

**Host-Pathogen Interactions of *Toxoplasma gondii*:  
Catecholamine Biosynthesis and Epigenetic Changes in  
Neuronal Cells During Infection**

Norhidayah Badya

Submitted in accordance with the requirements for the degree of

Doctor of Philosophy

The University of Leeds

School of Biology

October, 2019

## Intellectual Property and Publication Statements

The candidate confirms that the work submitted is her own and that appropriate credit has been given where reference has been made to the work of others.

This copy has been supplied on the understanding that it is copyright material and that no quotation from the thesis may be published without proper acknowledgement.

The right of Norhidayah Badya to be identified as Author of this work has been asserted by her in accordance with the Copyright, Designs and Patents Act 1988.

© 2019 The University of Leeds and Norhidayah Badya

## Acknowledgments

I would like to take the opportunity to thoroughly acknowledge the enormous amount of help I received in conducting this thesis work. I would like to thank my supervisor and mentor, Assoc. Professor Dr Glenn McConkey for his ideas and input, guidance, encouragement throughout this project and help over the years navigating this project through unexpected results and outcomes and continuously challenging me to think beyond, look further and investigate deeper. Thank you for introducing me to the world of neuroepigenetics, and also being patient throughout my journey of discovery.

I am also indebted to my laboratory mates, especially Francis, Mohammad, Ellie, Noha, Nok and Rosie for their kind help and guidance. Also, my thanks to Najihah, Sis Rosmaliza, Shazana, Hayati, Sis Nurha, Sis Nazlah, Fatin, Mokhtar (Jiji) and Ras Azira who provided limitless help for my work. I would also like to thank the entirety of the FBS faculty, especially the staff in the School of Biology.

Special gratitude goes to my family, in particular, my parents, Haji Badya Ngah and Hajjah Norehan Mohd Yunan, my siblings and all close family members. I am indebted to them for their never-ending support and love. Their presence has been critical in every stage of my life, championing my every success and sympathetic to every failure during the years of this PhD program. I could not have finished without their prayers and strength.

Last but not least to all my friends who have made life at Leeds wonderful, especially Najua, Adilla, Hanis, Nik Fatinah, Noorhidayah, Wafa, Amira, Farah Wahida, Farah Izyan, Sis Ziate, Farhain, Sis Nornizar, Sis Rafidah, Ust Daud and family and all members in the Malaysian Students and Community Leeds (MSCL) society and also, those I have forgotten to mention. Thank you very much for all your support, care, love, and fun times. I am grateful for a world of assistance that was given to me.

## Abstract

The apicomplexan parasite *Toxoplasma gondii* establishes chronic infection as intracellular cysts inside the brain and muscle tissue; able to infect virtually all mammals including humans. Modulation of host behaviour in rodents has been associated with promoting transmission and lifelong persistence. The neurophysiological changes associated with infection remain unclear, however catecholamine dysregulation has been observed in infected neurotransmitter-expressing cells and brain tissue. The experiments within this thesis examine the mechanisms whereby the parasite downregulates the expression of dopamine  $\beta$ -hydroxylase (DBH), the key enzyme required for converting dopamine into norepinephrine (NE), following prior studies showing NE suppression with infection. My experiments identified a long non-coding RNA (lncRNA) in infected cells that is in the antisense orientation to the DBH gene. This lncRNA may be associated with DNA methyltransferase 3 alpha (DNMT3a)-binding in the DBH promoter region which was elevated from day one post-infection rising to three-fold on day two. Time-dependent chromatin changes in the DBH promoter occurred with increased DNA methylation and dimethylation of H3K9 (H3K9me2) histone modifications, supporting previous findings of downregulation of the DBH gene. The minimal changes in chromatin observed in this study are consistent with the levels of NE and DBH suppression observed in the neural PC12 cells that were used. The presence of lncRNA in the DBH gene promoter in *T. gondii*-infected cells is proposed to play a role in alterations observed in host gene expression. The data in this thesis highlight a new form of epigenetic control of the host cell during parasitic infection. Model mechanisms of how the detected lncRNA control gene expression in *T. gondii*-infected neural cells are proposed.

## Table of Contents

<b>Acknowledgments</b> .....	<b>III</b>
<b>Abstract</b> .....	<b>IV</b>
<b>Table of Contents</b> .....	<b>V</b>
<b>List of Figures</b> .....	<b>X</b>
<b>List of Tables</b> .....	<b>XIII</b>
<b>Abbreviations</b> .....	<b>XIV</b>
<b>Chapter 1</b> .....	<b>1</b>
<b>General Introduction</b> .....	<b>1</b>
1.1 <i>Toxoplasma gondii</i> .....	1
1.2 Human toxoplasmosis .....	4
1.2.1 Dissemination to the host brain .....	6
1.2.2 CNS chronic infection.....	8
1.2.3 Parasite-induced behaviour changes in infected hosts .....	9
1.2.4 <i>Toxoplasma</i> -related psychiatric and neurological disorders.....	11
1.3 Host-pathogen interactions during chronic CNS <i>T. gondii</i> infection .....	13
1.3.1 Activation of chronic immune response and brain neuroinflammation causes neurodegeneration and neuroplasticity .....	14
1.3.2 Neuronal damage and dysfunction .....	16
1.3.3 Evading host-cell apoptosis.....	18
1.3.4 Dysregulation of neurotransmitters following infection .....	19
1.3.5 Effects of tryptophan degradation.....	22
1.3.6 Hormonal changes during infection .....	23
1.3.7 Parasite-derived mechanisms of neuro-modulation .....	23
1.4 Involvement of epigenetic modifications in transcriptional gene silencing (TGS).....	26
1.4.1 DNA methylation .....	27
1.4.2 Chromatin modification changes .....	29
1.4.3 Epigenetic regulation by antisense long non-coding RNAs.....	34
1.5 Conclusion .....	39
1.6 Research objectives .....	41

1.6.1	To evaluate DNA methylation patterns at the target DBH promoter gene induced by parasite infection coincident with downregulation of DBH gene expression. ....	41
1.6.2	To evaluate chromatin modification (H3K9me2) changes and measure DNA methyltransferase (DNMT3a) levels following infection in altering the DBH gene expression using a developed ChIP assay. ....	42
1.6.3	To repeat the DBH gene expression assay in <i>T. gondii</i> -infected rat PC12 cells. ....	42
1.6.4	To screen the involvement of antisense lncRNAs in downregulation of DBH transcription. ....	43
<b>Chapter 2</b>	.....	<b>44</b>
<b>Probing for DNA Methylation Changes Coincident with Downregulation of Dopamine <math>\beta</math>-hydroxylase Gene Expression</b>	.....	<b>44</b>
2.1	Overview .....	44
2.2	DNA methylation in transcription .....	46
2.2.1	Dynamic DNA methylation in the brain .....	47
2.2.2	Parasite-induced DNA methylation changes .....	48
2.2.3	Methylation regulates gene expression .....	49
2.3	Methods .....	50
2.3.1	Growth of parasite and host cell .....	50
2.3.2	Parasite conversion stage induction .....	50
2.3.3	Cells harvesting.....	51
2.3.4	Cell lysis.....	52
2.3.5	Phenol-chloroform DNA extraction .....	52
2.3.6	MeDIP: Sonication optimisation and DNA fragmentation.....	53
2.3.7	MeDIP: Immunoprecipitation of the methylated-DNA binding .....	54
2.3.8	Quantitative real-time PCR.....	55
2.3.9	MeDIP data analysis .....	57
2.3.10	Bisulphite treatment of the genomic DNA.....	59
2.3.11	Bisulphite-treated primer pair optimisation of rat 5'TSS DBH gene.....	60
2.3.12	Bisulphite-treated DNAs PCR amplifications .....	62
2.3.13	TOPO TA-cloning.....	63
2.3.14	Cloning plasmids in XL10-cells by transformation .....	65
2.3.15	Eco-RI digestion and confirmation of fragment insertion.....	65
2.3.16	Sequencing and data analysis.....	66
2.4	Results.....	67

2.4.1	MeDIP: Sample preparation and determination of sonication time and efficiency .....	67
2.4.2	Genomic DNA preparation from <i>T. gondii</i> -infected PC12 Cells.....	69
2.4.3	MeDIP-qPCR assay optimised .....	70
2.4.4	Primer optimisation for real-time qPCR .....	71
2.4.5	DNA methylation changes at the 5'TSS DBH gene region following infection.....	73
2.4.6	Bisulphite PCR primer design and optimisation .....	74
2.4.7	PCR amplification of the bisulphite-treated DNA of infected PC12 cell samples.....	77
2.4.8	Cloning procedure optimisation and plasmid digestion .....	79
2.4.9	Screening plasmid inserts by EcoRI plasmid digestion.....	80
2.4.10	Bisulphite PCR-cloning sequencing.....	82
2.4.11	DNA methylation pattern analysis by bisulphite sequencing.....	83
2.5	Discussion.....	89
2.6	Conclusion .....	95
<b>Chapter 3.....</b>		<b>96</b>
<b>Chromatin Modification Changes Coincident with DBH Gene Suppression in <i>T. gondii</i>-infected Neural PC12 Cells.....</b>		<b>96</b>
3.1	Overview .....	96
3.1.1	Repressive histone modification protein markers: Dimethyl-histone 3 lysine 9 (H3K9me2) and DNA methyltransferase 3 alpha (DNMT3a) 97	
3.1.2	Chromatin immunoprecipitation assay (ChIP) .....	98
3.2	Methods .....	100
3.2.1	Growth of host cells and parasites and induction of parasite conversion stage .....	100
3.2.2	Cell harvesting and formaldehyde-crosslinking .....	100
3.2.3	Chromatin extraction and shearing.....	101
3.2.4	Evaluation of chromatin shearing performance via agarose gel electrophoresis.....	102
3.2.5	Chromatin immunoprecipitation.....	102
3.2.6	DNA crosslinking reversal and isolation .....	103
3.2.7	Validation of the ChIP assay performance.....	104
3.2.8	Real-time qPCR and data analysis.....	104
3.3	Results.....	105
3.3.1	ChIP assay optimisation.....	105

3.3.2	Optimisation and validation of the ChIP assay performance.....	107
3.3.3	Summary of ChIP assay optimisation.....	109
3.3.4	ChIP real-time qPCR assay of <i>T. gondii</i> -infected PC12 cells.....	110
3.4	Discussion.....	114
3.5	Conclusion .....	119
<b>Chapter 4</b>	<b>.....</b>	<b>120</b>
<b>Assessing DBH Gene Expression in PC12 Cell Lines Used for Chromatin Studies</b>	<b>.....</b>	<b>120</b>
4.1	Overview .....	120
4.2	<i>Toxoplasma gondii</i> induces DBH down-regulation at the transcriptional level 121	
4.2.1	DBH catalyses the synthesis of norepinephrine from dopamine ..	122
4.3	Method.....	124
4.3.1	Cell plating and harvesting .....	124
4.3.2	Column RNA extraction and DNase treatment .....	124
4.3.3	Reverse-Transcriptase cDNA synthesis .....	125
4.3.4	RT-qPCR .....	125
4.3.5	Analysis of catecholamines secretion by HPLC-ECD .....	126
4.4	Results.....	128
4.4.1	Minimal changes in mRNA DBH expression during <i>T. gondii</i> infection in the rat PC12 cells .....	128
4.4.2	Reduced catecholamine secretion by rat PC12 cells .....	131
4.5	Discussion.....	134
4.6	Conclusion .....	135
<b>Chapter 5</b>	<b>.....</b>	<b>136</b>
<b>Antisense Long Non-coding RNA (lncRNA) Involvement in Post-infection DBH Gene Regulation</b>	<b>.....</b>	<b>136</b>
5.1	Overview .....	136
5.2	Long non-coding RNA-DNA interactions .....	137
5.3	Mechanisms of gene regulation by long non-coding RNAs.....	138
5.4	Methods .....	140
5.4.1	Primers targeting potential DBH antisense lncRNA .....	140
5.4.2	DBH lncRNA primer pair optimisation.....	141
5.4.3	RNA extraction and DNase TURBO treatment .....	142
5.4.4	First strand cDNA synthesis and RT-PCR.....	143

5.4.5	TA Cloning and DNA sequencing of the specific PCR bands .....	144
5.4.6	Validation of the RNA sample quality by RNase treatment .....	144
5.5	Results .....	145
5.5.1	Primer design and optimisation .....	145
5.5.2	Directional RT-PCR for lncRNA screening .....	148
5.5.3	DNA sequencing of positive RT-PCR products showed sequences complementary with the rat DBH promoter gene sequences .....	155
5.5.4	RNA sample quality control .....	158
5.6	Discussion .....	160
5.7	Conclusion .....	167
<b>Chapter 6</b>	.....	<b>168</b>
<b>Final Remarks</b>	.....	<b>168</b>
6.1	Final Remarks .....	168
6.1.1	Epigenetic changes at transcription start site associated with DBH transcriptional repression in <i>T. gondii</i> infection .....	169
6.2	Antisense long non-coding RNA could mediate epigenetic transcriptional gene silencing of the DBH gene .....	173
6.2.1	Involvement of other effectors in promoter DNA methylation-directed epigenetic gene repression .....	178
6.3	Study limitation; a relatively low DBH expression in catecholaminergic neural cell line .....	179
6.4	The effect of DBH downregulation and consequentially norepinephrine suppression on the host in initiating behavioural changes .....	180
6.5	Future investigations .....	181
6.5.1	Implement other cell lines and <i>in vivo</i> tissue .....	181
6.5.2	Broadening the studied promoter-region .....	181
6.5.3	Analysis of other related host epigenetic effector proteins .....	182
6.5.4	Characterise the detected-long non-coding RNA transcript at 5'TSS 182	
6.5.5	Assess chromatin accessibility changes throughout the neural cell genome with <i>T. gondii</i> infection .....	183
6.6	Conclusion .....	185
<b>List of References</b>	.....	<b>186</b>
<b>Appendix A</b>	.....	<b>210</b>
<b>Appendix B</b>	.....	<b>212</b>
<b>Appendix C</b>	.....	<b>225</b>

## List of Figures

Figure 1.1 Life cycle of <i>T. gondii</i> and the transmission routes in humans.....	3
Figure 1.2 Proposed mechanisms of <i>Toxoplasma</i> invasion to the brain.....	7
Figure 1.3 Proposed mechanisms of <i>T. gondii</i> alteration of neuronal functions. .....	14
Figure 1.4 Scenarios of DNA methylation patterns in gene regulation.....	29
Figure 1.5 Folding of DNA into chromatin. ....	30
Figure 1.6 Mechanisms of epigenomic gene regulation. ....	31
Figure 1.7 Long non-coding RNAs. ....	36
Figure 2.1 Threshold level and Cq value on the real-time qPCR amplification curve.....	56
Figure 2.2 Generalised MeDIP assay.....	58
Figure 2.3 Schematic representation of the steps in the MeDIP assay study design.....	59
Figure 2.4 Primer pair design of 5'TSS DBH gene sequences. ....	61
Figure 2.5 PCR4-TOPO TA vector.....	64
Figure 2.6 Time-based sonication determination. ....	67
Figure 2.7 Agarose gel electrophoresis of gDNA from rat PC12 cell samples sonicated for 1 minute.....	68
Figure 2.8 Melt peak analysis for MeDIP-qPCR primer pair optimisation. ....	72
Figure 2.9 DNA methylation pattern changes analysed by MeDIP-qPCR assay. .....	73
Figure 2.10 Gradient standard PCR of both sets of primer pairs tested on rat methylated and un-methylated gDNA standards.....	76
Figure 2.11 Set primer pair of 2.7k bp upstream tested on bisulphite-treated PC12 cell's gDNA. ....	77
Figure 2.12 PCR amplification of bisulphite-treated PC12 cell DNAs. ....	78
Figure 2.13 Gel-purified DNA isolation from PCR amplification products of bisulphite-treated PC12 cells. ....	78
Figure 2.14 Overall DNA methylation haplotypes (CpG 1 to CpG 8) at 5'TSS DBH gene of <i>T. gondii</i> -infected and uninfected control neural PC12 cells in a time-course on day 1, 3, and 5 post-infection as measured by cloning-PCR bisulphite sequencing analysis. ....	83
Figure 2.15 Bisulphite sequencing profile of differential DNA methylation changes on individual CpG site at 5'TSS DBH gene region following <i>T.</i> <i>gondii</i> infection. ....	84

Figure 2.16 Overall DNA methylation haplotypes at 2.7k bp upstream of DBH gene of <i>T. gondii</i> -infected and uninfected control neural PC12 cells days 1, 3, and 5 post-infection by cloning-PCR bisulphite sequencing analysis. ....	86
Figure 2.17 Bisulphite sequencing profile of the differential DNA methylation changes on individual CpG sites at 2.7k bp upstream of the DBH promoter region following infection.....	87
Figure 3.1 Outline of the ChIP-real time qPCR procedure. ....	99
Figure 3.2 Chromatin sonication time. ....	107
Figure 3.3 A working ChIP assay for protein binding. ....	108
Figure 3.4 ChIP assay parameters optimised for rat neural PC12 cells.....	109
Figure 3.5 ChIP analysis of DNMT3a binding at the 5'TSS of the DBH gene in <i>T. gondii</i> -infected PC12 cells.....	111
Figure 3.6 ChIP assay for DNMT3a binding 2.7k bp upstream of rat proximal promoter DBH gene. ....	112
Figure 3.7 ChIP analysis of H3K9me2 protein-binding patterns at the 5' promoter of the DBH gene in <i>T. gondii</i> -infected PC12 cells.....	113
Figure 4.1 The biosynthetic pathway of catecholamine neurotransmitters...	123
Figure 4.2 Plot showing DBH gene expression in MOI of <i>T. gondii</i> -infected PC12 cells with respect to the housekeeping gene, rat GAPDH, on day five post-infection, analysed by RT-qPCR. ....	128
Figure 4.3 Plot showing DBH gene expression of <i>T. gondii</i> -infected PC12 cells with respect to the housekeeping gene rat GAPDH at 1, 3, and 5 days post-infection, analysed by RT-qPCR. ....	129
Figure 4.4 BAG1 and Toxo-actin gene expression relative to rat GAPDH expression in <i>T. gondii</i> -infected PC12 cells at 1, 3, and 5 days post-infection, analysed by RT-qPCR. ....	130
Figure 4.5 Catecholamines released from rat neural PC12 cells, detected by HPLC-ECD. ....	132
Figure 4.6 Examples of HPLC chromatogram of different PC12 cell batches (A and B). ....	133
Figure 5.1 Interactions of lncRNAs with the genome.....	138
Figure 5.2 Primer map relative to the 5'TSS DBH gene.....	141
Figure 5.3 Schematic representation of the strand-specific RT-PCR assay designed for lncRNA screening at the DBH gene.....	146
Figure 5.4 Gradient PCR for primer optimisation of PCR Primer Set 1-4.....	147
Figure 5.5 PCR products of all primer sets; Set 1-4: 138bp, 132bp, 102bp, and 130bp, respectively.....	148
Figure 5.6 Agarose gel analysis of the PCR amplification of Primer Set 2....	149
Figure 5.7 Antisense lncRNA expressed at the 5'TSS DBH gene in infected PC12 cells.....	151
Figure 5.8 PCR amplification of Primer Set 3.....	152

**Figure 5.9 PCR amplification of primer Set 3 and Set 4 by RT-Primer 3 transcript.**  
.....153

**Figure 5.10 PCR amplification of Primer Set 4.....154**

**Figure 5.11 Predicted lncRNA-binding overlying the 5'TSS of the DBH gene.**  
.....157

**Figure 5.12 RNA sample quality control.....159**

**Figure 5.13 Map of the positive PCR bands in random hexamer +RT template,  
amplified by the primers of non-coding sites. ....166**

**Figure 6.1 Schematic model of how antisense long non-coding RNA could  
mediate epigenetic transcriptional gene silencing of the DBH gene in  
infected catecholaminergic cells. ....175**

**Figure 6.2 Schematic workflow of the ATAC-seq process.....184**

**List of Tables**

<b>Table 2.1 The final setting of the Real-Time qPCR. ....</b>	<b>56</b>
<b>Table 2.2 Ligation and cloning optimisation.....</b>	<b>80</b>
<b>Table 2.3 Total number of colonies with the positive fragment inserted.....</b>	<b>81</b>
<b>Table 2.4 Average DNA methylation percentage of each haplotype samples.</b>	<b>84</b>
<b>Table 2.5 Average methylation percentage of each haplotype sample.....</b>	<b>87</b>

**Abbreviations**

5-hmC	5-hydroxymethylcytosine
5-mC	5-methylcytosine
AADC	Aromatic amino acid decarboxylase
AGO1	Argonaute-1
AIDS	Acquired immune deficiency syndrome
ATAC-Seq	Assay for transposase-accessible chromatin with high-throughput sequencing
BBB	Blood-brain barrier
Bis-	Bisulphite
bp	Base pair
cDNA	Complementary DNA
ChIP	Chromatin immunoprecipitation assay
CNS	Central nervous system
CpG	Cytosine and guanine separated by a phosphate
Cq	Quantification cycle
DA	Dopamine
DBH	Dopamine $\beta$ -hydroxylase
DCs	Dendritic cells
DMEM	Dulbecco's modified eagles medium
DNA	Deoxyribonucleic acid

DNMT3a	DNA methyltransferase 3 alpha
DNMTs	DNA methyltransferases
e.g.	For example
ECACC	European Collection of Authenticated Cell Cultures
EZH2	Enhancer of zeste homolog 2
FBS	Foetal bovine serum
FOI	Fragment of interest
G9A	Histone methyltransferase G9A
GABA	Gamma-aminobutyric acid
GAD67	Glutamic acid decarboxylase 67
gDNA	Genomic DNA
GFP	Green fluorescent protein
GRA	Granule proteins
h	Hour
H3K27	Histone H3 lysine 27
H3K9	Histone H3 lysine 9
H3K9me2	Di-methylation of H3K9
H3K9me3	Tri-methylation of H3K9
H4K20	Histone H4 lysine 20
HDAC	Histone deacetylases
HFF	Human foreskin fibroblast
HMT	Histone methyltransferase
HOTAIR	Human HOX transcript antisense RNA

HPLC-ECD	High performance liquid chromatography-electrochemical detection
IDO	Indoleamine 2,3-dioxygenase
IFN- $\gamma$	Interferon gamma
IL	Interleukin
IP	Immunoprecipitation
IRGs	Immunity-related guanosine triphosphatases
KA	Kynurenic acid
lncRNA	Long noncoding-RNA
MAP2	Microtubule-associated protein-2
MBD	Methyl-CpG binding domain
MeDIP	Methylated DNA immunoprecipitation
miRNAs	microRNAs
MOI	Multiplicity of infection
mRNA	Messenger ribonucleic acid
ncRNA	Noncoding RNA
NE	Norepinephrine
NF- $\kappa$ B	Nuclear factor kappa-light-chain-enhancer of activated B cells
NMDARs	N-methyl-D-aspartate receptors
NO	Nitric oxide
NTC	No template control
PBS	Phosphate buffer saline

## XVII

PNMT	Phenylethanolamine N-methyltransferase
PRC2	Polycomb repressive complex 2
PTMs	Post-translational modifications
PV	Parasitophorous vacuole
RNA	Ribonucleic acid
RNA Pol II	RNA polymerase II
RNA-Seq	RNA sequencing
ROP	Rhopkinase proteins
RPMI	Roswell Park Memorial Institute
SDS	Sodium dodecyl sulfate
siRNAs	Short interfering RNAs
<i>T. gondii</i>	<i>Toxoplasma gondii</i>
T <sub>a</sub>	Annealing temperature
TE	Tris-EDTA
TET	Ten-eleven translocation
TGS	Transcriptional gene silencing
TH	Tyrosine hydroxylase
Th1	T helper cell type 1
TNF	Tumour necrosis factor
TSS	Transcriptional start site
UHRF1	Ubiquitin-like, containing PHD and RING finger domains 1
UTR	Untranslated region

# Chapter 1

## General Introduction

### 1.1 *Toxoplasma gondii*

The single-celled obligate intracellular parasite *T. gondii* is one of the most common global zoonotic pathogens and infects a wide range of animals, including humans (Dubey *et al.*, 1970). Generally categorised as a ubiquitous parasite, it is taxonomically classified in the phylum *Apicomplexa* (along with malaria parasites) and subclass *Coccidia*. Incidence of *T. gondii* infection in humans varies greatly between regions and overall high seroprevalence has been reported, approaching 30% to 80% worldwide (Tenter *et al.*, 2000; Pittman and Knoll, 2015; Tyebji *et al.*, 2019). In the United States, it is considered the second leading cause of foodborne-related deaths, mostly originated from poultry, pork, produced and complex foods (Scallan *et al.*, 2011; Batz *et al.*, 2012), and has emerged as one of the most common opportunistic infections in patients with AIDS (Luft and Remington, 1992; Ondounda *et al.*, 2016).

*Toxoplasma gondii* has a complex life cycle including sexual and asexual reproduction, and consisting of three infectious stages: bradyzoites, tachyzoites, and oocysts. All stages are capable of infecting intermediate (mammals) and definitive (cat) hosts (Tenter *et al.*, 2000; Dubey, 2008). The oocyst is the final product of the parasite's sexual cycle and is released in the cat intestine then excreted in the faeces. A single infected cat can

shed between 2 and 20 million oocysts per day and the cyst containing highly-infectious sporozoites can survive in humid soil for over a year (Dubey *et al.*, 1970; Flegr, 2015). Intermediate hosts are commonly infected by the ingestion of oocysts shed in the cat faeces, and infection by bradyzoite-containing cysts occurs in humans upon the ingestion of undercooked meat (Pittman and Knoll, 2015). Once ingested, the oocysts invade intestinal epithelial cells and transform into rapidly-dividing, free-moving tachyzoites in a parasitophorous vacuole (PV) which separates parasite from host cytoplasm. Unlimited replication will result in eventual cell rupture and the release of parasites into neighbouring cells, thereby activating the host immune response. Meanwhile, depending on the immune status of the infected host, some tachyzoites will successfully evade the immune response by transforming into slow-replicating bradyzoites in the chronic stage and settling inside the host cells as dormant cysts.

Human exposure to *T. gondii* occurs in a variety of ways, as shown in Figure 1.1. Firstly, humans can ingest tissue cysts containing bradyzoites present in undercooked infected meat (especially lamb and pork). Secondly, by ingesting highly infectious oocysts in the soil by consuming unwashed vegetables, contaminated water or unpasteurized milk. The transmission can also occur by direct exposure to infected cat faeces. Other possible routes are through errors in medical procedures such as in blood transfusion, organ transplantation and laboratory accidents involving biological materials. Some transmission is not due to error, e.g. in heart transplant mismatch (infected donor, uninfected recipient). The procedure goes ahead despite the risk, on the basis of a 'benefit versus harm' assessment, where risk of harm can be mitigated by prophylactic anti-toxoplasma treatment. Finally, infection via the transplacental transmission of rapidly replicating tachyzoites from mother to foetus can occur, endangering foetal development (Tenter *et al.*, 2000; Hill and Dubey, 2002; Jones and Dubey, 2012; Flegr, 2015).

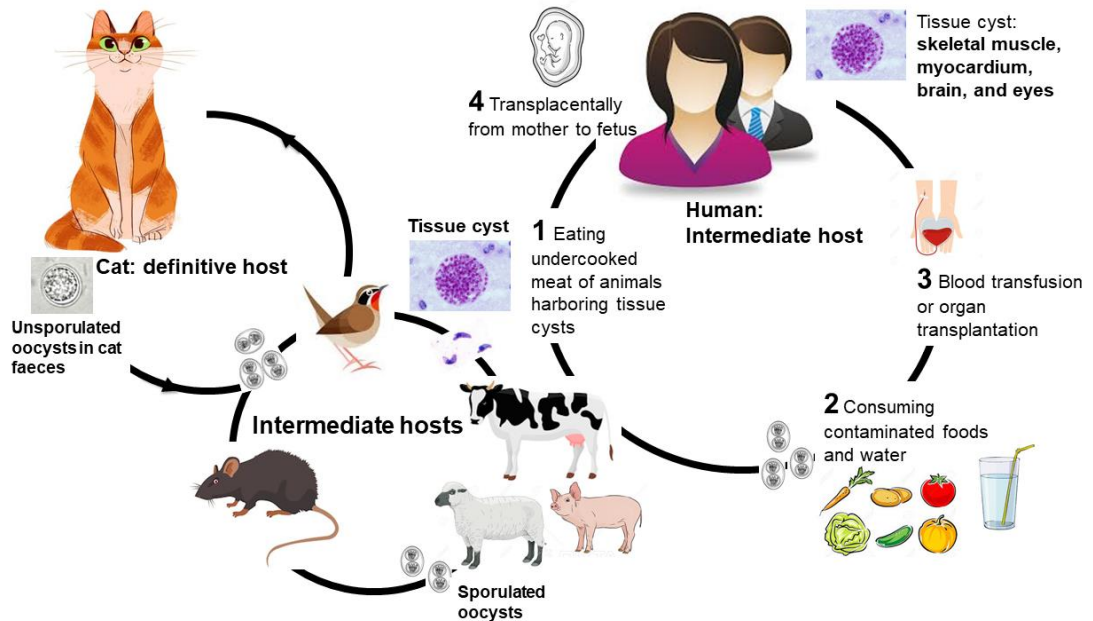


**Figure 1.1 Life cycle of *T. gondii* and the transmission routes in humans.** The cat is the only definitive host of *T. gondii* and rodents are natural intermediate hosts. Although toxoplasmosis has been broadly observed in a wide range of mammals including humans as an accidental intermediate host, sexual reproduction happens exclusively in the cat, resulting in environmental contamination after excretion of infective oocysts in cat faeces. Once ingested by the intermediate hosts where asexual reproduction takes place, the oocysts transform into freely-moving tachyzoites. Tachyzoites infect various cell types and differentiate into bradyzoite-containing cysts which persist chronically in the tissue. Cats become infected after consuming intermediate hosts harbouring tissue cysts, thus completing the parasite life cycle.

Three major genotypes or lineages of *T. gondii* have been identified: type I, II, and III (Howe and Sibley, 1995). Recently discovered is haplotype 12, a lineage associated with disease in North American wildlife (Khan *et al.*, 2011). Phenotypically, the lineages differ in virulence, growth rate, and cyst burdens in the host cells. Notably, differences in the dissemination of these strains correlate with disease pathogenesis and virulence (Saeij *et al.*, 2005; Sibley *et al.*, 2009; Harker *et al.*, 2015). The type I genotype (e.g. RH strain) is highly virulent in mice. Infection with this strain induces lethal acute toxoplasmosis in mice, even without inducing cyst formation (Blanchard *et al.*, 2015). However, the vast majority of human infection is caused by the type II strain (e.g. Prugniaud, ME49) which is commonly followed by cyst development in the brain, retina and skeletal and heart muscle. The strong association between the type II strain and human disease has

important implications for diagnosis, treatment, and prevention of toxoplasmosis (Howe and Sibley, 1995; Saeij *et al.*, 2005) even though type I, type III (e.g. CEP and VEG) and so-called atypical strains can also infect humans and cause the disease (Sibley *et al.*, 2009).

## 1.2 Human toxoplasmosis

In immunocompetent individuals, clinical disease due to *T. gondii* is uncommon. This is because, the fast-replicating tachyzoite stage is largely responsible for tissue destruction that results in clinical manifestations by which, at this stage, infection is typically well-controlled by an effective host immune response mediated by the cytokine interferon- $\gamma$  (IFN- $\gamma$ ) secreted by immune effector cells. Immunocompetent hosts usually show no or mild flu-like clinical symptoms during this primary infection although some individuals can develop lymphadenopathy with symptoms generally including fever, fatigue, muscle pain, sore throat and headache (Hill and Dubey, 2002). When threatened with elimination by the host's immune response, tachyzoites differentiate into long-lasting cysts containing slow-replicating bradyzoites resistant to immune clearance and are localised in the brain, eye, and muscles, persisting indefinitely. Bradyzoite chronic infection is latent and does not produce any noticeable symptoms (Flegr, 2015). However, once the host immune system is weakened, the encysted bradyzoites can transform back into rapidly-replicating virulent tachyzoites, thus reactivating and invading other tissues, causing chronic disease manifestations which can lead to patient death such as in fatal toxoplasmic encephalitis and pulmonary toxoplasmosis.

Two conditions confer heightened risk for clinical disease: (1) the reactivation of latent infection in immunodeficient persons such as AIDS patients or immunosuppressed transplant recipients, and (2) pregnant mothers with a *T. gondii* primary infection.

Immunodeficient persons commonly develop toxoplasmic encephalitis with the formation of CNS lesions and then, further disseminate the disease throughout their body. Meanwhile, infection in the pregnant mother can result in congenital toxoplasmosis that causes neurological defects and spontaneous abortion (Dubey, 2008; Weiss and Dubey, 2009; Flegr, 2015). In such cases, appropriate treatment is necessary to protect organs from irreversible damage. Finding the appropriate treatment for chronic toxoplasmic encephalitis is critical as the incidence of this disease is increasing with the increasing of AIDS population. In 2003 to 2012, the toxoplasmosis incidence rate in the US was 6137 cases per year of which 407 had meningoencephalitis (Lykins *et al.*, 2016). There is currently no anti-parasitic drug available capable of removing the intracellular cysts, in the brain or elsewhere in the body.

In addition, toxoplasmic retinochoroiditis contributes significantly to eye disease worldwide. The prevalence of ocular disease in patients with toxoplasmic infection is still not well established and likely under diagnosed, but the most severe manifestations are encountered in patients with an impaired immune system, the elderly and neonates (Furtado *et al.*, 2013). Therefore, ocular toxoplasmosis commonly results from both congenital and acquired infections. It can develop immediately after the initial infection, but more frequently months or years later, or during reactivation (Montoya and Remington, 1996). Parasites circulating in the blood may target the eye as, which thereafter stimulates host inflammatory responses. This results in intra-ocular inflammation called necrotizing retinochoroiditis (primary or recurrent), that can cause permanent retinal scarring, loss of retinal tissue and subsequent loss of vision (Holland, 2004; Maenz *et al.*, 2014).

### 1.2.1 Dissemination to the host brain

Upon host cell invasion, the fast-replicating tachyzoites unrestrictedly replicate by endodyogeny. This eventually leads to lysis of host cells and subsequent invasion of neighbouring cells, initiating the host's immune response and ultimately causing persistent host infection. The most severe inflammation often results when tachyzoites propagate in the retina and brain of the host. The high blood flow during the acute phase of infection promotes higher numbers of parasites to reach the brain region (Estate *et al.*, 2018). It has been reported that the parasite can break down the blood-brain barrier (BBB) as early as nine days following infection (Silva *et al.*, 2010).

The brain is considered a well-protected, immune-privileged organ. In order to reach the brain parenchyma from the cerebral blood circulation, *Toxoplasma* needs to pass through the brain endothelial cells lining the cerebral microvasculature of the BBB that is supported by a rich basement membrane network. The endothelial cells are wedged extremely close to each other, forming so-called tight junctions that, for CNS protection, strictly control the entry of large molecules and immune cells into the brain. The BBB is also lacking lymphatic vessels, thereby restricting lymphocyte access into the brain parenchyma. The surrounding pericytes and astrocytic endfeet function as structural and biochemical BBB supporters and epithelial protectors. There are multiple proposed mechanisms explaining how *T. gondii* breaches the BBB and gains access to the brain, but the exact mechanism is still under debate. A recent study suggested that the infection of endothelial cells is necessary for parasitic penetration into the CNS (Konradt *et al.*, 2016). The free parasite could then invade by one of two methods: (1) directly into the endothelial cell barrier transcellularly, thereafter rapidly replicating in and lysing the infected cells before bursting into the parenchyma brain, or (2) crossing the BBB paracellularly by passing through an intercellular space between the epithelial cells without invading the cells themselves (Tyebji *et al.*, 2019). Another proposed mechanism

is that parasites hijack blood-circulating cells such as leukocytes, macrophages or dendritic cells and use them as “Trojan horses” from local sites of infection to the brain (Fuks *et al.*, 2012). Such a mechanism was observed when *T. gondii*-infected monocytes were discovered transmigrating across an *in vitro* BBB model, shuttling the parasites into the brain of infected mice through a process dependent on host CD11b-expressing leukocytes. The study claimed that *T. gondii* hijacked CD11b-expressing leukocytes to reach the brain’s extravascular space (Courret *et al.*, 2006). The three proposed models are summarised in Figure 1.2.

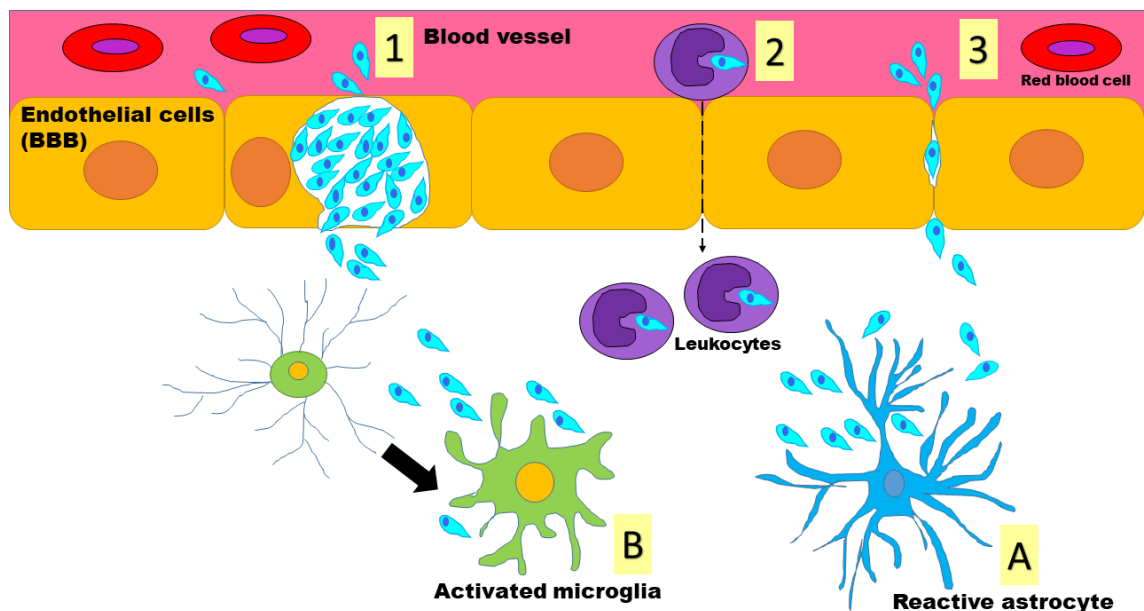


**Figure 1.2 Proposed mechanisms of *Toxoplasma* invasion to the brain.** Three proposed mechanisms of parasites entry into the brain; 1) transcellular entry, 2) “Trojan horses” entry and 3) paracellular entry. Parasite entry into the brain activates astrocytes (A) and microglia (B), thereby activating the immune response which then assists in parasite clearance.

Interestingly, tachyzoites can exploit the migratory properties of dendritic cells (DCs) without needing their activation. They accomplish this by manipulating the expression of DC chemokine receptor CCR7 (hallmarks of matured DCs) in which the infected DCs demonstrate a hypermigratory effect that aggravates spreading throughout the host. The hypermotility effect has also been proposed due to the response of functional GABA<sub>A</sub>

(gamma-aminobutyric acid) receptor expression and GABA released by infected DC soon after infection (Fuks *et al.*, 2012). Gamma-aminobutyric acid is used as a carbon source by *Toxoplasma* (MacRae *et al.*, 2012) and pre-treatment of infected-DC with GABAergic inhibitors reduced the parasite dissemination; hence, the parasite may alter GABAergic signalling in the cell host (Fuks *et al.*, 2012). Altogether, this evidence suggests that *Toxoplasma* utilises combined strategies for systemic dissemination into the brain.

### **1.2.2 CNS chronic infection**

Infection of the CNS is one of the hallmarks of toxoplasmosis and *T. gondii* can infect different types of brain cells including microglia, astrocytes, Purkinje cells and neurons and thereafter develop cysts within these cells (Blanchard *et al.*, 2015; Flegr, 2015), although cysts are predominantly found in neurons (Ferguson and Hutchison, 1987b; Lüder *et al.*, 1999; Melzer *et al.*, 2010; Haroon *et al.*, 2012). In fact, a recent *in vivo* study in mice reported the neuron was the primary target cell of *Toxoplasma* parasites (Cabral *et al.*, 2016). Immunohistochemical study showed that cysts can reside in all major parts of neurons including the neuronal soma, dendrites and axons (Haroon *et al.*, 2012). It is assumed that the parasite could possibly escape from detection by the immune system in the brain because of the lack of major histocompatibility complex antigen class I neurons, low IFN- $\gamma$  and/or TNF activity and non-response against CD8<sup>+</sup> T cells (Schlüter *et al.*, 2001; Schaeffer *et al.*, 2009; Salvioni *et al.*, 2019). It has been reported that host GABA can be utilised in parasite growth as a carbon source metabolite, therefore, it is scavenged by the parasite (MacRae *et al.*, 2012). Since neurons can release GABA, it explains the parasite's preference in targeting the cell for localisation. However, the exact mechanism on how the parasites reach and localise in the neurons remains unclear. As the neuron is the parasite's primary target, there are three neuronal subpopulations that

can be found during infection. The first subpopulation is uninfected neurons that contain the parasite's rhoptry proteins injected into the neuron during parasite entry. The second subpopulation is infected neurons with replicating or free-moving tachyzoites, and the third subpopulation is infected neurons with stable parasitic cysts containing hundreds of bradyzoites. The effect of the parasite on these neuronal subpopulations is unknown.

Literature on cyst distribution within the brain is speculative and sometimes controversial. Some studies have found higher numbers of tissue cysts located in the amygdala and nucleus accumbens, dopamine-containing limbic brain regions known to be important for motor control (basal ganglia) (Vyas *et al.*, 2007). In other studies, magnetic resonance imaging of cerebral toxoplasmosis patients revealed lesions were focused mainly in the cortex and cerebellum area, which is consistent with several rodent studies (Lüder *et al.*, 1999; Dellacasa-Lindberg *et al.*, 2007; Dubey *et al.*, 2016). Regardless, it is clear that *T. gondii* infects all regions of the whole brain area. Nevertheless, the cyst volume is considered small which makes it difficult to be detected, thus rendering study of cyst localisation in the human brain problematic. A recent study has provided strong evidence of infection via a population-based screening of autopsy cases, which found that 16.5% prevalence of *T. gondii* DNAs expression was within human brain tissue, although without any specific distribution (Samojłowicz *et al.*, 2019).

### **1.2.3 Parasite-induced behaviour changes in infected hosts**

Changes in behaviour have been observed in rodents infected with *T. gondii*, one of which is the phenomenon of "fatal attraction" (Berdy *et al.*, 2000; Webster, 2007). One implicit conclusion of the manipulation hypothesis is that *T. gondii* dynamically modifies host behaviour for its own selective benefit. Over decades of studies under various laboratory and experimental conditions, some highly specific and consistent behavioural

changes in infected rodents have been observed. One of the main captivating effects of *Toxoplasma* infection is the rodent's loss of innate fear and aversion towards the odour of cat urine, one result of which may be increased predation (Berdoy *et al.*, 2000; Vyas *et al.*, 2007; Webster, 2007). Many other behavioural changes in infected rodents have been observed such as weakened learning capacity and memory, lowered defensive response, location of time spent within vulnerable open areas, decreased fear of novel stimuli, increased psychomotor activity (Webster, 1994), decreased climbing and rearing and increased rate of entrapment (Hutchison *et al.*, 1980). All these behavioural changes are likely to increase the probability of parasite transmission from the intermediate to definitive host, thus conferring a sexual advantage to the parasite to complete its life cycle through increasing predation by the cat. Most studies also claim that behaviour changes are infection specific and not caused by general rodent illness, which can affect some learning and social interactions (Vyas *et al.*, 2007; Webster and McConkey, 2010).

Studies conducted using different rodent experimental models showed that behavioural changes occur in both acute and chronic *T. gondii* infections (Vyas *et al.*, 2007; Vyas, 2015). However, the mechanisms underlying the neurological alterations driving these behavioural modifications are still not clear. The elevated number of cysts in behaviourally-relevant brain regions has been proposed to play an important role in the behavioural changes of the host. However, the most comprehensive study to date analysing 100 infected rats found little preference for any specific region (Dubey *et al.*, 2016). Meanwhile, other studies showed that behaviour modifications persisted even with low numbers of brain cysts (Ingram *et al.*, 2013). Although this demonstrates that behaviour changes do not depend on high cyst density, some studies claimed that tropism in a specific relevant brain area may contribute towards certain behavioural impacts. Intriguingly, a recent discovery found that some behavioural changes in rodents were not associated with the parasite cyst burden in the brain, but rather by the degree of neuroinflammation produced by chronic infection. They also demonstrated that

behavioural changes can be reversed by the anti-inflammatory drug guanabenz (Martynowicz *et al.*, 2019).

Apart from rodents as one of its important intermediate host, toxoplasmosis may also affect human behaviour. Latent asymptomatic toxoplasmosis is believed to cause specific changes to human olfactory function whereby infected men rate the smell of diluted cat urine as relatively more pleasurable than those uninfected, although in infected women, the opposite effect was observed (Flegr *et al.*, 2011). Numerous other findings have also documented behaviour changes in the infected person upon infection, such as reduced novelty-seeking behaviours (Flegr, 2010), impaired psychomotor performance with prolonged reaction times (Havlíček *et al.*, 2001), personality profile changes, impairment of memory functions (Gajewski *et al.*, 2014), increased risk of suicide attempts (Bak *et al.*, 2018), greater risk of traffic accidents (Flegr, 2010), depression (Gale *et al.*, 2014) and developed general anxiety disorder (Markovitz *et al.*, 2015). These discoveries suggest possible indirect influences of the parasite on its accidental secondary intermediate hosts with regard to behavioural changes although many of these were small studies and need to be rigorously repeated.

#### **1.2.4 *Toxoplasma*-related psychiatric and neurological disorders**

Behavioural changes observed in rodents led to the discovery of a strong association between latent toxoplasmosis and many chronic psychiatric and neurodegenerative disorders, including schizophrenia (Torrey and Yolken, 2003; Horacek *et al.*, 2012; Holub *et al.*, 2013), Parkinson's disease (Miman *et al.*, 2010a), obsessive-compulsive disorder (Miman *et al.*, 2010b; Çakın Memik *et al.*, 2015), bipolar disorder (de Barros *et al.*, 2017) and a weak population-based study even suggested brain tumours (Thomas *et al.*, 2012). Serological studies have found that the presence of many psychological disorders

is correlated to higher seroprevalence of toxoplasmosis infection than in the rest of the population, but not correlated with infection with other CNS pathogens (Flegr, 2015). How the parasite interacts with the brain and how this interaction could contribute to our understanding of mental health disorders remains an unexplored area of research.

Although there a strong association has been reported, there is no definitive proof of the parasite as a primary cause of neuropsychiatric illness, there are few significant and noteworthy correlations, such as that observed in *Toxoplasma*-related schizophrenia. A meta-analysis of 23 studies of *T. gondii* seroprevalence and schizophrenia conducted out in 17 countries over five decades found that the likelihood of infection in schizophrenia patients was 2.7 times higher than in the rest of the population (odds ratio [OR]=2.73; 95% confidence interval;  $P < 0.000001$ ) (Torrey *et al.*, 2006). The strongest evidence to demonstrate the co-occurrence of *Toxoplasma* and schizophrenia is the correlation of *T. gondii* IgG antibody levels with schizophrenia severity. Elevated anti-*T. gondii* IgG antibody levels have been reported in first-onset schizophrenia patients, suggesting that *Toxoplasma* modulates the course of the disease (Torrey *et al.*, 2006). A recent large-scale serological study denoted 25.9% of the studied sample population was associated with schizophrenia (odds ratio [OR], 1.47; 95% confidence interval [CI], 1.03–2.09) and the data showed stronger association with pathogen exposure preceding outcome (incidence rate ratio [IRR], 2.78; 95% CI, 1.27–6.09) (Burgdorf *et al.*, 2019). In addition, latent toxoplasmosis has been ranked as one of the most important risk factors for schizophrenia. It is also noteworthy that some antipsychotic drugs used to treat schizophrenia have been shown to inhibit the growth of *T. gondii* in cell culture (Jones-Brando *et al.*, 2003).

### 1.3 Host-pathogen interactions during chronic CNS *T. gondii* infection

Chronic *T. gondii* infection is established in the CNS tissues where the parasite may directly or indirectly interfere with neuronal function leading to behavioural and neuropsychiatric illness. Inside the neuron, the parasite localises in an isolated PV within host cytoplasm, but is capable of recruiting host endoplasmic reticulum and mitochondria molecules into the PV to facilitate its growth, intracellular survival and transmission (Clough and Frickel, 2017). *Toxoplasma* is reported as auxotrophic for several nutrients such as tryptophan, cholesterol and iron (Dimier and Bout, 1998; Coppens *et al.*, 2000). Shared metabolite recruitment causes upregulation of the host genes involved in energy metabolism. This scenario describes an example of host-pathogen interaction following infection and it may be possible for the parasite to modulate the neurons and initiate neuronal changes for its own benefit.

Mechanisms underlying parasite-induced neuronal alterations remain unclear, but researchers have made recent progress. It is believed that *T. gondii* may have direct effects on the CNS due to the following observations: cyst tropism and its distribution in the brain, the dysregulation of host-dopamine metabolism and other catecholamines, the secretion of parasite proteins into non-invaded neurons, the functional silencing of the infected neuron and the capability to avoid cellular apoptosis. In addition to direct action, neuroinflammation effects caused by the parasite could indirectly induce neuronal alterations and also possibly mediate behavioural changes in the host. The involvement of a variety of inflammatory factors stimulate neurodegeneration, changes in neuroplasticity and neurotransmitter instability during latent toxoplasmosis. A summary of the possible mechanisms of neuronal alteration by *T. gondii* is shown in Figure 1.3.

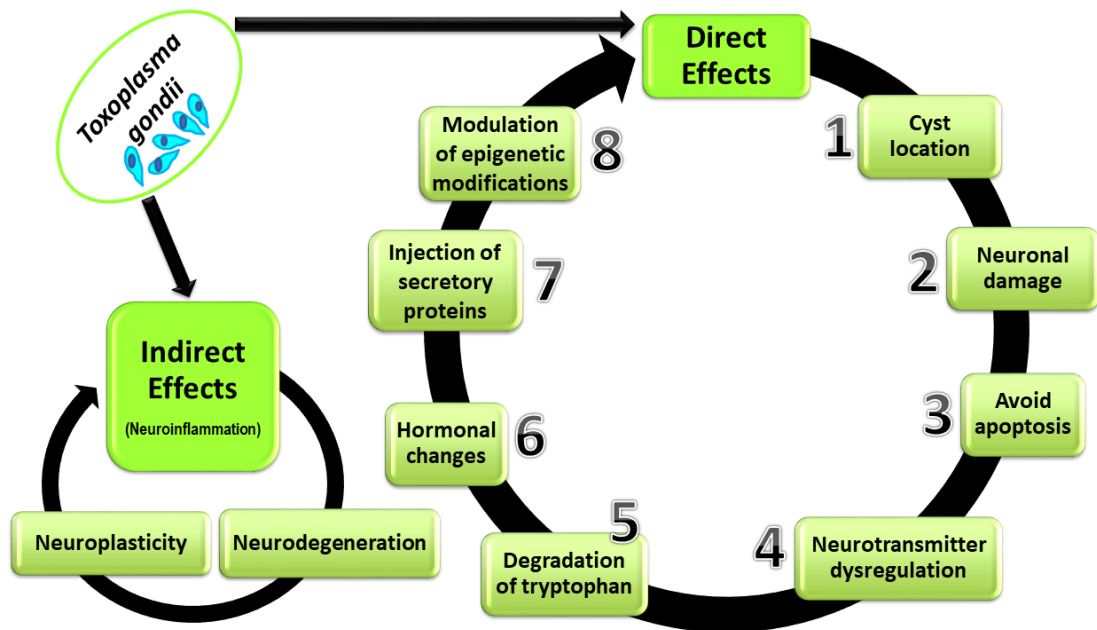


Figure 1.3 Proposed mechanisms of *T. gondii* alteration of neuronal functions.

### 1.3.1 Activation of chronic immune response and brain neuroinflammation causes neurodegeneration and neuroplasticity

Chronic *T. gondii* infection is associated with a neuroinflammatory response which is not limited to the areas surrounding the cysts but widespread through the CNS. The critical mechanism maintaining a benign host infection is to keep the CNS resident glia cells activated (Blanchard *et al.*, 2015). The parasite triggers the T helper cell type 1 (Th1) cell-mediated immune response by activation of this cell and recruited immune cells, resulting in the release of several cytokines and chemokines including interferon gamma (IFN- $\gamma$ ), interleukin-12 (IL-12), interleukin-1 (IL-1), interleukin-6 (IL-6) and tumour necrosis factor (TNF). With sustained neuroinflammation, the inflammatory mediators are potentially toxic to neurons.

For example, even when IFN- $\gamma$  is the main cytokine responsible for hosting immunological defence against *T. gondii* (Sarciron and Gherardi, 2000), the IFN- $\gamma$  activated by microglia can cause neuronal tissue injury through the production of toxic metabolites such as nitric oxide (NO), a strong inducer of CNS pathologies associated with oxidative stress and inflammatory neuronal disturbances. However, during *T. gondii* infection, there is evidence that NO production is inhibited by the parasite through stimulation of the transforming growth factor beta-1 production in favour of neuron viability. This can ensure decreased neuronal damages, presumably for the parasite's own benefits (Rozenfeld *et al.*, 2005). Infected astrocytes have been shown to secrete soluble factors that can inhibit NO release by the IFN- $\gamma$ -activated microglia, thus preventing neuronal degeneration (Rozenfeld *et al.*, 2003). These findings could explain why only limited neurodegeneration was observed in the CNS of chronically-infected mice (Möhle *et al.*, 2014; Parlog *et al.*, 2014). Study of astrocytes in human immunodeficiency virus patients showed astrocytes can produce arachidonic metabolites that can cause neuronal damage and could do so during *T. gondii* infection (Blumberg *et al.*, 1994). However, the Th1 cell-mediated biomarkers of inflammation including IFN- $\gamma$  have been shown to increase in *Toxoplasma* and patients diagnosed with other psychological diseases such as major depression, obsessive-compulsive disorder and schizophrenia (Parlog *et al.*, 2015). Hence, it is conceivable that the local immune response in the brain required to keep latent *T. gondii* may also alter cytokine levels that could then subsequently influence neuromodulator levels. Nevertheless, inflammation-induced neurodegeneration is at most, still considered a marginal contributor to the aetiology of behavioural and neurological changes in chronic toxoplasmosis. The presence of cysts and proliferation of tachyzoites in neurons has shown to stimulate a silent and sustained neuroinflammation that induces microvascular dysfunction with decreased vessel density and stability in infected mice (Estato *et al.*, 2018), thus contributing to a neurodegenerative process; which can explain the manifestation of host behavioural changes.

In order to maintain CNS function, the integrity and functionality of synapses in the brain need to be maintained. Chronic toxoplasmosis infection is able to trigger changes in the expression of presynaptic and postsynaptic proteins of mature synapses and synaptic deficits within the brain structure (Parlog *et al.*, 2015). Protein interruptions will lead to changes in synaptic plasticity and abnormal wiring of brain connections (Parlog *et al.*, 2014). Local neuroinflammation may also affect synaptic physiology and morphology of non-infected neurons, suggesting a potential explanation for widespread mental effects.

### **1.3.2 Neuronal damage and dysfunction**

As the parasite prefers to invade neurons, future investigation should focus on the effects of infection on neuronal cell biology. Infection causes local degenerative cell loss of the infected neurons, including their neighbouring cells, possibly by neurotoxicity of NO and other toxic oxygen products. Local immune activation helps to keep *T. gondii* maintained in the host cell by the production of proinflammatory cells (Webster and McConkey, 2010). However, knowledge on the interactions of *T. gondii* with brain cells and the immune system is still limited, while the exact mechanism on how intracerebral parasites develop is still unclear.

Damage to the structure and morphology of neurons following infection has been shown. At the macroscopic level, the infection causes lesions in the brain and modifies fibre density and grey matter volume. Magnetic resonance imaging data analysis of chronically *T. gondii*-infected mouse brain exhibited the presence of diverse lesions spread throughout all brain areas, with some high-density lesions observed within specific brain regions such as in the somatosensory cortex, hippocampus, and striatum (Parlog *et al.*, 2014). Lesions observed indicated damage to the brain tissue. This data coincides with the previous finding that showed a reduction in grey matter volume in the

brain cortical region in schizophrenia patients with seropositive *Toxoplasma* infection (Horacek *et al.*, 2012). Cysts were reported to establish predominantly in the grey matter region of the brain in the asymptomatic infected mice (Ferguson and Hutchison, 1987a).

Meanwhile, observation from the cellular level has shown that the activation of microglia upon parasite invasion initiates the host immune response and infiltration of lymphocyte T cells into the infected areas to counteract the invading parasite. The local ongoing basal inflammation contributes to the neuron damage and could lead to disturbed neuronal functions. A reduction of dendritic spines, a neuron structure that is responsible for information exchange, in the infected neurons was demonstrated and caused axon damage. Correspondingly, alterations in neuronal fibre density and fibre continuity have been observed that lead to the alteration of neuroconnectivity and synaptic plasticity (Mitra *et al.*, 2013; Parlog *et al.*, 2014). Furthermore, the size of progressive cysts larger than axons and synapses also accelerate neuron damage. Likewise, cell apoptosis, the host's programmed cell death to remove the pathogen by itself, lyses the cells and aggravates more neuron loss.

Observations deeper into the synaptic level found that microtubule structures were altered in the somatosensory cortex infected with ME49 strain parasite, wherein a significant reduction in neuronal neurofilament marker and microtubule-associated protein-2 (MAP2) were observed (Parlog *et al.*, 2014). This leads to perturbation in downstream post-synaptic signalling, interrupting gene expression. The expression levels of specific proteins that regulate key synaptic functions have been found altered in infected cells. A further significant effect is the parasite's ability to modulate neuronal functions. Encysted neurons become functionally impaired as shown by a decline of neuronal activity-dependent uptake of thallium, a potassium analogue (Haroon *et al.*, 2012).

### 1.3.3 Evading host-cell apoptosis

Infections may induce host cell apoptosis, a form of programmed cell death that can trigger the cell to die or commit “cell suicide”, and modulation of host cell apoptosis has been reported with *T. gondii* infection, which was described by inhibition of the invading cell from lysing for its own survival. In other words, blocking cell apoptosis allowed the infected host cell to remain alive (Nash *et al.*, 1998; Payne *et al.*, 2003; Keller *et al.*, 2006).

*Toxoplasma gondii* has evolved multiple mechanisms to resist destruction by apoptosis while intracellular (Halonen, 2015). *T. gondii* infection blocks the activation of caspase pathways that are involved in apoptosis machinery and activate host transcription factor NF- $\kappa$ B that mediates apoptosis blockage (Goebel *et al.*, 2001; Payne *et al.*, 2003). It has also been reported to manipulate host microRNAs (miRNAs) that leads to anti-apoptosis in infected macrophages (Cai *et al.*, 2014). Parasite secretory proteins released from the PV during invasion have been found to be able to modulate host cell apoptosis and prevent rapid clearance by immune cells (Sinai *et al.*, 2004; Blader and Koshy, 2014; Seizova *et al.*, 2019). The parasite efficiently manipulates host transcription, specifically of genes involved in the anti-apoptotic response, into an anti-death state. On the other hand, the parasite is capable of inducing apoptosis in immune cells, suppressing the host immune response and assisting it in establishing the infection.

### 1.3.4 Dysregulation of neurotransmitters following infection

Neurotransmitters are chemical messengers in the brain that function to transmit signals at synaptic junctions. Examples of neurotransmitters are dopamine, glutamate, GABA and serotonin. Abnormal levels of extracellular neurotransmitters, especially alteration in the dopamine metabolism, is a primary hypothesis supporting the link between latent toxoplasmosis and behavioural alterations. Correspondingly, many studies have observed changes in neurotransmission as a result of *T. gondii* infection in the brain, which focused on dopamine, glutamate, GABA and decreased serotonin.

Several studies have found dopamine alterations following *T. gondii* infection. Increased dopamine levels have been reported in both rodents and humans infected with *T. gondii* and within human patients with schizophrenia (Stibbs, 1985; Flegr *et al.*, 2003; Torrey and Yolken, 2003; Skallova *et al.*, 2006; Prandovszky *et al.*, 2011; Martin *et al.*, 2015), which provided a plausible link for the observed close association of *Toxoplasma* with severe forms of schizophrenia (Holub *et al.*, 2013). Correspondingly, high dopamine secretion in infected brain cells has been suggested to accompany host behavioural changes. Dopamine plays a critical role in body movement, motivation, memory and reinforcement of rewarding behaviours. It is also involved in anxiety-related behaviour (Kaushik *et al.*, 2012). Evidence linking dopamine and behavioural changes in infected rodents is supported by studies that found dopamine antagonists (including drugs such haloperidol and GBR 12909) could prevent behavioural alterations in *T. gondii*-infected rats (Jones-Brando *et al.*, 2003; Webster *et al.*, 2006). Therefore, the brain's dopamine signalling system might be involved in mediating behaviour changes in the infected host (Flegr *et al.*, 2003). At present, there is no concrete evidence that *Toxoplasma* directly increases CNS dopamine levels following infection, but evidence supports that dopaminergic pathways are indeed altered. Interestingly, *T. gondii* contains two genes encoding aromatic amino acid tyrosine hydroxylase (TgTH) that can produce the

dopamine precursor (Gaskell *et al.*, 2009) although their role in dopaminergic signalling remains unclear. Recently, a mechanism in dopamine signalling alteration was proposed by which *Toxoplasma* upregulates host small non-coding RNA, microRNA-132 (miR-132), expression during infection that represses the expression of relevant proteins associated with dopamine receptor signalling (Xiao *et al.*, 2014). Additional reviewing of dysregulation of dopamine synthesis will be discussed further in the next following sections.

Meanwhile, glutamate levels were also altered following *Toxoplasma* infection. Glutamate is a major excitatory neurotransmitter in CNS that regulates cognitive processes. During the signalling process, extracellular glutamate is removed from the synaptic cleft by GLT-1, a primary astrocytic glutamate transporter. Following infection, the regulation of glutamate by astrocytes was disrupted when GLT-1 expression was downregulated by the parasite two-fold, leading to increased levels of extracellular glutamate in the synaptic cleft and a surge in the excitatory glutamatergic signalling (Wohlfert *et al.*, 2017). This can cause neuronal damage due to glutamate excitotoxicity (Barker-Haliski and White, 2015; David *et al.*, 2016). The study also revealed that these disruptions were correlated with loss in neuronal dendritic spine density (David *et al.*, 2016). The finding suggests that *T. gondii* tachyzoites directly alter neuronal functions by changing Ca<sup>2+</sup> signalling when glutamate is activated, thereby causing hyper or hypo responsive neurons (Haroon *et al.*, 2012).

Another CNS inhibitory neurotransmitter, GABA, regulates the flow and timing of excitatory neurotransmission in the brain to maintain normal synaptic activity. Alterations in GABA signalling may lead to seizures. Since seizures have been observed in toxoplasmosis patients, this suggests an interference in GABAergic signalling in the brain. Gamma-Aminobutyric acid is also utilised as a carbon source for parasite metabolism (Fuks *et al.*, 2012; MacRae *et al.*, 2012). Changes in GABA levels have not

been reported, but a recent study (Brooks *et al.*, 2015) showed that the *T. gondii* cysts caused glutamic acid decarboxylase 67 (GAD67) redistribution throughout the neurons. Glutamic acid decarboxylase 67 is the key enzyme that catalyses the conversion of glutamate to GABA in the brain (Rowley *et al.*, 2012). Changes in GAD67 distribution may reduce its ability to synthesize GABA (Chattopadhyaya *et al.*, 2007) that could explain the link with seizures. Studies need to assess the effects of GAD67 redistribution on GABA levels in the brain.

Although earlier studies failed to detect serotonin changes in the brain (Stibbs, 1985), it was recently found that serotonin was reduced in acute and chronic brain infections of wild-type BALB/c mice infected with the type II *T. gondii* strain (Mahmoud *et al.*, 2017). A different study also showed decreased serotonin in the amygdala of the same strain of *T. gondii*-infected mice (Ihara *et al.*, 2016). However, another study found that the serotonin increased in acutely-infected C3H/HeJ inbred mice (three weeks post-infection), mostly in males, while there was a slight increase in serotonin system activity in the female mice during chronic infection (six weeks post-infection). A different type II *T. gondii* strain, ME49, was used in the study (Gatkowska *et al.*, 2013). These inconsistent findings might be due to differences in experimental methods including experimental species, line of species, parasite strain or length or method of infection. In addition, the imbalance of serotonin synthesis during infection could be associated with the degradation of tryptophan that is mediated by the immune response. Hence, further investigation into tryptophan and its association with brain serotonin synthesis and imbalance during *T. gondii* infection is necessary.

### 1.3.5 Effects of tryptophan degradation

Tryptophan is an essential amino acid and acts as a precursor for neurochemical mediators such as serotonin and melatonin (Fabiani *et al.*, 2015). Host cells defend themselves against *T. gondii* through interferon IFN- $\gamma$  activation which initiates synthesis of the indoleamine 2,3-dioxygenase (IDO-1 and IDO-2) enzyme that metabolises tryptophan into N-formylkynurenine (Divanovic *et al.*, 2011). Tryptophan is required for *T. gondii* growth so degradation of tryptophan by the immune response inhibits parasitic growth (Sibley *et al.*, 1994; Henriquez *et al.*, 2009). However, tryptophan degradation by IDO leads to the increased concentrations of a few neuroactive metabolites such as 3-hydroxykynurenine, quinolinic acid, and kynurenic acid (KA) in the brain of infected mice (Silva *et al.*, 2002; Notarangelo *et al.*, 2014). Quinolinic acid binds to glutamate N-methyl-D-aspartate receptors (NMDARs) and stimulates excitotoxicity and oxidative stress in the brain, damaging cells and eventually leading to apoptosis. Meanwhile, KA, the potent NMDAR antagonist, can cause glutamatergic and dopaminergic neurotransmission disturbances, thereby altering the brain function (Schwarcz and Pellicciari, 2002; Guillemin *et al.*, 2005).

In human patients, high quinolinic acid and KA levels have been correlated with the presence of neurodegenerative disorders and these compounds are claimed to be partly responsible for memory defects and other cognitive symptoms in schizophrenia patients (Schwarcz and Pellicciari, 2002; Schwarcz and Hunter, 2007). In addition, inhibition of parasitic growth by tryptophan starvation is suggested to cause host depression. There is an increased risk of suicide among seropositive psychiatric patients that could be related to tryptophan decrement (Okusaga *et al.*, 2011).

### **1.3.6 Hormonal changes during infection**

Steroid hormone testosterone synthesis has been found upregulated during *Toxoplasma* infection in male rats. *Toxoplasma* enhances the expression of luteinizing hormone receptor genes in Leydig cells, which is also involved in assisting testosterone synthesis in testicular Leydig cells. As a result, testosterone synthesis is increased upon *Toxoplasma* infection (Lim *et al.*, 2013), and this finding clarifies why testosterone is increased only in infected men, but not women (Flegr *et al.*, 2008). Enhanced testosterone levels may explain the observations of fear reduction and increase in attractiveness of infected male rats. Additionally, neither testosterone nor behavioural changes were observed in castrated male rats (Lim *et al.*, 2013).

### **1.3.7 Parasite-derived mechanisms of neuro-modulation**

#### **1.3.7.1 Parasite secretes effector molecules**

During invasion, specialised parasite organelles such as micronemes, dense granules and rhoptry release a range of effector proteins into the host neuronal cells. These proteins can modify host cell functions and hinder immune responses which are directed towards the parasite to prevent its clearance, thus enabling chronic infection (Coffey *et al.*, 2016). These findings are supported by the detection of many rhoptries proteins in the cytosol and nucleus of the host cell, including on the surface of the parasite PV. The involvement of a profilin-like protein of *Toxoplasma*, toxofilin, has been suggested in the tachyzoite invasion via depolymerisation of the host actin which facilitates parasite entry (Delorme-Walker *et al.*, 2012). Rhopkinase proteins such as ROP5, ROP17 and ROP18 are described as capable of forming complexes on the PV membrane, thus preventing

the host immunity-related guanosine triphosphatases (IRGs) binding to the parasite' vacuole (Fentress and Sibley, 2011). Other ROP proteins such as ROP16 can activate the transcription factors, STAT3 and STAT6, by direct phosphorylation. These modulations result in the downregulation of IL-12 and upregulation of the IL-4 and Th2 responses (Butcher *et al.*, 2011).

After invading, the parasites will reside in the cytoplasm of the host cells, enclosed in a PV, and then induce another stage of effector proteins that are exported via dense granules into the host cells. The dense granule proteins (GRA) modulate the immune signalling and upregulate host-survival pathways. One of the proteins, identified as MYR1 novel protein, has been found to play a role in translocating *Toxoplasma* effectors into the host cytosol (Franco *et al.*, 2016). The GRA24 and GRA16 are translocated into the host nucleus, whilst GRA15 and GRA6 are localised to the PV membrane (Bougdoor *et al.*, 2013). An immunohistochemical study showed that the host cell cytoplasm and some axons stained positive for *Toxoplasma* antigen, thus signifying that parasitic proteins might directly disturb the neuronal functions (Haroon *et al.*, 2012). Dense granule protein 15 activates TRAF6 and I $\kappa$ B kinase, leading to the translocation of NF- $\kappa$ B, resulting in the release of inflammatory cytokines, including IL-12 (Morgado *et al.*, 2014). Most of these GRA proteins are believed to play key roles in vacuolar remodelling, nutrient uptake and immune evasion while the parasite is replicating within the host cell. However, to date there is no evidence showing that encysted bradyzoites can export proteins, but, it is reasonable to consider that the bradyzoite stage employs specific mechanisms or/and similar strategies as tachyzoites to maintain its persistence while avoiding clearance by the host immune system.

Given that tissue cysts are only found in a limited number of neurons at a distinct loci in the brain, thus how the diffuse effects are spread become an interesting investigation. The parasite-secreted factors would provide a mechanism for exerting global effects. A

significant finding is the discovery that the parasite also injects proteins into brain cells that are not invaded, providing a mechanism of manipulating host cells outwardly without cyst persistence (Koshy *et al.*, 2012). This strategy can prevent the parasite's removal by the host immune system and maintain prolonged persistence in the brain. What is more important, these findings also raise the possibility that the parasites can provoke alterations in more neurons, both infected and uninfected, that may lead to neuronal and behavioural changes. However, it is still unclear the extent of how far these proteins could spread in these regions, how long they can persist within the injected neurons and how they can alter cell mechanism. Summarised by Hakimi *et al.* (2017), several secretory parasite effector proteins can interfere with host gene expression by activating host transcription factors, through the modification of chromatin or by inducing small non-coding RNAs, which suggests the involvement of epigenetic and host gene manipulations. The effects in neuronal cells have not been thoroughly investigated.

### **1.3.7.2 Hijacked host gene regulation**

Little is known about events occurring during the chronic stages, which needs further study of the influences of parasitic infection on host genome expression. The discovery of *Toxoplasma*-secreted effector proteins which can alter host genomes has given new insight into potential regulation of host genes in a gene-specific manner, causing explicit effects (Bougdour *et al.*, 2014; Hakimi and Bougdour, 2015; Hakimi *et al.*, 2017). Transcriptomic analysis using RNA-Seq data evaluated the host gene expression in infected mouse brain and showed that 935 genes were upregulated, whereas 12 genes primarily involved in host immune responses and cell activation were downregulated, in this mixture of brain cell types (Tanaka *et al.*, 2013). Meanwhile, downregulation of the dopamine  $\beta$ -hydroxylase (DBH) gene has been observed in RNA-seq data of *T. gondii*-infected noradrenergic neurons, both in *in vivo* (rat and mouse brain) and *in vitro* (human

and rat cell lines). The massive changes in mRNA gene expression of the infected cells showed that the parasite can alter genes at the transcriptional level (Alsaady *et al.*, 2019). Dopamine  $\beta$ -hydroxylase is a key enzyme in the biosynthesis of norepinephrine that is converted from dopamine. Further discussion related to the DBH gene will be elaborated in the next few sections.

#### **1.4 Involvement of epigenetic modifications in transcriptional gene silencing (TGS)**

Epigenetic refers to the combination of mechanisms that confer long-term and heritable changes in gene expression without changing the DNA sequence itself. Even when all the cells in a human body share the same genetic information, not all genes in a cell are expressed at the same time. At a given time, only restricted functional subsets of genes are allowed to be expressed, while other non-functional genes are depressed. It is still unknown how the same genetic information in every cell can lead to so many different cell types with each of them having their own specialised functions. One level of regulation of expression of these genes is by epigenetic marks applied to the DNA. Epigenetics is mediated by three main processes; DNA methylation, histone modifications, and non-coding RNA (ncRNA)-associated gene silencing. In the human body, epigenetic regulation is one of the central mechanisms involved in embryonic development and tissue differentiation. Epigenetic alterations in neuronal cells are stimulated by external stimuli such as microorganism infections which can influence gene expressions and therefore, may initiate neuronal function changes in the brain. Epigenetic control provides the pathogen with substantial opportunity to manipulate host gene expression to its own advantages.

The emerging development of epigenetic studies has revealed the parasite's capability to interrupt the host epigenome and silence a gene, thereby manipulating the brain and inducing host behaviour changes. Alteration in one epigenetic marker in response to infection, the vasopressin receptor, and its involvement in fear has been studied in *T. gondii*-infected hosts (Hari Dass and Vyas, 2014). Clarifying the specificity of these modifications with respect to specific gene targets is necessary to understand how the resulting changes in gene expression can control host behavioural changes.

There is growing evidence that epigenetic aberrations contribute a role in the aetiology and development of many brain and neurological disorders, including schizophrenia. For example, most schizophrenia patients have impairments in GABAergic neuron transmission. Consistent evidence shows that the dysfunction of GABAergic neurons involves DNA methylation and histone modification alterations. Protein markers expressed in GABAergic neurons of the mammalian brain cortex, GAD67 and reelin genes, were found downregulated. Repression of these genes is associated with hypermethylation of their promoter genes and decreased acetylated histone levels (Grayson *et al.*, 2005; Gavin and Sharma, 2010). The findings provide compelling evidence that aberrant methylation and histone modifications may be part of the core dysfunction causing a primary defect in brain GABAergic transmission, which might be related to *T. gondii* intracellular parasite infection causing neuro-epigenetic alterations.

#### **1.4.1 DNA methylation**

The most commonly studied epigenetic modification is DNA methylation, an addition of a methyl group (-CH<sub>3</sub>) at 5 cytosine site within genomic sequences, called 5-methylcytosine (5-mC). Cytosine methylation predominantly occurs at, but is not restricted to, the CpG site in genomic DNA in mammals, which is commonly located in

the promoter regions of genes and less frequently in introns. The 'p' in CpG represents the phosphodiester bond linking the cytosine and guanine-containing nucleotides. In mammalian genomes, 60–90% of CpG sites are globally methylated and most of the unmethylated DNA is located in CpG islands within the gene promoters (Razin and Cedar, 1991; Tucker, 2001; Weber and Schübeler, 2007). DNA methylation is essential for normal development, genomic imprinting, X-chromosome inactivation and maintenance of genomic integrity (Bird, 1980). It also plays important roles in neuronal functions and morphology (Feng *et al.*, 2010). DNA methyltransferases (DNMTs) are enzymes catalysing the transfer of methyl groups to DNA and DNA methylation is conserved and maintained by the activity of DNMT1, known as maintenance methylase, which is the most abundant DNMT in the cell. DNA methyltransferase 1 methylates hemimethylated CpG dinucleotide DNA during DNA replication and cell division to maintain the DNA methylation patterns of the parental strands. Meanwhile, *de novo* DNA methylation is mediated by the activity of DNMT3a and DNMT3b, responsible for establishing the patterns of new DNA methylation, especially during embryonic development (Newell-Price *et al.*, 2000; Weber and Schübeler, 2007).

Generally, gene expression is highly reliant on the location of DNA methylation (e.g. promoter, gene body). For example, DNA methylation in the promoter is observed to be negatively correlated with gene expression, while in the gene body, it is more commonly positively correlated (Yeivin and Razin, 1993). This raises the question of how gene silencing is achieved. Methylation is mostly associated with a repressed chromatin state and inhibition of promoter activity by two avenues. First, by direct interference of the binding of specific transcription factors or second, by affecting the chromatin structure resulting from the recruitment of methyl-CpG binding domain (MBD) proteins that mediate repression (refer Figure 1.4). For example, in the brain, MeCP2, a type of MBD protein, has been known to recognise the methylated CpG and then initiate the recruitment of chromatin remodelling complexes (multiprotein repression complexes)

including histone deacetylases (HDAC) and histone methyltransferases, which in turn induce major deacetylation of histone proteins and repress the chromatin structure which will ultimately lead to gene silencing (Jones *et al.*, 1998; Razin, 1998). Mutations of the MeCP2 gene causes a mental disorder in females known as Rett syndrome, a type of a neuro-developmental disorder (Tucker, 2001). Maintained and conserved over long chromosomal regions to keep the gene expression consistent, DNA methylation is postulated as a highly stable silencing mark that may be inherited from generation to generation.

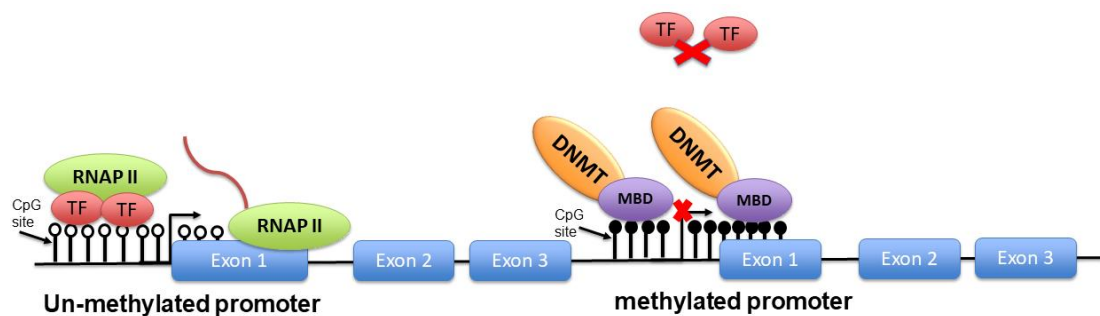


**Figure 1.4 Scenarios of DNA methylation patterns in gene regulation.** Left: Normal unmethylated condition at CpG islands of a promoter gene where the gene is expressed. The CpG is unmethylated and allows TF binding which is required for transcription initiation. Right: Hypermethylated condition at CpG islands where the gene is repressed. In general, DNMTs enzymes initiate MBD binding and methylate DNA at the promoter gene, and thus interfere with TF binding sites resulting in gene silencing. Abbreviations: RNA Pol II (RNA polymerase II enzyme; TF (transcription factors); DNMT (DNA methyltransferase); MBD (methyl-binding domain proteins).

### 1.4.2 Chromatin modification changes

The second type of epigenetic regulation of gene expression involves chemical modifications of DNA-bound histones, called chromatin. Chromatin is comprised of 147 bp DNA wrapped around a core complex of an octamer of four different histone proteins (H2A, H2B, H3 and H4) that altogether form a nucleosome (Kouzarides, 2007) (Figure 1.5). Histones represent 50% of the total weight of chromatin that functions to regulate access to information contained in the DNA. It consists of two main structural domains

known as the flexible domains (N and C terminal tails) and the globular domains (that includes the conserved histone fold). The flexible domains are exposed outside the nucleosome and are the targets of numerous post-translational modifications (PTMs). A combination of PTMs generate a complex network that can change chromatin structure by modifying the interactions between histone, DNA, and associated complexes, thereby promoting or preventing the binding of specific proteins to the DNA and directly activating or repressing the expression of a gene.

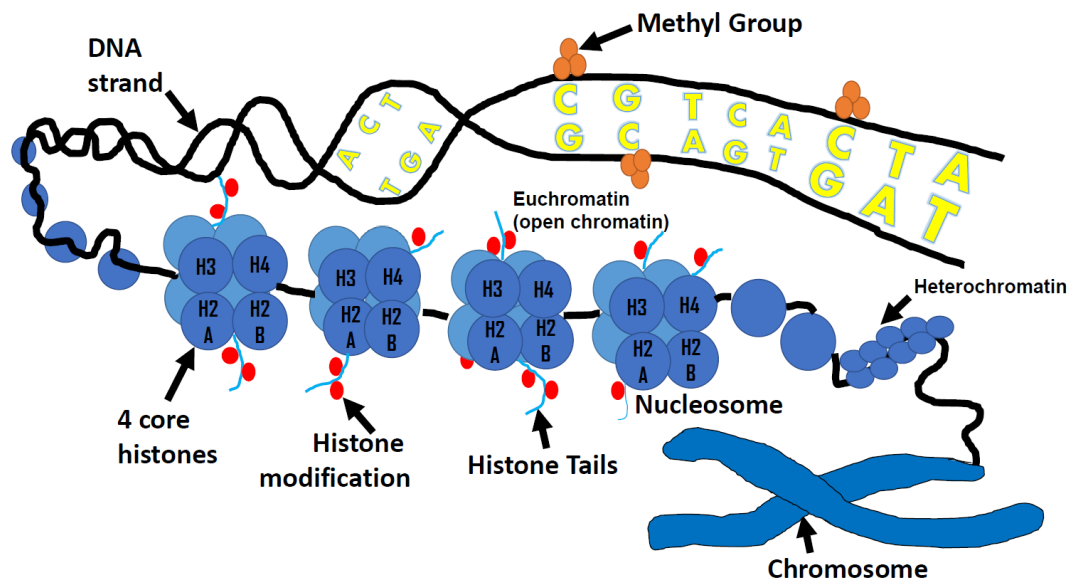


**Figure 1.5 Folding of DNA into chromatin.** DNA is assembled with histone to form the nucleosome, in which 147 base pairs of DNA are wrapped around an octameric complex composed of four core histones (H3, H4, H2A, H2B). The core histones are predominantly globular, except for terminal tails. The histone terminal tail contains diverse PTMs that determine the overall chromatin structure: in an open state called euchromatin or packed heterochromatin state by which access to genomic DNA is regulated.

Histone modifications can be both activated and deactivated depending on the type of modifications and the specific residues modified. The transcriptionally-silent, condensed form is called heterochromatin, whereas the euchromatin form is less condensed and contains the most actively transcribed genes (Li *et al.*, 2007). Modifications of chromatin

include acetylation, methylation, phosphorylation, ubiquitination and sumoylation processes which control the accessibility of the chromatin to transcriptional machinery in a sequence- and activity-dependent manner. There are various modifications of core histones at the lysine, arginine and serine residues that reside in the amino-terminal tails of histones. They are added or removed by chromatin-modifying enzymes, which in turn are subject to transcriptional and post-translational regulations.

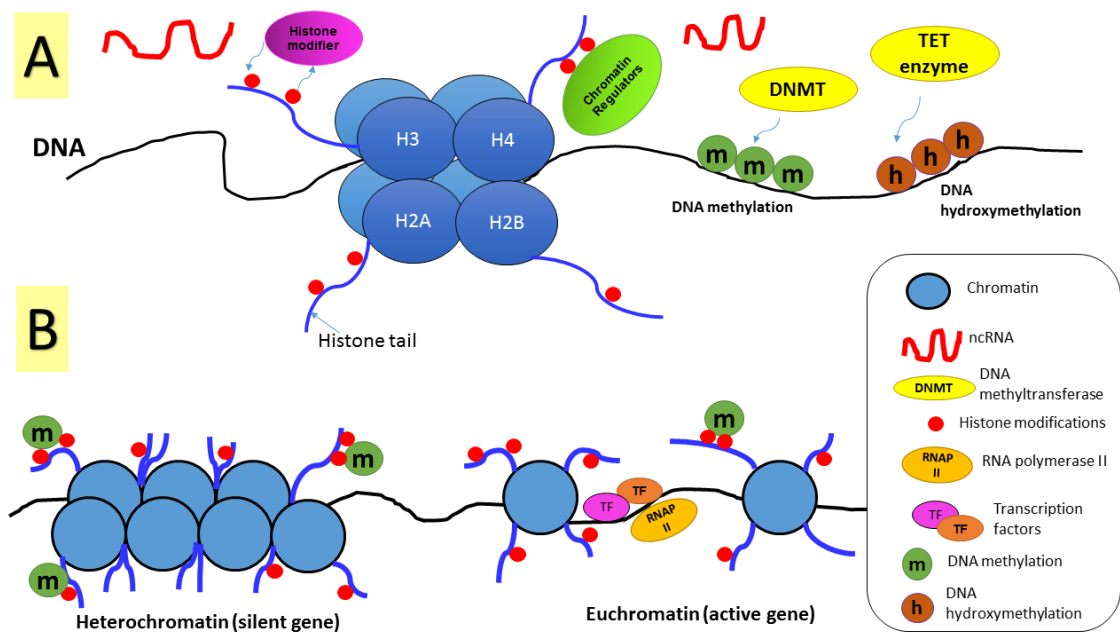


**Figure 1.6 Mechanisms of epigenomic gene regulation.** A. Three main epigenetic mechanisms of gene regulation consist of chromatin packaging of DNA via transcriptional modification of histone tails (acetylation, methylation, phosphorylation, etc), DNA methylation/demethylation is established and maintained by DNMTs and TET enzymes, and non-coding RNAs, in addition to subsequent histone protein regulator/modifier recruitment to specific regions of DNA. B. Two main chromatin structure states are heterochromatin (silent gene) with tightly bound chromatin conformations and euchromatin (active gene) with less condensed, open chromatin.

Histone acetylation is usually linked with transcriptional activation in which acetylation affects the interaction of histones with DNA, keeping the chromatin packaging in a more relaxed state. For example, acetylation of histone 3 or 4 proteins at lysine amino acids on the N-terminal tails, catalysed by histone acetyltransferase, can increase gene promoter accessibility. The acetyl-binding neutralises the protein-DNA binding charged

molecule and thereby loosens the interactions, thus making the DNA more accessible to transcription. Conversely, the removal of acetyl groups by HDAC condenses chromatin around gene promoters which generally results in the decreased gene expression. This charge-neutralisation model has been proposed to explain the role of histone modifications in transcription (Shogren-Knaak *et al.*, 2006).

In contrast, histone methylation can induce either a transcriptionally facilitative or repressive state depending on histone number and position of the lysine residues that are methylated. For example, histone H3 methylation at lysine 9 (H3K9) and lysine 27 (H3K27), and histone H4 methylation at lysine 20 (H4K20) are generally associated with heterochromatin and gene silencing, yet histone H3 at lysine 4 (H3K4), lysine 39 (H3K39), and lysine 79 (H3K79) are often associated with active transcription (Jones, 2012). Each lysine residue may be methylated in the form of mono-, di-, or tri-methylation which adds to a vast chromatin complexity. The functional consequences of histone PTMs can be direct, leading to chromatin structural changes, or indirect, acting through the recruitment of effector proteins. The 'histone code' hypothesis states that the diverse covalent modifications within open histone tails are read by effector molecules, which in turn mediate outcomes. The PTMs can influence each other and the combination of them can form a complex and dynamic code (Strahl and Allis, 2000; Turner, 2007).

The repressive processes of histone deacetylation, H3K9 or H3K27 methylation and DNA methylation does not necessarily interact independently, but have been reported to act in concert with each other in repressing gene expression. Direct recruitments of HDAC and HMT by DNMT and DNMT by HMT have been reported. For indirect MBD binding, such as MeCP2, it can lead to the increased histone methylation and histone deacetylation. The connection between histone methylation and DNA methylation is demonstrated most convincingly in earlier research studies of *Neurospora* and an

*Arabidopsis* plant wherein mutations in histone methyltransferase genes at H3K9 resulted in a complete loss of DNA methylation (Tamaru and Selker, 2001).

Research interest in the modulation of epigenetic modifications by *T. gondii* has increased in an effort to increase understanding of host-parasite interactions. One finding demonstrated that lysine acetylation patterns were altered upon *T. gondii* infection in a proteome-wide analysis of lysine-acetylated proteins in rat cortical astrocytes and those alterations could affect the host protein localisation, function, stability and interactions (Bouchut *et al.*, 2015). Another study showed that the *T. gondii* proliferation in infected cells can be stopped by knocking-down the UHRF1 gene (Unoki *et al.*, 2009) which is believed to be used by the parasite to enhance its proliferation (Brunet *et al.*, 2008). The study demonstrated UHRF1 was significantly over-expressed in *T. gondii*-infected cells. The UHRF1 gene plays a central role in maintaining methylation status in host cells by recruiting MBD and DNMT1 to the site, and has also been linked with a variety of histone modifications and heterochromatin formation. This finding suggests the capability of *T. gondii* to exploit UHRF1 and other epigenetic regulators to control host cell epigenetic machinery (Unoki *et al.*, 2009). In addition, enzymes important for regulation of major histone PTMs, such as HATs, HDACs and HMTs are abundant in the brain. As *T. gondii* has established a privileged interaction within the CNS, specifically in the brain, it would not be surprising if the parasite can dysregulate histone PTM functions, thus interfering with the host epigenome to mediate changes to the parasite's advantage.

### 1.4.3 Epigenetic regulation by antisense long non-coding RNAs

Studies related to RNA-based gene regulation in human cells have created another avenue in study of mechanisms of RNA-directed gene regulation and silencing the epigenome. Over the last decade, a lot of interest has been generated around non-coding RNAs. A large percentage of the human genome (70–90%) is composed of non-coding DNA, regions that do not code for proteins. Interestingly, in the more than 80% of the human genome that is transcribed, only 2% represents protein-encoding genes of which a vast majority of other transcribed genes are encoded by non-coding RNAs (Consortium, 2001). The function of abundant ncRNAs transcription in humans has not been elucidated and with limited knowledge of their functions known. There is still no clear molecular distinction to categorise the ncRNAs, but they have been roughly classified as microRNAs (miRNAs), short interfering RNAs (siRNAs), small antisense RNAs (sasRNAs), PIWI-interacting RNAs (piRNAs), small nucleolar RNAs (snoRNAs), large intergenic non-coding RNAs (lincRNAs) and long non-coding RNAs (lncRNAs) (Esteller, 2011). Arbitrarily, ncRNAs are simply being classified into two groups based on the transcript sizes; short RNAs with less than 200 nucleotides and long ncRNAs with more than 200 nucleotides.

More recently, endogenous ncRNAs have been shown to act as epigenetic regulators that can regulate the epigenome by controlling gene transcription and manipulating the epigenetic state, thus mediating gene silencing in humans. The initial finding of RNA-directed gene silencing in human cells was observed when siRNAs were found to inhibit the transcription of a transgenic elongation factor 1 alpha (EF1A) promoter gene expressed in a green fluorescent protein (GFP) reporter gene (Morris *et al.*, 2004). The EF1A is a protein that promotes aminoacyl tRNA binding to the ribosome site during protein biosynthesis. The silencing was associated with DNA methylation and chromatin modifications of the targeted gene. Gene silencing was eliminated when induced with 5'

Aza-cytadine and Trichostation A compounds, inhibitors of DNA methylation and histone deacetylation, respectively.

Although the current literature is dominated by study of short RNAs, there is an increasing number of reports describing long transcripts that function as RNAs, even without encoding proteins. Longer than 200 nucleotides, the lncRNA is an RNA transcript without translated open-reading frames, thus exhibiting low protein-coding expression. They are described as biochemically similar to mRNA as they are frequently transcribed by RNA polymerase II, share the same chromatin state, contain conserved RNA intron splice sites (5'-GU/AG-3'), have similar intron/exon lengths to mRNAs, are partially polyadenylated and have methylguanosine capped at 5' termini. The lncRNAs show far lower expression levels than protein-coding genes and they are mostly expressed in a cell and tissue type-specific fashion, with large fractions expressed in the brain. Moreover, whereas mRNAs localise specifically in the ribosomes of cytoplasm, lncRNA localisation is much more diverse and can be found located within nuclear or cytosolic fractions. Interestingly, they are reported to be particularly enriched in the chromatin fraction in the nucleus, consistent with its proposed role as an epigenetic regulator in gene expression (Mondal *et al.*, 2010; Derrien *et al.*, 2012; Roberts *et al.*, 2014b; Quinn and Chang, 2015).

Long non-coding RNAs are characterised with respect to their complimentary protein-coding genes which can be oriented in a sense or antisense strand direction (exonic). Others can be localised in the intron (intronic) or within two genes (intergenic). Refer to Figure 1.7.

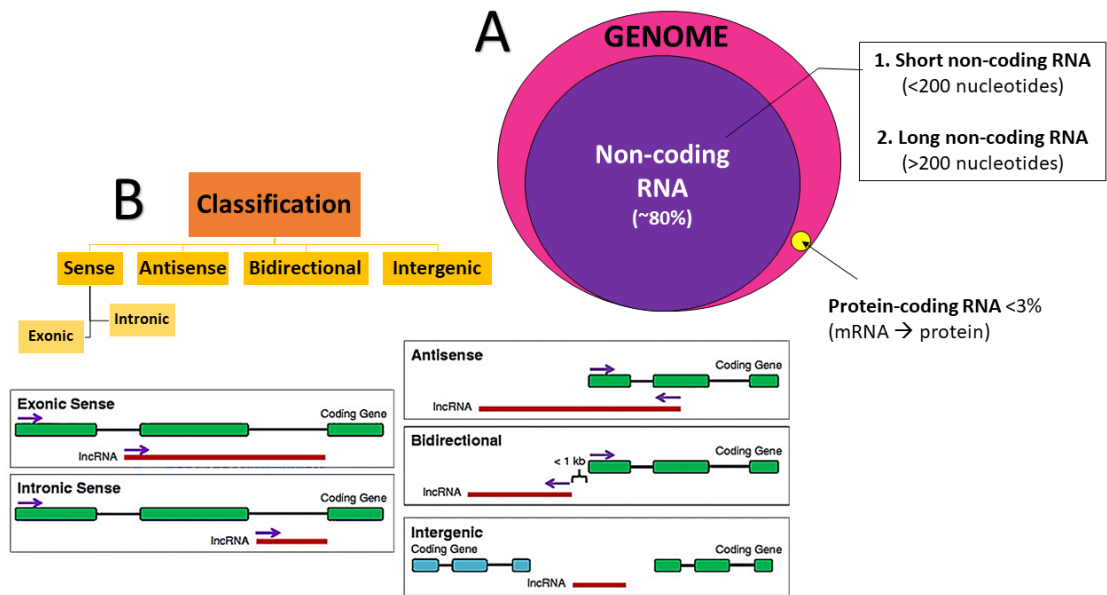


**Figure 1.7 Long non-coding RNAs.** A. Non-coding RNAs (ncRNAs) are diverse, numerous and consist of a much larger percentage of the human genome than protein-coding genes. In general, ncRNAs are divided into short and long ncRNAs based on the RNA transcript nucleotide size. B. The genomic organisation of non-coding transcripts, where the location and position of lncRNAs are dependent upon the protein-coding genes.

Further observations have proposed that the antisense lncRNAs could play a role as epigenetic regulators of transcription in human cells (Weinberg and Morris, 2016). Many lncRNAs with a known function, such as *Xist* (lncRNA that mediated X chromosome inactivation (Penny *et al.*, 1996)), only exhibit high conservation over short sequences from their full length, thus explaining why small antisense RNAs were observed in early findings to silence transcription via directed epigenetic changes at the target loci (Wutz, 2003; Pang *et al.*, 2006).

There are several proposed mechanisms in the regulation of gene expression involved by lncRNAs. The lncRNA is capable of regulating gene expression at the level of chromatin modification, transcription, and post-transcriptional processing (Mercer *et al.*, 2009). First, lncRNA can mediate epigenetic changes by recruiting chromatin remodelling complexes to specific loci. For instance, human HOX transcript antisense

RNA (HOTAIR), located within the homeobox C (HOXC) gene locus, induces a repressive chromatin state in adjacent protein-coding genes. The inducement is by recruitment of polycomb repressive complex 2 (PRC2) to the HOXD gene locus to silence the gene (Rinn *et al.*, 2007). HOTAIR is a key example demonstrating that RNA can play a direct role in silencing large genomic regions. Aberrant expression of lncRNA HOTAIR has been reported in cancers including breast cancer (Gupta *et al.*, 2010). LncRNA *Xist* acts similarly by implementing this mechanism to mediate transcriptional repression (Wutz, 2003). In a study by Khalil *et al.* (2009), 20% of the lncRNA expressed in a variety of human cell types can bind to PRC2, while some other lncRNAs are bound with other chromatin-modifying complexes, suggesting the major involvement of lncRNAs in gene regulation.

Second, lncRNAs can regulate the transcriptional process by forming a RNA-DNA triplex structure at major promoters, such as seen in human dihydrofolate reductase promoter that creates a blocking site for transcription factor TFIID binding, thereby silencing dihydrofolate reductase gene expression in a homology-dependent manner (Martianov *et al.*, 2007). The complementary triplex formed has also been reported to direct DNA methylation in the promoter of targeted genes (Martianov *et al.*, 2007). LncRNAs can also directly interfere with transcription by Polymerase II when the antisense lncRNA overlaps with protein-coding genes and initiates antisense transcription which can then interfere with sense transcription of the gene (Pelechano and Steinmetz, 2013). Antisense transcription arises from promoters and their expressions commonly have similar regulations as those for other genes. Finally, the ability to bind with complementary sequences allows antisense lncRNAs to regulate various steps in the post-transcriptional processing of mRNAs, such as splicing, editing, transport, translation and RNA degradation.

The capability of ncRNAs to regulate associated protein-coding genes might contribute to gene dysregulation under aberrant conditions. A number of studies have shown that some protozoan parasites such as *Plasmodium*, *Toxoplasma*, and *Leishmania* can manipulate ncRNAs in host-pathogen interactions. These intracellular pathogens are able to transfer their small ncRNA molecules to the host cells, usually via extracellular vesicles, to modulate their functions. They are also capable of modulating the host ncRNAs expression for their own survival (Bayer-Santos *et al.*, 2017). Such a manipulation example was observed in *T. gondii* infection wherein the host cell's miRNA profile was altered in infected human fibroblast cells (Zeiner *et al.*, 2010). One recent study (Menard *et al.*, 2018) revealed that *T. gondii* can directly manipulate the host lncRNA expression, in which secretory kinase ROP16 has been found to play a role in upregulating the expression of some lncRNAs upon infection. Microarray data analysis showed hundreds of lncRNAs were differentially regulated during infection with approximately 900 lncRNAs upregulated and an equal number of lncRNAs downregulated (Menard *et al.*, 2018). This finding is similar to that in another study which found lncRNAs that were mainly involved in the host-immune responses were significantly and differentially expressed in *T. gondii*-infected HFF cells. The study proposed that lncRNAs induced during infection were used by the parasite as a modulating mechanism to regulate host immune signalling (Liu *et al.*, 2018).

## 1.5 Conclusion

*T. gondii* induces many neurophysiological changes in the CNS, allowing it to quickly adapt to the host environment and facilitating its proliferation and survival. Once it invades the CNS, the parasite activates the host immune system and causes neuroinflammation. Many effector proteins are released to help the parasite avoid immune clearance, keeping it safely dormant in infected cells. Chronic infection is established with many cysts localised throughout the brain, specifically residing in the neurons. Persistent cyst localisations cause neuronal damage and dysfunction. To survive, the parasite employs other mechanisms, such as preventing host cell apoptosis and disturbing catecholamine biosynthesis and signalling to support parasite proliferation and growth. The activated host immune system attempts to counteract parasite activities in a number of ways, such as by degrading tryptophan which unfortunately causes further catecholamine disturbances. The capability to reside in the brain provides the parasite with direct access to the host brain epigenetic machinery and the parasites often hijack host gene regulation. Manipulating the brain's cognition and behaviour confers advantages to the parasite as they can accelerate life cycle completion in the definitive host by inducing host behavioural changes, even though humans only exhibit accidental effects that clearly do not support the parasite's life goal. However, the parasite-induced behavioural changes in humans have been associated with many brain and neuropsychological disorders.

Nonetheless, with growing evidence from studies of many aspects of host-parasite interactions, and interrelation demonstrated between some of these studies, no research has yet confirmed the exact mechanisms by which *Toxoplasma* alters the brain and mediates behavioural changes. The question of whether the parasite is capable of inducing behavioural alterations in infected humans by itself, or only as a result of the

host immune response, is still unresolved. Therefore, understanding the molecular phenomena involved in *T. gondii* pathogenesis, exploring causal effects of host-parasite relationships and knowing how the parasite alters neuronal functions might help explain the behavioural changes.

## 1.6 Research objectives

The general objective of this thesis was to investigate the molecular mechanisms by which the *T. gondii* parasite manipulates the neurological host-parasite interactions during chronic brain infection and which interactions may lead to the behavioural changes in the hosts. In an attempt to gain an overall understanding of the neurobiology of *Toxoplasma* chronic infection, this study aimed to achieve the following specific objectives:

### **1.6.1 To evaluate DNA methylation patterns at the target DBH promoter gene induced by parasite infection coincident with downregulation of DBH gene expression.**

DNA methylation has a well-known association with chromatin modifications to repress a gene so was evaluated. This involved the development of MEDIP-qPCR assay and primer optimisation. Then, the percentage of methylation pattern changes at 5' transcriptional start site DBH gene in a time-course manner following *T. gondii* infection in rat neural pheochromocytoma (PC12) cells was evaluated. The results achieved were compared with another developed methylation assay, the bisulphite-cloning sequencing method, by broadening the region of interest to include upstream of the DBH promoter region.

**1.6.2 To evaluate chromatin modification (H3K9me2) changes and measure DNA methyltransferase (DNMT3a) levels following infection in altering the DBH gene expression using a developed ChIP assay.**

A chromatin immunoprecipitation (ChIP) assay was optimised to quantitate chromatin modification protein-related suppression, H3K9me2 binding at DBH promoter gene, following chronic infection as it is involved with DNA methylation. Using the same method and cell conditions, the amount of bound enzyme that is responsible to dynamically methylate DNA, DNMT3a, was also measured to further investigate DNA methylation involvement. All evaluations were done in a time-course manner for five days following *T. gondii* infection to analyse the DNA chromatin of rat PC12 cells. Correlations between the histone-modification proteins and the changes in DNA methylation patterns in *T. gondii* infection were observed.

**1.6.3 To repeat the DBH gene expression assay in *T. gondii*-infected rat PC12 cells.**

This chapter (Chapter 3) repeated the gene expression assay to observe downregulation of DBH targeted gene in rat PC12 cells following *T. gondii* infection. *Toxoplasma gondii* is capable of manipulating host gene expression, and my group research has found that the DBH gene was downregulated following *T. gondii* infection. Repetition of this experiment was done as a control study to confirm that the DBH gene was depressed in the studied host cells after analysing the epigenetic manipulation assays, that was important for results validation and confirmation. The capability of PC12 cell to produce dopamine also was observed by analysing the sample in HPLC-ECD.

#### **1.6.4 To screen the involvement of antisense lncRNAs in downregulation of DBH transcription.**

It has become clear that knowledge of the presence and function of specific RNAs is important in understanding gene repression. Thus, this study aimed to screen for the presence of antisense lncRNAs binding at DBH gene sequences, which may interfere with gene transcription in the *T. gondii*-infected PC12 cells. The RT-PCR assay was implemented to achieve this aim with specific designated primers.

## Chapter 2

### Probing for DNA Methylation Changes Coincident with Downregulation of Dopamine $\beta$ -hydroxylase Gene Expression

#### 2.1 Overview

Previous work in this laboratory has found that DBH gene expression is downregulated following *T. gondii* infection (Alsaady *et al.*, 2019). Epigenetic alterations associated with decreased DBH gene expression was further investigated under the assumption that the increase of methylation localised to the 5' transcriptional start site (5'TSS) and the upstream promoter may be associated with DBH gene expression during *T. gondii* infection. To determine this, two methods were applied: an immunoprecipitation (IP) assay known as methylated DNA immunoprecipitation (MeDIP) combined with real-time qPCR and bisulphite PCR-clone sequencing (bis-sequencing). Both assays quantified methylated DNAs of CpG sites and its pattern changes were observed in a time-course manner. The assays were developed and optimised before the *T. gondii*-infected and uninfected rat neural cell line samples were used. The MeDIP method detected overall pattern changes in methylation, whereas the bisulphite method, which analysed methylation per CpG site, did not show any methylation changes in both compared samples.

DNA methylation is a covalent modification of the cytosine ring at the 5 position of a CpG dinucleotide. Its presence at CpG sites within the promoters, the surrounding TSS, and the first exon of genes has commonly been reported to lead to epigenetic gene inactivation (Brenet *et al.*, 2011). Genes with tissue-specific expression patterns such as the DBH gene often have CpGs close to their promoter (Tate and Bird, 1993). Thus, in this study, a set of primer pairs was designed to flank the 5'TSS region in the DBH gene sequences to measure the DNA methylation levels of its covered CpG sites by implementing the MeDIP assay. The DNA methylation pattern changes were compared with uninfected neural cell controls. The MeDIP assay relies upon protein-antibody binding in an IP reaction and is an efficient technique to extract the methylated DNAs from gDNA samples. The methylated DNAs were then amplified by a direct qPCR reaction to quantify the enrichment of bound methylated protein at a locus-specific level, making it a highly specific method for measuring DNA methylation.

The second approach to measure DNA methylation states of the studied region is the bis-sequencing analysis. Identifying which fraction in the promoter region or near 5'TSS consists of functional CpG sites that can control gene expression in the context of gene regulation is difficult due to the relatively small fraction of genomic CpGs assayed. Also, despite recent advances, we still have a limited understanding of when, where, how many and which CpGs participate in genomic regulation as CpG methylation is well-known to suppress transcription. Identifying a specific CpG site specifically within the promoter and surrounding the 5'TSS regions which controls methylation and gene regulation may be critical for modulating transcriptional repression of genes such as the DBH gene. To investigate further, this study analysed an extra subset of CpG sites within the same endogenous proximal DBH gene region as in the MeDIP assay and 2k bp further upstream of the gene promoter region. Earlier findings from methylation-sensitive restriction enzyme sequencing (MSRE-Seq) data in assessing global DNA methylation of *T. gondii*-infected brain samples demonstrated that 2k bp further upstream of the DBH

promoter region contains more CpG sites (Tedford, 2018). Afar *et al.* (1996) found that a sequence 1k bp upstream of the DBH promoter could direct gene expression in DBH-expressing cells, including rat PC12 cells. However, most evidence suggests gene expression variations are located predominantly near surrounding 5'TSS genes. As another study found that the methylation of the first exon is critical for transcriptional silencing (Brenet *et al.*, 2011), I designed new primers that cover more CpG sites in the first exon and nearby 5'TSS DBH gene sequences. Our hypothesis was that it is possible that changes in 5-methylcytosine (5-mC) at a single specific locus can be sufficient to modify gene expression. The bisulphite sequencing method, which investigates differential DNA methylation at single-base resolution, was implemented as the MeDIP assay could not give detailed methylation information regarding which CpG sites were methylated or associated with DNA methylation at single nucleotide resolution. The first step in this method, sodium bisulphite treatment, creates sequence differences by converting unmethylated cytosines to uracils, but leaving methylated cytosine unchanged (Frommer *et al.*, 1992). The differences were detected by sequencing the PCR products or its sub-clones. In the final sequence output, all original cytosines appeared as thymines, while methylated cytosines would remain cytosines.

## **2.2 DNA methylation in transcription**

Methylation of cytosine adds a methyl group to the 5 carbon of cytosine, converting it to 5-mC. It is found in the genomes of a wide range of organisms including both prokaryotes and eukaryotes. In mammals, it occurs mainly at cytosine residues followed by a guanine residue, known as CpG dinucleotides sites. There are roughly 28 million CpGs in the human genome with an average 60–80% methylation rate (Smith and Meissner, 2013). It has been demonstrated that DNA methylation is not uniformly distributed over the genome, but rather is associated with CpG density. Genomes are largely CpG deficient

except at CpG islands, regions dense with CpG sites. Commonly found at gene promoters, the methylation of these islands plays a significant role in the regulation of gene expression. The density of CpG methylation has proven to be closely associated with transcriptional gene silencing in the context of promoter methylation; however, related information on the CpG-deficient promoter gene is still lacking. In addition, DNA methylation profiles can be highly tissue-specific due to their role in gene regulation (Schübeler, 2015).

### **2.2.1 Dynamic DNA methylation in the brain**

Epigenetic alterations have a strong impact on the brain; the modifications are not static, but change dynamically in response to external stimuli including alterations in neuronal synaptic activity. It has been reported that DNA methylation is involved in controlling long-term synaptic plasticity in many areas in the brain where its dynamic changes contribute to neuronal diversity and plasticity. DNA methylation in neurons mostly occurs in low CpG density regions and intergenic (between annotated genes) regions in the genome (Guo *et al.*, 2011). Mapping of DNA methylation in the brain has uncovered unexpected differences compared to that of other somatic tissues, including unprecedentedly high levels of non-CpG methylation and the 5-hydroxymethylcytosine (5-hmC), an oxidised form of 5-mC. The formation of 5-hmC is catalysed by the ten-eleven translocation (TET) family of proteins (Tahiliani *et al.*, 2009). It is believed that 5-hmC is involved in the demethylation process.

Alterations of this dynamic regulation pattern may cause damage to tissue and brain function, potentially leading to many brain disorders. A genome-wide study conducted to investigate the extent of DNA methylation changes in the brain has found that the regulation pattern is altered in the brains of those who commit suicide, suggesting a link

between gene expression alterations and suicide (Labonté *et al.*, 2013). Furthermore, post-mortem analysis of human brain tissue from 24 patients with schizophrenia and an equal number of unaffected controls showed significantly different DNA methylation rates (Wockner *et al.*, 2014).

### **2.2.2 Parasite-induced DNA methylation changes**

Recent studies have shown that *Toxoplasma* infection can result in DNA methylation changes. One study (Hari Dass and Vyas, 2014) showed that *T. gondii* is able to induce hypomethylation in the promoter of the gene encoding arginine vasopressin, a hormone involved in the behavioural response, in the amygdala, a part of the brain that controls behavioural responses. The study showed that fear aversion to cat odour can be restored by inducing systemic global hypermethylation throughout the genome with L-methionine administration in infected rats. Another recent study found that *T. gondii* infection causes genome-wide changes in host gene expression, evaluated by examining host cell methylome perturbations. The parasite altered amyloid precursor protein levels following infection in a human eye cell line, and the study determined that seven significant biological pathways were enriched six hours post-infection in a developed gene-network analysis, in which neurologically associated dopamine-DARRP32 feedback in the cAMP signalling was among the most-altered pathways (Syn *et al.*, 2018). This demonstrates a possible alteration in the dopamine signalling pathway, consistent with the literature (Chapter 1) reporting dopamine alterations during *Toxoplasma* infection. However, the duration of the experiment was very short relative to cyst persistence *in vivo* (months or years). It is unknown how *T. gondii* causes these changes in DNA methylation, but the finding suggests that targeting and altering host genes or genomes through this mechanism could be an effective way for the parasite to adapt host physiology for its own benefit.

### 2.2.3 Methylation regulates gene expression

Combined methylome and gene expression profile analysis have demonstrated a strong correlation of DNA methylation with gene repression. Changes in DNA methylation are associated with the changes in the chromatin structures that cause a closed chromatin state. Methylated cytosines can prevent the binding of some transcription factors with their recognition sites in the promoter region. Yet, the methylated condition is also capable of recruiting CpG binding proteins that can modify the chromatin states.

DNA modifications are commonly affected by external stimuli including drugs, infections and development. This has been shown to occur at the glutamatergic synapses, in which the neurons exposed to methamphetamine, a type of dopamine stimulant, cause hypoacetylation of histone H4 on GluA1, GluA2, and GluN1 promoters and decrease striatal glutamate receptor expression. Methamphetamine-induced neurons also caused hypomethylation at GluA1 and GluA2 promoter sequences (Jayanthi *et al.*, 2014). This finding provides strong evidence that gene expression can be modulated by external stimuli beside the invading intracellular parasite.

## **2.3 Methods**

### **2.3.1 Growth of parasite and host cell**

Wild type II *T. gondii* Prugniard strain was isolated from infected mouse brain. The parasites were maintained in human foreskin fibroblast (HFF) cell line Hs27 (ECACC 94041901) in Dulbecco's Modified Eagle's Medium (DMEM, GIBCO Life Technology, Paisley, UK) containing 10% foetal bovine serum (FBS) and 100 units/mL penicillin/streptomycin (Sigma, UK)

Dopaminergic rat neural cell line pheochromocytoma (PC12) cells (a gift from C. Peers; ECACC 88022401), a neuron-like cell capable of secreting catecholamines, was used for all assays in this study. PC12 cells were maintained in Roswell Park Memorial Institute (RPMI) 1640 Medium (GIBCO Life Technology, Paisley, UK) and supplemented with 10% horse serum (Life Technology, UK), 5% FBS (Life Technology, UK) and 100 units/mL penicillin-streptomycin (Sigma, Poole, UK). Normal PC12 cells growth in RPMI medium was showed in Appendix A.

### **2.3.2 Parasite conversion stage induction**

For the induction of parasite differentiation to bradyzoites, pH manipulation technique was used. First, the tachyzoites were free released from HFF cells by vigorously passing through a 27-gauge needle, re-suspended in alkaline RPMI supplemented with 1% FBS (pH 8.2) and incubated at 37°C for 16 to 18 h in ambient air. After incubation, the parasites were pelleted by centrifugation to remove the alkaline medium and rinsed once

with DMEM medium (Invitrogen, UK), isolated by centrifugation and returned to standard PC12 cell culturing conditions; the completed RPMI medium (pH 7.4) containing 10% horse serum (Invitrogen, UK), 5% FBS pH 8.2 (Invitrogen, UK) and 1% penicillin-streptomycin (Sigma, Poole, UK) prior to cell infection. The shocked liberated tachyzoite number was determined by microscopy and used for infection of PC12 cells with a parasite:cell ratio of 1:1. Bradyzoite stage was determined by the gene expression assay of the bradyzoite-stage gene markers, e.g. BAG1, LDH2, SAG4, ENO1, etc. and through light microscopy by observing the morphology of bradyzoite-encysted cyst. The photo of shocked-parasite in PC12 and HFF cells were showed in Appendix A.

### **2.3.3 Cells harvesting**

Two T-75 (75 cm<sup>2</sup>) flasks of PC12 cells, one each for *T. gondii*-infected and uninfected control cells, were cultured in 30 mL of completed RPMI medium at a density of  $5 \times 10^5$  cell/mL. Culture growth was monitored daily by light microscopy and the RPMI medium was changed after three days of infection. The cells were harvested daily for five days following *T. gondii* infection by removing 5 mL of the cell culture ( $2.5 \times 10^6$  cells) for DNA extraction and pelleted by centrifugation at  $3250 \times g$  (2500 rpm) for 10 min, then rinsed twice with ice-cold PBS (pH 7.4). The pellets were kept in a -80 °C freezer to be processed after the completion of five days of the cell harvesting. Assays were performed for three biological repeats. For the MeDIP assay, cells were harvested on day one to day five following infection. For the bisulphite PCR-cloning and sequencing assay, cells were harvested on days 1, 3, and 5 post-infection.

### **2.3.4 Cell lysis**

The cell pellet was lysed in 350  $\mu$ L cell lysis buffer containing 20 mM EDTA, 10 mM Tris-HCl (pH 8) and 1% sodium dodecyl sulfate (SDS) and incubated for 2 h at 37 °C with 5  $\mu$ L RNase A (10 mg/mL) prior to overnight incubation with 5  $\mu$ L Proteinase-K (20 mg/mL) at 55 °C.

### **2.3.5 Phenol-chloroform DNA extraction**

For DNA extraction, an equal volume (of starting sample volume) of phenol-chloroform-isoamyl alcohol (25:24:1) (PanReac AppliChem, USA) was added to the lysed cell pellet, then the tube was mixed by inverting, and centrifuged at 16,000 x g for 10 min to allow for phase separation. Two separate layers of solvent were formed.

Then, the top aqueous layer was transferred to a new tube, and an equal volume (sample) of chloroform (Fisher Scientific, UK) was added. The tube was mixed by inverting and centrifuged at 16,000 x g for 10 min. The above steps were repeated for chloroform.

Next, the top aqueous layer was transferred into a new tube and an equal volume (sample) of hydrated diethyl ether (Fisher Scientific, UK) was added, the tube was mixed, and centrifuged at 16,000 x g for 10 min. The above steps were repeated for the hydrated diethyl ether. The top aqueous layer was discarded while the bottom layer was transferred into a new tube.

Then, 1/10 volume (of the sample's volume) of 3 M sodium acetate (pH 5.2) and 0.75 volume (of the sample's volume) of isopropanol was added. The mixture was left at room temperature for 1 h to precipitate the DNA. Then, the mixtures was centrifuged at 16,000 x g for 1 h to pellet the DNA. The supernatant was removed while the pellet was washed with freshly-prepared 70% ethanol. Then, the mixtures was centrifuged for 30 min. The supernatant was removed and the DNA pellet was air-dried. The air-dried DNA pellet was eluted with 100  $\mu$ L elution buffer (TE buffer).

DNA concentration was measured by NanoDrop spectrophotometer (ThermoFisher, UK) and fluorescence assay; the QuantiFluor® dsDNA system fluorescence assay kit (Promega Corporation, UK), following manufacturer's instructions. The fluorescence assay was done at wavelengths 504nm<sub>Ex</sub>/531nm<sub>Em</sub>) using the Polarstar Omega microplate reader (BMG Labtech, UK).

### **2.3.6 MeDIP: Sonication optimisation and DNA fragmentation**

Optimal length of time for sonication of each sample was determined prior to the IP assay. This optimisation was important in order to achieve an average length of fragmented gDNA sizes to assist with DNA-antibody binding during the IP process. The standard published fragments were between 300 bp and 1k bp (Weber *et al.*, 2005) was achieved, and the optimal average selected was 500 bp. Optimal DNA sonication was performed using the EpiSonic Multifunctional 1100 Bioprocessor (Epigentek, USA) sonicator, and purified gDNAs were sonicated for 10 sec on, 30 sec off for a total time of 0.5 to 5 min. The sonicator was set to a standardised amplitude setting of 17%. After sonication, the sonicated DNAs were loaded onto 2% agarose gel (Bio-Rad Laboratories, California) containing 0.5  $\mu$ L/mL GelRed nucleic acid stain (Biotium, USA). A 2-log ladder (New England Biolabs, USA) was used for size comparison. Electrophoresis was

performed at room temperature for 80 min at 75 volts. Gel images were captured by a gel imager (Syngene Ingenius BioImaging, UK).

### **2.3.6.1 Evaluation of sheared DNA via agarose gel electrophoresis**

After sonication optimisation, the extracted DNAs of PC12 cell samples were sonicated simultaneously to avoid any variance in sonication efficiency. Thereafter, the sonicated-DNAs were loaded (2 µg of DNA per lane) onto a 2% agarose gel for average fragment size confirmation prior to assays.

### **2.3.7 MeDIP: Immunoprecipitation of the methylated-DNA binding**

An aliquot of 3.5 µg of fragmented gDNA was used for IP (per assay) and 180 ng of the DNA was kept as input (contained total methylated DNA and unmethylated DNA). In a total volume of 250 µL IP buffer (10 mM sodium phosphate pH 7, 140 mM NaCl and 0.05% Triton X-100), the DNA was denatured for 10 min at 95 °C then immunoprecipitated with 10 µL of monoclonal antibody against 5-methylcytidine (5-mC) Rabbit mAb D3S2Z (Cell Signaling Technology, USA) for 3 h at 4 °C on a rotator. Subsequently, 30 µL of Dynabeads Protein G (Invitrogen, UK) magnetic beads containing the secondary antibody with affinity for the primary antibody 5-mC was added and incubated for 2 h at 4 °C on a rotator. To remove the unbound, non-methylated DNA, the washing steps required 500 µL of IP buffer (10 mM sodium phosphate pH 7.0, 140 mM NaCl, 0.05% Triton X-100) for five washes, and the sample was incubated for 4 min on a rotator for each wash. An aliquot of 250 µL dilution buffer (0.1M NaHCO<sub>3</sub>, 1% SDS) was added to the methylated DNA-antibody-magnetic beads mixture to dissociate the complexes from the magnetic beads. The mixture was incubated overnight at 50 °C for

Proteinase-K antibody digestion, leaving only the methylated DNA intact. The methylated DNA was separated from the magnetic beads and purified using ChIP DNA Clean and Concentrator extraction kit (Zymo Research, California) according to the manufacturer's instructions. Figure 2.2 demonstrated a generalised MeDIP assay principle.

### 2.3.8 Quantitative real-time PCR

Real-time qPCR was performed in a Bio-Rad CFX thermocycler (Bio-Rad Laboratories, California) in duplicate per sample reactions. For each reaction, a qPCR reaction mixture was made as follows: 12.5  $\mu$ L Brilliant III Ultra-Fast SYBR® Green QPCR Master Mix (Agilent Technology, USA), 1  $\mu$ L 200nM forward primer, 1  $\mu$ L 200nM reverse primer, 10  $\mu$ L template DNA, and 0.5  $\mu$ L DNase/RNase free water added to give a total volume of 25  $\mu$ L. The primers were designed to be specific to the 5'TSS DBH gene: forward 5'-GCATGGGCTGGTGGGAGAG-3' and reverse 5'-CCACCAGGATGACCAGGAAGATGG-3'. Prior to amplification, the primer pair was optimised to determine the appropriate annealing temperature ( $T_a$ ) and PCR conditions by gradient qPCR. The gradient qPCR thermocycler setting for  $T_a$  was set within the range of 58–68 °C in the Bio-Rad thermocycler where the gDNA input samples were loaded in duplicate (by column) in a 96 well plate (each row representing one specific gradient temperature). The qPCR plate was incubated in a G1000 Thermal cycler (Bio-Rad Laboratories, California) at 95 °C for 2 min, followed by 40 cycles of 95 °C for 30 sec,  $T_a$  for 30 sec, and 72 °C for 30 sec, then final extension at 72 °C for 5 min prior to melting curve analysis, as summarised in the Table 2.1. Input amount were determined beforehand by loading a serial dilution of 1  $\mu$ g gDNAs into the real-time qPCR to obtain an acceptable quantification cycle ( $C_q$ ) scale ( $5 < C_q < 40$ ), in which 180 ng of input sample was obtained in the range of  $C_q$ s 22–23. The same amount of DNA input (180

ng) was standardised for each sample. The Figure 2.1 demonstrates how Cq value is measured using BioRad CFX-manager software (USA).

**Table 2.1 The final setting of the Real-Time qPCR.**

Step	Temperature (°C)	Time
Initial Denaturation	95	2 min
Denaturation	95	30 sec
Annealing	62	30 sec
Extension	72	30 sec
Final Extension	72	5 min
Melt Curve Analysis	65–95	

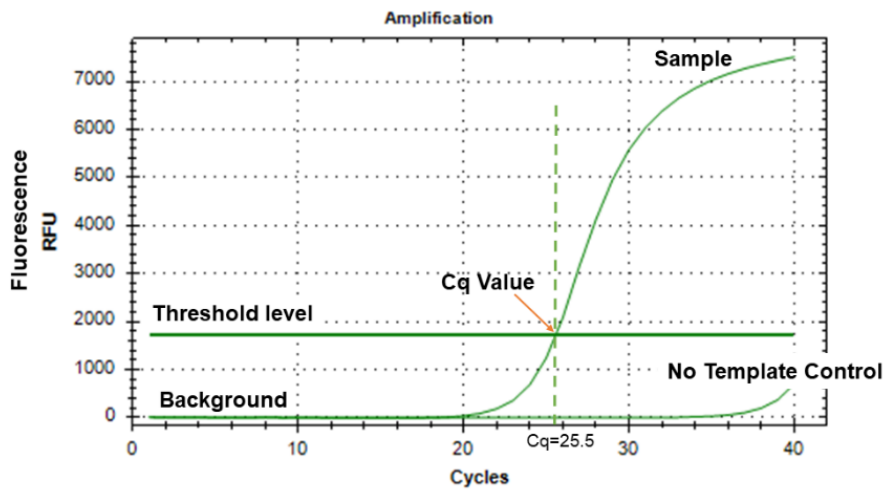


**Figure 2.1 Threshold level and Cq value on the real-time qPCR amplification curve.**

The threshold level is the level of detection at which a reaction reaches a fluorescent intensity above the background level. The Cq value shows the total number of cycles required to detect a real signal from the sample that intersects the threshold line.

### 2.3.9 MeDIP data analysis

The data were analysed by the percent input method which measures the IP value relative to the input, wherein the input value was used for data normalisation. This method was used as it includes normalisation for both background levels and input IPs samples. The input sample represents the amount of DNA used in the MeDIP assay. As assay controls, the rabbit anti-IgG was used as an IP negative control, while no antibody-binding sample reaction was used as background control. Both controls were subject to the same procedures as the sample.

To obtain percent input, the Cq value (Figure 2.1) obtained from IP was divided by the value obtained from an input sample in the following steps:

1. The Cq starting input was adjusted to 100%. As the total of input used was 180 ng and the total DNA for the sample reaction was 3500 ng, the dilution factor was 19.44 or 4.28 cycles (i.e.  $\log_2$  of 19.44). To normalise the input cycle, the dilution factor cycle value was subtracted from the Cq value of the input.
2. To obtain the delta Cq, the average of the Cq IP sample was subtracted from the adjusted input value. (Mock [IgG] was calculated in the same way).
3. Percent input (%) of each sample was calculated based on this formula:

$$100 * 2^{(\text{adjusted input Cq} - \text{Cq IP})}$$

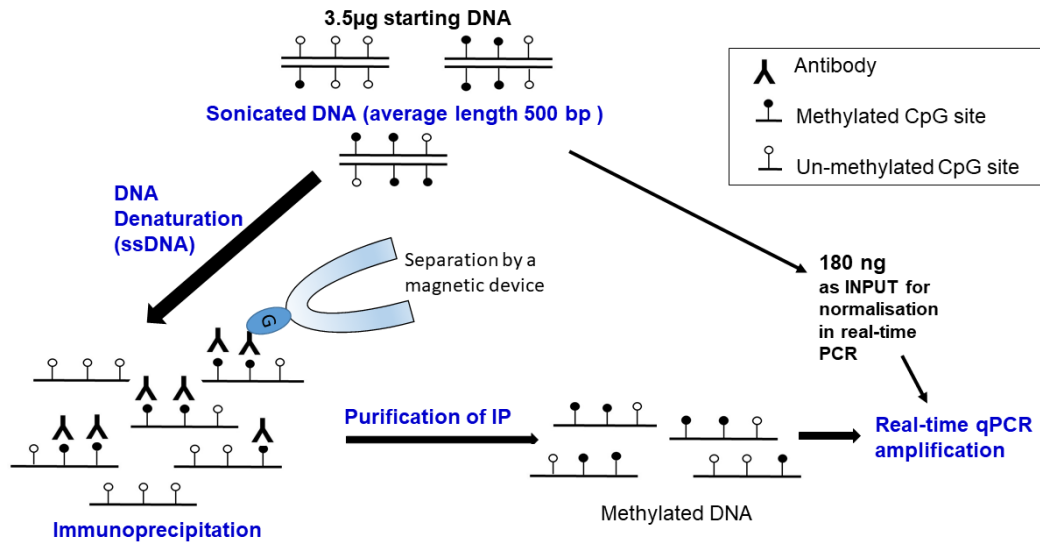


**Figure 2.2 Generalised MeDIP assay.** Total gDNA is fragmented by sonication and denatured into single-stranded DNA fragments which are then immunoprecipitated with an antibody that recognises the methylated DNA. The methylated DNA-antibody complexes are then immunocaptured by a secondary antibody prior to separation by magnetic beads. The purified methylated fragments are amplified by real-time qPCR. The IP value is measured relative to the input sample which is the starting sonicated genomic DNA that contains both methylated and un-methylated fragments.

Figure 2.3 provides a summary of the steps involved in the MeDIP assay. One set of primer pairs was designed specific to the first exon including the 5'TSS proximal promoter of the DBH gene. The studied region included four CpG sites in a 242 bp length DNA sequence.

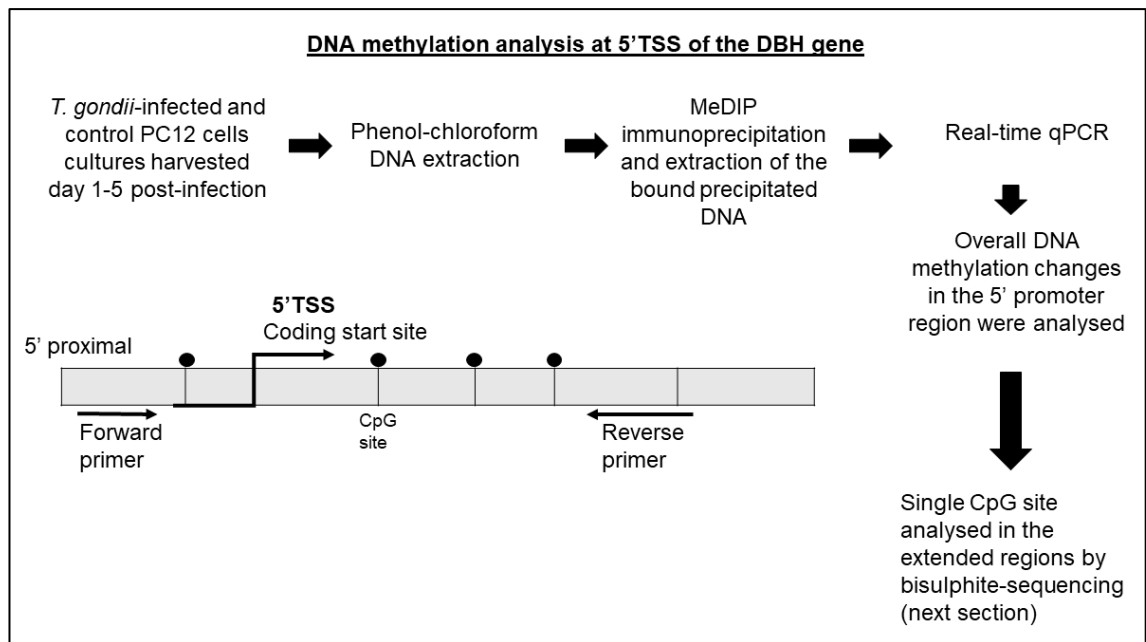


**Figure 2.3 Schematic representation of the steps in the MeDIP assay study design**

### 2.3.10 Bisulphite treatment of the genomic DNA

Purified gDNA was treated with bisulphite using the EZ DNA Methylation Gold kit (Zymo Research, California), following manufacturer protocols. Two standard genomic DNAs, CpGenome™ rat methylated genomic DNA standard (Millipore Cat:S7855) and CpGenome™ rat unmethylated genomic DNA standard (Millipore Cat:S7860), were used as controls to test and optimise the primers; they were treated with bisulphite using Zymo Methylation Gold kit prior to PCR primer pair optimisation. Briefly, 700 ng (diluted in a total of 20  $\mu$ L DNase/RNase-free water) of the purified DNA was added directly to the 130  $\mu$ L of CT-conversion reagent and incubated in a thermocycler for 10 min at 98  $^{\circ}$ C

and then at 64 °C for 2.5 h. Strand denaturation and bisulphite conversion were completed in a single-tube reaction. Next, the sample was transferred into a column that contained 600 µL of M-binding buffer to bind the bisulphite-treated DNA onto the column. The desulphonation process (by addition of M-desulphonation buffer) and the recovery of the bisulphite-treated DNA occurred in a spin column. The spin column allowed for elution of bisulphite-converted DNA in as little as 10 µL DNase/RNase-free water and was ready for immediate PCR analysis. A 2 µL aliquot of the eluted DNA was used for the next PCR amplification region. The PCR products were visualised by agarose gel electrophoresis.

### **2.3.11 Bisulphite-treated primer pair optimisation of rat 5'TSS DBH gene**

Primer pairs specific for the bisulphite-treated DNAs were designed with the help of MethPrimer software, a program for designing bisulphite-conversion-based methylation PCR primers for bisulphite-sequencing PCR (Li and Dahiya, 2002). Two regions of interest in the DBH promoter gene sequences were chosen based on the location relative to the DBH gene coding region. The first primers were designed to be near the 5' DBH gene coding region (hereafter labelled as "5'TSS"), while the second primers were designed to be 2700 bp upstream of the coding region (hereafter labelled as "2.7k bp upstream"). More than six pairs of primers for each region were screened and optimised for their propensity for the correct binding and amplification, covering five to eight densities of CpG sites. A working primer pair of each region with the correct template binding and covers the highest CpG sites was chosen for further investigation. The lengths of each fragment of interest (FOI) for the 5'TSS and 2.7k bp upstream of the DBH promoter gene were 367 bp and 316 bp, respectively.

### DNA methylation analysis at 5'TSS of the DBH gene

CpG site analyses of the extended regions by bisulphite sequencing

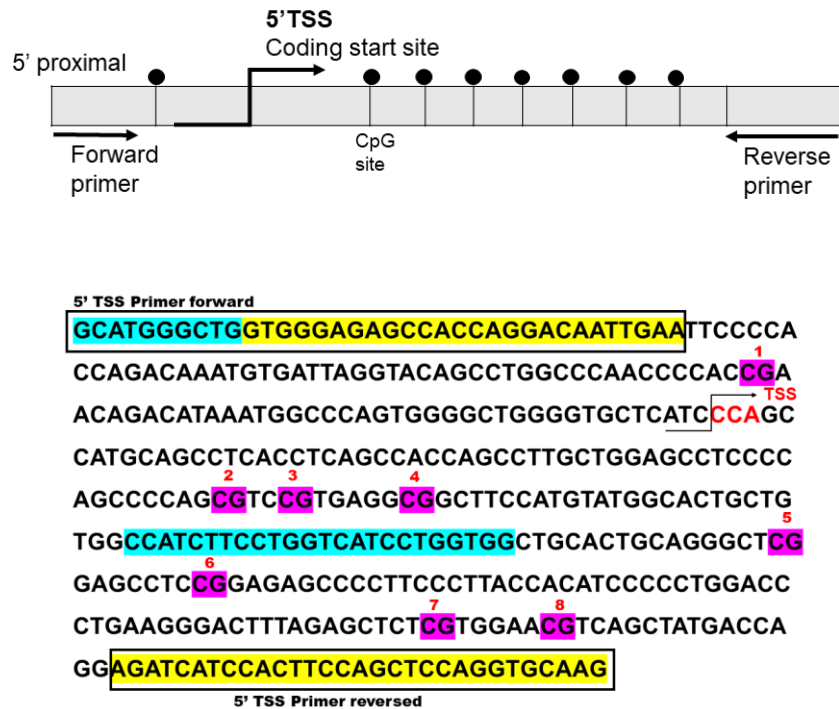


**Figure 2.4 Primer pair design of 5'TSS DBH gene sequences.** A total of eight CpG sites were covered in this region, the majority of which is embedded in Exon 1. Below the diagram is the full nucleotide sequences covered in the MeDIP and bisulphite sequencing assays. Yellow highlighted sequences were the primer pairs in bisulphite sequencing analysis. Blue highlighted sequences denote primer pairs of the MeDIP assay analysis.

The 5'TSS DBH gene bisulphite-treated primer pair (367 bp) was as follows: forward 5'-GTGGGAGAGTTATTAGGATAATTGAA-3' and reverse 5'-CTTACACCTAAACTAAAATAAATAATCT-3'. Meanwhile, the primer pair of 2.7k bp upstream (316bp) were: forward 5'-TTGTTTTTTTGGTTGTTATTATTTA-3' and reverse 5'-ACCCCCACCCTAATAACTCTACTATAT-3'. For both regions, eight CpG sites were covered in each of the designated primer pairs. The primers were designed with a few considerations. Each FOI contained a maximised CpG sites in the nucleotide sequences of the PCR products while maintaining shorter, acceptable PCR product lengths (<500 bp). As the methylation status of CpG dinucleotides was unknown, the bisulphite-primer binding sites were designed without containing any CpG dinucleotides, and thus

amplified the target regardless of methylation status. After bisulphite treatment, all unmethylated cytosines were converted to thymines and methylated cytosines remained cytosines. Therefore, the cytosine bases in the primer sequences would also need to be converted into thymine. For that reason, all forward primers contained no cytosine bases.

Gradient PCR was performed to determine the optimum annealing temperatures of each primer using a MasterCycler gradient thermal cycler (Eppendorf, UK). The PCR setting was standardised with an initial DNA denaturation at 95 °C for 2 min, denaturation 95 °C for 30 sec, specific annealing  $T_a$  for 30 sec, extension 72 °C for 20 sec and a final extension at 72 °C for 7 min. Each PCR cycle required 30 to 40 cycles and a 25- $\mu$ L reaction volume using GoTaq® G2 Hot Start Green Master Mix (Promega, USA).

### **2.3.12 Bisulphite-treated DNAs PCR amplifications**

The bis-treated DNA samples were amplified by a 50- $\mu$ L reaction of PCR using both sets of primer pairs, 5'TSS and 2.7k bp upstream, to create and amplify the FOI prior to ligation into a TOPO vector by TOPO® TA Cloning® Kit for Sequencing (Invitrogen, UK). PCR cycling conditions were as follows: 2 min at 95 °C, 40 cycles of 30 sec at 95 °C, 30 sec at 53 °C, 20 sec at 72 °C and 8 min at 72 °C. Both primers were found to have the same annealing  $T_a$  at 53 °C. The PCR products were electrophoresed on a 0.75% agarose gel (50 V, 60 min) and the specific band was gel-excised and gel-extracted by QIAquick Gel Extraction Kit (Qiagen, Germany). The kit implemented a simple bind-wash-elute procedure in a silica membrane column that supported the binding of DNA with the high-salt buffer and DNA elution with the low-salt buffer or water. Next, the eluted DNA concentrations were measured by the NanoDrop spectrophotometer (Thermo Fisher Scientific, UK). The PCR products were subcloned into a TOPO TA cloning vector (PCR™4-TOPO–Invitrogen TA cloning kit) (Thermo Fisher Scientific, UK).

### **2.3.13 TOPO TA-cloning**

The purified fragment was inserted into a TOPO-TA cloning vector. The vector used was PCR4-TOPO TA vector from Invitrogen (UK), which was specifically designed for cloning PCR products amplified by Taq DNA polymerase. Usage of Taq DNA polymerase in PCR often leaves an adenine at the 3' end of the product, creating overhangs, and the usage of the TOPO vector is suitable because it includes a 3'-thymidine overhang for direct ligation with the fragment (Figure 2.5). Briefly, 50 ng of gel-extracted DNA (diluted in 4  $\mu$ L DNase/RNase-free water) was added with 1  $\mu$ L salt solution and 1  $\mu$ L of TOPO TA vector for a total solution volume of 6  $\mu$ L, then the mixture was properly mixed by finger vortexing and incubated at room temperature for 15 min then placed on ice prior to plasmid-cell transformation steps.

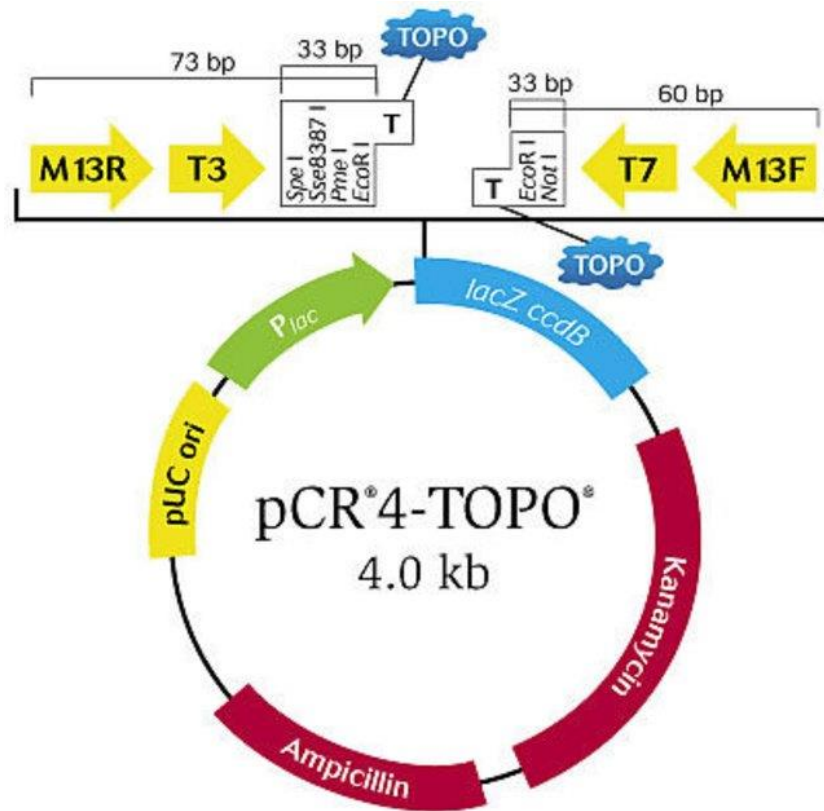


**Figure 2.5 PCR4-TOPO TA vector (Invitrogen, UK).** TOPO vector contained 3'-thymidine overhang for direct ligation with fragment of interest, amplified by Taq polymerase II enzyme that created 3'-adenine overhang during PCR amplification. The key of TOPO TA cloning was the enzyme DNA topoisomerase I which functioned as a restriction enzyme and as a ligase; to cleave and rejoin DNA. The TOPO enzyme formed a covalent bond with the phosphate group attached to each of the 3'-thymidine overhang of the vector. During incubation with a fragment having 3'-adenine overhang at both ends (PCR product), the TOPO enzyme ligated the fragment sequences with compatible ends, and released itself from the DNA. The positive fragment-insert formed a recombinant cloning-plasmid. Insertion was done at lacZ $\alpha$  ccdB gene site, which disrupted the expression of the lacZ $\alpha$ -ccdB gene fusion, permitting growth of only positive recombinants upon transformation in competent cells. This vector also consisted a group of restriction cut sites, designated for *Spe I*, *Sse8387 I*, *Pme I* and *EcoR I* enzymes. The yellow bar denoted a flanking sequencing primers (forward and reversed), M13 and T3, for DNA sequencing. Kanamycin and ampicillin in the vector sequences were antibiotic resistance genes that enable a positive selection of transformed colonies. Meanwhile plasmid pUC ori functioned to copy plasmid inside the bacteria cells.

### **2.3.14 Cloning plasmids in XL10-cells by transformation**

The fragment inserted-vector (plasmid) was transformed into XL-10 Gold ultracompetent cells (Agilent Technologies, USA) by following the manufacturer's suggested protocols. Briefly, 50  $\mu\text{L}$  of the XL-10 Gold ultracompetent cells were added with 2  $\mu\text{L}$   $\beta$ -mercaptoethanol mix (to increase transformation efficiency) prior to adding 3  $\mu\text{L}$  TOPO TA ligation mixture. The mixture was incubated on ice for 30 min in a 14 mL BD falcon tube (Appleton Woods Ltd, UK). Next, the tube was heat-pulsed in a 42 °C water bath for 30 sec and quickly incubated on ice for 2 min. Preheated NZY<sup>+</sup> broth (450  $\mu\text{L}$ ) was added and the mixture incubated at 37 °C for 1 h in a shaking incubator. The transformation mixture was plated on Luria-Bertani (LB) agar plate with ampicillin (100  $\mu\text{g}/\text{mL}$ ) and incubated overnight at 37 °C. The following day, a single colony of the transformed cells was then grown in 2 mL of LB broth with ampicillin (100  $\mu\text{g}/\text{mL}$ ) for overnight growth in the shaking incubator at 37 °C. The bacterial suspension was extracted with a plasmid extraction purification column kit (NucleoSpin Plasmid, Macherey-Nagel, Germany). At least 20 colonies were picked up for each sample (infected and uninfected cells for days 1, 3, and 5 post-infection).

### **2.3.15 Eco-RI digestion and confirmation of fragment insertion**

The vector consisted of flanking EcoRI restriction sites in the cloned PCR product inserted site. Digestion of the plasmid with EcoRI digestion enzyme produced the inserted fragment size on an agarose gel. Five hundred ng of plasmid was incubated at 37 °C with 0.5  $\mu\text{L}$  of restriction enzyme and 2.5  $\mu\text{L}$  cut smart buffer in a total reaction volume of 25  $\mu\text{L}$  for 1 h prior to electrophoresis on 1% agarose gel to visualise the cut bands.

### **2.3.16 Sequencing and data analysis**

At least 20 plasmid clones of each sample were sent for Sanger sequencing to Genewiz, UK. Sequencing was done by flanking sequencing primers M13F and M13R of the plasmid sequences.

## 2.4 Results

### 2.4.1 MeDIP: Sample preparation and determination of sonication time and efficiency

Cells were cultured and infected as previously described (method section; 2.3.1 - 2.3.2). Prior to the assay, the extracted DNA was sonicated using the EpiSonic sonicator for different time periods to determine appropriate sonication time. A total sonication time of one minute was found to work best for this assay, providing optimal average fragment lengths of 500 bp (Figure 2.6). It was found that the quantity of gDNAs used did not influence the sonication efficiency: the same length of fragmented DNA at low or high DNA amounts was generated. However, different cell lines may require different sonication times.

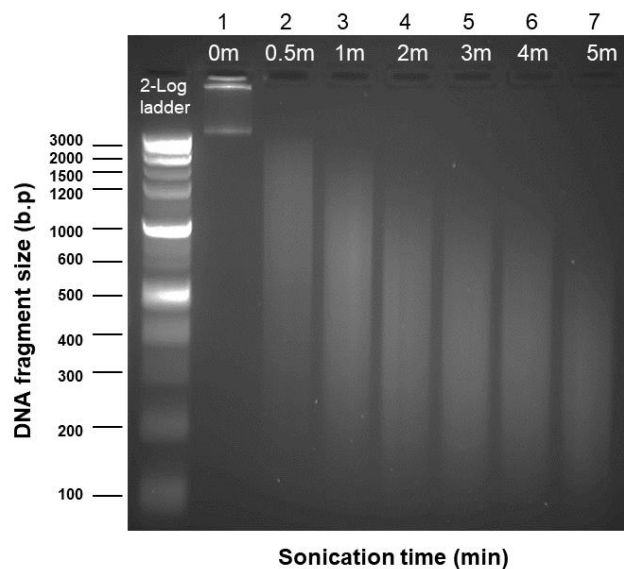


**Figure 2.6 Time-based sonication determination.** Gel image showed fragments of sonicated gDNA rat PC12 cells (400 ng per well), sonicated for 0.5 min to 5 min with a 2-log ladder as a reference length. The sonication time of the preferable length (average 500 bp) chosen was 1 min (Lane 3). Lane 1: unsonicated gDNA, Lane 2–7: gDNA sonicated from 0.5 min to 5 min.

In this study, the EpiSonic sonicator implemented a cooling system with a recirculating chilled water pump to promote an isothermal sample environment, prevent thermal degradation and maintain sample integrity. The presence of SDS (detergent) in the sonication buffer improved sonication efficiency, especially for the cell lysate. For the DNA sample, sonication performed appropriately using Tris-EDTA (TE) buffer, which was routinely used in avoiding DNA degradation.

#### 2.4.1.1 Evaluation of sheared DNA via agarose gel electrophoresis

Prior to the assay, to reconfirm an ideal total sonication time of one minute, five gDNAs of extracted PC12 cells were run on a gel to confirm the average fragment sizes.

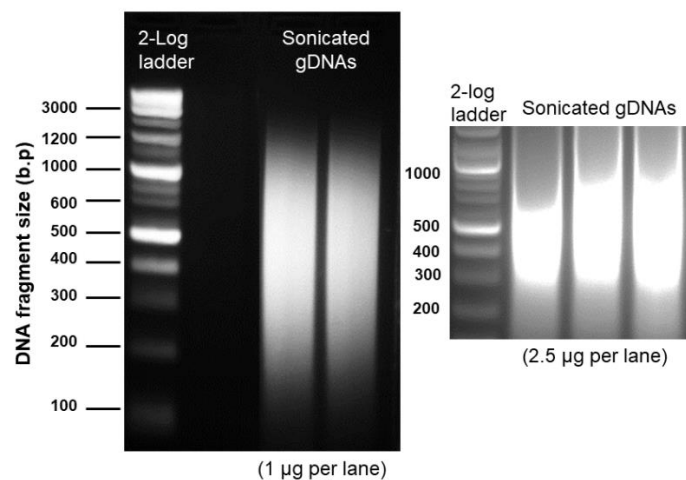


**Figure 2.7 Agarose gel electrophoresis of gDNA from rat PC12 cell samples sonicated for 1 minute.** The average fragmented DNA size is approximately 500 bp.

### 2.4.2 Genomic DNA preparation from *T. gondii*-infected PC12 Cells

Purified gDNA was eluted with TE elution buffer and sonicated for one minute prior to DNA quantification. The first quantification of total gDNA concentrations, as well as screening for quality and purity of the DNA, was done using spectrophotometry (NanoDrop spectrophotometer). The second quantification was done by a fluorescence-based assay (QuantiFluor kit) to accurately quantify the ratios and screen for quality and purity of the DNA. The 260/280 ratio and the 260/230 ratio were approximately 1.80 and above 2.0, respectively, and the ranges obtained indicated the samples were pure DNA without protein or reagent contamination. The fluorescence assay gave more sensitive values in DNA concentration than DNA quantitation by spectrophotometry, though differences were minor. The QuantiFluor® dsDNA reagent (Promega, UK) used contained a fluorescent DNA-binding dye that enables sensitive quantitation of even small amounts of double-stranded DNA (dsDNA) in a purified sample.

Consistent purification of high-quality gDNA and accurate DNA quantification of sonicated gDNA are important for the MeDIP and bisulphite sequencing methods. MeDIP is a sensitive IP assay that requires pure DNA for accuracy as contaminations might interfere with the protein-antibody binding. Downstream real-time qPCR and bisulphite-treated DNA sequencing are also highly sensitive methods. Thus, an accurate quantitation was needed for optimum working assays, especially for sample normalisation and comparison between the time-course samples.

### 2.4.3 MeDIP-qPCR assay optimised

The MeDIP assay involves the capture of methylated DNA by an antibody specific to 5-mC (Figure 2.2). This assay used a standard, validated commercial 5-mC rabbit antibody (Cell Signaling Technology, USA) that increased the assay specificity and selectivity for 5-mC, thus avoiding nonspecific interactions or binding. The assay procedure was modified and optimised from the original MeDIP method (Weber *et al.*, 2005). The incubation time for IP steps for DNA-antibody-magnetic beads bindings required only 5 h without compromising the quality of the results for the rat neural PC12 cell lines. The magnet-based purification was chosen because it provides a fast, simple and efficient antibody-complex separation by a magnetic rack. In addition, increased washes in the IP washing steps showed improved removal of unbound fragments (Lee *et al.*, 2006; Gade and Kalvakolanu, 2012). The standard method to purify methylated DNAs was also modified by incorporating DNA silica column extraction, eliminating a lengthy phenol and chloroform: isoamyl alcohol extraction, and thus avoiding further loss of the precipitated methylated DNAs. This resulted in a much faster method than the method proposed in the original protocol. Overall, the procedures of the MeDIP assay required only two days to be completed.

A minimum of 200 ng (5–6%) from a total of 3.5  $\mu$ g starting gDNA was successfully precipitated by this assay. Due to the low amount of the precipitated IP DNAs, the DNAs were directly subjected to real-time qPCR for MeDIP analysis. The amplification resulted in Cq values between 20 and 26 for all subsequent qPCR sample reactions (data not shown). The MeDIP analysis was calculated based on the percent input method described in the method section, where the Cq value of the IP was calculated relative to the normalised Cq input. PCR reactions were performed in triplicate and product specificity was confirmed with melt curve analysis. A single product peak was obtained for each reaction of this assay, demonstrating a working optimised MeDIP assay.

## **2.4.4 Primer optimisation for real-time qPCR**

Real-time qPCR conditions were optimised by testing different primer concentrations (0.2  $\mu$ M to 0.5  $\mu$ M) and discovered to work well even at the lowest concentration of 0.2  $\mu$ M. Thus, the primer concentration was standardised to 0.2  $\mu$ M for all real-time qPCR reactions in this assay.

### **2.4.4.1 DBH primer optimisation using gradient qPCR**

The primer pair annealing temperature was determined by gradient qPCR. As most of the Cqs (24-25) of the PCR products were within an acceptable range (Cq=20-35), the determination was based on the melt peak analysis with a single optimum product peak (Figure 2.8). It is important to optimise the PCR conditions to confirm the primer specificity and to avoid primer-dimers and non-specific bindings. The primers showed an annealing  $T_a$  of 62° C worked best for this primer pair which gave a single product (shown as a single peak in the melt curve graph in Figure 2.8).

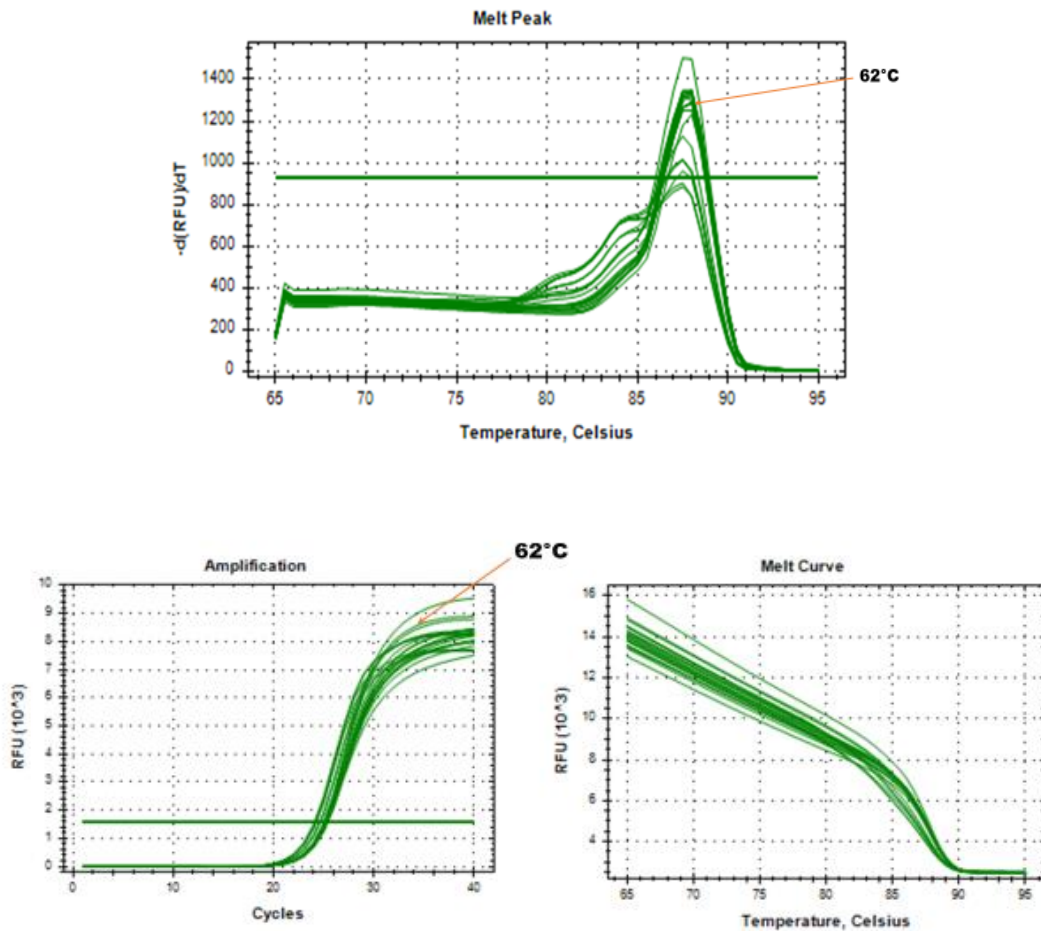


**Figure 2.8 Melt peak analysis for MeDIP-qPCR primer pair optimisation.** Analysis of the melt peaks at annealing  $T_a=62$  °C; the primer-DNA binding worked best in the gradient qPCR reaction assay for primer pairs that displayed a single, optimal peak, indicating one amplification product. Amplification graph showed normal sigmoidal shapes. The melt curve monitored the fluorescence as temperature increased. The SYBR dissociated as DNA melted into single strand DNA, hence, the fluorescence intensity decreased as SYBR dissociated.

## 2.4.5 DNA methylation changes at the 5'TSS DBH gene region following infection

The expression and methylation patterns in *T. gondii*-infected neural PC12 cells were compared to that of uninfected control cells for five consecutive days following infection. The percent input of DNA methylation at the 5'TSS region of the DBH gene by MeDIP-qPCR assay are shown in Figure 2.9:

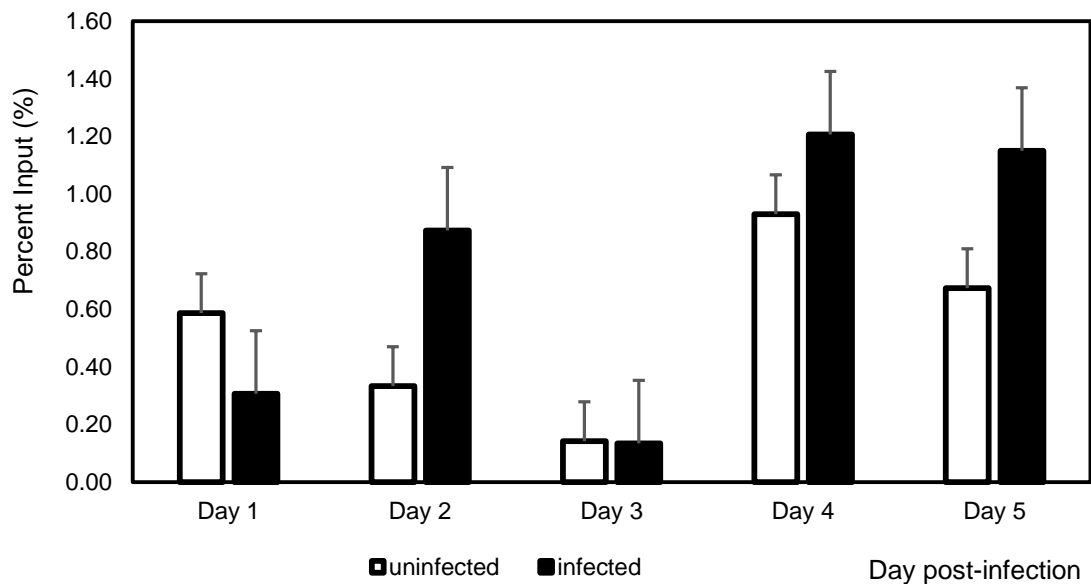


**Figure 2.9 DNA methylation pattern changes analysed by MeDIP-qPCR assay.** The bar graph shows DNA methylation patterns at the 5'TSS DBH gene on day one to day five following *T. gondii* infection in the catecholaminergic neural PC12 cells. The white bar denotes the percent input of uninfected control PC12 cells, while the black bar denotes percent input of infected PC12 cells. Day one post-infection showed a difference with a less percentage per input of DNA methylation of the infected cells compared to uninfected control, but showed a 2.5-fold increased on day two. There were no difference on day three but the DNA methylation level on day four post-infection was slightly increased up to 1-fold and continued increasing with 1.7 folds on day five compared to the uninfected samples. Overall, DNA methylation patterns increased following the time-course study. The two-way ANOVA test showed there was a significant change in the DNA methylation patterns in the five continuous days ( $F=6.562$ ,  $*p=0.0015$ ). However, the data was found to be not significant in two-way ANOVA among the samples of each day between the infected and control samples ( $F=1.468$ ,  $p>0.05$ ). Error bars are shown.

A general trend was observed where DNA methylation increased in the infected cells following *T. gondii* infection in the PC12 cells up to day five post-infection ( $F=6.562$ ,  $p<0.005$ ). The F ratio value in two-way ANOVA test was significant with  $p<0.05$  indicating a pattern changes from day one to day five. However, the changes were not statistically significant in two-way ANOVA ( $F=1.468$ ,  $p>0.05$ ) in comparing between infected sample (mean=0.73) and uninfected control (mean=0.53) for each day. Therefore, the involvement of DNA methylation changes at the 5'TSS region of the gene following *T. gondii* infection cannot be confirmed. MeDIP is limited by the ability of the antibody to immunoprecipitate the fragmented DNA based on the density of CpGs. It is notable that the DBH promoter does not contain a CpG island that may limit the sensitivity of this assay.

The next step was to determine whether methylation changes in specific CpGs relative to the DBH gene could be detected.

#### **2.4.6 Bisulphite PCR primer design and optimisation**

The DBH promoter region was screened for the density of CpG sites. Two regions of interest in the 5'UTR upstream of the DBH promoter gene were chosen based on their distance from the DBH gene initiation coding region. The first region was the extended Exon 1 sequences of downstream 5'TSS DBH gene region from the MeDIP assay, which included more CpG sites. Meanwhile, the second region was designed to be 2.7k bp further upstream of the promoter. The DBH gene does not have obvious CpG islands in its promoter; thus, the 2.7k bp upstream region from the start codon, even with only sparse CpG sites, was chosen to be evaluated and compared with the 5'TSS region as illustrated in Figure 2.4.

Successful primer design is challenging for bisulphite-treated DNA because the bisulphite-converted DNA has lower-complexity primers which are often AT-rich. Therefore, the primer sequences need to be longer to bring them up to an acceptable annealing  $T_a$  in PCR, as they need to anneal outside the CpG sites. Bisulphite treatment causes the DNA structures to become unstable as a result of the non-complementary strands. As optimal primer annealing temperatures are important for successful and specific primer binding, they need to be optimised prior to each assay. Too low temperatures can cause primer-dimer and non-specific product formation, whilst too high annealing temperatures decrease product yields due to poor primer annealing. Increasing the length of forward primers which lack cytosine bases increases the annealing  $T_a$ . The primer length is ideally around 25 to 30 nucleotides, which helps in increasing the specificity of the binding (Li and Tollefsbol, 2011). PCR bias was also minimised during optimisation by increasing the annealing  $T_a$  for methylated DNA, which improves the PCR efficiency (Shen *et al.*, 2007). As the bisulphite treatment reduces the specificity of dsDNA, a gradient PCR was used to optimise the PCR conditions when determining the primers' annealing  $T_a$ . In addition, the G2 Hot Start DNA polymerase enzyme (Promega, USA) was employed in the PCR reaction to increase the binding specificity, thus improving the PCR yield which greatly reduces the primer-dimer formation.

#### **2.4.6.1 Bisulphite-treated DNA standards tested with set primer pairs of 5'TSS and 2.7k bp upstream of DBH promoter gene**

The optimal bisulphite method must deliver the complete conversion of cytosine residues to uracil while the 5-mC remains intact. Standard DNA controls were used to mimic the effects while unconverted gDNA was used as a negative control template to confirm a completed DNA conversion after bisulphite treatment as the primers only bind to the

converted DNA. The primers were optimised to correctly bind to the converted modified gDNA in a gradient standard PCR. The agarose gel of the PCR products of methylated and unmethylated standard DNAs is shown in Figure 2.10.

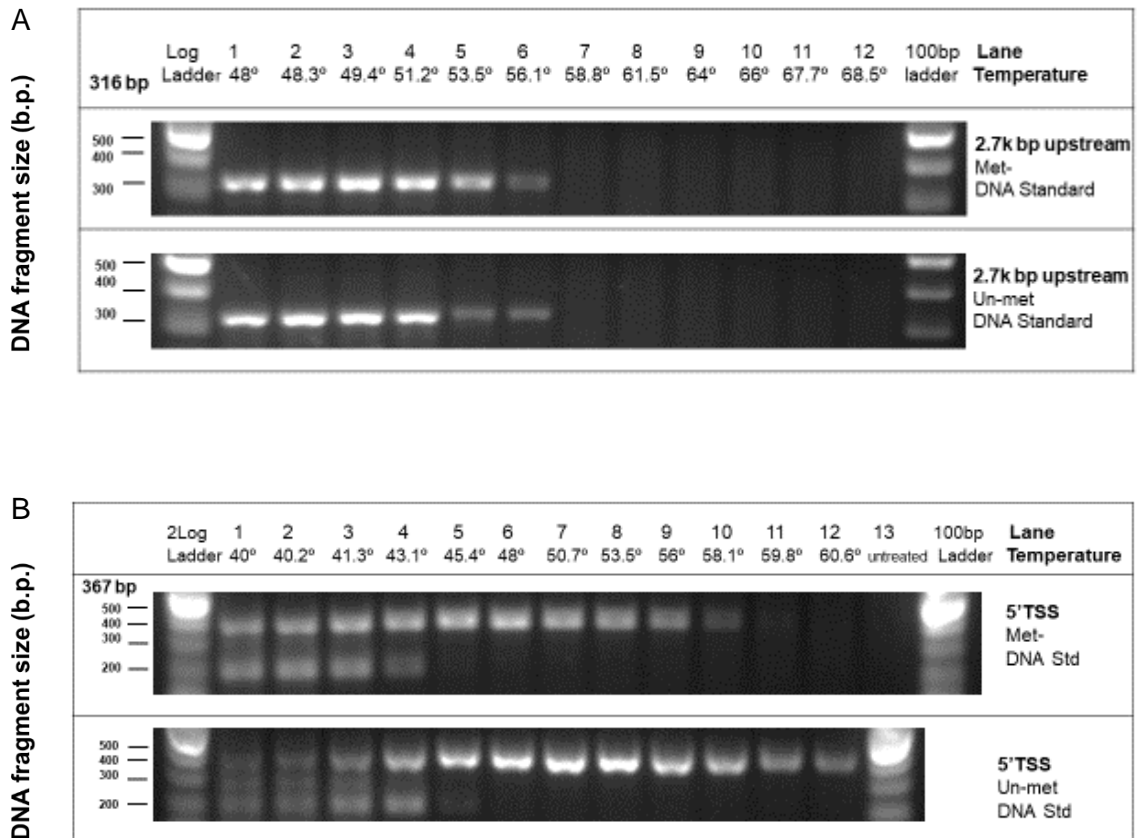


**Figure 2.10 Gradient standard PCR of both sets of primer pairs tested on rat methylated and un-methylated gDNA standards.** A. Primer pair 1: 2.7k bp upstream: the gradient thermocycler (Eppendorf, UK) annealing temperature was set from 48 °C to 68 °C, with the mean  $T_a$  at 50 °C and G:10° increment. B. Primer pair 2; 5'TSS: the gradient thermocycler (Eppendorf, UK) annealing temperature was set from 40 °C to 60 °C, with the mean  $T_a$  at 58 °C and G: 10° increment. For both primer pairs, an optimum annealing  $T_a$  was chosen to be 53 °C. Met: methylated DNA; Un-met: un-methylated DNA.

Based on the gradient standard PCR, the annealing temperatures of both primer pairs for the two studied regions were in the range of 48 °C to 56 °C, which were evaluated using methylated and un-methylated gDNA standards with a single product produced. The highest optimum temperature with a single product ( $T_a=53$  °C) was chosen for the standard PCR reaction of both primers.

For confirmation of working primers, one of the primer pair was applied to and found to work with the gDNA sample, the bisulphite-treated rat PC12 cells (Figure 2.11).

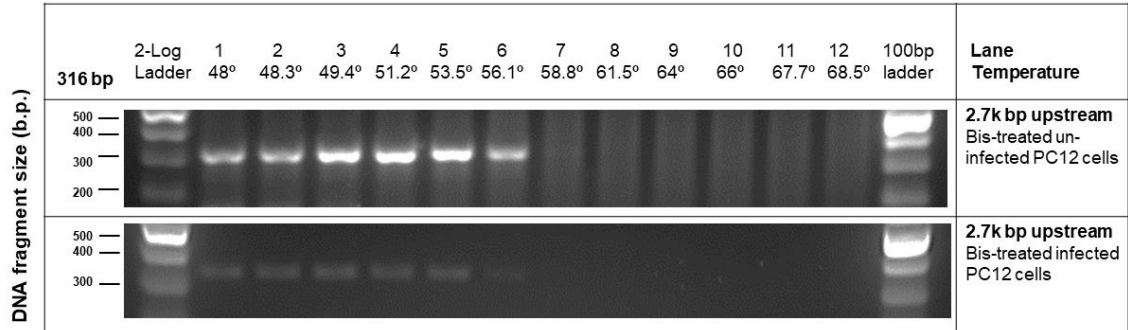


**Figure 2.11 Set primer pair of 2.7k bp upstream tested on bisulphite-treated PC12 cell's gDNA.** The primer pair amplified the gDNA-converted sample from rat PC12 cells indicated of a working primer pairs. An optimum annealing  $T_a$  was chosen to be 53 °C.

#### 2.4.7 PCR amplification of the bisulphite-treated DNA of infected PC12 cell samples

After establishing the annealing temperature for both primer pairs ( $T_a=53$  °C), all bisulphite-treated rat PC12 cell gDNAs samples of day 1, 3 and 5 post-infections were amplified with the specific PCR primer pairs for single product verification and visualised on agarose gel prior to ligation into a cloning vector (Figure 2.12).

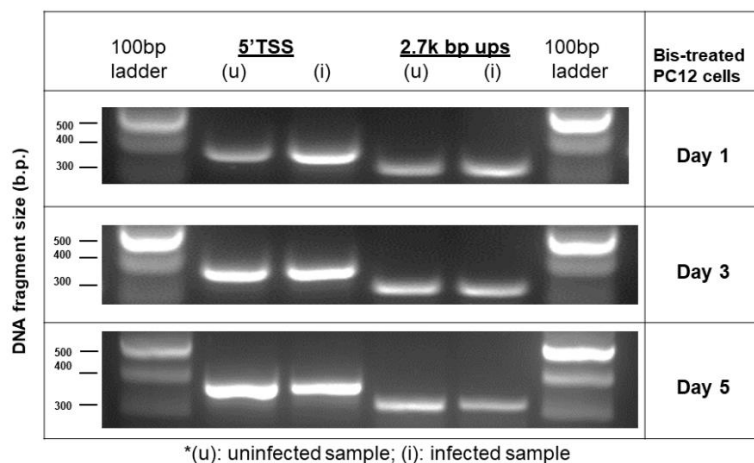


**Figure 2.12 PCR amplification of bisulphite-treated PC12 cell DNAs.** A single PCR amplification product was observed on agarose gel of each primer set for both regions; 5'TSS and 2.7k bp ups.

The PCR fragment bands were excised and extracted by a gel purification kit (Qiagen, Germany). Prior to ligation, gel-purified DNAs were run on a new agarose gel as a final confirmation for correct fragment amplification and extraction.

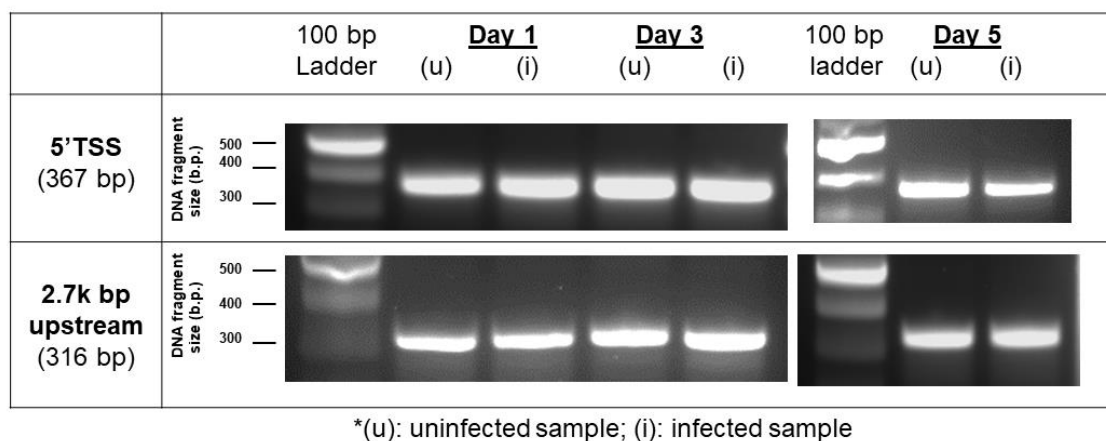


**Figure 2.13 Gel-purified DNA isolation from PCR amplification products of bisulphite-treated PC12 cells.**

### 2.4.8 Cloning procedure optimisation and plasmid digestion

TOPO TA cloning method required an optimisation to correctly insert the FOI into a cloning vector. The ligation of FOI into the TOPO 4 TA vector was done in insert:vector ratios of 1:20, 1:50, and 1:70. Successful ligation was determined by the percentage of correct fragment-insert by RE digestion enzyme analysis in the plasmid clones per total randomly acquired plasmid extracted. The insert:vector ratio of 1:50 worked with the highest number of fragment-inserted plasmids for the ligation step and was used for subsequent sample batches (Table 2.2). In addition, two PCR product purification techniques were implemented prior to vector ligation (using 1:20 insert ratio), which used the purified PCR product directly and used a purified gel-cut fragment from an agarose gel. The ligation step was done by directly using the purified PCR products as the ligation template, tested in parallel for both fragment regions; 2.7kb bp and 5'TSS (namely, Fragment 1 and Fragment 2, respectively). Fragment 1 showed a lower percentage of insert success rate (25–35%) compared to Fragment 2 (65–80%). Therefore, another trial was needed for Fragment 1 (new gDNA) by running the PCR product on agarose gel and the fragment of interest excised and purified. The insert success rate had increased to 56.5%. By increasing the insert:vector ratio to 1:50, the same fragment provided a 79% insert success rate. Hence, for this sample, the gel cut and extraction method was more effective and gave a better insert success rate. However, both methods worked with ligation into the TOPO vector.

**Table 2.2 Ligation and cloning optimisation.** Two techniques of ligation were implemented; by direct insert of PCR amplification products and, agarose gel cut and extraction prior to the ligation into the cloning vector. Ratios (insert:vector) of 1:20, 1:50 and 1:70 were tested to evaluate the successful rate. A clone with a correct insert denoted a successful ligation, analysed by EcoR I digestion analysis.

<b>Insert Ratio Ligation (insert:vector)</b>	<b>Successful rate (%)</b>	
1:20	<u><b>Direct insert of PCR product:</b></u> <b>Fragment 1:</b> Uninfected: 5/20 (25%) and infected: 7/20 (35%) <b>Fragment 2:</b> Uninfected: 13/20 (65%); infected: 16/20 (80%)	<u><b>Gel cut and extraction:</b></u> <b>Fragment 1 (2.7kb):</b> Uninfected: 13/23 (56.5%) and infected: 11/23: (47.83%)
1:50	19/24 (79%)	
1:70	5/24 (20.8%)	

\*Fragment 1 (2.7k bp region); Fragment 2 (5'TSS region)

#### 2.4.9 Screening plasmid inserts by EcoRI plasmid digestion

Table 2.3 shows the total number of clones containing both studied fragments of the DBH promoter gene from day 1, 3 and 5 post-infection samples. Randomly acquired clones were grown overnight in LB broth and extracted using a plasmid extraction kit. Thereafter, the plasmids were screened for fragment insert by EcoRI endonuclease restriction enzyme digestion.

**Table 2.3 Total number of colonies with the positive fragment inserted.**

Region	Sample	Day 1		Day 3		Day 5	
		+	-	+	-	+	-
5'TSS	Uninfected	21	9	22	4	32	10
	Infected	22	4	30	5	25	6
2.7k bp upstream	Uninfected	24	2	21	13	32	15
	Infected	22	4	24	2	23	44

\*The "+" denoted as correct FOI inserted and "-" denoted as negative FOI inserted by EcoRI endonuclease RE digestion analysis.

#### 2.4.9.1 Cloning plasmid of the 5'TSS DBH gene region

On day one, 26 colonies were randomly selected from LB agar plates of both infected and uninfected control samples (Table 2.3). An additional few colonies were picked and added after plasmid RE-digestion screening on uninfected control samples in order to acquire at least 20 plasmids with positive FOI insertion for sequencing, which provided 30 total extracted cloning plasmid samples. Meanwhile, the same concept was applied to another batch of samples on day three, in which 26 plasmids from uninfected control and 35 plasmids from infected plasmids were extracted. On day five, a total of 42 uninfected control plasmids and 31 infected plasmids were extracted with 32 and 25 plasmids, respectively, containing the FOI.

#### 2.4.9.2 Cloning plasmid of the 2.7k bp upstream region

As shown in Table 2.3, a total of 26 cloning plasmids containing the fragment from uninfected and infected cells on day one, and 34 uninfected and 26 infected positive plasmids on day three. Meanwhile, 47 uninfected control colonies and 67 infected colonies were extracted from day five samples in which there were 32 and 23 plasmids, respectively, with positive inserts. The higher number of plasmids extracted in this batch was due to the plasmid optimisation method described above.

#### **2.4.10 Bisulphite PCR-cloning sequencing**

Sequencing a CpG-containing region will help measure the methylation states of all the CpG sites within the region in which the distribution of methylation patterns can be observed. To determine the average cytosine methylation patterns in the DBH gene and the promoter regions, gDNAs were first subjected to the bisulphite treatment and PCR amplified using the G2 Hot Start DNA polymerase and the previously optimised primers. Each PCR product was cloned into a TOPO vector and an average of 20 randomly picked clones were sequenced. Sequence reading was done by using flanking sequencing primers M13F and M13R for the plasmid vector (Figure 2.5). Each fragment was inserted into a plasmid by either orientation. The sequencing process unexpectedly malfunctioned for the forward inserted sequence orientation (sense strand) for all plasmid samples with early termination; meanwhile, an optimal sequencing reading was obtained for the opposite orientation (antisense) of the inserted fragment in the plasmid vector. Surprisingly, the same reading patterns were observed for both studied regions. The reason for this is not clear, but it was suspected this was due to hairpin or secondary structure formation. Hence, only data with full fragment-covered sequencing readings were counted for DNA methylation pattern analysis. M13 primers reading were implemented for both directions to obtain at least one complete reading per sample. In addition, PCR bias produced by the difference in amplification efficiencies of sequences within a PCR process could skew the sequencing results. To avoid this PCR bias, an additional step, the cloning of the purified specific PCR products, was done prior to submitting the samples for bisulphite sequencing.

## 2.4.11 DNA methylation pattern analysis by bisulphite sequencing

Each of the eight CpG sites for both regions was analysed from sequencing data by comparing sequence output from at least 20 sequences of clone plasmids per sample. To calculate the conversion rate, the resulting clones from each bisulphite treatment were aligned and the converted cytosine nucleotides were counted. The fraction of converted cytosines to total cytosines before the treatment was calculated in percent as presented in the graph of Figure 2.14. The resulting percentage averages were referred to as DNA methylation haplotypes. The graph showed a four percent difference with 82% (SEM=1.53) of total methylated cytosines in the infected fragment versus 78% (SEM=1.28) of uninfected control from the overall total CpG sites on day one, 79% (SEM=1.34) infected versus 76% (SEM 1.18) control on day three, and on day five, 79% (SEM=0.28) control over 77% (SEM=0.29) infected.

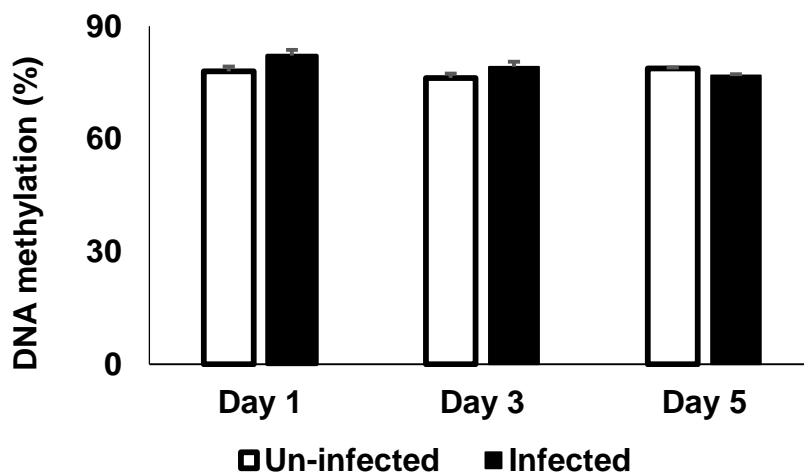


**Figure 2.14 Overall DNA methylation haplotypes (CpG 1 to CpG 8) at 5'TSS DBH gene of *T. gondii*-infected and uninfected control neural PC12 cells in a time-course on day 1, 3, and 5 post-infection as measured by cloning-PCR bisulphite sequencing analysis.** All mean  $\pm$ SEM shown is based on the total clones sequenced per sample ( $n \geq 20$ ). Data showed no statistical difference in uninfected and infected samples analysed by the two-way ANOVA statistical test,  $p > 0.05$  on day 1, 3, and 5 post-infection. The assay was analysed based on a single biological repeat.

Data in Table 2.4 shows the average methylation percentage of haplotypes of each CpG site (%) that was determined by the number of methylated sites per the total number of clones sequenced. The assay was analysed based on one biological repeat.

**Table 2.4 Average DNA methylation percentage of each haplotype samples.**

		CpG site							
		CpG 1	CpG 2	CpG 3	CpG 4	CpG 5	CpG 6	CpG 7	CpG 8
<b>DAY 1</b>	un-infected	19.05	61.90	71.43	76.19	100.00	100.00	95.24	100.00
	infected	0.00	90.48	90.48	95.24	100.00	95.24	95.24	90.48
<b>DAY 3</b>	un-infected	19.05	66.67	66.67	85.71	90.48	95.24	95.24	90.48
	infected	9.52	85.71	71.43	90.48	95.24	95.24	95.24	90.48
<b>DAY 5</b>	un-infected	15.00	80.00	75.00	75.00	95.00	95.00	100.00	95.00
	infected	10.00	65.00	80.00	85.00	90.00	95.00	100.00	90.00

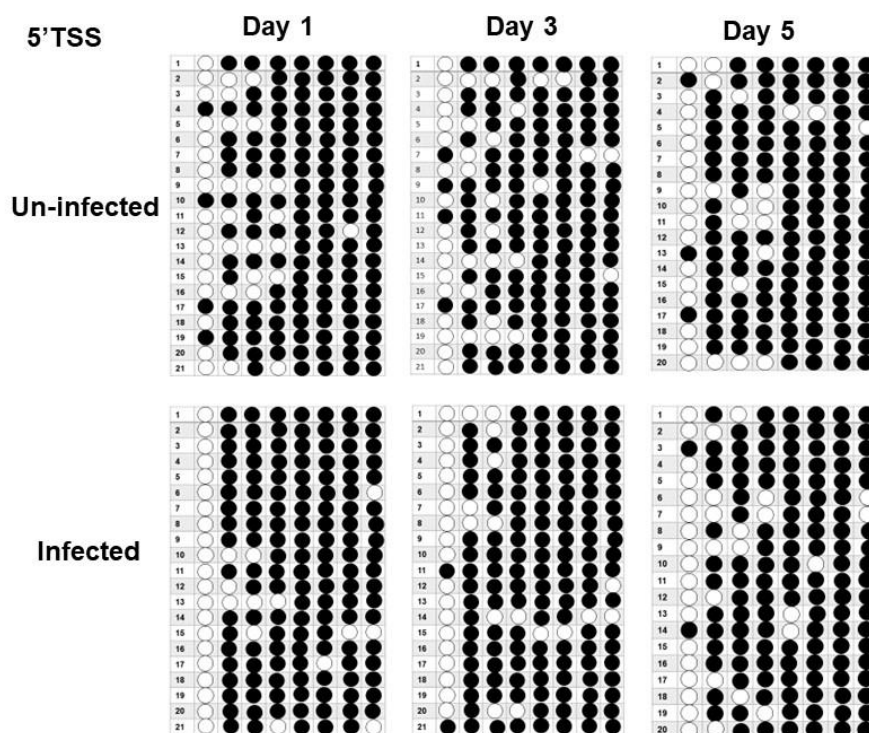


**Figure 2.15 Bisulphite sequencing profile of differential DNA methylation changes on individual CpG site at 5'TSS DBH gene region following *T. gondii* infection.** Each dot represents a single CpG site. Open circles indicate unmethylated CpGs and filled circles indicate methylated CpGs. Each column represents a single CpG site in the region of interest (a total of eight CpG sites were covered). Each box represents the day of post-infection sample harvest. Each horizontal row within each box represents a single sequenced clone (at least 20 clones for each sample).

Overall, high levels of basal methylation were shown in all of the CpGs sites studied except CpG 1 (column 1 within each box). A DNA methylation level at the promoter gene of 10–15% is expected for an expressed gene. In contrast, a high level of DNA methylation is normally associated with low levels of gene expression. Differential DNA methylation of the CpG 2 to CpG 4 sites in the infected samples were slightly higher than in the control. However, CpG 5 to CpG 8 sites showed no differential methylation changes between the infected and control samples. Hence, no substantial findings were observed.

Analysis of differential DNA methylation pattern changes at 2.7k bp upstream of the promoter is shown in Figure 2.16. A 6% reduction in overall DNA methylation was shown in infected samples compared to controls on day one post-infection with 82% infected and 88% control. Only 2% difference in differential methylation changes was observed in the infected sample on day three and 1% on day five over control samples. There were no significant changes in overall methylation pattern changes at 2.7k bp upstream of the proximal DBH promoter gene in *T. gondii*-infected cells analysed by bisulphite sequencing.

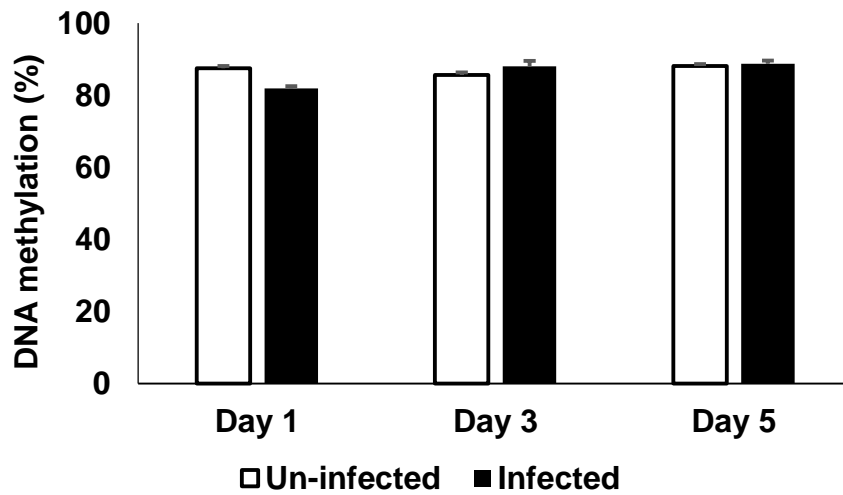


**Figure 2.16 Overall DNA methylation haplotypes at 2.7k bp upstream of DBH gene of *T. gondii*-infected and uninfected control neural PC12 cells days 1, 3, and 5 post-infection by cloning-PCR bisulphite sequencing analysis.** All mean  $\pm$ SEM shown is from the total clones sequenced per sample. Data showed no statistical difference in the uninfected and infected samples analysed by the two-way ANOVA statistical test,  $p > 0.05$  of day 1, 3, and 5 post-infection. The assay was analysed based on one biological repeat.

More data on CpG sites in this 2.7k bp upstream region is shown in Figure 2.17. Data in Table 2.5 shows the average percentage of haplotypes for each CpG site (%).

**Table 2.5 Average methylation percentage of each haplotype sample.**

		CpG site							
		CpG 1	CpG 2	CpG 3	CpG 4	CpG 5	CpG 6	CpG 7	CpG 8
<b>DAY 1</b>	un-infected	100.00	100.00	95.65	65.22	91.30	82.61	86.96	78.26
	infected	95.00	90.00	90.00	65.00	90.00	95.00	60.00	70.00
<b>DAY 3</b>	un-infected	95.00	95.00	95.00	65.00	100.00	100.00	75.00	60.00
	infected	100.00	100.00	100.00	91.30	100.00	100.00	95.65	17.39
<b>DAY 5</b>	un-infected	100.00	100.00	100.00	80.00	80.00	75.00	95.00	75.00
	infected	100.00	100.00	100.00	100.00	70.00	100.00	90.00	50.00

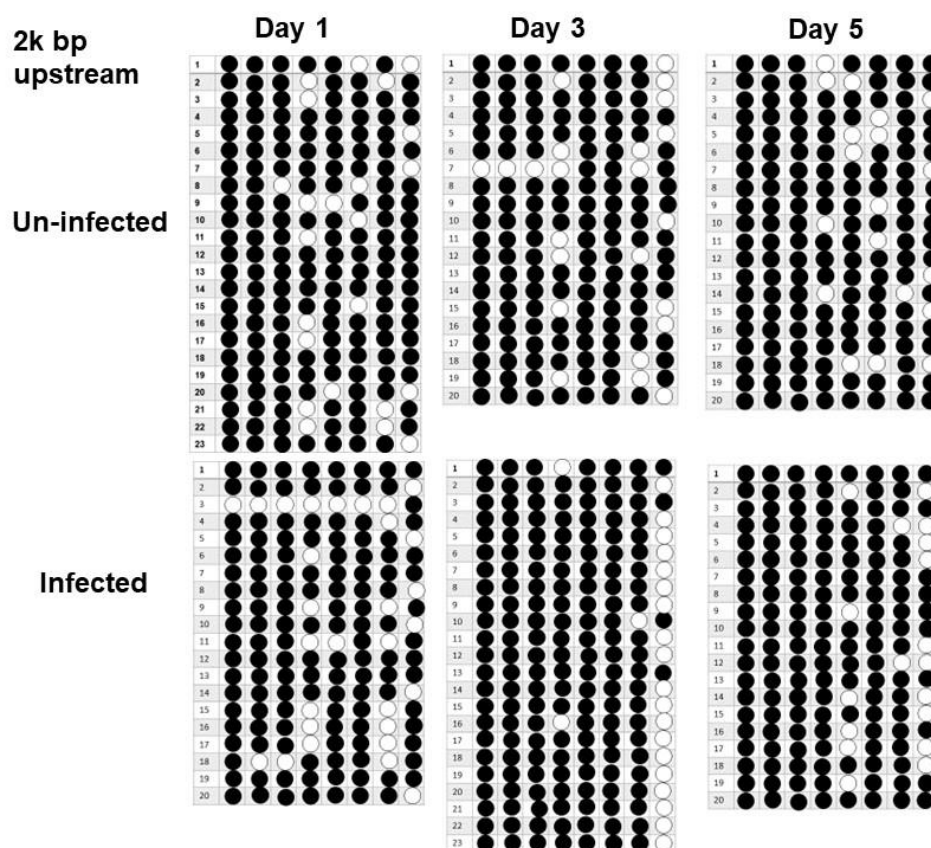


**Figure 2.17 Bisulphite sequencing profile of the differential DNA methylation changes on individual CpG sites at 2.7k bp upstream of the DBH promoter region following infection.** Each dot represents a single CpG site. Open circles indicate unmethylated CpGs and filled circles indicate methylated CpGs. Each column represents a single CpG site in the region of interest (total eight CpGs sites were covered). Each box represents the day of post-infection sample harvest. Each horizontal row within each box represents a single sequenced clone (at least 20 clones for each sample).

Overall, CpG sites 1 to 3 maintained methylated states in both infected and control samples. Interestingly, CpG 4 showed some differential changes over the time course of the infection with hypermethylation of the cytosine observed day three to day five post-infection. Meanwhile, CpG sites 5 to 7 showed unstable methylation changes over time. The CpG 8 had lost most of its methylated states on day three with an obvious 43% reduction, but it gained methylation back on day five. However, the methylation changes at these specific CpG sites shown in the data were still inconclusive in demonstrating a significant difference between the infected and control samples.

## 2.5 Discussion

The general consensus on DNA methylation is that it silences gene expression and even though it has long been considered a key gene expression regulator, not much is known about the precise mechanisms by which methylation status can modify gene expression. Studying DNA methylation, a prevalent epigenetic mark that can directly target DNA of a specific gene to regulate gene expression, is currently a topic of increasing interest. PCR-based methods permit detailed analysis of a specific region in the genome. Many studies have focused on CpG islands in the promoter region, known to consist of many CpG sites that are easy to detect and recognise. However, genes without CpG islands at their promoters, such as the DBH gene, have limited CpG sites, making measurement of methylated DNA more difficult. A MeDIP-qPCR assay was developed to give a detailed and specific view of DNA methylation patterns within a gene region by analysing the relative enrichment of methylated DNAs at a specific locus to that of the whole sample region. The MeDIP assay is based on affinity purification of methylated DNAs in a region, captured by an antibody binding directed against 5-mC. It has a profound sensitivity to methylated DNA. In the past few decades, however, bisulphite sequencing has emerged as the 'gold standard' technology for assessing DNA methylation and has been widely used as a targeted approach to investigating specific candidate regions of interest. Both assays were implemented in this methylation study.

Expression of the DBH gene is controlled by multiple regulatory interactions on gene sequences acting together to maintain the basal level of DBH transcription in noradrenergic cell types (Greco *et al.*, 1995). In the brain, DBH expression is restricted to specific regions, including the brain nucleus locus coeruleus, sympathetic ganglia and adrenal medulla (Greco *et al.*, 1995). Epigenetic alterations at the promoter loci encoding critical regulatory elements of gene expression may reduce or increase gene

transcription. The target region in this study is specific for the 5'TSS, the first exon and the upstream region of the proximal promoter gene. My earlier prediction was that DNA methylation at the 5'TSS and surrounding promoter regions could block the initiation of DBH gene transcript synthesis. This hypothesis is supported by many studies that found a strong correlation between hypermethylation at the surrounding 5'TSS gene site and transcriptional gene silencing (Brenet *et al.*, 2011; Jones, 2012; Ando *et al.*, 2019).

In this study, an increasing trend of DNA methylation levels, specifically surrounding the 5'TSS of the DBH gene in the infected host in response to chronic *T. gondii* infection, was observed, even though the data showed no significant changes between samples in the statistical tests. Generally, most CpG-poor promoters are reported to be methylated when the genes are not active (Schübeler, 2015). As the DBH promoter gene represented by this group is CpG-deficient, only a slight difference in the percent input between the infected samples and uninfected controls was detected in MeDIP result data. The DBH gene lacked CpG islands and the target study areas consisted of fewer CpG sites. This may have made it difficult to immunoprecipitate the gene. Further analysis of the downstream region of the 5'TSS Exon 1 gene by bisulphite sequencing assay also showed no significant alterations in DNA methylation. Thus, the low number of CpG sites may explain the negative MeDIP and bisulphite sequencing results. Indeed, in CpG-poor regions, both MeDIP-seq and MBDCap-seq (an assay that uses methyl-CpG-binding domain protein to capture methylated DNA in the genome) showed low statistical power to detect differentially-methylated regions (Robinson *et al.*, 2010; Yong *et al.*, 2016).

However, a clear trend towards increased DNA methylation in the 5'TSS region is noteworthy (Figure 2.9). The MeDIP assay demonstrated that DNA methylation increased two days post-infection and continued increasing until day five, the end of cell culture collection. This finding was consistent with previous data published by our group

which showed that DBH expression started decreasing after three days post-infection (Alsaady *et al.*, 2019). Hypermethylation may initiate DBH depression on the following day. However, the graphed data showed an outlier value for day three samples. In comparing the bisulphite sequencing analysis of the same studied region on day three, the DNA methylation percentage was found to increase in the infected sample (Figure 2.14). The lowest percent input values on day three for both infected and control samples in the MeDIP assay graph (Figure 2.9) suggest technical laboratory errors might have occurred during sample processing.

In the antibody-binding MeDIP assay, I could not identify which specific CpG sites were methylated and also, which of these specific sites could be associated with gene repression. The MeDIP assay can only measure all methylated DNAs in the studied region as a whole. Bisulphite sequencing offers a better resolution of the methylation status at a single nucleotide-level. Unfortunately, my bisulphite sequencing results also showed no difference between the average overall cytosine methylation in the infected neural cells and control samples in a time-course analysis following parasitic infection. The same methylation pattern was observed at the 2.7k bp sequences upstream of the DBH promoter gene, which suggests that this region may exert no repressive activity in DBH expression. Even analysis at each single CpG site resolution of the region did not reveal any substantial changes between the compared samples, as shown in the mapping of the CpG site profiles (Figures 2.15 and 2.17). Therefore, whether transcriptional repression relies on methylation at specific critical CpGs or on the overall level of promoter methylation remains uncertain, although it is known that promoter strength and methylation density do play some role in gene expression (Bird, 1992; Tate and Bird, 1993). In a promoter with rich-CpG sites or containing CpG islands, one methylation change at a CpG site may not contribute to any changes in gene transcription. Conversely, even a single methylated DNA change at CpG sites on a CpG-deficient promoter, which can be categorised as a weak promoter, could have major

consequences in gene expression (Bird, 1992). One such example was shown in studies where the methylation of a single site in a brain-derived neurotrophic factor exon promoter could silence the gene (Martinowich *et al.*, 2003). Moreover, it is also unclear if the methylation repression occurs in an all-or-none fashion at some critical methylation density and whether a half density of methylation can cause an intermediate level of gene repression.

One of the major assay-specific issues is that bisulphite sequencing cannot distinguish between 5-mC and 5-hmC, suggesting that methylated and hydroxymethylated regions of DNA may be underrepresented in this quantitative methylation analyses (Huang *et al.*, 2010). Thus, 5-hmCs may have been present in the genomic samples, which are possible since the 5-hmCs are abundantly found specifically in post-mitotic neurons (Kriaucionis and Heintz, 2009), although their potential function in gene regulation remains largely unknown. The 5-hmC mediated by TET proteins is a mechanism of non-passive DNA demethylation. Hence, bisulphite treatment methylation measurements for cells having high 5-hmC/5-mC will be unreliable, at least in certain genomic regions.

Collectively, one plausible explanation for the negative or weak findings in both assays is that the methylation does not appear to always be very specific in its suppression. The regions assessed in this study may not be involved in the repression; other locations in the promoter can exist since methylation can act in a distance-independent manner relative to the promoter of the gene sequences. There might be subtle changes in methylation that occur in regions that were not covered in this study, hence not detectable given my small target region size. Alternatively, the DBH gene may be represented as a strong promoter that can override the effect of methylation since most of the CpG haplotypes mapping were methylated, thus a small locus-specific comparison was not comparable (Figure 2.15 and 2.17). The molecular mechanism by which a strong promoter prevails over methylation is unknown. Another remarkable explanation for this

weak DNA methylation data finding suggests that the DBH gene was not active in the uninfected control cultures. Thus, it was necessary to repeat the DBH expression assay to check the capability of the control host PC12 cells to express the DBH gene at levels seen in previously published studies.

Not all methylation changes will elicit biological effects. It is possible that transcriptional repression does not require promoter DNA methylation. Transcriptional activity of some genes may be independent of DNA methylation status, although other genes are tightly regulated by it. Other genetic mechanisms may act in accordance with or independent with the methylation changes. Indeed, some studies showed that for some low CpG promoters, there was no significant correlation between gene activity and richness of methylated cytosines, wherein the majority of low CpG promoters are predominantly methylated in both active as well as inactive state regardless of the methylation status at the promoter CpG sites (Eckhardt *et al.*, 2006; Weber *et al.*, 2007). This hypermethylation does not preclude gene expression. Notably, several low CpG promoters were unmethylated, but still showed active gene expression. Due to limited changes in the percent input values observed, neither assay can significantly prove that DNA methylation plays a part in gene repression observed in *T. gondii* infection. Statistically insignificant changes may imply no impact on DBH expression in general. However, the increasing methylated DNA pattern change results may suggest a small contribution of DNA methylation in mediating DBH gene repression.

While there is evidence that *T. gondii* infection can cause epigenetic changes to host cell gene expression (Hari Dass and Vyas, 2014), it is not always clear whether the changes are directly induced by the parasite. Even with many epigenetic modulators well-characterised, the mechanism involved or molecules that initiate the changes and their origin are not known. Understanding the mechanisms by which DNA methylation targets specific regions of the genome and interpreted is of paramount importance. As the

ultimate effect of *T. gondii* infection is the initiation of behavioural changes, altering the DBH gene is a key control in neurotransmitter biosynthesis and metabolism. Once triggered, changes in DNA methylation can be self-perpetuating within the host cell. Thus, transiently altering the DNA methylation can trigger permanent effects on gene expression, in this case, downregulation of DBH expression that can lead to dopamine/norepinephrine dysregulation. This could explain the behavioural changes seen in the infected host (as described in Chapter 1), which are claimed to be consistently associated with the deposition of dopamine production.

## 2.6 Conclusion

The lack of changes in DNA methylation mediated by the *T. gondii* parasite shown in this study still provide a limited understanding of its significance and role in DBH gene repression. The data did not confirm our predictions, in which variable CpG methylation levels shown in both compared samples may be due to poor CpG density at this promoter gene. This, eventually, limited the outcome of this study. The DBH gene may not be over-expressed and is produced in a very small amount in the studied control neural cells, which could explain the lack of apparent effects observed specifically in DNA methylation pattern changes. However, it is also possible that the promoter CpG methylation may not be the dominant event that causes DBH gene transcriptional repression upon neural cell infection.

## Chapter 3

### Chromatin Modification Changes Coincident with DBH Gene Suppression in *T. gondii*-infected Neural PC12 Cells

#### 3.1 Overview

Previous work in this laboratory (Tedford, 2018) suggested dynamic DNA methylation occurs coincidentally with suppression of DBH gene expression in infected catecholamine-producing cells. In this chapter, a chromatin immunoprecipitation assay (ChIP) was developed to further investigate the mechanism in DBH gene suppression at the chromatin level. Changes in chromatin proteins and DNA methylation levels were compared. It was postulated that the small difference in DNA methylation changes in the DBH promoter gene (Chapter 2) may be due to the fact the cells have chromatin changes suppressing transcription that were not yet observable as changes in the DNA, since the gene expression can also be suppressed by chromatin (i.e. histone modifications) without changes in DNA methylation (Fuks *et al.*, 2001; Ting *et al.*, 2005). My finding in the ChIP-qPCR analysis revealed that dimethyl-histone H3 at lysine 9 (H3K9me2) protein binding at the 5'TSS DBH gene was increased three days after *T. gondii* infection. The ChIP analysis also showed the deposition of an enzyme that methylates CpG sites; DNA methyltransferase 3 alpha (DNMT3a) protein at the same locus was increased after 24-48 h post-infection. The DNMT3a is responsible for establishing genomic DNA methylation patterns which can lead to transcriptional gene silencing (TGS). It also has been shown to act as a transcriptional co-repressor required for the initiation of gene

silencing (Fuks *et al.*, 2001; Hawkins *et al.*, 2009). These findings suggest histone modification proteins and DNMT3a can initiate DBH chromatin condensation and transcriptional gene repression.

### **3.1.1 Repressive histone modification protein markers: Dimethyl-histone 3 lysine 9 (H3K9me2) and DNA methyltransferase 3 alpha (DNMT3a)**

The packaging of DNA into chromatin is recognised to be a major mechanism by which the access of genomic DNA is restricted, thereby regulating gene expression. Chromatin can be modified at both the histone and DNA levels with histone modification proteins controlling the chromatin structure and DNA packaging. Among histone modifications implicated in gene silencing is the methylation of H3K9, where one of its prominent roles include X-chromosome inactivation in females. The methylation of H3K9 was the first methyl-lysine residue characterised on histone proteins; the di- and tri-methylation of H3K9 (H3K9me2 and H3K9me3, respectively) are well-known hallmarks of heterochromatin (Rea *et al.*, 2000; Allis and Jenuwein, 2016). Histone modifications can act singly or in combination with other proteins to orchestrate the dynamic gene functions associated with chromatin and to mediate the chromatin structure changes controlling gene expression.

As DNA methylation is often found in conjunction with the H3K9 methyl mark, the relationship could suggest a direct interplay between histone and DNA methylation, which work in concert to repress gene transcription. The DNA methylation machinery includes the enzyme responsible for methylating DNA, DNMT3a. It is abundantly present in neurons and appears to be critical in maintaining their *de novo* dynamic DNA

methylation patterns (Goto *et al.*, 1994; Feng *et al.*, 2005). Even though there are two major DNA methyltransferases, DNMT3a and DNMT3b, studies found that CpG site-specific methylation is DNMT3a-dependent for certain genomic loci in *de novo* DNA methylation, although both major enzymes are known to methylate DNAs (Oka *et al.*, 2006). In addition, DNMT3a expression is ubiquitous which makes its detection much easier than DNMT3b, limited to low-level expression in most tissues (Xie *et al.*, 1999). Binding of DNMT3a at the locus site would imply a mechanism for the down-regulation of DBH gene expression. However, a role for DNA methylation in this process remains questionable due to inconclusive MeDIP and bisulphite sequencing data (Chapter 2) that failed to demonstrate the involvement of direct DNA methylation at this site. Thus, quantitation of the enzyme-binding levels that methylate these DNAs, as such DNMT3a, could give further information. As DNMT3a also associates with TGS and is needed in pre-initial starts of gene silencing, it is worth knowing its role in DBH down-regulation. The CHIP assay method was implemented for such aims.

### **3.1.2 Chromatin immunoprecipitation assay (ChIP)**

The use of the ChIP assay in discerning protein-DNA interactions has increased in recent years, allowing for the study of epigenetic markers and transcription factors binding DNA and by extension, gene regulation. The ChIP coupled with real-time qPCR has become the gold standard assay for chromatin organisation studies (Kuo and Allis, 1999; Nelson *et al.*, 2006; Dahl and Collas, 2008; Collas, 2010). In this chapter, I describe some ChIP method optimisations relevant to the current study. The original conventional ChIP protocol (Orlando *et al.*, 1997; Kuo and Allis, 1999) was amended to make the assay applicable for the extracted chromatin of rat PC12 cells. The procedure, briefly, consists of a formaldehyde crosslinking fixation step to fuse the DNA-protein interactions, followed by a series of cell lysis steps to extract the nuclear chromatin, then finally,

chromatin fragmentation by sonication prior to immunoprecipitation (IP) of the antibody-protein chromatin complexes (Figure 3.1). The formaldehyde-crosslink is then reversed and the immunoprecipitated bound-DNA is purified. Subsequently, downstream applications such as real-time qPCR are used to quantify the enrichment of the precipitated protein-binding relative to the total extracted protein DNA.

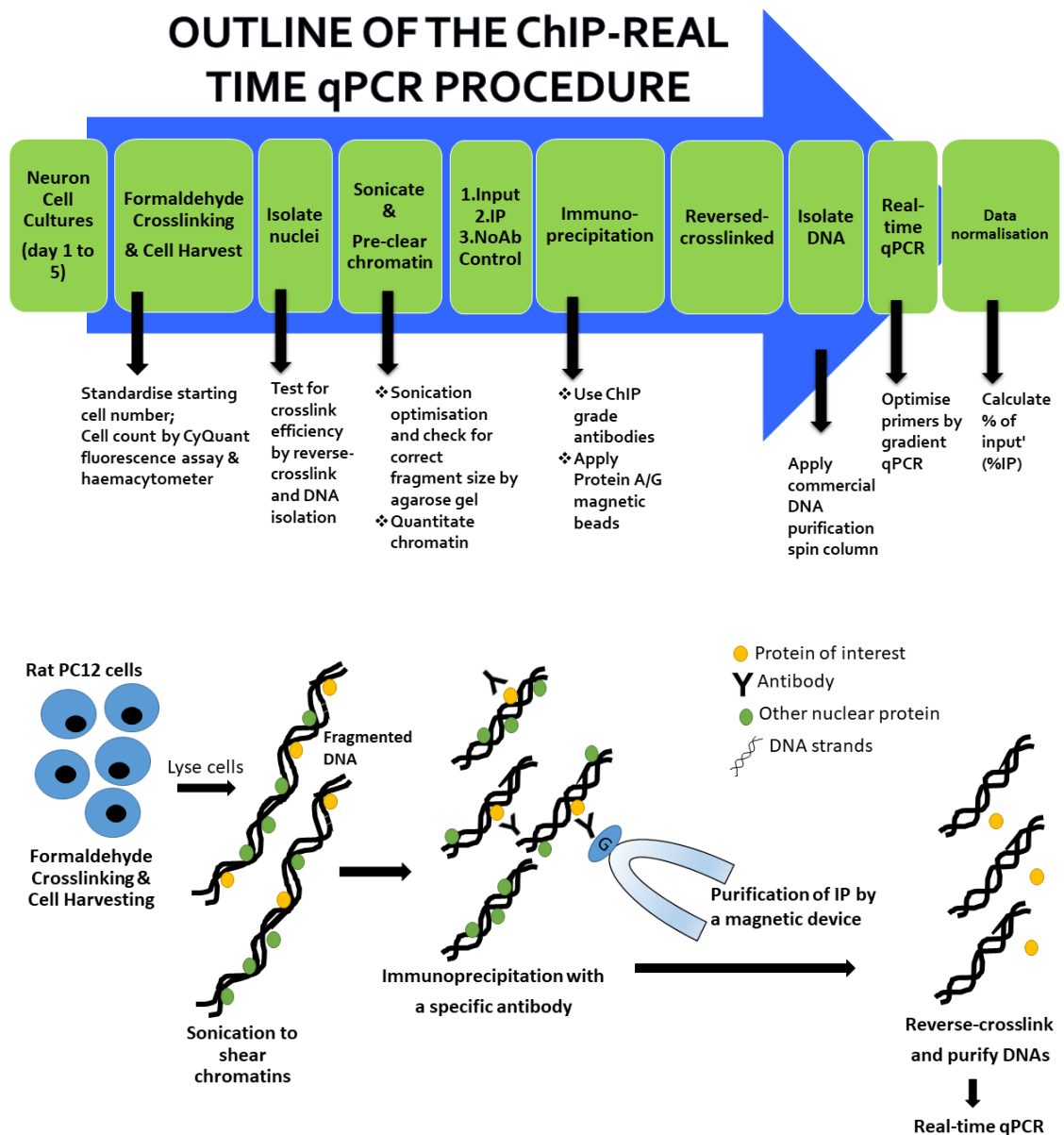


Figure 3.1 Outline of the CHIP-real time qPCR procedure.

## 3.2 Methods

### 3.2.1 Growth of host cells and parasites and induction of parasite conversion stage

As described in Chapter 2 (Sections 2.3.1 and 2.3.2), shocked and liberated type II Prugniard strain tachyzoites were prepared and used in this chapter. PC12 cells were infected with a parasite:cell of 1:1.

### 3.2.2 Cell harvesting and formaldehyde-crosslinking

A cell count was visually conducted using a haemocytometer. However, for an accurate measurement of cell number, important for sample standardisation in this time-course study, the CyQuant® Cell Proliferation Assay kit (Invitrogen, UK), a fluorescence-based assay, was also employed. The fluorescence assay was measured by the Polarstar Omega microplate reader (BMG Labtech, UK). PC12 cells at a density of  $5 \times 10^5$  cell/mL in 50 mL RPMI medium were cultured in a T175 (175 cm<sup>2</sup>) flask. While harvesting, four culture flasks were used per assay sample, two each for infected and uninfected cells. Samples were collected for five continuous days following *T. gondii* infection. The cell culture samples were pelleted by centrifugation for 10 min at 3250 x g (2500 rpm). Cross-linking was then allowed to proceed for 10 min at room temperature with 1% formaldehyde (in 10 mL phosphate buffer saline [PBS] solution, pH 7.4) and the process was stopped by the addition of 0.125 M glycine. After an additional 5 min incubation at room temperature, the cross-linked cells were collected by centrifugation for 10 min at 3250 x g (2500 rpm) and the cell pellet was rinsed twice with 10 mL PBS buffer. The cell pellets were stored at -80 °C.

### **3.2.3 Chromatin extraction and shearing**

The cell pellet was resuspended in 1.0 mL of ChIP lysis buffer (20 mM Tris HCl pH 8.0, 85 mM KCl, 0.5% Igepal CA-630) supplemented with a protease inhibitor cocktail (Roche, UK). The suspension was incubated for 10 min, then passed through a mixing needle (19 gauge) 20 times to break apart the clumped PC12 cells while keeping the nuclei mostly intact. The crude nuclear preparation was then collected by centrifugation at 8609 x g (10,000 rpm) for 5 min at 4 °C in a 2.0 mL microcentrifuge tube. The supernatant was removed and was resuspended by finger vortex in 350 µL nuclei lysis buffer (50 mM Tris HCl pH 8.0, 10 mM EDTA, 1% sodium dodecyl sulfate (SDS), and protease inhibitor cocktail). For the sonication step, the cell lysates were aliquoted into 0.2 mL tubes, 50 µL volume each, to meet the sonicator requirements. Sonication was performed for 5 min on the EpiSonic Multifunctional 1100 Bioprocessor (Epigentek, USA). The sonication conditions were optimised prior to the IP assay.

#### **3.2.3.1 Sonication optimisation for chromatin shearing**

The sonication time was determined by sonicating the cell lysate (formaldehyde-crosslinked), prepared as above, in a time-based manner. By choosing a constant amplitude of 17% (amplitude machine ranges from 1% to 20%, corresponding to average power delivery to the sample), the sample was sonicated for 10 sec on, 30 sec off for a total process time of 1 to 5 min. The chromatin sample was then reverse cross-linked with a concentrated salt solution containing 0.2 M NaCl, treated with 2 µL of Proteinase-K (20 mg/mL) and incubated overnight at 60 °C prior to gDNA extraction. The chromatin shearing performance was tested by loading the purified gDNAs onto 1% agarose gel to determine the fragment sizes for each sonicated-minute samples. The ideal fragment sizes range from 400 bp to 1000 bp, with the most fragments at 500 bp.

### **3.2.4 Evaluation of chromatin shearing performance via agarose gel electrophoresis**

Extracted gDNAs were loaded (1 µg of gDNAs per lane) in a 1% agarose gel (Bio-Rad Laboratories, USA) containing 0.5 µL/mL GelRed Nucleic Acid stain (Biotium, USA). A 2-log ladder (New England Biolabs, UK) was used for size comparison. Electrophoresis was performed at room temperature for 50 min at 75 volts. Gel images were captured by a gel imager (Syngene Ingenius Biolmaging, UK).

### **3.2.5 Chromatin immunoprecipitation**

Prior to IP reaction, the chromatin was diluted six-fold with ChIP dilution buffer (0.01% SDS, 1.1% Triton X-100, 1.1 mM EDTA, 20 mM Tris HCl pH 8.0 and 167 mM NaCl) which gave a total chromatin sample volume of 1.75 mL. The optimal amount of antibody needed depends upon the individual antibody used, as recommended by the manufacturer and published literature (typically 1–10 µg, diluted with PBS-Tween 20). The antibodies used were anti-DNMT3a antibody-ChIP grade ab2850 (Abcam, UK) and anti-histone H3 (di-methyl K9) antibody-ChIP grade ab194680 (Abcam, UK). At first, each specific antibody was added to the 500 µL chromatin sample (for each IP protein) and incubated overnight on a rotator at 4 °C. For an IP control, another 500 µL chromatin sample was incubated with rabbit anti-IgG (Sigma, USA). A pre-cleaned 50 µL (1.5 mg) of Dynabeads® Protein G magnetic beads (Life Technologies, UK) was added to collect the antibody-protein-DNA complex, then incubated for 4 h on a rotator at 4 °C. Pre-cleaned magnetic beads were used in order to minimise unspecific chromatin binding prior to the IP step. Then, a series of washing steps of the complex were done, starting with (1) low-salt buffer (0.1% SDS, 1% Triton X-100, 2 mM EDTA pH 8.0, 20 mM Tris-HCl pH 8.0 and 150 mM NaCl); (2) high-salt buffer (0.1% SDS, 1% Triton X-100, 2 mM

EDTA pH 8.0, 20 mM Tris-HCl pH 8.0 and 500 mM NaCl); (3) LiCl buffer (100 mM Tris pH 8.0, 500 mM LiCl, 1% NP-40 and 1% Deoxycholate); and then completed with three additional washes with (4) TE buffer (1 mM EDTA and 10 mM Tris-HCl pH 8.0). The protein complexes were separated by using a magnetic separation device.

### **3.2.6 DNA crosslinking reversal and isolation**

After IP, the protein-DNA was eluted from the magnetic beads by adding freshly prepared 25  $\mu$ L elution buffer (1% SDS and 0.1 M  $\text{NaHCO}_3$ ) and incubated at room temperature for 15 min with rotation. The supernatant was transferred into a new tube and the elution process was repeated once. The two supernatants were pooled, making the total volume 50  $\mu$ L. Thereafter, the pooled eluate was reverse formaldehyde-crosslinked in a high TES salt buffer consisting of 0.2 M NaCl, 50 mM Tris-HCl pH 8.0 and 10 mM EDTA. Then 2  $\mu$ L of Proteinase-K (20 mg/mL) was added and the samples incubated overnight at 60 °C on an incubator shaker in order to facilitate DNA release. The reverse formaldehyde-crosslinking step was done in combination with this Proteinase-K digestion step. To normalise the results, an Input volume (the chromatin without IP reaction) for each sample also was established. A 250  $\mu$ L from the total diluted chromatin was used for the Input (1% SDS in the TES buffer was added for reverse formaldehyde-crosslinking), which was processed afterward in parallel with the immunoprecipitated samples. On the following days, 2  $\mu$ L of RNAse A (10 mg/mL) was added and further incubated for 2.5 h at 50 °C on an incubator shaker. Afterward, the digested-chromatin was separated from the magnetic beads, and the eluted DNA was purified by using Zymo Chip DNA Clean and Concentrator extraction kit (Zymo Research, California) in accordance with the manufacturer's instructions. Additional washing steps were added to the column. The Inputs and CHIP DNAs were recovered with 30  $\mu$ L elution buffer and stored at -20 °C prior to further downstream tests.

### **3.2.7 Validation of the ChIP assay performance**

Before proceeding with the real-time qPCR, the immunoprecipitated products were validated to ensure that the protein-captured steps were successful. The extracted DNA of the precipitated samples were amplified using standard PCR in which 5'TSS DBH gene primer pairs were used (MeDIP primers in Chapter 2). The PCR products of both protein-bindings were loaded onto 1.5% agarose gel electrophoresis. The Input samples were used as controls.

### **3.2.8 Real-time qPCR and data analysis**

The real-time qPCR, data analysis were performed as stated in the previous chapter (Chapter 2; see MeDIP assay).

## **3.3 Results**

### **3.3.1 ChIP assay optimisation**

#### **3.3.1.1 Cell harvesting and formaldehyde cross-linking**

Several important measures were carefully considered while optimising the assay. A large culture density was used for sample collection to get a high chromatin yield and protein recovery. Based on the literature, at least  $1 \times 10^7$  cells are needed for an IP reaction. Prior to cell harvesting, formaldehyde-crosslinking was applied to the culture to bind the chromatin modification proteins to DNA. The duration of the formaldehyde-crosslinking is important as too little can result in inefficient crosslinking, while too much can result in difficulty lysing cells and shearing chromatin, thus reducing protein recovery. Therefore, the recommended 10 min standard time was used and I found it worked well for the rat PC12 cell line used in this study. However, a duration of 8 min was tested and can also be used without giving any noticeable change in the effects of the sonication process. The formaldehyde-crosslinking and glycine steps were performed in a conical Falcon tube rather than in the large culture flask for easy handling of the large cell culture volumes and also, to minimise using a large volume of the hazardous formaldehyde reagent. For chromatin extraction, I decided to increase the proportion of buffers used for the cell pellet to aid the chromatin extraction process. This is due to the large cell culture volume that was used in this study. Accumulation of very thick cell lysates derived from the large culture could hinder the nucleus release, as protein-DNA interaction occurs primarily in the nuclear compartment. Apart from that, since the concentration of the SDS in the buffers also influences the cell lysis and sonication process, three different buffers were implemented to assist in extracting the tight binding of the proteins-DNA

that is formed by formaldehyde-crosslinking, prior to the IP step. SDS is a detergent that helps in nuclear chromatin extraction but its presence would interfere with the IP steps. Diluting the chromatin with the ChIP dilution buffer prior to the precipitation process can reduce the SDS concentration. Furthermore, these implemented buffers allow for the recovery of cleaner nucleus lysate pellets that can improve the sonication process and chromatin release. Moreover, chromatin shearing is a key step to success in the following IP steps.

### **3.3.1.2 Determination of chromatin sonication time**

The sonication setting is highly variable depending on the type of sonicator used; thus, optimisation is needed to determine the ideal time to achieve DNAs with target lengths. The best workable fragment length is approximately 500 bp as fragments of such a small size can increase the antibody-binding specificity, thus facilitating the IP process. This study employed an EpiSonic multifunctional bioprocessor sonicator (Epigentek, USA) with a recirculating chiller embedded. This chiller provides a cold environment in the designated water bath for the sample at all times, specifically during the sonication process. In addition, a proper shearing method is acquired not only for each device but for each kind of cell, tissue, or gDNA. I tested the chromatin lysates from the PC12 cells for a duration of 1-5 min, sonicating for 6 to 30 cycles at high power. A 5-min sonication time worked best for this extracted chromatin. As shown in Figure 3.2, a 5-min sonication time was enough to shear the gDNA strands from the chromatin lysates into fragmented strands with an average length of 500 bp.

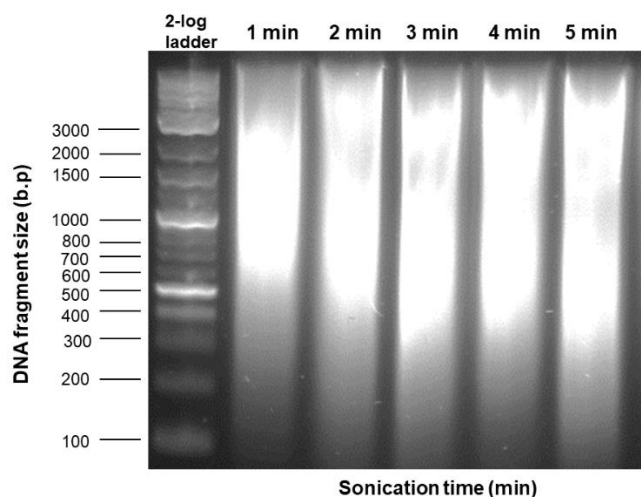


**Figure 3.2 Chromatin sonication time.** Chromatin extracted from PC12 cell lysates was sonicated in a time-based manner, from 1 to 5 min in a pattern of 10 sec on, 30 sec off with an amplitude of 17% using an EpiSonic multifunctional 1100 bioprocessor sonicator (Epigentek, USA) followed by reversal of formaldehyde crosslinking and DNA purification. The average suitable length for the ChIP assay, which is 500 bp fragmented DNA, was determined to be 5 min.

### 3.3.2 Optimisation and validation of the ChIP assay performance

The diluted sonicated chromatin was used for the IP assay in which two protein antibodies of interest, anti-DNMT3a and anti-H3K9me2, were tested. A range of chromatin volumes (standardised by the starting cell numbers) was tested to obtain positive protein bindings with an ideal antibody:chromatin ratio (data not shown). The manufacturer's suggested antibody concentrations were used as stated in the product sheet and published literature, where both commercial antibodies used were ChIP-grade quality (Abcam, UK). Negative control IP with rabbit anti-IgG antibody was at very low levels, confirming the specificity of these studied antibodies. Commercial magnetic bead complexes were used to facilitate protein separation by a magnetic technique which eases visibility. Magnetic beads eliminate the needed for centrifugation and thus can reduce the potential of sample loss and contamination compared to agarose beads used in the original ChIP protocol (Orlando *et al.*, 1997; Kuo and Allis, 1999), and offers highly reproducible results. However, agarose beads have a higher capacity for binding due to

their porous nature and thus higher surface area. The ChIP assay ended with DNA extraction of the bound immunoprecipitated DNA by a commercial spin-column DNA extraction kit that is specifically designed for the ChIP reaction. I used the spin-column for DNA recovery in the final IP step to minimise DNA loss from the minute precipitated proteins recovered. It also helps avoid phenol contamination in the end product if the phenol-chloroform extraction method is used beforehand as it is in the original ChIP protocol. Excess detergents in the buffers that can interfere with the downstream step in qPCR reaction could also be removed easily by the spin-column.

The positive bound-proteins were verified with a standard PCR amplification as shown in Figure 3.3. Gel electrophoresis analysis of both protein bindings confirmed the presence of a single fragment with the correct size (242 bp), indicating an optimised, working ChIP assay. This assay also managed to recover both of two DNA binding-proteins that were processed in parallel, originating from a single chromatin extraction of large-scale cell culture, thus saving processing time. The enrichment of each protein recovered from the same cell cultures can be compared.

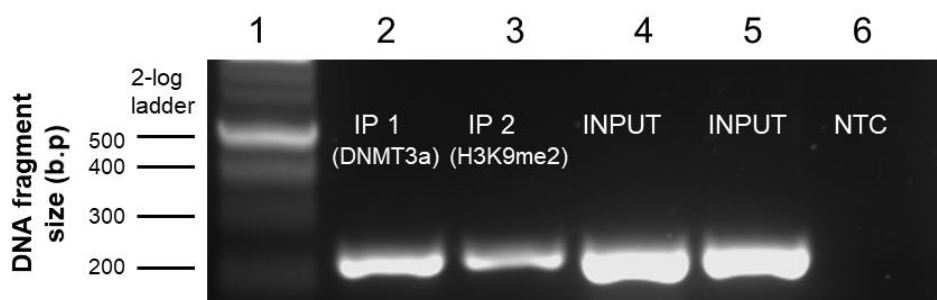


**Figure 3.3 A working ChIP assay for protein binding.** Immunoprecipitated DNAs from immunoprecipitation (IP) with DNMT3a and H3K9me2 antibodies and purified gDNAs were amplified by a standard PCR. The primer pairs of the 5'TSS DBH gene region were used with the expected PCR products at 242 bp in length. Lane 1: 2-log ladder (New England Biolabs, UK); Lanes 2 and 3: IPs of DNMT3a and H3K9me, respectively; Lanes 4 and 5: gDNA starting material from the two IP tests; Lane 6: no template control (NTC).

### 3.3.3 Summary of ChIP assay optimisation

In each ChIP assay step, a number of parameters were measured for optimisation as aforementioned and the optimal conditions summarised (Figure 3.4). The ChIP assay is amenable to variations in virtually every aspect of the assay, from the size of chromatin input, the time dedicated for IP, washing, elution, reverse cross-linked and Proteinase-K incubation to precipitate DNA recovery, which has made it a very complex and sensitive method. This study has tried to develop a simplified method that is shorter, uses a minimal amount of costly reagents and equipment, and provides a reduced potential for sample loss or contamination. Taken together, these considered measures have resulted in an improved and optimised ChIP assay that is suitable for rat dopaminergic neural PC12 cells and could also be implemented with other neural cell lines.

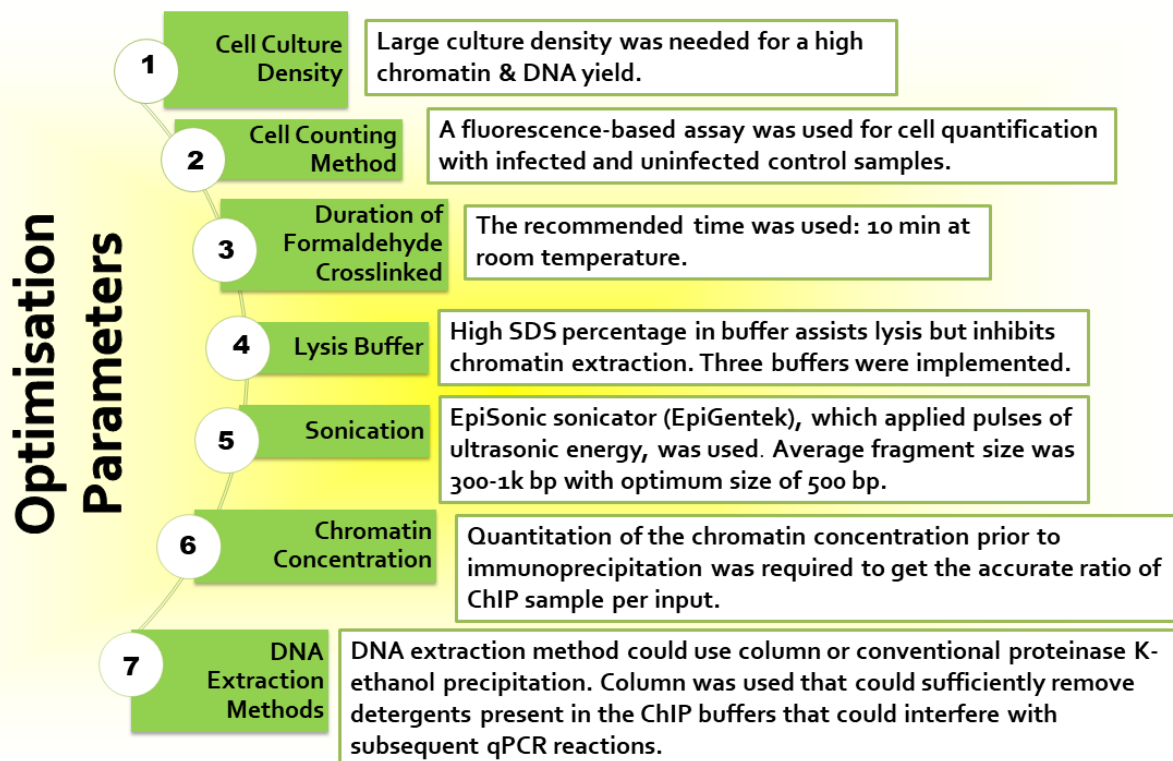


Figure 3.4 ChIP assay parameters optimised for rat neural PC12 cells.

### 3.3.4 ChIP real-time qPCR assay of *T. gondii*-infected PC12 cells

After obtaining an optimised and working ChIP protocol, the enrichment patterns of the DNMT3a enzyme and H3K9me2 histone modification protein in *T. gondii*-infected and control PC12 cells were quantitated and analysed by real-time qPCR.

#### 3.3.4.1 DNMT3a-ChIP protein-binding patterns in five days following *T. gondii* post-infection

Overall, the ChIP assay demonstrated small percent input values (0.08 – 0.58 %) of DNMT3a protein binding at the region immediately 5' of the DBH gene, thus suggesting low binding of this enzyme to the chromatin. On day 1, 0.58 percent input of infected sample versus 0.47 percent input control was observed, while 0.26 percent input in infected versus 0.09 percent input of control on day two, 0.25 percent input of control over 0.13 percent input of infected sample on day three, 0.10 percent input of infected over 0.08 over control on day four and 0.11 percent input of infected over 0.10 percent input sample on day five. As demonstrated, overall, the small values demonstrated no apparent changes between the infected and uninfected samples. However, during this time-course study, day two showed greater DNMT3a binding in the infected cell than the uninfected control at this site (Figure 3.5).

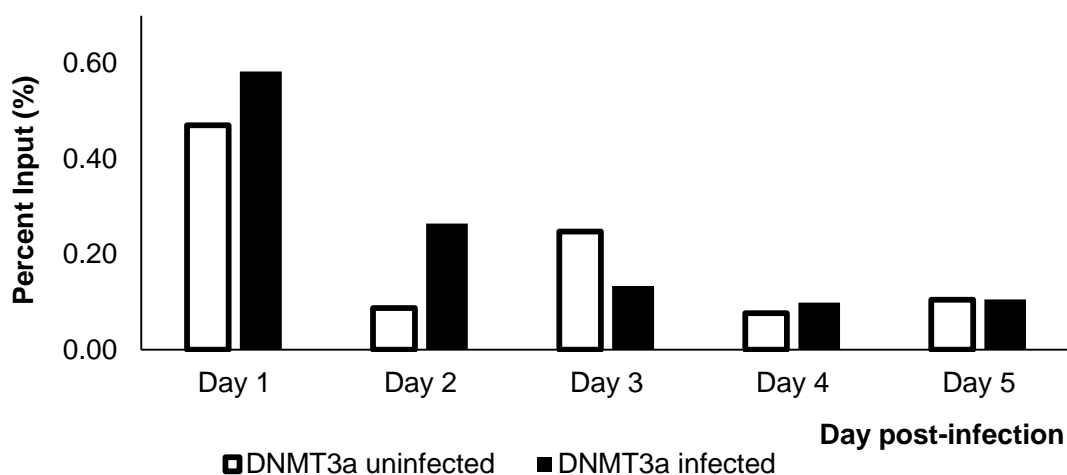


**Figure 3.5 ChIP analysis of DNMT3a binding at the 5'TSS of the DBH gene in *T. gondii*-infected PC12 cells.** A time course of infection (day 1 to day 5) was performed and DNMT3a binding at the 5'TSS of the DBH gene measured in the cells by immunoprecipitation and quantitated by real-time qPCR. On day two, levels in infected cells are three times greater than uninfected cells on the same day. The DNMT3a levels in infected and uninfected cells were comparable on all days except day two. The percent input values of the protein bindings (500  $\mu$ L starting volume) were negligible compared to the total starting chromatin input (250  $\mu$ L starting volume). A single biological repeat is shown with duplicate technical repeats in the ChIP test. Statistical test could not be made due to uncompleted triplicate data values that was required to generate an acceptable statistical test.

Binding of DNMT3a at a region 2.7k bp upstream of the DBH gene was also measured (Figure 3.6). Daily samples beginning only at day three of infection were analysed as a preliminary evaluation of this region a few days post-infection plus with time limitation. The protocol was modified to use Magna ChIP™ Protein A+G magnetic beads (EMD Millipore, USA) to increase the protein-antibody binding. Protein G has the best affinity for a range of antibody, and experiments comparing protein A, G, and A/G magnetic bead blends revealed that a combination of both protein A and G beads worked and had higher sensitivity and recovery, improving signal-to-noise ratios (Sikes *et al.*, 2009). Interestingly, the levels of DNMT3a bound were increased 1.6-fold at day three (5.5 % uninfected and 9.2 % infected), 14.5-fold on day four (0.6 % uninfected and 8.7 % infected) and 1.8-fold on day five (3.2 % uninfected and 5.8 % infected) although these experiments need more biological repeats to verify the findings.

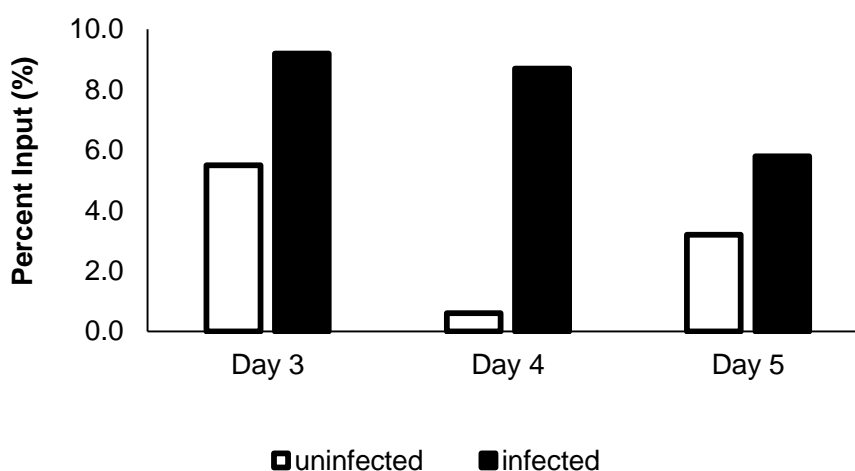


**Figure 3.6** ChIP assay for DNMT3a binding 2.7k bp upstream of rat proximal promoter DBH gene. A bar graph of DNMT3a binding for days 3-5 post-infection comparing infected and parallel uninfected cultures. ChIP and real-time qPCR were applied. Higher amounts of DNMT3a protein was bound at all infected time points. Bar graph data shows a single independent IP experiment with duplicate technical repeats in the qPCR. Statistical test could not be made due to uncompleted triplicate data values that was required to generate an acceptable statistical test.

### 3.3.4.2 ChIP analysis of H3K9me2 in chromatin associated with the DBH gene following *T. gondii* infection

A time-course analysis for H3K9me2 histone protein modification was also performed with infected cultures and showed changed levels at the 5'TSS DBH gene in infected cells, suggesting a role for chromatin modifications in the suppression of DBH gene expression during parasitic infections (Figure 3.7). Not surprisingly, the amount bound of this histone marker overall was higher than the DNMT3a enzyme (in Figure 3.5). Over the course of the infection, the H3K9me2 mark increased on day three onwards post-infection. On day three, H3K9me2 increased 1.9-fold with infection, 1.6-fold on day four, and the highest percent input value on day five, which showed a 3.8-fold increase. This analysis should be subject to more biological repeats.

Unfortunately, due to time constraints, the 2.7k bp region was not examined for H3K9me2 binding.

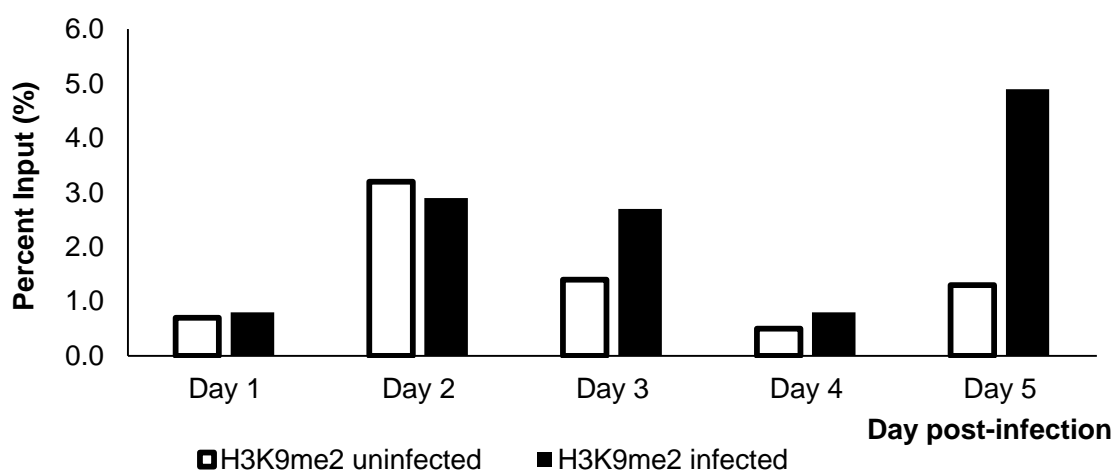


**Figure 3.7 ChIP analysis of H3K9me2 protein-binding patterns at the 5' promoter of the DBH gene in *T. gondii*-infected PC12 cells.** A time course of infection with daily time points was performed and H3K9me2 levels adjacent to the DBH gene monitored by ChIP and real-time qPCR. A bar graph of the data shows a pattern of increasing H3K9me2 mark with infection compared to controls. Graphed data showed one independent IP experiment with duplicate technical repeats in the qPCR. Statistical test could not be made due to uncompleted triplicate data values required for a statistical test.

### 3.4 Discussion

A major goal of the ongoing work was to understand the underlying mechanisms of chromatin complex assembly at a single gene locus. Hence, the ChIP assay provides fundamental insights into where and when regulatory factors bind to the DNA template. The development of experimental strategies to achieve these goals requires a more comprehensive understanding of how the procedures were performed and can be fully optimised to obtain true snapshots of the chromatin states. Certainly, it is evident that variations in protocols can yield different interpretations. All modifications and optimisation in each step of the ChIP assay implemented in this study were described in detail in the Results section. The optimised ChIP assay successfully immunoprecipitated and PCR-amplified both the studied proteins, DNMT3a and H3K9me2, isolated from the extracted chromatin of rat neural PC12 cell line. Henceforward, this working assay could be implemented on other histone modification proteins.

This is the first study to characterise the epigenetic modification changes; including the DNA methylation catalyser, DNMT3a, and histone lysine modification, H3K9me2, at the rat DBH promoter gene, analysed by the ChIP assay. The ChIP assay analysis produced incremental DNMT3a and H3K9me2 protein levels upon *T. gondii* infection, suggesting their role in modulating DBH gene transcription activity. This study postulated that there was involvement of epigenetic factors in regulating DBH gene expression; they could act as main regulators that reduce endogenous DBH mRNA expression levels upon infection.

The ChIP analysis of the 5' region of the DBH gene showed that level of DNMT3a, which is responsible for *de novo* methylation, in infected cells were higher than in uninfected cells at day one and day two. This is in accordance with Chapter 2 results that DNA

methylation pattern was higher in infected sample at the 5'TSS DBH gene 48 hours following infection. In one possible pathway, DNA methylation is the first event that initiates the repression resulting in modification of the histone terminal tails forming a silenced chromatin (Jones *et al.*, 1998; Nan *et al.*, 1998; Schübeler *et al.*, 2000). However, the ChIP data showed that the DNMT3a level in the infected sample on day three was less than uninfected control as compared to day one and day two which showed infected samples with greater percent inputs than uninfected controls (Figure 3.5). These results could be due to DNMT3a finishing its methylation catalysis and leaving the DBH gene or technical reasons regarding the minute amounts of precipitated-bound proteins captured by the ChIP assay and the low enzyme expression level. Meanwhile, analysis of the 2.7k bp upstream region of the DBH gene demonstrated an increased pattern of DNMT3a binding at the locus from day three onwards (samples on day one and day two were not collected due to time limitation). As DNA methylation in this 2.7 kb upstream region was not observable (Chapter 2), re-evaluating the bisulphite sequencing finding at this site is recommended for further investigation.

Meanwhile, in a second possible mechanism, the DNA methylation might not be required for gene silencing at all, or could take place as a secondary event after the chromatin has been silenced, where it is involved mainly for maintaining the inactive chromatin state (Fuks *et al.*, 2001; Bird, 2002; Mutskov and Felsenfeld, 2004). DNMT3a was reported can be targeted to specific regulatory loci through its association with DNA-binding transcription factors. Increasingly studies have claimed that DNMT3a can operate to depress transcription independently of its *de novo* methylation activity (Fuks *et al.*, 2001; Weinberg and Morris, 2013); this could provide an explanation for the apparent contradiction between the data on DNA methylation in Chapter 2 and the data in this chapter. DNMT3a has also been reported to interact with non-coding RNAs to regulate transcription (Holz-Schietinger and Reich, 2012; Miller *et al.*, 2012). Increasing evidence suggests that it is required for small and long non-coding RNA-directed TGS in

human cells (Weinberg *et al.*, 2006; Hawkins *et al.*, 2009; Morris, 2009). However, the site-specific recruitment of DNA methyltransferases on genes and thereby targeted *de novo* promoter hypermethylation (to promote transcriptional repression) is the most commonly reported mechanism in the published literature (Bird and Wolffe, 1999; Stirzaker *et al.*, 2004; Hervouet *et al.*, 2009). Even though a trend of increased DNMT3a and H3K9me2 with infection was observed in these ChIP analyses, this experiment requires more than one replicate.

Meanwhile, an increase of the repressive histone modification mark, H3K9me2, with infection was also observed in this study. The ChIP assay revealed that H3K9me2 could specifically bind to the 5'TSS region of the DBH gene (Figure 3.7). The increasing histone marker in the infected cells compared to control suggests an epigenetic mechanism that could be induced by the parasite. This histone protein-binding is postulated to be able to promote a repressed chromatin structure, forming a heterochromatin state, and thereafter hindering transcription factor binding to the DBH promoter via inaccessibility to the transcriptional machinery and subsequent shut down of the gene transcription. An important role for H3K9me2 in mediating gene repression is well-established (Grewal and Moazed, 2003; Stewart *et al.*, 2005; Mozzetta *et al.*, 2014; Weinberg and Morris, 2016). Direct H3K9me2-binding to the locus site results in chromatin structure changes that create a compact chromatin that does not permit transcription. It is thought that methyl-K9 facilitates the formation of heterochromatin whereas histone deacetylation is required for the repressive function of dimethyl-K9 (Stewart *et al.*, 2005). Also, another study reported dimethylation of H3K9 creates a high-affinity binding site for the heterochromatin protein HP1, an essential component of heterochromatin formation state (Lachner *et al.*, 2001). Similarly, it was recently reported that *T. gondii*-induced host chromatin remodelling at a STAT1-regulated gene led to the unresponsiveness of infected macrophages to IFN- $\gamma$ , a cytokine crucial for controlling parasite replication (Lang *et al.*, 2012). The study showed that epigenetic alterations can be implemented by

this parasite in its host cell, whether it was used to evade the host immune system, adapt to a new niche, reproduce or manipulate the host brain.

Remarkably, ChIP data showed that the H3K9me2 protein level started to increase on day three post-infection, by comparing day one and day two which demonstrated less protein-binding in the infected samples (Figure 3.7), signifying its binding to the locus site in an ordered manner after DNMT3a protein-binding and DNA methylation at the DNA locus site. Although it is still too early to predict, the data may suggest that the methylation-dependent repression of DBH gene activity influenced the assembly of chromatin proteins to the locus site, initiated by the invading parasite to the host cell. How the protein-binding was attracted to the site remains unclear, although the effector proteins secreted by the parasite could play a role. However, due to practical constraints, this ChIP assay data was produced by only a single biological replicate and demonstrated minimal changes with no substantial difference between the compared samples. Thus, the reported changes in the histone modification protein-binding cannot be definitively credited. Furthermore, the current study has only examined one repressive histone protein mark. The involvement of other chromatin modification proteins needs to be assessed by the ChIP assay. Therefore, the precise sequence of events in the mechanism of DBH gene repression remains unknown.

Accumulating evidence suggests that an epigenetic cross-talk, the interplay between DNA methylation and histone modification proteins, may be involved in the process of gene transcription and aberrant gene silencing. However, the ChIP analysis in this study could not observe any direct interaction between the DNMT3a enzyme and the histone protein-binding at the 5'TSS DBH gene. This time-course analysis gave a too broad prediction with wide observation windows, thus limiting observation of more direct interactions and alterations of both protein-bindings. Further follow-up experiments utilising an hourly time-course may be preferable. Nevertheless, this study demonstrated

an increased level of DNMT3a on day one to day two, while the dimethylation of H3K9me2 occurred on day three. Direct interaction of both protein bindings on day two to day three could possibly take place at the locus site.

Of note, repressive effect has been reported by the trimethylation of H3K9 (Bulut-Karslioglu *et al.*, 2014; Becker *et al.*, 2016) instead of the dimethylation to detect significant changes in values for the ChIP assay. As this study used an antibody that was specific to the H3K9me2 protein, the influence of H3K9me3 proteins was not evaluated. Thus, it is possible that the H3K9me3 contributes jointly with H3K9me2 in silencing the DBH gene. Hence, a more repressive effect could be observed in the ChIP analysis. The interplay among these two distinct modification states is currently poorly understood in the literature. However, both histone modifications are reported to correlate with heterochromatin and gene silencing. Even though H3K9me2 and H3K9me3 modify the same amino acid residue (lysine 9), the trimethyl modification of H3K9 is not built upon the dimethyl modification as the H3K9 demonstrates independent acquisition to the targeted site, exhibits divergent localisation and requires different histone methyltransferases (Rice *et al.*, 2003; Bessler *et al.*, 2010). Furthermore, the trimethylated H3K9, but not the dimethylated H3K9 was shown to mark chromatin regions for cytosine methylation in *Neurospora crassa* fungi (Tamaru *et al.*, 2003). Thus, different protein antibody-binding is needed to capture the protein-binding at the studied region for more clarification. However, it is possible that the modified protein works singly as well as in combination to mediate the distinct associated functions.

The weak histone protein-binding pattern changes observed in the infected cells may only denote a normal state of the dynamic changes of histone protein-bindings at a specific locus site. The presence of certain protein modifications may not indicate a unique regulatory status (that is, 'on' or 'off') against the gene expression. However, further experiments are needed for a clear interpretation. Almost all of the current

knowledge supports the idea that there is an accumulation of effector protein repressive complexes at the specific locus site that play a role in controlling gene expression. It is believed that they act in concert to regulate the transcription of a gene. Alterations in the chromatin modification proteins are highly associated with chromatin remodelling; changes in the chromatin structures will affect which genes are expressed in the cell genome.

### 3.5 Conclusion

Studying protein-binding interactions and epigenetic protein changes in the parasite-host relationship may facilitate a renewed approach to deal with parasite infection. The present study was designed to determine the involvement of the repressive histone protein modification marker, H3K9me2, in the downregulation of DBH gene expression in the infected rat neural PC12 cell. The implemented ChIP assay successfully showed that the H3K9me2 protein-binding was increased in a time-based manner upon *T. gondii* infection. Meanwhile, the level of DNMT3a enzyme was increased at the beginning of parasite infection, and thereafter maintained the same level as the controls. Both pattern changes might have been involved in the DBH gene repression upon *T. gondii* infection. Hence, this study has provided the first insight into the regulation of H3K9me2 and DNMT3a protein at the DBH gene upon *T. gondii* infection. However, more studies are needed to characterise the complete set of factors that affect gene transcription to gain a better understanding of the mechanisms underlying epigenetic DBH gene regulations.

## Chapter 4

### Assessing DBH Gene Expression in PC12 Cell Lines Used for Chromatin Studies

#### 4.1 Overview

Based on the high basal level of DNA methylation found for the upstream DBH gene region (Chapter 2) in the uninfected PC12 cells used and the minimal change in histone modifications with infection measured by ChIP (Chapter 3), we felt that it would be reasonable to screen the expression of dopamine (DA) and norepinephrine (NE) in the cell stocks that were used. As several prior published studies (Prandovszky *et al.*, 2011; Martin *et al.*, 2015; Alsaady *et al.*, 2019) and two PhD theses (Al-Saady, 2016; Tedford, 2018) in this laboratory had used these cells, we had assumed that the expression of DA and NE would demonstrate the same expression levels as previously observed. Therefore, for thoroughness of this PhD study, I reassessed and determined their expression levels by repeating a gene expression assay evaluating the transcriptional activity of mRNA dopamine  $\beta$ -hydroxylase (DBH) gene in the rat neural PC12 cells in response to *T. gondii* infection, as published previously by this laboratory (Alsaady *et al.*, 2019). As expected from my earlier findings (Chapters 2 and 3), only minimal changes were found in DBH gene expression after *T. gondii* infection over a time course qPCR analysis. The parasites were confirmed viable by an increase in BAG1 and Toxo-actin over time. Catecholamines measurement by HPLC-ECD showed DA biosynthesis but low NE production in the uninfected control cells, indicating low DBH expression, as DBH

is the enzyme responsible for converting DA into NE. Low expression of the DBH gene in uninfected control cells overlaid the observed outcomes in these epigenetic modification assays studying transcriptional DBH gene silencing in parasite-infected cells.

#### **4.2 *Toxoplasma gondii* induces DBH down-regulation at the transcriptional level**

Expression of the gene encoding the neurotransmitter biosynthetic enzyme DBH is regulated in tissue-specific patterns, in, among others, noradrenergic and adrenergic brain cells. Transcription of the DBH gene is influenced by environmental stimuli including parasitic infections. Alterations in DBH expression have been implicated in the pathogenesis of cardiovascular and neuropsychiatric disorders such as hypertension (Chen *et al.*, 2010), major depression (Cubells *et al.*, 2002), Parkinson's disease (Healy *et al.*, 2004), and Alzheimer's disease (Combarros *et al.*, 2010; Mustapic *et al.*, 2013), which is potentially connected to changes in central catecholamine levels. The rat neural PC12 cell line is derived from the rat adrenal gland. These cells are capable of producing and releasing catecholamines, including DA and NE, and their catalyser, DBH. Thus, it has been commonly used in neurobiological and neurochemical studies to create artificial nervous system tissue models in brain function studies.

It is currently unknown whether infection by the intracellular *T. gondii* parasite, specifically the chronic bradyzoite stage that resides in neuron cells, is able to modulate host gene regulation. Localised within host cells, the parasites have a chance to directly interfere with the host genome and manipulate gene transcription. As brain cells act as major regulators of human body systems controlling all aspects of memory, cognition, movement, and emotion, any system aberration may interrupt normal regulation of

cellular and physiological functions. Even if only a single gene is forced to be over-expressed or depressed in a normal cell, it may cause chaos in the synapses and receptor networks. Indeed, many infections result in differential host gene expressions, especially those involved in stress responses or inflammation which can lead to changes in the expression of specific genes, such as shown in the *T. gondii* infection. The infection causes changes in host transcript expression, such as that of chemokines, cytokines, extracellular matrices, and growth factors that regulate various cell functions. Some host gene expression changes are often organism-specific, suggesting that these effects are orchestrated by the invading organism. Our group previously found that gene expression of mRNA DBH was specifically depressed following *T. gondii* infection, in parallel with a decline of NE in the brain of the infected hosts, both *in vivo* and *in vitro* (Alsaady *et al.*, 2019). The decreased NE was suspected of having an association with DBH suppression.

#### **4.2.1 DBH catalyses the synthesis of norepinephrine from dopamine**

Classified as catecholamines, monoamines containing a catechol group, DA and NE are the principal neurotransmitters localised in discrete brain regions that play essential roles and mediate a variety of CNS functions such as movement control, emotional cognition, memory processing, and endocrine modulation in the brain. Central nervous system catecholamine is synthesized from the amino acid tyrosine, which is actively transported from the liver to the brain. The biosynthetic pathway (Figure 4.1) is catalysed by the consecutive action of four enzymes: tyrosine hydroxylase (TH), aromatic amino acid decarboxylase (AADC), dopamine  $\beta$ -hydroxylase (DBH), and phenylethanolamine N-methyltransferase (PNMT). Tyrosine hydroxylase is the initial and rate-limiting enzyme in the pathway which converts tyrosine to L-dopa, which in turn is acted upon by AADC for rapid conversion to dopamine. Norepinephrine is then produced from DA by

hydroxylation of DBH and finally, in adrenergic neurons in the peripheral system, NE is methylated by PNMT to produce epinephrine (Hoyle *et al.*, 1994; Daubner *et al.*, 2011).

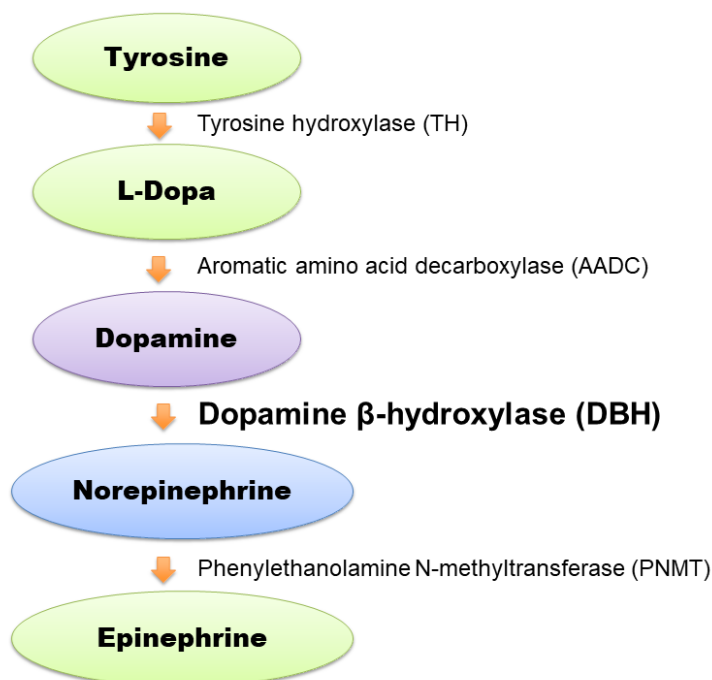


**Figure 4.1 The biosynthetic pathway of catecholamine neurotransmitters.**

As DBH is the final enzyme in NE biosynthesis in the noradrenergic nerve endings of the central and peripheral nervous systems, alteration of its transcription and expression will affect the ratio of DA/NE levels in the synapses. This provides a reasonable explanation for increased DA levels and a corresponding decrease in NE levels shown in chronic *T. gondii* infection (Alsaady *et al.*, 2019). This gene suppression demonstrates the capability of this intracellular parasite to modulate host genomic functions that may lead to neuronal alterations. To further explore this, I repeated the DBH gene expression assay, focusing on the intensity of mRNA expression following multiplicity of infection (MOI) by the shocked liberated tachyzoite *T. gondii* in infected PC12 cells. The gene expression was evaluated in a time-course manner to observe any pattern changes. The assay served as a control to check PC12 cells' capability to produce the same catecholamine secretion properties reported in earlier works.

## **4.3 Method**

### **4.3.1 Cell plating and harvesting**

PC12 cells were standardised to a total of  $2.0 \times 10^5$  cell in 2.0 mL completed RPMI medium ( $1.0 \times 10^5$  cell/mL) for each well in a 6-well plate. The cells were infected with parasites in a ratio based manner, by MOI, with parasite:cell ratios of 1:1, 2:1, 3:1, 4:1, and 5:1 and a range of parasite numbers from  $2.0 \times 10^5$  to  $1.0 \times 10^6$  per assay. Another plate of cells was prepared for the uninfected control. Meanwhile, another set of cells was prepared for day-based culturing, where the cell cultures were harvested on days 1, 3, and 5. This cell batch was infected with 1:1 ratio of parasite:cell. The assay plates were incubated in 5% CO<sub>2</sub> incubator at 37 °C for five days post-infection. The cell growth was monitored by microscopy on each day. For harvesting, the cells were removed with a scraper and pelleted by centrifugation at 3250 x g (2500 rpm) for 10 min. Cell pellet was lysed in 300 µL TRI reagent (Sigma, USA) and was stored in -80 °C freezer or proceeded with RNA extraction.

### **4.3.2 Column RNA extraction and DNase treatment**

RNA extraction was done by Direct-zol™ RNA MiniPrep Plus kit (Zymo Research, USA) according to the manufacturer's instruction. Briefly, a prepared resuspended pellet of cells dissolved in 300 µL TRI reagent was mixed with an equal volume ethanol (95–100%) and directly applied to Zymo-Spin column in a collection tube. The column was centrifuged at 16,000 x g for 30 sec. The flow-through was discarded. The column was then washed with 400 µL RNA wash buffer. The removal of co-purified contaminating DNA through DNase I treatment was done twice with 15 min incubation in the column by adding 5 µL DNase I (6 U/µL) with 75 µL DNA digestion buffer and then incubated for 15

min at room temperature. Thereafter, the column was washed two times with 400  $\mu$ L Direct-zol™ RNA PreWash and one time with 700  $\mu$ L RNA Wash Buffer. Finally, the binding-RNA in the column was eluted with 40  $\mu$ L DNase/RNase-free water. The concentrations of extracted RNA was measured with the NanoDrop spectrophotometer (Thermo Fisher Scientific, USA).

### **4.3.3 Reverse-Transcriptase cDNA synthesis**

The eluted RNAs were converted into first strand cDNA using using Maxima H Minus First strand cDNA synthesis kit (Thermo Scientific, USA) according to the manufacturer's protocol. A total of 150 ng RNA was used per 20  $\mu$ L reaction for each sample mixtures containing oligo (dT)18 primers, dNTP mix, 5X RT buffer, and Maxima H Minus Enzyme mix. The reaction mixtures were incubated for 10 min at 25 °C followed by 30 min at 50 °C, 20 min at 65 °C, and terminated at 85 °C for 5 min. The reverse transcription reaction products were 20 times diluted with DNase/RNase free water and 1  $\mu$ L of each was directly used for RT-qPCR per 25  $\mu$ L reaction volume. Control reactions, RT negative and no template controls, were included for verification of cDNA synthesis.

### **4.3.4 RT-qPCR**

The product of first strand cDNA synthesis reaction was directly used for qPCR reactions. The qPCR was performed in a Bio-Rad CFX thermocycler (Bio-Rad Technologies, California) in triplicate per sample reaction. GAPDH was used as a control reference gene. For each reaction, a qPCR reaction mixture was made as follows: 12.5  $\mu$ L Brilliant III Ultra-Fast SYBR® Green qPCR master mix (Agilent Technology), 1  $\mu$ L 200 nM forward primer, 1  $\mu$ L 200 nM reverse primer, 1  $\mu$ L template DNA, and 9.5  $\mu$ L DNase/RNase-free water were added for a total volume of 25  $\mu$ L. The primer pairs used

were as follows: the rat DBH gene primers, forward: 5'-CCACAATCCACGGAATATACAAG-3' and reverse: 5'-GATGCCTGCCTCATTGGG-3'; and the rat GAPDH gene primers pair, forward: 5'-GTGGACCTCATGGCCTACAT-3' and reverse: 5'-TGTGAGGGAGATGCTCAGTG-3'. The rat GAPDH was used as reference gene for the qPCR reaction to normalised the rat DBH gene expression. Another two primer pairs used were rat BAG1 gene primers, forward: 5'-TCCGCCGGGAGCTTGTCCACC-3' and reverse: 5'-GCAAGTCAGCCAAATTAATCA-3', and Toxo-actin gene primers, forward: 5'-CGAGCTGGTCAGTTCCTCAT-3' and reversed: 5'-CATCGGGCAATTCATAGGAC-3'. The qPCR plate was incubated in a G1000 Thermal cycler (Bio-Rad Laboratories, California) at 95 °C for 5 min, followed by 40 cycles of 95 °C for 15 sec, 55 °C for 15 sec, and 60 °C for 45 sec, and ended with melting curve analysis. Both sets of primer pairs used the same  $T_a=55$  °C. Data analysis was calculated by implementing  $-\Delta Cq$  method ( $\Delta Cq = Cq_{\text{sample}} - Cq_{\text{GAPDH}}$ ). The  $\Delta Cq$  was the difference in Cq values, between Cq sample and Cq reference gene (GAPDH) by which the average of  $Cq_{\text{GAPDH}}$  was subtracted from the average  $Cq_{\text{sample}}$ .

#### **4.3.5 Analysis of catecholamines secretion by HPLC-ECD**

For total DA and NE measurements, the PC12 cell cultures were counted and harvested by microcentrifugation at 5510 x g (8,000 rpm) for 1 min and rinsed once with 1.0 mL phosphate buffer saline (PBS). Thereafter, it was re-pelleted with centrifugation prior to a lysing step by 20 sec sonication in 200  $\mu$ L 0.1 M perchlorate. Finally, the lysates were centrifuged at 14,549 x g (13,000 rpm) at 4 °C for 20 min to remove all cell debris. Supernatants were taken for HPLC-ECD for neurotransmitters measurement. Reverse phase chromatography, combined with electrochemical detection (HPLC-ED) was performed with a Dionex HPLC system consisting of a P580 Pump (Dionex, USA) and Ultimate 3000 Autosampler Column Compartment (Thermo Fisher Scientific, USA). The mobile phase consists of 43 mM sodium acetate trihydrate, 0.1 mM sodium EDTA, 57

mM anhydrous citric acid, 1 mM sodium octane-1-sulphonate monohydrate and 10% methanol where the pH was adjusted to 4.0. The mobile phase was delivered at a flow rate of 0.8 mL/min, and the column temperature was set at 40 °C. Applied standards (norepinephrine and dopamine) were dissolved in 0.1 M perchlorate for chromatography. The peaks were observed using Chromeleon software.

## 4.4 Results

### 4.4.1 Minimal changes in mRNA DBH expression during *T. gondii* infection in the rat PC12 cells

A plot of the relationship between the number of parasites and the reduction in DBH mRNA expression (Figure 4.2) shows DBH expression in neural PC12 cells were unaffected by an increasing number of parasites. These observations demonstrate that DBH was expressed equally in the neural PC12 cells regardless of the degree of parasitic infection. However, it was clear that all of the infected cells showed a minimal amount of repression of DBH gene expression compared to the control cells.

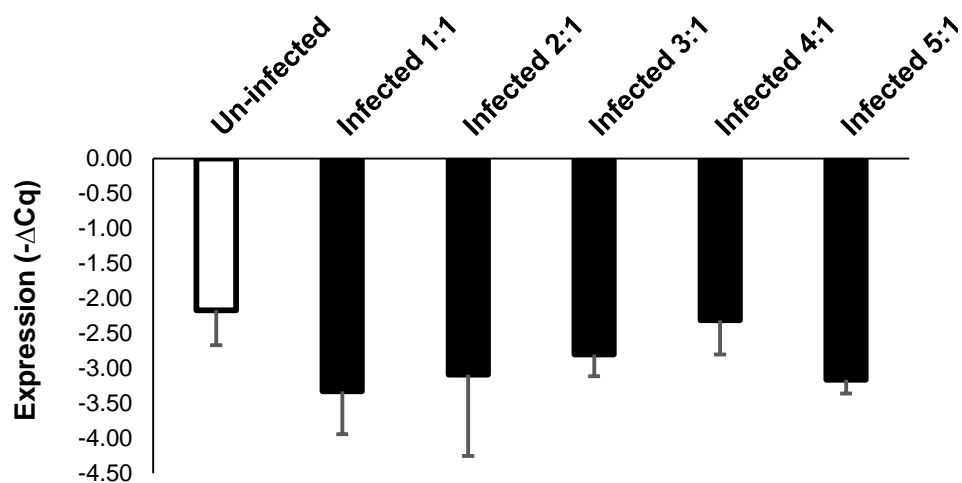


**Figure 4.2** Plot showing DBH gene expression in MOI of *T. gondii*-infected PC12 cells with respect to the housekeeping gene, rat GAPDH, on day five post-infection, analysed by RT-qPCR. The PC12 cells were infected with MOI of bradyzoite-induced *T. gondii* (parasite: cell in 1:1 to 1:5 ratios), and the RNAs were collected on day five. The experiment was done in three independent biological repeats (with triplicate technical repeats in RT-qPCR). Mean  $\pm$ SEM values are shown. One-way ANOVA was performed to measure significant differences between the samples ( $p > 0.05$ ;  $n=3$ ).

Although not statistically significant based on variability between biological repeats (one-way ANOVA;  $p > 0.05$ ), DBH gene expression values were downregulated at least 1.5-fold in all of the infected cells compared to the control. Detail data calculation and analysis in Appendix B.

Further evaluation of DBH gene expression in the time course samples infected with a parasite:cell ratio of 1:1 (Figure 4.3) showed minimal changes in gene expression between infected and control samples for each day. The cells showed a slightly depressed DBH expression pattern from day 1 to day 5; however, the change was not supported by statistical testing ( $p > 0.05$ ). Detail data calculation and analysis in Appendix B.

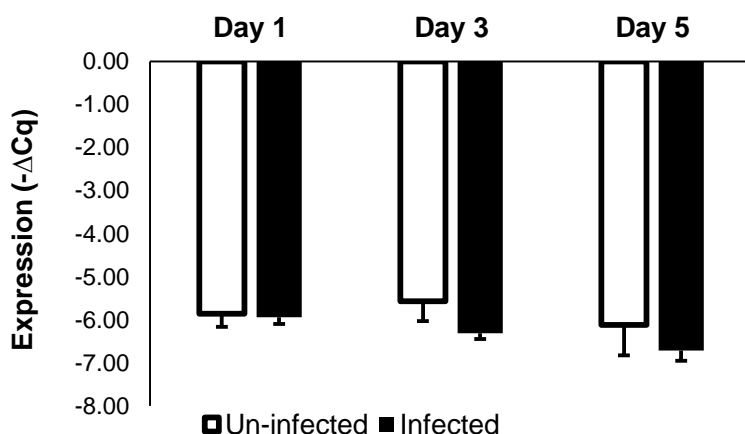


**Figure 4.3** Plot showing DBH gene expression of *T. gondii*-infected PC12 cells with respect to the housekeeping gene rat GAPDH at 1, 3, and 5 days post-infection, analysed by RT-qPCR. The PC12 cells were infected with bradyzoite-induced *T. gondii*, and the RNAs were collected at 0, 3, and 5 days post-infection. The experiment was done in three independent biological repeats (with triplicate technical repeats in RT-qPCR). Mean  $\pm$ SEM values are shown. Two-way ANOVA was performed to measure the significant differences between ( $p > 0.05$ ) and within samples from day 1 to day 5 ( $p > 0.05$ ). MOI=1; n=3.

To confirm that there were live parasites in the samples, *T. gondii* BAG1 and actin gene expression were also evaluated in the infected samples, analysed by RT-qPCR. The BAG1 gene is a stage marker for bradyzoites and the actin gene is a parasite marker for gene expression of both *T. gondii* stages (bradyzoite and tachyzoite). The level of parasite gene expression was compared relative to rat GAPDH expression. Figure 4.4 shows that both genes were expressed in the infected samples, indicating the presence of live *T. gondii* parasites in the host cells. The increase in expression relative to host cell number monitored by rat GAPDH expression from day one to day five post-infection suggests that both genes were increasingly expressed over time with an increase of approximately four-fold. More parasites were therefore assumed to be present in day five samples than day one although it is unclear why there is no increase from day three to day five. Detail data calculation and analysis in Appendix B.

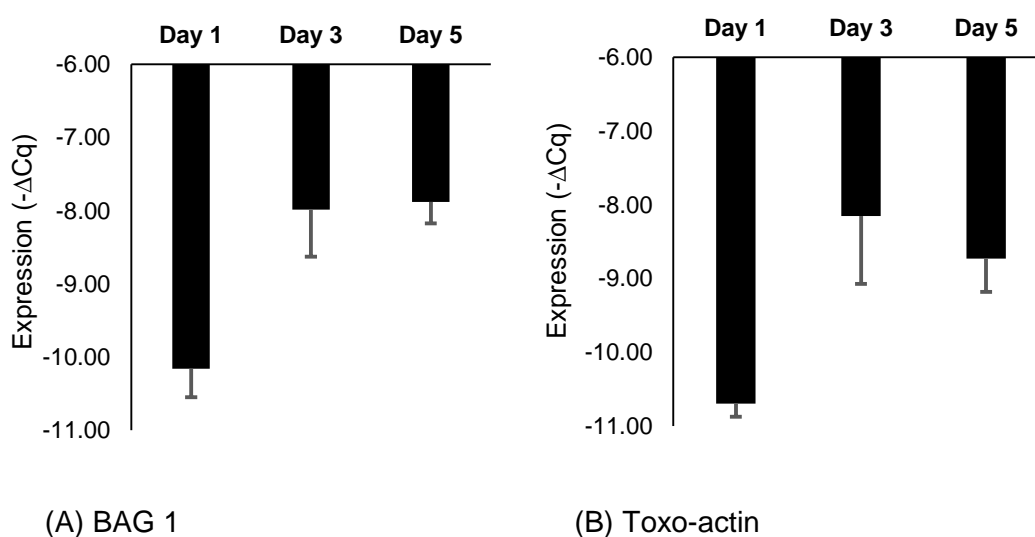
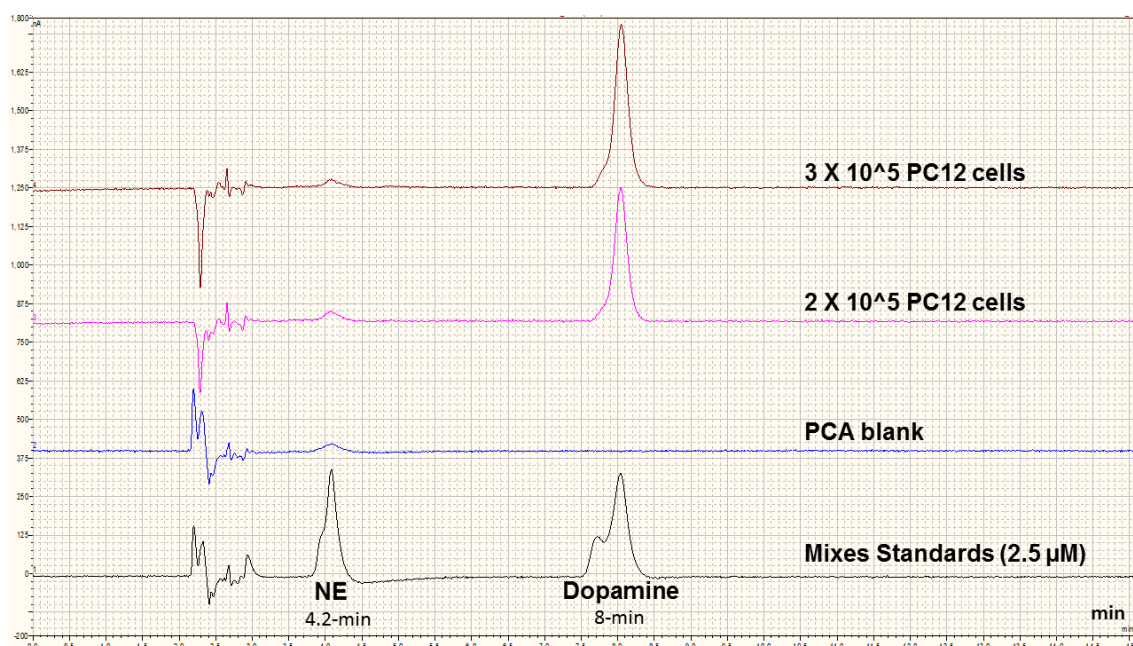


**Figure 4.4 BAG1 and Toxo-actin gene expression relative to rat GAPDH expression in *T. gondii*-infected PC12 cells at 1, 3, and 5 days post-infection, analysed by RT-qPCR.** (A) BAG1 gene expression for bradyzoite chronic stage detection. The gene expression increased from day 1 to day 5. One-way ANOVA was performed to measure the significant differences between samples ( $p = 0.066$ ) (B) Toxo-actin gene expression for parasite detection. The gene expression was increased over time from day 1 to day 5. One-way ANOVA was performed to measure the significant differences between samples ( $p = 0.111$ ;  $p > 0.05$ ). All data represent two independent biological repeats for both genes (with triplicate technical repeats in qPCR). Error bars are shown. MOI=1; n=2.

These observations have verified my predictions that the PC12 cells might not produce enough DBH to signify genuine repression effects by the parasite obtained in our earlier work. Nevertheless, PC12 cells clearly demonstrated a slight but consistent change in DBH gene downregulation upon infection.

#### **4.4.2 Reduced catecholamine secretion by rat PC12 cells**

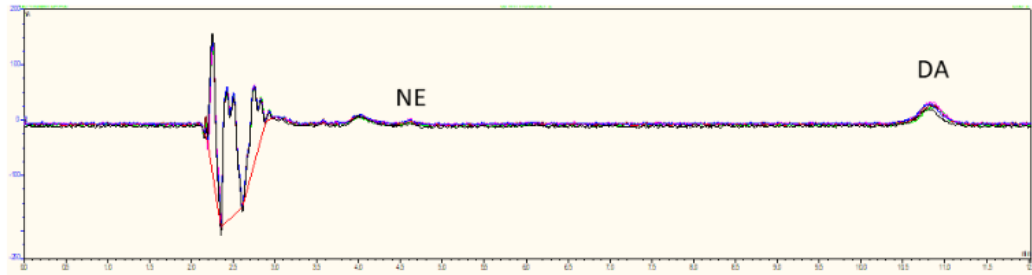
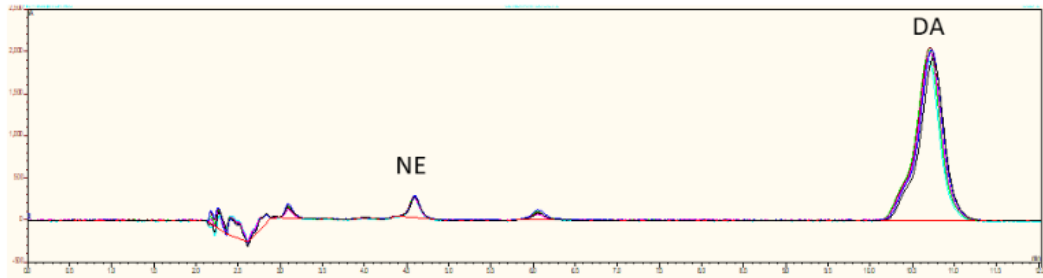
Catecholamine release by the PC12 cell line was analysed by HPLC-ECD (Dionex Thermo Fisher Scientific, USA). The chromatogram in Figure 4.5 shows that the uninfected control PC12 cells were still producing and releasing total DA, detected at min-8 relative to the beginning of electrochemical detection. However, there was no peak detected in the chromatogram for NE at min-4.2, suggesting very little NE was released by the cells. Thus, it can be proposed that there may be no or little DBH released by the PC12 cells since DBH is the rate-limiting enzyme in converting DA into NE.



**Figure 4.5 Catecholamines released from rat neural PC12 cells, detected by HPLC-ECD.** A total of  $2 \times 10^5$  and  $3 \times 10^5$  PC12 cells were harvested, and the catecholamines released were measured. Both cell samples showed an increase in total dopamine (DA) released (peak at minute 8) with increasing cell numbers. However, no norepinephrine (NE) peaks were observed at minute 4.2. Two catecholamine standards ( $2.5 \mu\text{M}$ , NE and DA), were used as neurotransmitter peak references (black line) and perchloric acid (PCA) was used as a blank (background) sample (blue line).

#### 4.4.2.1 Variability of the PC12 cell lines between cell batches

For quality control, several batches of the PC12 cells that had been stored in liquid nitrogen were analysed. There was a variability of the cells' capability to produce DA and NE (Figure 4.6). Quality checks prior to epigenetic assays of each batch of the PC12 cell line used is necessary to validate research findings.

**Batch A****Batch B**

**Figure 4.6** Examples of HPLC chromatogram of different PC12 cell batches (A and B). Batch A shows a reduction in DA and NE release whereas Batch B shows normal PC12 cell DA (41.0 ng per  $1.0 \times 10^5$  cells) and NE (6.15 ng per  $1.0 \times 10^5$  cells) secretion.

## 4.5 Discussion

The noradrenergic PC12 cell line was originally established from an adrenal medulla tumour in a rat (*Rattus norvegicus*) (Greene and Tischler, 1976) that have been used in thousands of published studies as model neurons for studying neurotransmission and neurological diseases. The rat neural PC12 cells closely resemble neurons with some characteristics of nerve cells, thereby creating an artificial neuronal environment for the parasite; the neuron is well-documented as the most favourable spot for developing a chronic infection. In addition, PC12 cells are capable of synthesising, storing, and secreting catecholamines, specifically DA and NE, thus making it particularly relevant to study DBH gene expression and catecholamine biosynthesis. Meanwhile, DA biosynthesis pathway alterations accompanying *T. gondii* infection are well-documented to strongly associate with neurobehavioral changes associated with toxoplasmosis.

The expression of mRNA DBH showed only slight changes between infected and control cells, regardless of parasite load that may be explained by the low level of NE being produced. With little DBH expressed, there is very little to be suppressed. This fits well with the observation of a 1.5 fold decrease in DBH gene expression with infection in this study (Figure 4.2) when prior published work from our laboratory found parasites significantly down-regulated DBH gene expression greater than 8-fold (Alsaady *et al.*, 2019). The low level of DBH expression in the cells used in this study may explain the high background of DNA methylation observed in the DBH upstream/promoter region (Chapter 2). The minimal downregulation of DBH expression with infection is also consistent with the small change in modified histones H3K9me2 and DNMT3a binding to the DBH gene (Chapter 3). Changes in NE expression may be due to selective pressures stimulated in the culture environment and genetic instability mediated by continuous culturing and passaging, as stated by the European Collection of Authenticated Cell Cultures (ECACC). Thus, it is possible that the changes in phenotype

and genotype of cells have altered its ability to produce certain proteins, and in this case, lower DBH expression. Quality control of the cell line used thus becomes of utmost importance for this research study.

## 4.6 Conclusion

The capability of the rat PC12 cell line used in this study to express the DBH gene has probably been lost during the extended period of *in vitro* culture or due to the original cell line stored for a long period in liquid nitrogen. These unanticipated observations cannot confirm the results obtained from this work. However, they may explain negative bisulphite sequencing data and weak outcomes in the MeDIP and CHIP assay. Although it was clear that the cells were still producing DBH, and regardless of its low expression, downregulation of gene transcription post-infection was still observed.

## Chapter 5

### Antisense Long Non-coding RNA (lncRNA) Involvement in Post-infection DBH Gene Regulation

#### 5.1 Overview

Numerous studies have proposed functional roles for short miRNAs in *T. gondii* infection (Pope and Lässer, 2013; Jia *et al.*, 2014; Kim *et al.*, 2016; Hu *et al.*, 2018) and recently there is increasing interest in longer non-coding transcripts, called long non-coding RNAs (lncRNAs). In this chapter, my study of how *T. gondii* downregulates DBH gene expression in host cells continues with an attempt to detect the presence of an antisense lncRNA that binds the DBH gene promoter in *T. gondii*-infected rat neural PC12 cells. Due to time constrain, only infected sample of day five was used throughout this study. I implemented a two-step directional reverse transcription-polymerase chain reaction (RT-PCR) method to detect the complementary antisense lncRNA at a specific locus region in the DBH promoter sequences in *T. gondii*-infected rat PC12 cells. This approach is based on the assumption that the antisense lncRNA exists and primers can be designed to detect it. Several specific bands representing each PCR primer set (Set 1, 3 and 4) present at the DBH gene locus of interest were observed in agarose gel electrophoresis. This indicates the presence of an antisense lncRNA with an estimated 470 bp bound-transcript complementary to the DNA strand.

## 5.2 Long non-coding RNA-DNA interactions

As described in detail in Chapter 1, lncRNAs are generated by the same transcriptional machinery as mRNA transcripts and other non-coding RNA classes (Mercer and Mattick, 2013). The lncRNAs are categorised with respect to their complementarity to the coding region of protein-producing genes. A vast number of the potentially functional lncRNAs are in an antisense orientation. Most antisense lncRNAs are transcribed in the opposite direction of protein-coding genes and overlap the exons. The ability of lncRNA to base pair with protein-coding genes was the basis of postulating that they can also modulate gene transcription or repression. Long non-coding RNAs are known to be able to influence the gene expression at both the transcriptional and post-transcriptional levels including altering chromatin structure organisation. Moreover, these transcripts have been observed to play an important role in the regulations of protein-coding genes (Magistri *et al.*, 2012; Vadaie and Morris, 2013; Weinberg and Morris, 2013). An estimated 72% of transcripts in the mouse genome is overlapped by the antisense strand, strongly suggesting the existence of regulatory interactions (Katayama *et al.*, 2005; Whitehead *et al.*, 2009). Aberrant expression of lncRNAs and dysregulation of its related-mRNAs have been associated with various diseases (Faghihi *et al.*, 2008; Taft *et al.*, 2010; Ng *et al.*, 2013). As yet, their functions and impact on disease are not well-understood. Recent evidence suggests that *T. gondii* can directly manipulate host lncRNAs expression in evading the host immune response (Liu *et al.*, 2018; Menard *et al.*, 2018).

The lncRNAs can interact with gDNA and chromatin in multiple ways (Cao, 2014; Roberts *et al.*, 2014a; Fernandes *et al.*, 2019). Modes of interaction are summarised by five scenarios illustrated in Figure 5.1.

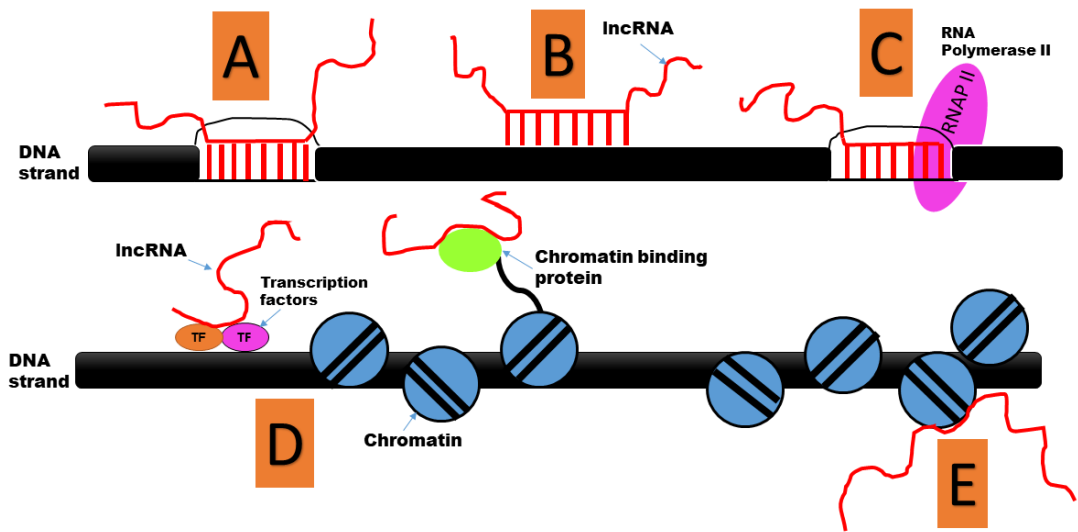


**Figure 5.1 Interactions of lncRNAs with the genome.** (A) Form a DNA-RNA heteroduplex. (B) Form DNA-DNA-RNA triplexes. (C) Associate with the RNA Polymerase II transcription machinery at transcribed loci. (D) Indirect binding to chromatin-associated proteins or sequence-specific DNA binding transcription factors. (E) Direct binding to chromatin structure.

### 5.3 Mechanisms of gene regulation by long non-coding RNAs

Long non-coding RNA can regulate the transcriptional process through several mechanisms. First, lncRNAs are able to control gene expression at the level of chromatin remodelling as they can bind one or more chromatin-modifying complexes and guide their activities to specific genomic DNA loci. In addition, they can directly interfere with the transcriptional machinery where the binding of lncRNA with repressive chromatin-modifying complexes at the locus site can modify terminal histone proteins, causing chromatin structure changes and repressing gene transcription. Transcription of lncRNAs can also result in chromatin remodelling by either favouring or inhibiting the binding of gene regulatory factors. Besides, lncRNA is able to interfere with general transcriptional machinery where it can directly bind to RNA Pol II to inhibit transcription. Meanwhile, the lncRNA transcript can form a stable lncRNA-DNA triplex structure that

can inhibit the assembly of the pre-initiation complex, thus repressing gene expression. Exclusively, some lncRNAs can modulate specific transcriptional regulators by folding into structures that mimic DNA-binding sites that generally inhibit or enhance the activity of specific transcription factors. LncRNAs can also act at the pre-initiation transcription stage by binding to specific transport factors in the cytoplasm, where they thereafter avoid nuclear localisation binding of specific transcription factors (Geisler and Coller, 2013; Kornienko *et al.*, 2013; Cao, 2014).

## 5.4 Methods

### 5.4.1 Primers targeting potential DBH antisense lncRNA

Three single-stranded forward (ie. sense) directional primers for reversed transcriptase (RT) synthesis of potential DBH gene-specific lncRNAs were synthesised. These were designed to be complementary to the predicted antisense lncRNA transcript and are labelled RT-Primer 1, RT-Primer 2, and RT-Primer 3 (Figure 5.2). The RT-designed primers are located (1) in the first exon, (2) near 5'TSS (transcription start site), and (3) -378 bp upstream of the DBH coding sequence. Four pairs of PCR primers were then designed to amplify products from the RT primer synthesized-template to screen for the presence of antisense lncRNA at the covered site.

The following directional RT gene-specific primers were used (Ups: upstream to the 5'TSS DBH gene site; Down: downstream of the 5'TSS gene site):

- 1) RT Primer 1 (Down+12): 5'-CCTCACCTCAGCCACCAG-3'
- 2) RT Primer 2 (Ups-180): 5'-TCCATGCGTCATTAGTGTC-3'
- 3) RT Primer 3 (Ups-378): 5'-CACTCACTGTCACTCAGGAAGG-3'

The following PCR primer sets were used:

- 1) Primer Set 1
  - F (Ups-46): 5'-CCCACCGAACAGACATAA-3'
  - R (Down+92): 5'-ACAGCAGTGCCATACAT-3'
- 2) Primer Set 2
  - F (Down+100): 5'-TCCTGGTCATCCTGGTG-3'
  - R (Down+232): 5'-GGATGATCTCCTGGTCATAG-3'

## 3) Primer Set 3

F (Ups-153): 5'-GAGGATCGGAGCAAAGT-3'

R (Ups-51): 5'-GCCAGGCTGTACCTAAT-3'

## 4) Primer Set 4

F (Ups-310): 5'-TATGAGGCATTCAGCAG-3'

R (Ups-180): 5'-CATCATCAAGAGAATCGAAG-3'

Figure 5.2 shows the locations of RT Primers and each of the primer sets relative to the DBH 5'TSS.

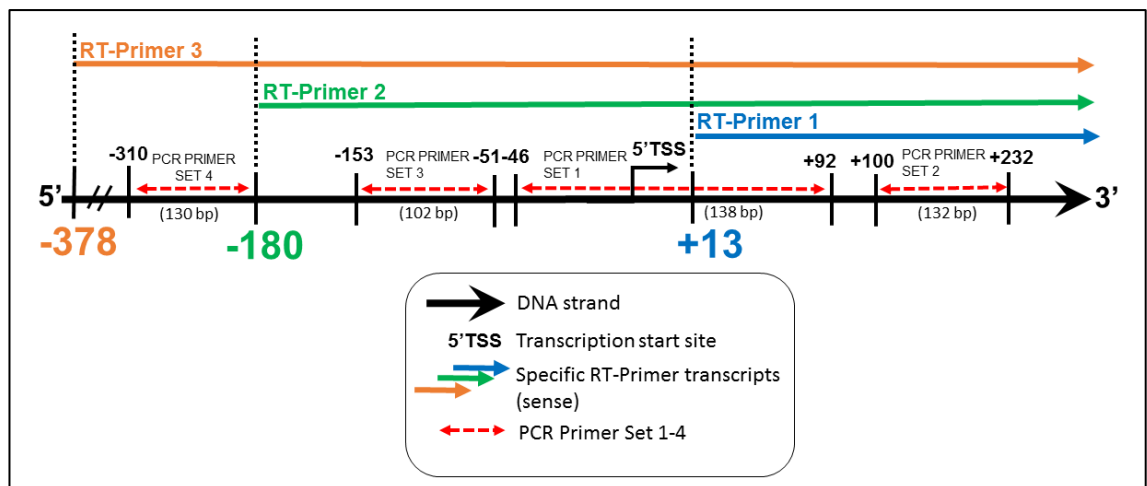


Figure 5.2 Primer map relative to the 5'TSS DBH gene.

#### 5.4.2 DBH IncRNA primer pair optimisation

All four primer pairs (PCR Primer Set 1–4) were optimised by amplifying purified PC12 cell gDNAs using a MasterCycler Gradient Thermal Cycler PCR (Eppendorf, Germany). The gradient PCR was used to determine the optimal PCR annealing  $T_a$  cycle of each set of primers with all sets of the primers designed with similar annealing  $T_a$ s, the range was 43 °C to 58 °C. The optimum PCR conditions for each primer pair was then verified

by standard PCR and visualised on agarose gel electrophoresis for a single specific PCR product. The PCR cycle utilised a 25- $\mu$ L reaction volume containing 12.5  $\mu$ L GoTaq<sup>®</sup> G2 Hot Start Colorless Master Mix (Promega, USA), 300 nM forward primer, 300 nM reverse primer, 2  $\mu$ L template DNA and DNase/RNase-free water. Final thermal cycling of the standard PCR setting started with 3 min at 95 °C, followed by 30 to 40 cycles of 95 °C for 30 sec, 57 °C for 30 sec, 72 °C for 20 sec and final termination at 72 °C for 5 min by incubation in a PCR thermocycler (Applied Biosystems, USA).

### **5.4.3 RNA extraction and DNase TURBO treatment**

Total RNA was extracted from *T. gondii* infected-PC12 cells that were harvested on day five post-infection by a Direct-zol RNA MiniPrep Plus kit (Zymo Research, USA) according to the manufacturer's instructions. DNase I treatment was implemented once as suggested by the manufacturer. In addition, to ensure that all trace amounts of DNA contamination were removed, the eluted RNA sample was re-treated with DNase enzyme by TURBO DNA-free™ kit (Invitrogen, USA). Briefly, 0.1 sample volume of 10X TURBO DNase buffer and 1  $\mu$ L TURBO DNase enzyme was added to the RNA sample, mixed and incubated for 30 min at 37 °C. Thereafter, the enzyme reaction was inactivated by adding 2  $\mu$ L of DNase inactivation reagent and incubated at room temperature for 5 min with finger vortexing to re-disperse the reagent. The inactivation reagent was removed by centrifugation at 10,000  $\times$  g for 1.5 min and the supernatant (treated RNA) was transferred to a clean tube.

#### 5.4.4 First strand cDNA synthesis and RT-PCR

First strand cDNA was primed with gene-specific designated RT-primer (RT-1 to RT-3) or random hexamer primer (as control) using a Maxima H Minus First Strand cDNA synthesis kit (Thermo Scientific, USA). Briefly, an estimated 400 ng DNase-treated RNA template was used as the starting RNA, then 0.2  $\mu\text{L}$  gene-specific primer (20 pmol) or 1  $\mu\text{L}$  of random hexamer primer (100 pmol), 1  $\mu\text{L}$  10 mM dNTP mix (0.5 mM final concentration) and nuclease-free water were added to give a total reaction volume of 15  $\mu\text{L}$  and placed on ice. Next, 4  $\mu\text{L}$  of 5  $\times$  RT buffer and 1  $\mu\text{L}$  Maxima H Minus enzyme mix were added to the component mixture. For each of the samples, a negative control reaction was prepared in parallel to assess the gDNA contamination in the RNA sample containing all components for RT-PCR except the Maxima H Minus enzyme mix. Another control, labelled as no template control (NTC), was performed to assess reagent contamination, contained all components in the reaction except the RNA template. The mixtures were incubated as follows: 25  $^{\circ}\text{C}$  for 10 min, 50  $^{\circ}\text{C}$  for 30 min, 65  $^{\circ}\text{C}$  for 20 min and then the reaction was terminated by heating at 85  $^{\circ}\text{C}$  for 5 min to inactivate reverse transcriptases. The reaction product of the synthesized first strand cDNA was directly used as a template for standard PCR. Two different DNA volumes, 2  $\mu\text{L}$  and 4  $\mu\text{L}$  of the cDNA samples, was diluted to 25  $\mu\text{L}$  total reaction volumes each and used as a template for the subsequent PCR. A random hexamer cDNA transcript (2  $\mu\text{L}$ ) was used as a positive control template. The PCR settings were as described as in the previous primer optimisation section (Section 5.4.2). All PCR products were visualised in 1.5% to 2% agarose gel electrophoresis, running at 65 to 80 V for 45 to 60 min.

#### **5.4.5 TA Cloning and DNA sequencing of the specific PCR bands**

The PCR products were run on 1% agarose gel electrophoresis (65 V, 60 min) and the specific band was gel-excised and gel-extracted by QIAQuick Gel Extraction Kit (Qiagen, Germany). The eluted DNA concentrations were then measured by the NanoDrop spectrophotometer (Thermo Fisher Scientific, UK). The PCR products were subcloned into a TOPO TA cloning vector (PCR<sup>TM</sup>4-TOPO–Invitrogen TA cloning kit) (Thermo Fisher Scientific, UK) and transformed into XL-10 Gold ultracompetent cells (Agilent Technologies, USA). Two clones bearing inserts of each sample were sent for Sanger Sequencing to Genewiz, UK. Detailed procedures were as described in the methods Section 2.3.13 – 2.3.16 in Chapter 2.

#### **5.4.6 Validation of the RNA sample quality by RNase treatment**

To validate the DNA-free RNA sample quality, the RNA was treated with RNase-A and compared to the +RT sample, in which both samples were treated with TURBO DNase enzyme to remove all RNA and DNA in the sample. Briefly, 1 µL of RNase A (20 mg/mL) was added to 2 µg of TURBO-DNase treated-RNA and incubated at 37 °C for an hour prior to first strand cDNA synthesis and PCR amplification. The Set 1 PCR primer pair was used for PCR amplification and verified by agarose gel electrophoresis. As the RNA extraction by the Direct-zol RNA MiniPrep Plus (Zymo Research, USA) resulted in RNA samples contaminated with DNA (even after DNase I treatment on the column), this RNA sample was compared to a positive band that originated from the DNA template. Also, an RNA-free sample was generated by treating the RNA sample with RNase (but without Turbo DNase treatment to maintain the presence of DNA). The RNA-free sample and both RNA-DNA-free controls were compared to the positive sample of +RT Set 1.

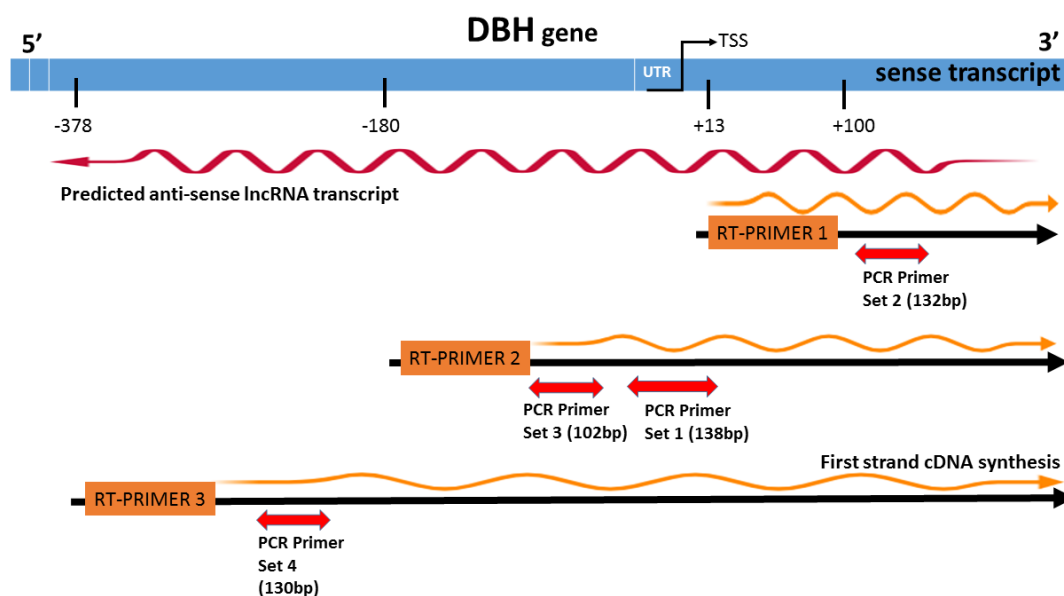
## 5.5 Results

### 5.5.1 Primer design and optimisation

RNA expression can be detected by northern blotting and ribonuclease protection assays, but these methods lack sensitivity and require a high volume of RNA, making it unsuitable for detecting low levels of RNA expression. Meanwhile, the sensitive high-throughput RNA-sequencing has been constrained to some extent, due to the high cost. Hence, RT-PCR has become the method of choice to detect ncRNAs with low expression, as this method is uncomplicated and provides results at much lower cost. The proper experimental design is very important in preventing false positives in searching for antisense lncRNAs (Haddad *et al.*, 2007). The pitfalls to consider are RNA purity, strand specificity in primed cDNA synthesis and mRNA transcribed from the complementary RNA template. In this study, the strand specificity of RT-PCR is established via the use of a specific directional primer in the reverse transcription reaction, producing a single sense strand. Meanwhile, a random hexamer primer was used in detecting mRNA transcription from the RNA template. A random hexamer primer is used to generate cDNA of the entire RNA population in the analysed sample including poly A-RNAs and ribosomal RNAs. However, the major concern in using this assay is genomic DNA contamination in RNA preparation which can give a false-positive PCR product, especially in antisense RNA detection. Carrying out appropriate contamination precautions is of utmost importance.

This is especially critical as many regulatory antisense lncRNAs map near to the transcription initiation site (Bonasio and Shiekhattar, 2014). Specific sense-strand primers are needed for the reverse transcriptase reaction to ensure that mRNA or coding strand transcripts are not amplified in the subsequent PCR detection step. As only a

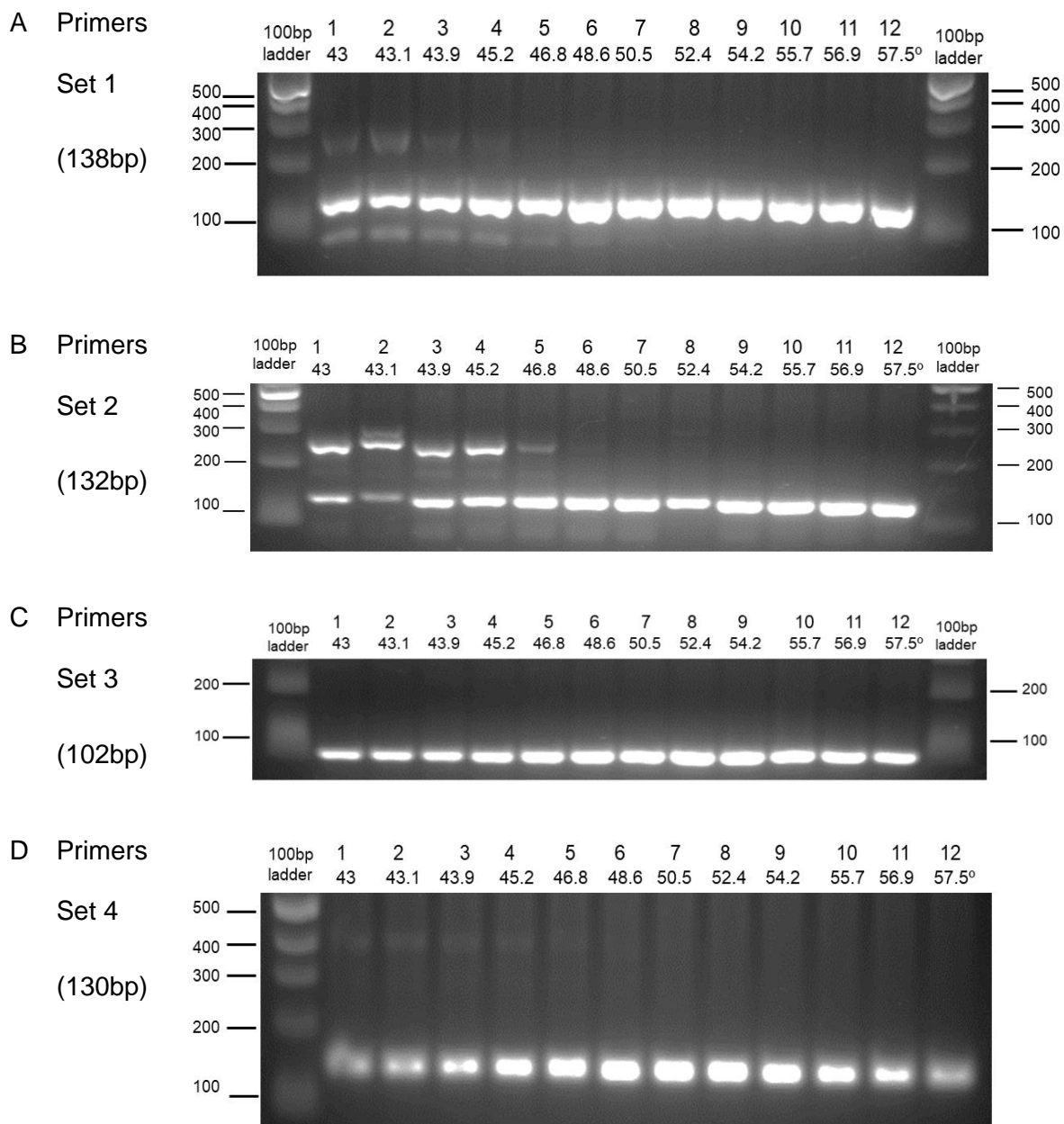
single sense strand is produced, the corresponding transcribed RNA is expressed in a single orientation. As it is unknown whether a lncRNA exists and where it initiates on the upstream region, three primers were designed to map at the TSS, 180 bp and 378 bp upstream of the DBH coding sequence (Ups-180 and Ups-378, respectively). Then all four pairs of primers were designed (Figure 5.3) to detect products of the reverse transcriptase reaction. Two primer sets were designed for RT-primer 2 with one set overlapping the TSS and TATA box region (PCR primer set 1).



**Figure 5.3 Schematic representation of the strand-specific RT-PCR assay designed for lncRNA screening at the DBH gene.** Three single-stranded directed RT primers labelled as RT-Primer 1 (TSS), RT-Primer 2 (Ups-180), and RT-Primer 3 (Ups-378) (depicted by orange arrows) were used in a directional reverse transcription synthesis. Then the synthesized-cDNA templates were amplified by standard RT-PCR to detect the presence of antisense lncRNA by implementing four pairs of PCR primer for different locations covering the synthesized-template, labelled as PCR Primer Set 1–4 (depicted by red arrows). The size of each set of primer products is as stated under the red arrows in the figure.

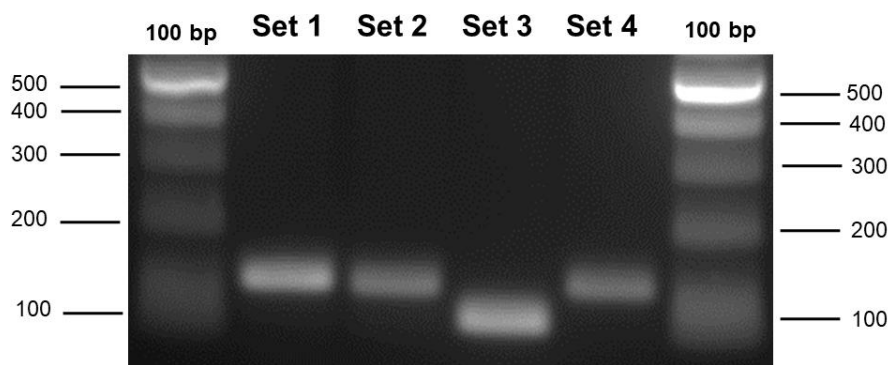
First, the PCR conditions for the four primer sets were optimised by gradient PCR and visualised by agarose gel electrophoresis. Most PCR annealing  $T_{as}$  showed a single specific PCR product for each lane with the increasing annealing  $T_a$ . As shown in the gel

photo in Figure 5.4, the highest annealing  $T_a$  at 57 °C was chosen for subsequent PCR reactions for all primer sets.



**Figure 5.4 Gradient PCR for primer optimisation of PCR Primer Set 1-4.** Gel agarose analyses showed PCR products of each primer set (A-D). Each lane represents an annealing temperature ( $T_a$ ) in the range of 43-58 °C as labelled. A single product was produced starting from an annealing  $T_a$  of 50 °C, but the highest annealing  $T_a$  at 57 °C was chosen for subsequent PCR reactions for all primer pairs.

Thereafter, a single PCR reaction was performed at annealing  $T_a=57$  °C for all primer sets to verify the final PCR setting and conditions. Agarose gel (Figure 5.5) showed a single specific band of each pair which indicates working primer pairs.



**Figure 5.5 PCR products of all primer sets; Set 1-4: 138bp, 132bp, 102bp, and 130bp, respectively.** The 100 bp DNA ladder was used as a DNA size marker.

### 5.5.2 Directional RT-PCR for lncRNA screening

Negative control reactions were used to verify the results of the first strand cDNA synthesis. All negative controls worked as expected in the PCR reactions: -RT indicated no gDNA contamination in the RNA template, while the NTC sample showed that there was no reagent contamination during the reaction. The PCR reaction with the specific PCR primer set was done with a specific RT-synthesized template based on the designated location (illustrated in Figure 5.2). The +RT samples with random hexamer primer-synthesized template of each primer set showed a positive band indicating positive DNA transcription, hence acting as a positive control for the cDNA template. It is notable that random hexamer samples showed a positive band in each set of primers (Set 1-4), signifying the presence of antisense transcripts lining targeted DNA regions, including non-coding regions (Sets 1, 3 and 4).

### 5.5.2.1 PCR primer Set 2 amplification: Negative finding

Putative sense RT-transcript 1 was designed to be amplified by PCR primer pair Set 2. The agarose gel analysis showed no specific PCR product band in the +RT samples of Set 2 (Figure 5.6). It was assumed that no antisense lncRNA overlaid the downstream region of the DBH gene at this primer pair-covered region in PC12 cells post-infection.

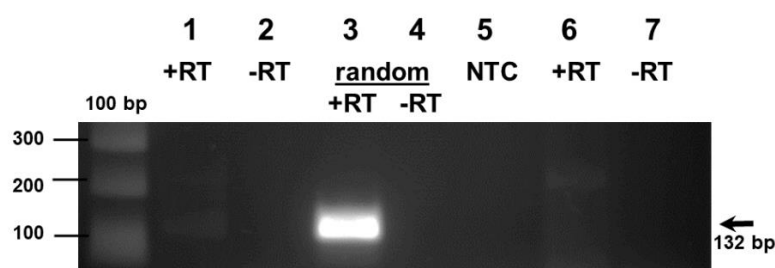


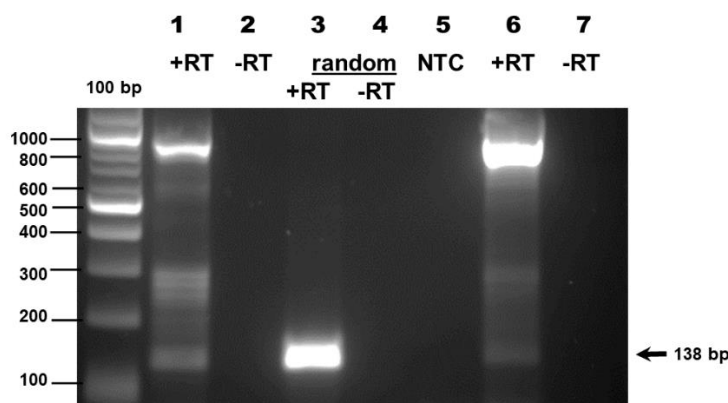
**Figure 5.6 Agarose gel analysis of the PCR amplification of Primer Set 2.** No band appeared at the specific PCR product size of the +RT samples in lane 1 and lane 6. Lanes 1 and 2 (sample) used 2  $\mu$ L of cDNA template, while lanes 6 and 7 (sample) used 4  $\mu$ L of cDNA template in the PCR reaction for both +RT and -RT sample reactions. A random hexamer synthesized-template was used as a positive control for the cDNA template, and a positive band indicates DBH mRNA strand was transcribed. +RT: reversed transcriptase-inserted in the first strand cDNA synthesis; -RT no reversed transcriptase inserted in the first strand cDNA synthesis; NTC: no template control. A 100bp DNA ladder used as a size marker.

### 5.5.2.2 Ups-378 bp and Ups-180 sense transcripts: Detection of antisense lncRNA expression

Putative sense RT-transcript 2 (Ups-180) was designed to be amplified by Primer Set 1 and Set 3 and putative sense RT-transcript 3 (Ups-378) was designed to be amplified by Primer Set 4. Each PCR-amplified region covered a different locus in the DBH gene region as illustrated in Figure 5.3. Interestingly, the gel image in Figure 5.7 showed +RT samples with a positive band for each of the PCR reactions in the region covered by Primer Set 1. Primer Set 1 was successful as the predicted band at 138 bp was visible.

The positive band supported the initial prediction of the presence of antisense RNA overlying the sense strand of DBH gene coding. Therefore, the PCR reaction was re-run and the specific band was gel-excised for DNA sequencing. The region covered was at -46 bp upstream of the promoter to +92 bp downstream of the first exon 1, including the 5'TSS site. Two biological repeats and two technical replicates were performed to confirm the specific band (Figure 5.7). No band was present in the -RT reaction, which indicated no DNA contamination in the initial RNA template during the cDNA first strand synthesis, and a positive band was observed for the random hexamer template control sample suggesting positive RNA DBH transcriptions. However, the gel showed the presence of multiple product bands in the +RT sample reactions with an obvious unknown clear band at approximately 900 bp length. As the cDNA synthesis products were directly used in the PCR amplification step, the specific RT-Primer 2 primer possibly worked with the Reverse Primer Set 1 in the PCR reaction to produce a predicted 272 bp band. In the gels, several bands between 236 and 296 were visible including the predicted product band (Lane 1 and Lane 6; Figure 5.7). The predicted band suggests a positive binding from Ups-180 to the +92 downstream of the TSS (272 bp length).

(A) Repeat 1

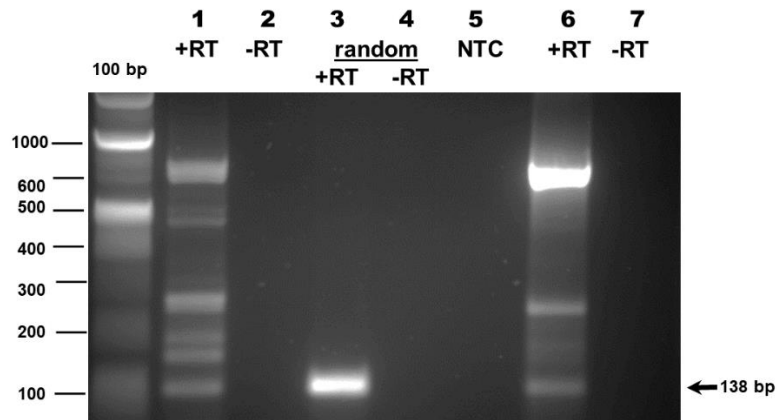


Gel 1

\*(Figure images continue next page)

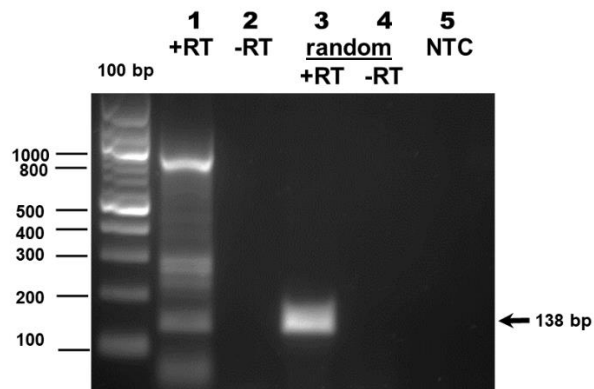
(B) Repeat 2

(i) Technical replicate 1



Gel 2

(ii) Technical replicate 2



Gel 3

**Figure 5.7 Antisense lncRNA expressed at the 5'TSS DBH gene in infected PC12 cells.** The region was amplified by a Set 1 primer pair. The predicted band at 138 bp is visible, indicating a positive antisense-binding lncRNA transcript. Another expected band formed by RT-Primer 2 primer:Reversed Set 1 primer at 272 bp is also visible. Lanes 1 and 2 (sample) used 2  $\mu$ L of cDNA template, while Lanes 6 and 7 (sample) used 4  $\mu$ L of cDNA template in the PCR reaction for both +RT and -RT sample reactions. A random hexamer-synthesized template was used as a positive control for the cDNA template. Gel 1 and Gel 2 show two biological repeats from two different starting RNA samples and Gel 3 was reproduced as technical repeats using RT-2 template, as in Gel 2. +RT: reversed transcriptase inserted in the first strand cDNA synthesis; -RT no reversed transcriptase inserted in the first strand cDNA synthesis; NTC: no template control. A 100bp DNA ladder was used as a size marker.

Primer Set 3 may have worked as there is a very faint band visible at 102 bp (Figure 5.8). Interestingly, the predicted RT-Primer 2 primer with Reverse Set 3 primer yielded a clear band at 129 bp which also may indicate a positive antisense-binding transcript between Ups-51 and Ups-180 in the DBH promoter region.

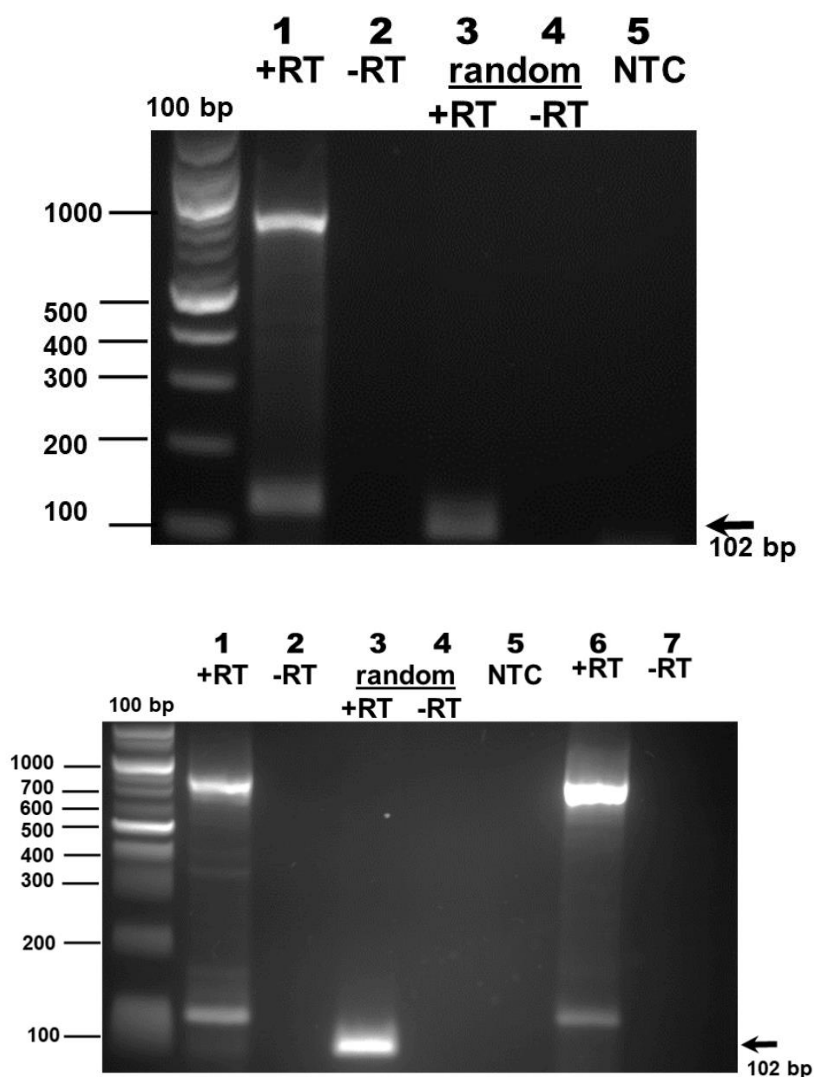


**Figure 5.8 PCR amplification of Primer Set 3.** Gel showing two technical replicates of the PCR amplification Set 3 produced from RT-transcript 2. A faint band is visible at 102 bp, but an expected clear band appeared at 129 bp that was amplified by RT-Primer 2:Reversed Set 3 primer paired. Lanes 1 and 2 (sample) used 2  $\mu$ L of cDNA template, while Lanes 6 and 7 (sample) used 4  $\mu$ L of cDNA template in the PCR reaction for both +RT and -RT sample reactions. A random hexamer-synthesized template produced a band indicating a positive antisense transcript was transcribed in the RT reaction at this specific Set 3 locus. +RT: reversed transcriptase inserted in the first strand cDNA synthesis; -RT: no reversed transcriptase inserted in the first strand cDNA synthesis; NTC: no template control. A 100bp DNA ladder was used as a size marker.

To confirm the band patterns, the putative RT-Primer 3 transcript was used in the PCR reaction and amplified using primer Set 3 and Set 4. Using RT-transcript 3 template, Set 3 yielded a clearer positive band at 102 bp (Figure 5.9) than in a previous amplification by RT-Primer 2 transcript (Figure 5.8). In addition, a clear band at 327 bp also appeared in the gel, amplified as expected by primer pairing of RT-Primer 3:Reverse Set 3 (Figure 5.9) which strongly suggests the presence of antisense lncRNA across the primer pair Set 3-covered region. To identify the sequence, the band was gel-excised, cloned into a TA-vector and then, the transformed purified-plasmid was sent for DNA sequencing for transcript confirmation.

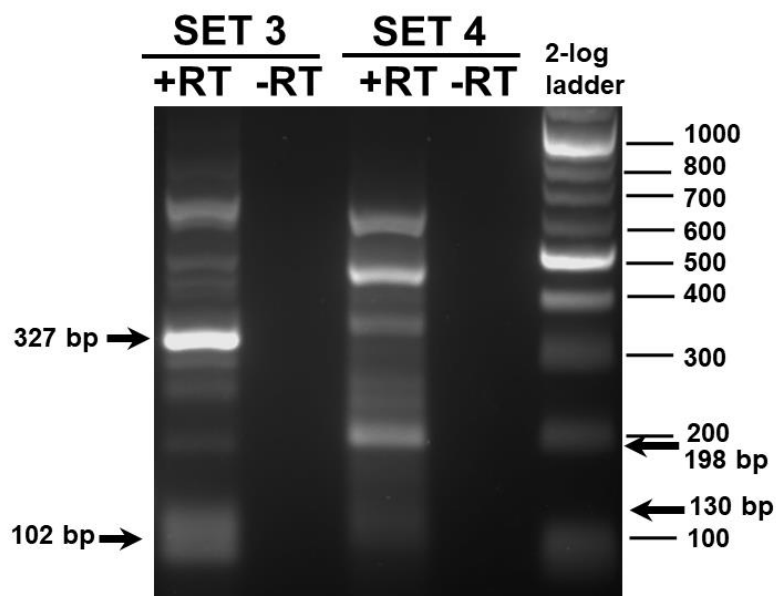


**Figure 5.9 PCR amplification of primer Set 3 and Set 4 by RT-Primer 3 transcript.** +RT: reversed transcriptase inserted in the first strand cDNA synthesis; -RT no reversed transcriptase inserted in the first strand cDNA synthesis. A 2-log DNA ladder was used as a size marker.

Lastly, the predicted 130 bp product from primer Set 4 was faint, but a 198 bp band is visible that fits the predicted RT-Primer 3 with Reverse Set 4 primer-pairing (Figures 5.9 and 5.10). The predicted band covered the region located at Ups-180 to Ups-378 of the DBH promoter gene (198 bp length). The band was gel-excised, cloned into a TA-cloning vector and the resultant plasmid sequenced to identify the band sequences.

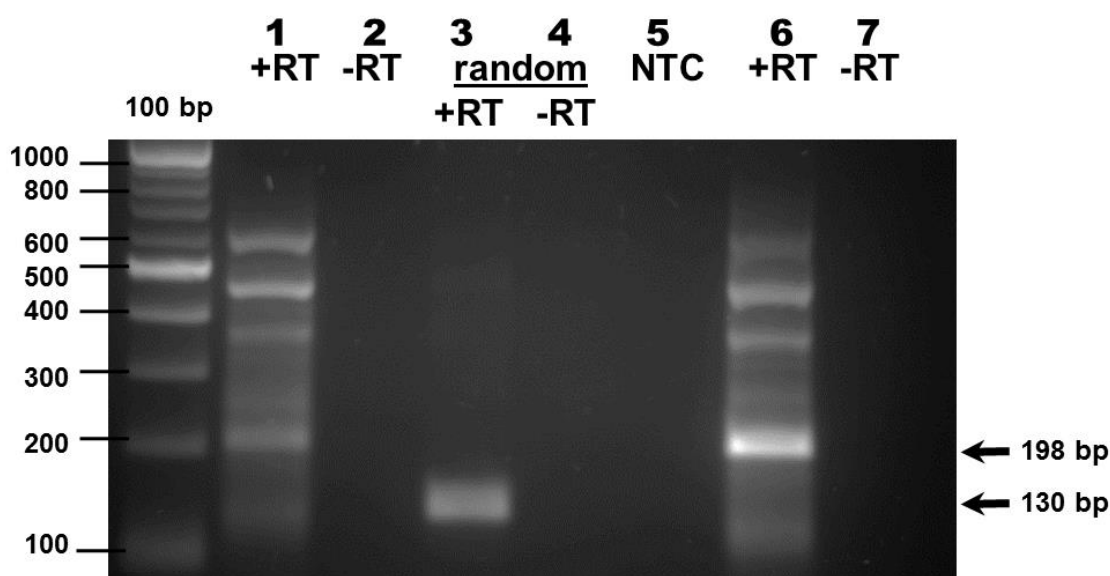


**Figure 5.10 PCR amplification of Primer Set 4.** A faint product is visible at 130 bp of primer pair Set 4. However, a clear band appeared at 198 bp that was amplified by RT-Primer 3:Reversed Set 4 primer-paired (+RT samples; Lanes 1 and 6), as expected. A random hexamer-synthesized template showed a band indicating a positive antisense transcript was transcribed in the RT reaction at this specific Set 4 locus. Lanes 1 and 2 (sample) used 2  $\mu$ L of cDNA template, while Lanes 6 and 7 (sample) used 4  $\mu$ L of cDNA template in the PCR reaction for both +RT and -RT sample reactions. +RT: reversed transcriptase-inserted in the first strand cDNA synthesis; -RT: no reversed transcriptase-inserted in the first strand cDNA synthesis; NTC: no template control. A 100bp DNA ladder was used as a size marker.

### **5.5.3 DNA sequencing of positive RT-PCR products showed sequences complementary with the rat DBH promoter gene sequences**

Three RT-PCR product bands, processed from the *T. gondii*-infected PC12 cells, were extracted from the agarose gels and cloned for DNA sequencing. The nucleotide sequence obtained by Sanger sequencing of the RT-PCR products followed by the Basic Local Alignment and Search Tool (BLAST) for nucleotide searches, BLASTN alignment of the cDNA to the genomic sequence (<https://blast.ncbi.nlm.nih.gov/Blast.cgi>), showed an identical match between the RT-PCR products and rat DBH promoter sequences from the genome database assembly.

#### **5.5.3.1 Primer Set 1**

The first output sequence originated from the positive band at 138 bp of the +RT-PCR products from Set 1 amplification. The sequence was matched with *Rattus norvegicus* DBH promoter gene sequence, underlying the 5'TSS (sequence ID: M96011.1, range 1: 353 to 442). The data confirmed the correct PCR product of the primer pair Set 1 (Appendix A.1.1).

#### **5.5.3.2 Primer Set 3**

The second output sequence originated from an expected band at 327 bp of the +RT-PCR products from Set 3 amplification (RT-Primer 3 as template). The sequence was matched with *Rattus norvegicus* DBH promoter gene sequence (sequence ID: L12409.1,

range 1: 633 to 959). The data confirmed the PCR product of the extracted band was produced from the amplification of primer-paired RT-Primer 3 primer and reversed Set 3 primer (Appendix A.1.2).

#### **5.5.3.3 Primer Set 4**

The third output sequence originated from an expected band at 198 bp of the +RT-PCR product from Set 4. The sequence was matched with *Rattus norvegicus* DBH promoter gene sequence (sequence ID: L12409.1, range 1: 633 to 830). The data confirmed the extracted band was formed by the amplification of RT-Primer 3 and Reversed Set 4 primer pairing (Appendix A.1.3).

As summarised in Figure 5.11, an antisense lncRNA was detected at the proximal promoter including 5'TSS of the DBH gene by PCR Primer Sets 1, 3 and 4. However, there was no lncRNA-binding detected from the 92 bp onwards downstream of the gene with no band of the correct size detected in gel agarose analysis in Set 2.

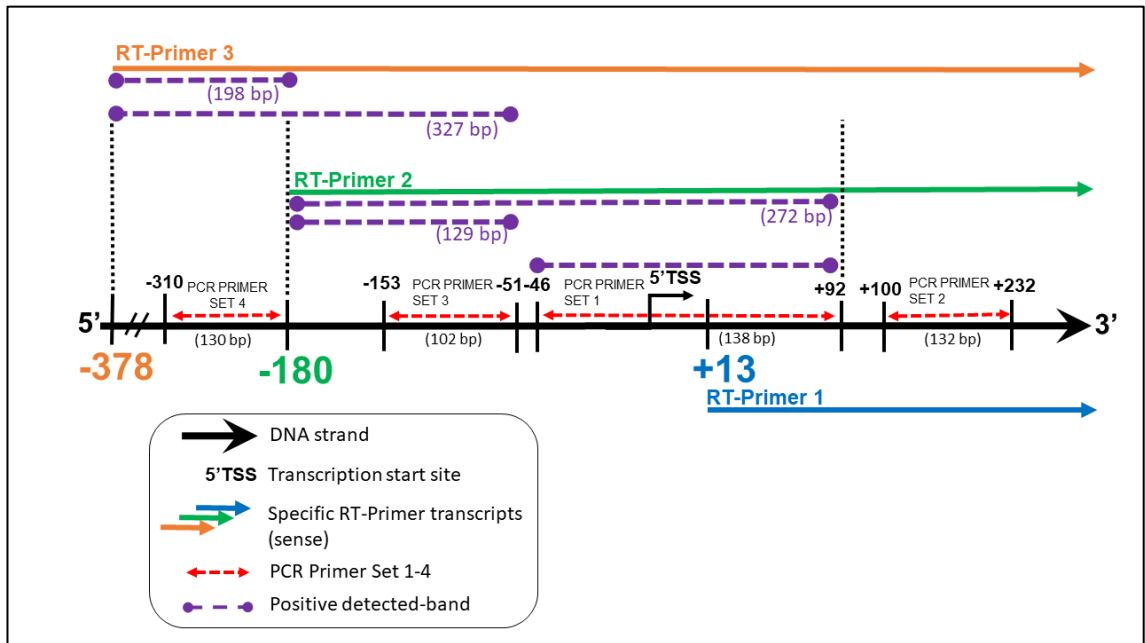


**Figure 5.11 Predicted lncRNA-binding overlying the 5'TSS of the DBH gene.** The positive binding covered a region 470 bp long. The putative sense RT-transcript 2 amplified RT-Primer 2 with both Reverse primers from Set 3 and Set 1, with 129 bp and 272 bp of the predicted PCR product size, respectively. Meanwhile, the putative sense RT-transcript 3 amplified RT-Primer 3 with Reverse primer Set 3 and Set 4 producing 327 bp and 198 bp PCR products, respectively. The visible predicted bands indicated the presence of antisense lncRNA that overlayed the DNA sequences with a total bound-transcript length of 470 bp. Meanwhile, no bands were found in the PCR amplification of primer pair Set 2 that covers +100 bp region downstream of Exon 1. The red sequence line marks the nucleotides-covered region of each primer.

#### 5.5.4 RNA sample quality control

The agarose gel image in Figure 5.12 shows that RNase plus TURBO DNase-treated samples (both RNA and DNA free) were used for reverse transcriptase reactions in this assay and no bands were detectable. This indicates that the bands observed in the experiments of this study originated from the RNA template products of the first strand-specific RT-primer synthesis. In contrast, samples treated with RNase only yielded a band indicating DNA contamination in samples and the necessity for TURBO DNase treatment (as recommended by others identifying antisense lncRNAs (Saayman *et al.*, 2014). Indeed, samples in which the reverse transcription reaction did not contain an RT enzyme (-RT samples) showed no product and hence no DNA contamination in the RNA starting sample. Additionally, the pattern of bands present on the gels from RNA-free and +RT samples were different from each other. The clear band size at 272 bp in the RNA-free sample (Lane 1) was expected, formed by RT-Primer 2:Reversed Set 1 primer pair. However, the unknown PCR products at 900 bp sizes in the respective +RT sample remain unidentified.

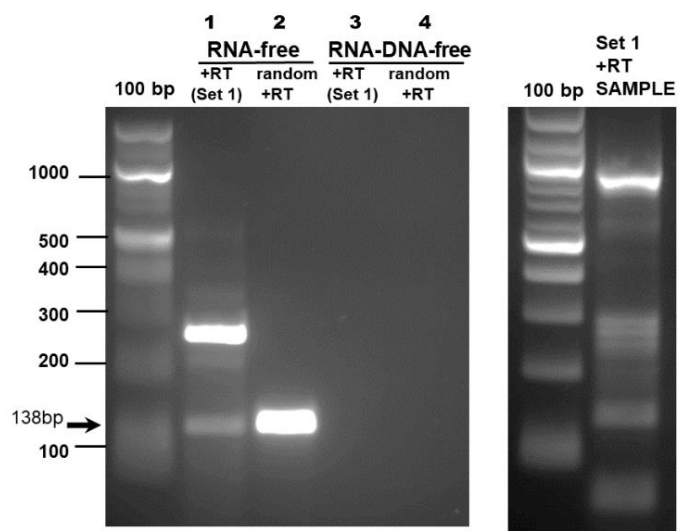


**Figure 5.12 RNA sample quality control.** The gel photo on the left shows no bands visible in RNase and DNase-treated (RNA-DNA-free) samples for both RT-Primer 2 and random-hexamer primed samples (Lanes 3 and 4, respectively). Products were visible for those samples with only RNase-treated, which cDNA synthesised with RT-Primer 2 and random hexamer (Lane 1 and 2, respectively), implicating DNA contamination in samples removed with TURBO DNase. The expected PCR product of primer pair Set 1 with RT-primer 2 is 138 bp long. The 272 bp band is a product from RT-Primer 2:Reversed Set 1 primer pair. Meanwhile, the gel photo on the right shows the positive result from Figure 5.7 of DNase-treated RNA reverse transcribed with RT-primer 2 and amplified with Set 1 primers, for comparison. Directional RT-Primer 2 template; random hexamer template; + reversed transcriptase-inserted in the first strand cDNA synthesis. A 100 bp DNA ladder was used as a DNA size marker.

Even after DNase I treatment, the specific band in the RNA-free samples (and not TURBO DNase treated) at the 138 bp size originated from a trace amount of DNA template present during RNA extraction using the Zymo Direct-zol kits detected during the first trial assay (Figure 5.12; Lane 1). My study implemented TURBO DNase enzyme treatment of the purified RNA samples to completely remove all the DNA as described in the method section, as in Haddad *et al.* (2007) and Saayman *et al.* (2014). Controls throughout the experiments above (Figures 5.7-5.10) further demonstrate starting RNA purity throughout the experiment with products dependent on the primer in first-strand synthesis.

## 5.6 Discussion

The discovery of abundant lncRNAs transcribed in the genome and in transcriptions of most of the genome has been a surprising finding as it was previously described as “junk” transcripts with no apparent potential role. Recent efforts focussed on determining their roles have found antisense lncRNAs play a role in facilitating epigenetic complex targeting of gene promoters, resulting in transcriptional gene silencing (TGS) of the targeted gene (Hawkins and Morris, 2008). They mediate changes in chromatin structure at the targeted promoter thereby forming a heterochromatin state, a key step in silencing a gene. For the first time, I present evidence of the presence of antisense lncRNA-binding at the DBH promoter gene in *T. gondii*-infected rat PC12 cells. This sequence-specific binding of lncRNA could potentially exert a regulatory function in DBH gene promoter activity. Analysis of GENCODE RNA-sequencing catalogue data shows approximately 40% of lncRNAs (3934 lncRNA genes, 5361 transcripts) intersect protein-coding gene loci. Potentially, according to data from Derrien *et al.* (2012), such lncRNAs, specifically exonic antisense lncRNAs, were positively correlated with host mRNA expression. Studies have reported that expression of sense mRNAs in mammals are altered by perturbation in antisense RNA expression, which strongly suggests the antisense transcript can interfere with gene transcription and control gene outputs (Katayama *et al.*, 2005; Pelechano and Steinmetz, 2013). In addition, lncRNAs are also predominantly located in the chromatin and nucleus of the cell, with a large fraction preferentially expressed in the brain specific-tissue, further supporting a regulatory role in gene transcription (Derrien *et al.*, 2012; Quinn and Chang, 2015).

In this assay, RT-Primer 1 transcript did not yield any bands, although a random hexamer control sample detected the DBH mRNA transcript (Figure 5.6). This indicates no lncRNA this far downstream into the gene (+100 bp onwards). Remarkably, RT-Primer 2

transcript detected a correct band for the RT-PCR products with primer Set 1 (138 bp), confirmed by DNA sequencing. Additionally, the primer Set 3 yielded a faint band for its specific primer-paired products, but showed a clear band of the correct size for RT-Primer 2:Reversed Set 3 primer, indicating a lncRNA from RT-Primer 2 transcript. While RT-Primer 3 transcript only produced a faint band for primer Set 4, interestingly, it yielded a band of the correct size for RT-Primer 3:Reversed Set 4 (198 bp) that was confirmed by DNA sequencing. The amplification of RT-Primer 3 transcript using primer Set 3 also gave a correct size for RT-Primer 3:Reversed Set 3 primer (327 bp), validated by DNA sequencing. These bands suggest the presence of antisense lncRNA transcript-binding upstream of the DBH promoter gene. Through DNA sequencing, the allele transcript was confirmed complementary to the DBH gene promoter strand in antisense orientation and it is clear that direct interaction of antisense lncRNA-DNA offers a potent mechanism for gene regulation.

Intriguingly, the antisense strand is localised at TSS and TATA loci of the DBH promoter gene. These sites are the essential starting points for mRNA DBH synthesis. Thus, the presence of this transcript at the locus site potentially has direct involvement in the DBH gene transcription that can disturb or obstruct RNA Polymerase II activity, hence dampening the mRNA expression. Undeniably, divergent transcription at the DBH promoter gene can occur where RNA polymerase II binding to the 5'TSS promoter initiates the transcription of the antisense lncRNA in both directions, giving a bidirectional regulatory effect to the gene expression. Since the antisense transcriptions of most lncRNA genes are coordinated with the transcriptional outputs in protein-coding genes (Derrien *et al.*, 2012; Sigova *et al.*, 2013), overexpression of lncRNA at this initiation site could contribute to a lower mRNA DBH transcription activity, thus demonstrating possible effects by the parasite-directed triggering effector proteins. These observations could indicate that transcription at TSS, specifically at the RNA Polymerase II binding-site, could be the main requirement for an effector RNA target site involved in transcription

regulation. Indeed, previous studies have demonstrated that perturbations of an antisense RNA can alter the expression of mRNAs in mammals (Katayama *et al.*, 2005; Sigova *et al.*, 2013; Weinberg and Morris, 2016). It is important to note that the involvement of the lncRNA presented in this study was at the transcriptional gene level, interfering with DNA in the cell chromatin. Most of the lncRNAs are expressed at low levels in a cell (Derrien *et al.*, 2012) and are generally less conserved than protein-coding sequences, which makes them difficult to detect. In this study, by implementing the directional RT-PCR amplification technique using various sets of primers, detection of the antisense lncRNA lining the gene coding sequence is possible, as the lncRNA acts in a DNA sequence-specific manner.

Based on gel electrophoresis of the positive amplification bands from each primer pair set (summarised in Figure 5.11), the bound-lncRNA transcript is estimated to be approximately 470 nucleotides in length. The positive PCR bands of Sets 1, 3 and 4 show the transcript strand extending from +92 to -378 (relative to 5'TSS) in the DBH gene. Based on cDNA amplification patterns of the +RT samples observed in gel electrophoresis, the 5' end of the lncRNA transcript is located between +92 to +100 downstream of the DBH gene. This is also the possible location of the lncRNA transcript TSS locus, although the 3' end of the transcript could be longer (Figures 5.7-5.10; Lanes 1 and 6). The reason for the variety of PCR product band sizes is unclear. It is possible the 3' end of the transcript does not bind to the gene and has a folding secondary/tertiary/circular structure that could yield a longer transcript. Scenarios A-C (Figure 5.1) are possible mechanisms of direct RNA-DNA interactions of the lncRNA-binding of the DBH gene. This prediction is based on the observation that it may not be necessary to have a full-length lncRNA sequence to depress a gene, as a partial, short sequence of the strand is enough to exert control; this is demonstrated by the targeted gene silencing activities of short interference RNAs (siRNAs; 21-25 nucleotides) (McManus and Sharp, 2002; Yu *et al.*, 2002; Weinberg *et al.*, 2006). It has been

demonstrated that using only a 21 bp antisense “guide” strand of the promoter-targeted small RNA is required to modulate TGS (Weinberg *et al.*, 2006), however, the vast majority of short miRNA studies have reported that miRNAs play a more prominent role in post-transcription than in TGS. Thus, the bound-lncRNA revealed in this study could be constructed from a longer transcribed lncRNA strand. Indeed, lncRNA is the largest group of RNA species produced in the genome and accounts for up to 68% of the transcriptomes (Iyer *et al.*, 2015), which are mostly retained in the nucleus, specifically in the chromatin (Derrien *et al.*, 2012). A more recent *in vitro* study identified as many as 996 host lncRNAs differentially expressed after infection by the Type II *T. gondii* parasite (Liu *et al.*, 2018).

This study was conducted using the infected sample only; thus, comparison with uninfected control cells could not be made. Further use of the assay with uninfected controls for band comparison may help explain the lncRNA status. It is too early to predict whether or not the bound-lncRNA at the DBH promoter site originated by host overexpression induced by the parasitic infection as it is still unknown if this lncRNA is related to infection and correlated with DBH downregulation. Thus, quantification of the found lncRNA expressions between infected and uninfected cells is needed to allow the transcript expression levels of both samples to be predicted and compared. Supporting the concept of parasite manipulation of the host genome, lncRNA is thought to possibly have greater transcript expression than uninfected host cells, exaggerated by parasite effectors.

The form, structure and functionality of the lncRNA also require further exploration. The timescale of this antisense transcript-binding to the DNA is also still unknown as this study was performed at a single time point on samples harvested day five post-infection. It is possible that transcript synthesis occurs much earlier. Knowing the exact time of the

initial lncRNA overexpression can help determine the mechanism of post-infection epigenetic DBH gene regulation.

To date, this is the first study to observe the lncRNA transcript expression at the DBH promoter gene during chronic *T. gondii* infection. However, understanding of the function and mechanism of lncRNA expressions in the genome, especially during infection, is still lacking. The first recognised lncRNA, Xist (Brown *et al.*, 1991), was reported capable of guiding gene expression due to its special capability to base-pair with the DNA protein-coding strand (Wutz, 2003; Zhao *et al.*, 2008). The lncRNAs have been shown to perform vital functions in the formation of a repressive chromatin state in the genome, including the recruitment of chromatin modifiers that lead to gene repression (Whitehead *et al.*, 2009; Kornienko *et al.*, 2013). They have been proven capable of associating with transcriptional silencing complexes containing repressive proteins such as AGO1, EZH2, DNMT3a and HDAC1, which bind to the targeted loci (Hawkins and Morris, 2008; Khalil *et al.*, 2009; Morris, 2009; Vadaie and Morris, 2013; Weinberg and Morris, 2013). The accumulation of chromatin-modifying and repression complex elements may be induced upon infection through histone-mediated protein alterations as shown in Chapter 3. *Toxoplasma gondii* infection resulted in an enrichment of repressive histone modifications such as H3K9me2. Thus, DBH repression may also utilise the H3K9me2-mediated mechanism in conjunction with that of lncRNA. Meanwhile, some lncRNAs are reported to be able to act as scaffolds that can recruit multiple proteins simultaneously, thereby coordinating their activity to alter gene expression (Tsai *et al.*, 2010; Kornienko *et al.*, 2013).

The mechanisms of promoter-specific transcriptional repression may vary by gene. Some genes can have alternative promoters within the same gene. For example, the human dihydrofolate reductase gene encodes a ncRNA initiated upstream of its minor promoter that can regulate RNA expression from downstream of its major promoter. The

gene's ncRNA sense transcript interacts with transcription factors which thereafter initiate the recruitment and formation of a repressive chromatin complex to the major promoter initiation start site. Through these interactions, ncRNA disassembled the pre-initiation mRNA transcription complex from the regulatory promoter, thereby leading to suppression of dihydrofolate reductase expression. The transcript forms a highly specific and stable triplex structure with the major promoter, which strongly supports a direct role of ncRNA regulation in gene repression (Martianov *et al.*, 2007). Such a mechanism can also be implemented by the *T. gondii* parasite to depress the DBH gene in host cells although current knowledge about the presence of alternative DBH gene promoters is lacking. The exact TSS and end sites for this antisense lncRNA could not be confirmed in this study. We can only speculate that the intracellular parasite *T. gondii* can most likely manipulate host lncRNA expression via secretion of its effector proteins where the transcribed-lncRNA possibly interferes with DBH mRNA gene expression. However, this study did not investigate the presence of any parasite-derived effector proteins associated with the locus site, and indeed, the functions of many of these effector proteins remain unknown.

Using a random hexamer primer to prime the RNA template and as a template-synthesis control for each of the synthesized-RT transcripts provided at least one notable supporting observation. Under standard conditions, I was expecting many DBH mRNA transcripts in the sample to be generated by RT-Primer 1 template (starting at 5'TSS to downstream). Normal mRNA transcription starts at the 5'TSS codon, producing a sense transcript. The region was detected by the PCR primer of Set 2 with a clear PCR product band shown in the electrophoresed gel (Figure 5.6) as expected. However, interestingly, the data showed all the random hexamer samples generated a positive PCR product band in the gels with a specific size for each primer pair including the primer pair Sets 1, 3, and 4 which had been designed to be located in the promoter site of a non-coding sequence upstream of 5'TSS locus (Figure 5.13).

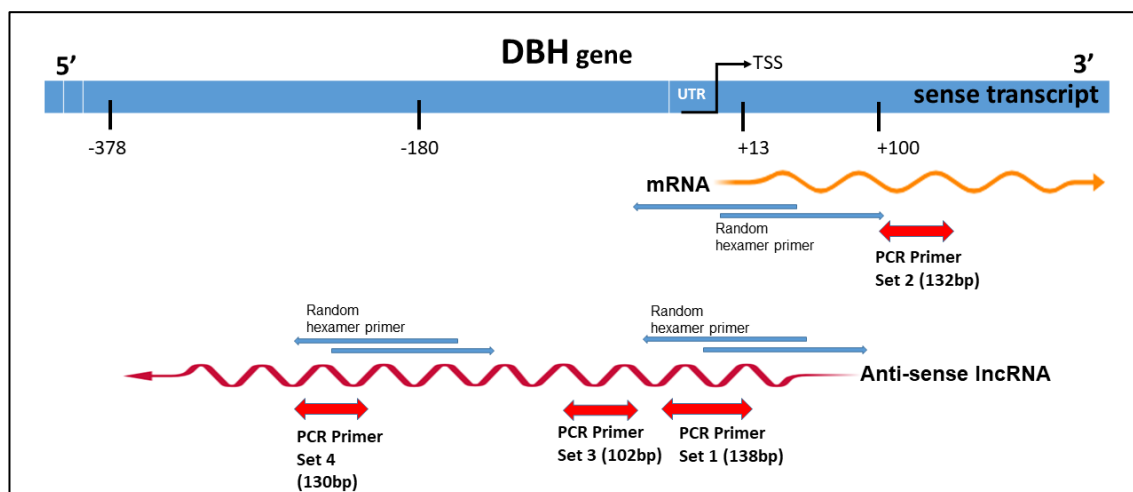


**Figure 5.13** Map of the positive PCR bands in random hexamer +RT template, amplified by the primers of non-coding sites.

Positive amplification by the primer pairs of Sets 1, 3, and 4 from the random hexamer RT-synthesized templates was observed (Figures 5.7-5.10). Random hexamer primers primed any sense and antisense RNA and therefore yielded a positive PCR product for any of the samples that were positive with the sense specific RT-primer (e.g. RT-Primer 2 or 3). This observation supports the presence of antisense lncRNA binding upstream of the DBH gene, as observed in the sense-specific primer data. The DBH gene may have pervasive transcription, thus transcribing not only the mRNA strand, but also other non-coding RNA transcripts. An alternative promoter may exist in the DBH gene that transcribes and regulates lncRNA expression. Recent studies have shown pervasive transcription throughout the genome, generating a large number of lncRNAs, most transcribed in the antisense direction of the protein-coding gene with which they often share sequence complementarities (Djebali *et al.*, 2012; Hangauer *et al.*, 2013). However, only a few of these RNAs have been shown to perform regulatory functions. Equally important, this study has screened for the presence of an antisense lncRNA that binds to DBH gene promoter sequences post-infection. The parasite thereby manipulates the lncRNA to mediate epigenetic changes in regulating gene expression.

## 5.7 Conclusion

Thus far, this study has provided evidence of the presence of host lncRNA at the 5'TSS DBH gene in *T. gondii*-infected rat PC12 cells. The antisense DNA complementary transcript could have originated from parasite triggering such as by its effector proteins, thus causing over-transcription of the lncRNA transcript by the host cell. The presence of antisense lncRNA may indicate the existence of another possible mode of epigenetic gene regulation involving RNA-mediated interactions in DBH gene transcriptional expression. The lncRNA may regulate transcription by targeting epigenetic silencing complexes to homology-containing loci. This direct involvement can influence the DBH transcriptional rate causing downregulation of the gene post-infection. Long non-coding RNA binding future research could explore how it exerts its effect, especially during parasite chronic infection. The data shown in this study provides a resource to facilitate future examination of the specific functional relevance of these transcriptional perturbations.

## Chapter 6

### Final Remarks

#### 6.1 Final Remarks

Lifelong persistence of parasite cysts in the brain creates a plausible vehicle by which the parasite can act upon and affect the host genome through epigenetic modulation. Exploring the epigenetic 'conversation' between the histones and DNA, specifically cytosine and histone H3K9 methylation, and the involvement of non-coding RNAs upon parasitic infection can lead to understanding the mechanism of parasite manipulation in DBH transcriptional gene silencing (TGS) that was previously described (Tedford, 2018; Alsaady *et al.*, 2019). This thesis has attempted to reveal information on how epigenetic exploitations of the host genome are implemented by the parasite to provide its prolonged survival in host cells and completing its life cycle. Intracellular *T. gondii* is capable of manipulating and interfering with the host genome, and subsequent gene silencing. Downregulation of the DBH gene occurring at the transcriptional level was observed post-infection, which led to speculation that epigenetic modification was involved in the mechanism and to determine this, various epigenetic modification assays such as the MeDIP, ChIP, and bisulphite-sequencing were performed. This study is relevant in delineating how catecholamine biosynthesis pathway changes and DBH dysregulation can contribute to various phenotypes associated with *T. gondii* brain infection. My final observations in this thesis are presented in the following sections.

### 6.1.1 Epigenetic changes at transcription start site associated with DBH transcriptional repression in *T. gondii* infection

A lncRNA was identified that could be involved in DBH gene regulation and could initiate histone and DNA methylation changes to suppress gene expression. Some evidence for histone modification, H3K9 methylation, was observed, but investigations of DNA methylation changes, as assessed by MeDIP and bisulfite sequencing, were not definitive. Data from the MeDIP assay presented in Chapter 2 of this thesis demonstrated that the infection had induced only a subtle changes in DNA methylation patterns at CpG sites close to the 5'TSS of the DBH gene. Meanwhile, the bis-sequencing analysis showed that most CpG sites in both covered regions of the uninfected cell controls were found in methylated states (80–90%), and this was only minimally different from the infected sample. This may be due to technical issues as the background level of methylation in the DBH promoter of these cells was high for an expressed gene and considerably greater than prior unpublished work (Tedford, 2018). Nevertheless, another reasonable explanations may exist for the subtle DNA methylation changes. First, as the studied regions showed little change in DNA methylation patterns upon perturbation, there could be other functional CpG sites in the promoter sequences that were not covered in the study. Indeed, this study only analysed a small section of the upstream region that is 2.7 kb away from the 5'TSS and another small section surrounding 5'TSS. It is possible that there was a global increase in DNA methylation in the promoter region post-infection and the effect on gene regulation was not locus-specific. However, the increasing methylation trend at the 5'TSS region in the MeDIP-qPCR analysis gave some indication of the involvement of DNA methylation post-infection. Second, it is possible that DNA methylation only provided a small contribution, partially, or may not be involved at all in DBH gene regulation, regardless of its methylation states. It is, however, difficult to prove that DNA methylation had no impact post-infection especially because the covered regions of the studied loci sites were relatively small. Further analysis by the

ChIP assay found that presence of the enzyme responsible for DNA methylation, DNMT3a, increased with infection (Chapter 3). The percent input of the infected sample was greater than uninfected control on day one and day two that suggested an increasing trend upon parasite invasion in the host cell. Indeed, on day two (48 h) post-invasion, the binding had greater percent input relative to control with three-fold. At the same time, DNA methylation began to incrementally increase post-infection. Though the timescale was still unclear, the accumulation of DNMT3a protein-binding to the locus site signifies an active process of DNA methylation at the DBH promoter region. However, this study failed to show that the enzyme levels continued to increase to maintain the hypermethylation process in the infected sample, as evident in the DNA methylation assays. There might be a few explanations for this. First, secretion of the DNMT3a enzyme was too low in the nuclei of PC12 cells, making protein-capture by the ChIP assay more difficult. Limited CpG sites present in the studied region may also explain this. Second, the bound proteins may have been lost in the ChIP processing procedures, as the assay involved a longer, multi-step protocol. Technical laboratory errors can happen in a single biological replicate. Also, the implemented formaldehyde-crosslinking exposure in the assay may not have been enough to bind all the enzyme-proteins to DNA. Conversely, the recruitment of DNA methyltransferase to the locus site may not have caused enough repressive activity at the onset of the infection, as denoted by the statistically insignificant differences between the infected and control samples. However, by comparing the MeDIP-qPCR for DNA methylation assay with DNMT3a-bindings in the ChIP-qPCR, it can be concluded that the higher level of methylase-binding upon infection allowed for the prediction that DNA methylation also increased in the infected cells despite the observation of a minimal increase in the MeDIP assay. However, possibly due to the aforementioned reasons, both specific DNA methylation assays could not confirm the changes. Interestingly, DNMT3a might not only function as a *de novo* DNA methyltransferase but can also participate in repressive complexes involving histone modifications, specifically histone deacetylation and methylation. It has been shown that DNMT3a can associate with many repressor proteins such as histone deacetylase

(HDAC) to repress gene expression (Fuks *et al.*, 2001; Morris, 2005). Thus, a second alternative regulation scenario can be proposed. Without forming hypermethylation states causing promoter-directed DNA methylation, the DNMT3a can also act as a co-repressor protein in initiating the TGS. The data showed an increased protein binding up to 48 h upon infection, postulated at this time to be the formation of a repressive complex at the site locus. The enzyme-binding values dropped on day three, as compared to day one and day two, as the enzyme had started to dissociate from the locus site, usually when the accumulation of other repressive proteins takes place. These findings raise the possibility that DNMT3a enzyme is a dual-function protein that silences gene expression, both directly through association with chromatin remodelling complexes and indirectly through epigenetic modification of cytosine in DNA methylation. Hence, further analysis of a repressive histone modifications protein mark; H3K9me2 showed an increasing protein-binding pattern at the TSS after day three post-infection, suggesting its inhibitory role in DBH transcription activity. The histone-modifying H3K9me2 repressive protein functions specifically to alter the chromatin to form a more compacted structure, thus hiding gene sequences and blocking the transcription activity of the active genes and initiating a heterochromatin state. The increase occurred after increasing DNA methylation activity and DNMT3a binding that had started earlier on day two, suggesting that the chromatin modification protein worked in a methylation-dependent manner. However, the exact timing was still unclear and the question as to whether DNA methylation was involved or only partially involved in the DBH gene repression remains uncertain due to the above mentioned data limitations. Also, I had assumed that dimethyl H3K9 may work in parallel with the trimethyl H3K9 in remodelling the chromatin structure to form a repressed heterochromatin state. Insight into whether the global heterochromatin state repressed the gene is still largely unsolved as a gene can be silenced without needing the overall shift into heterochromatin. A local chromatin structure change modified by a histone modification is enough to hide the transcriptional machinery of a gene. Further investigation relates on how chromatin-remodelling complexes were targeted to the targeted site and initiated the histone modification

changes. Chapter 5 data provided evidence of the presence of long non-coding RNA (lncRNA) at the TSS of DBH mRNA, suggesting its possible inhibitory role in epigenetics DBH gene expression. The RNA transcript was bound complementary to the promoter DNA protein-coding sequence, in the antisense orientation. The lncRNA expression could be triggered by the parasite-derived effector proteins that activated lncRNA transcriptions by the host cell. Long non-coding RNA induced during infection could be a general mechanism used by the parasite to alter host gene expression, such as immune-related genes in macrophage. For example, *T. gondii*-infected bone marrow-derived mouse macrophages have a substantial number of host lncRNAs involved in the immune response dysregulated, possibly mediated by a direct effect from parasite ROP16 protein, although the direct roles are still being clarified (Menard *et al.*, 2018). The same mechanism of inducing lncRNAs might be found for other intracellular pathogens and parasites, such as *Leishmania* (McMaster *et al.*, 2016) and trypanosomes (Bayer-Santos *et al.*, 2017). Numerous lncRNAs have been reported to participate in gene regulation by interacting with various types of proteins involved in histone modifications or chromatin-remodelling complexes. The lncRNAs have demonstrated an ability to guide epigenetic silencing complexes to targeted loci in the gene promoter. Based on the literature, in this scenario, two potential mechanisms of lncRNA promoting DBH downregulation are proposed. The first is that lncRNA can recruit proteins such as chromatin modifiers (e.g. DNMT3a) to the targeted DNA, and the second is that it can function as a scaffold to bring multiple proteins into a complex by its homology sequences with DNA.

## **6.2 Antisense long non-coding RNA could mediate epigenetic transcriptional gene silencing of the DBH gene**

By understanding the mechanism of the DBH gene silencing, new insight into host-parasite interactions can be obtained as it is the key enzyme involved in the catecholamine biosynthesis pathway. While it is of the utmost importance to understand the underlying mechanism of how the DBH gene is regulated, it is also essential to identify the associated regulatory elements to further understanding of how the gene can be depressed by an infection. An inhibitory role by epigenetic effectors on DBH promoter-driven transcription is the most likely target mechanism at this transcriptional level. A question arises if there is a general chronological order in protein recruitment to the specific targeted site of gene regulation. But most studies indicate that each individual gene promoter works using a sequence of actions that differs from one promoter to another. The three distinct mechanisms that appear to be implicated in initiating and sustaining epigenetic modifications are RNA-associated silencing, DNA methylation and histone modification.

In this study, the level of DNMT3a in infected cells was greater than uninfected control observed 24 h post-infection, signifying that it was the first protein recruited to the target locus. Meanwhile, DNA methylation was observed after day two (48 h) post-infection and continued to increase until day five. This suggests the establishment of promoter DNA methylation patterns resulting in the modulation of DBH gene repression. Although many studies have proposed that DNA methylation can act as a primary player in silencing a gene preceding other epigenetic pathways, there are also events in which DNA methylation can act as a secondary action that takes place to stabilise the gene silencing status after chromatin modifications. Perturbations on H3K9me2 histone at the DBH promoter was observed on day three post-infection, which suggests that the local

repressive chromatin structure had changed. This is consistent with our group finding; decreased DBH expression three days post-infection (Alsaady *et al.*, 2019). An immediate inquiry emerged on whether the DBH downregulation resulted from the presence of a ncRNA. Both short and long antisense ncRNAs have been demonstrated to be functional in epigenetically-regulated gene transcriptions (Weinberg *et al.*, 2006; Morris, 2009). I have predicted that a lncRNA may play a functional role in regulating DBH gene expression. In this study, an antisense lncRNA at the locus site was detected in samples harvested on day five post-infection. The lncRNA-binding could be transcribed earlier at the targeted locus, possibly right after the parasite invasion. One plausible theory is the lncRNA can guide the silencing complexes to the targeted site. Despite small target loci being generally understudied, a wide diversity of interactions between short and long noncoding RNAs and different chromatin-modifying complexes have been described in the literature (Hawkins and Morris, 2008; Geisler and Coller, 2013; Weinberg and Morris, 2013; Weinberg and Morris, 2016). The antisense lncRNAs detected in this study could act as a “guide RNA” in directing the repressive protein complexes to the targeted locus. Intriguingly, many reported ncRNAs are thought to have an initial association with DNMT3a, histone deacetylases 1 (HDAC1) and Argonaute-1 (AGO1) proteins and form the complexes that function as co-repressors to silence a gene in TGS (Hawkins and Morris, 2008; Morris, 2009; Weinberg and Morris, 2013). Or the lncRNA could bind first to the DBH promoter region and recruit repressive protein complexes with its functional secondary structures to the targeted site. There is an alternative model where the antisense RNA could act directly via binding close to the TSS through its sequence homology, and form a hybrid (such as a triplex RNA:DNA:DNA) with opened DNA helix at the promoter and this blocks the transcription machinery (Martianov *et al.*, 2007). It does not require DNA methylation or histone changes but is likely to be short-lived, a longer term study would be required for this. Considering both the literature and data presented in this thesis, a sequence of events that may involve in the DBH repression machinery can be proposed.

A model for the mechanism of antisense lncRNA-directed transcriptional regulation in rat neural PC12 cells consistent with my data is proposed (Figure 6.1).

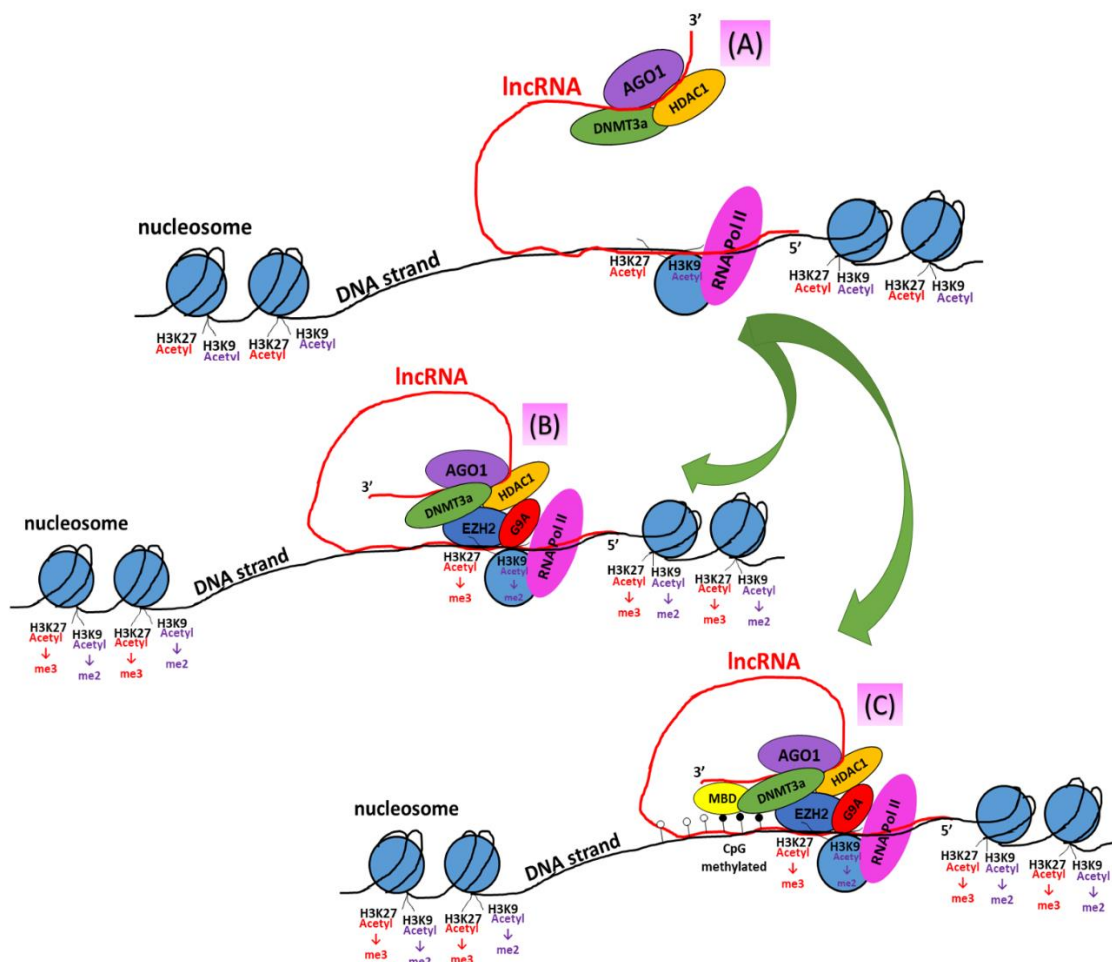


**Figure 6.1 Schematic model of how antisense long non-coding RNA could mediate epigenetic transcriptional gene silencing of the DBH gene in infected catecholaminergic cells.** (A) The lncRNA targeting the repressive proteins (AGO1, HDAC1, DNMT3a) to the targeted locus. This is followed by one of two proposed scenarios: (B) Chromatin modification changes without promoter DNA methylation and (C) involving DNA methylation. The HDAC1 binding leads to histone de-acetylation; meanwhile, DNMT3a and AGO1 binding can lead to DNA methylation. The co-repressor complex binding attracts the accumulation of other repressive proteins such as EZH2 that functions to methylate histone H3K27, and histone methyltransferase G9A that functions to methylate histone H3K9 at the locus site. Meanwhile, the MBDs protein which binds specifically to 5-methylcytosine, associates with DNMT3a to methylate a CpG site. Epigenetic histone modifications at the locus site change the chromatin structure that leads to TGS by interrupting the RNA Pol II transcriptional machinery activity. Abbreviation: lncRNA (long non-coding RNA); AGO1 (argonaute-1); HDAC1 (histone deacetylases 1); DNMT3a (DNA methyltransferase 3 alpha); EZH2 (enhancer of zeste homolog 2); G9A (histone methyltransferase G9A); MBD (methyl-CpG binding domain protein); RNA Pol II (RNA Polymerase II).

Two epigenetic regulation scenarios are proposed, one which involves DNA methylation at the promoter region and one that does not. The lncRNA-guide allows the recruitment of DNMT3a, which then methylates the sense DNA promoter (Figure 6.1C). This scenario is consistent with the data obtained in this study that demonstrated a greater level of DNMT3a enzyme than uninfected cells 24 h post-infection and increased DNA methylation patterns starting at day two and continuing afterward. However, as previously mentioned, the presence of DNA methylation in this study could not be confirmed. Thus, another scenario is proposed that does not include the effect of DNA methylation on gene regulation. The binding of lncRNA and co-repressor proteins at the 5'TSS may have manifested enough repressive effect on its own to silence the DBH gene (Figure 6.1B). Hyper-acetylation of histones has been shown to mark open chromatin and is a required step for transcriptional activation. Accordingly, the de-acetylation process may be the first required mechanism that has to take place to enable chromatin structure changes. Thus, the initial step in transcriptional gene repression is histone de-acetylation: the removal of the acetyl group from H3K9 terminal histone, catalysed by HDAC1 enzyme. The HDAC1-bindings cause a localised histone de-acetylation (Figure 6.1A). The AGO1 protein is an effector protein that facilitates the “guide lncRNA” to form a silencing complex with HDAC1. The AGO1 can associate with RNA polymerase II, and it is also required in the H3K9me2 modifications process (Kim *et al.*, 2006). Interestingly, the *T. gondii* parasite itself harbours a single gene encoding an argonaute protein (Riyahi *et al.*, 2006) that may be associated with DBH repression.

After HDAC1-complexes bind, the recruitment of other proteins such as polycomb group protein enhancer of zeste homolog 2 (EZH2) and G9A protein could take place, accumulate at the 5'TSS locus site and then block RNA Polymerase II transcription. The EZH2 is a lysine methyltransferase enzyme that methylates H3K27 histone, another major repressive histone marker, and the enzyme usually interacts within the polycomb repressive complex 2 (Viré *et al.*, 2006). Remarkably, the EZH2 is also reported to be

able to directly control DNA methylation, and thus might be involved in establishing DNA methylation in the promoter gene to mediate changes (Viré *et al.*, 2006). Hence, assessing the EZH2-binding pattern changes at the DBH promoter site may provide insight into the DNA methylation. Additionally, the G9A protein is a well-known H3K9 lysine methyltransferase enzyme primarily responsible for mono- and dimethylation of H3K9 histone in mammalian euchromatin (Mozzetta *et al.*, 2014). Since this thesis analysed the H3K9me2, evaluating its catalyser enzyme, the G9A, can support the data.

This would permit chromatin remodelling by the addition of methyl groups to the H3K9 and H3K27 histones, forming H3K9me2 and H3K27me3, respectively. Both are major repressive histone marks that have been shown to direct the formation of a repressive heterochromatin state through the recruitment of silencing complexes. There is evidence in which the H3K9me2 modification can act in concert with H3K27me3, suggesting positive crosstalk between these two mechanisms. The alterations cause the chromatin structure to change to a condensed state and silence the gene. Herein, my data showed an increased level of H3K9me2 binding after three days post-infection, which occurred after DNMT3a binding at the locus site on day two. This suggests that the chromatin structure changes were mediated on day three, in agreement with the finding of low transcriptions activity of mRNA DBH, *in vitro*. The DBH gene was significantly downregulated after day five post-infection (Alsaady *et al.*, 2019).

## 6.2.1 Involvement of other effectors in promoter DNA methylation-directed epigenetic gene repression

### 6.2.1.1 Methyl-CpG binding domain proteins (MeCP2 and UHRF1)

Epigenetic regulations including DNA methylation are commonly mediated by multiple proteins that add, remove, or interpret the chromatin structures (Readers and Writers). With regard to DNA methylation, gene suppression is generally mediated partly by the recruitment of the methyl-CpG binding domain protein (MBDs) which selectively recognises methylated CpG sites. The 5-mC site is recognized by three separate families of proteins: the MBD proteins, the UHRF proteins, and the zinc-finger proteins (Moore *et al.*, 2012). In the brain, methylated DNA may be bound by MBDs proteins such as MeCP2 that can thereafter recruit additional proteins to the gene locus, such as HDACs and other chromatin remodelling proteins that can modify the local chromatin structure, thereby forming compact, inactive heterochromatin states (Amir *et al.*, 1999). There is growing evidence that MBD proteins interact with HDACs, suggesting that methylation represses transcription by recruiting HDAC activity, resulting in hypo-acetylation of histones residing in the region of methylated DNA. As such, the MeCP2 was shown to associate and assist histone methylation at lysine 9 of H3 (H3K9me), which is a key epigenetic modification involved in gene silencing (Nan *et al.*, 1998; Fuks *et al.*, 2003). The UHRF1, another type of MBD protein, has a critical role in cell cycle progression. The *T. gondii* parasite exploits the host UHRF1 gene to control the cell cycle phase and enhance its proliferation, as the gene has been found significantly overexpressed following infection. Hence, the UHRF1 has been used as a promising drug target to treat toxoplasmosis because it can act as a transcriptional repressor through its variety of functional domains that can bind to the epigenetic modification proteins (Brunet *et al.*, 2008; Unoki *et al.*, 2009). The latest finding reported that *T. gondii* ROP16 protein kinase

initiated the epigenetic events which targets host UHRF1 (Sabou *et al.*, 2019). Indeed, both the MBDs and the UHRF proteins interact with methylated DNA and histones to increase gene repression. Based on this evidence, it is proposed there could be other specific MBD proteins that are involved and play some roles in the heterochromatin formation in DBH gene downregulation, modulated directly by *T. gondii* infection or from the host's response following infection. Therefore, MBD protein binding status can help to further determine DNA methylation involvement in DBH gene repression.

### **6.3 Study limitation; a relatively low DBH expression in catecholaminergic neural cell line**

While much effort has been expended on studying the mechanisms of epigenetic changes in the infected cells, my latest finding has found that the DBH protein was expressed at relatively low levels in the cell line utilised. The cell line used failed to repeat the same outcome in expressing the mRNA DBH post-infection shown in previous experiments. The HPLC-ECD analysis of catecholamines released by the cells also showed undetectable NE levels in the line of cells, confirming the lower DBH enzyme. Thus, this could provide an explanation for the insignificant changes in the epigenetic assay data described in DNA methylation assays and very high background methylation in the DBH promoter (Chapter 2). The low level of DBH transcription in the PC12 cells is due to unknown causes, but it was believed that the cells show low inherent competency to produce the DBH protein over time.

## **6.4 The effect of DBH downregulation and consequentially norepinephrine suppression on the host in initiating behavioural changes**

The brain's central place for noradrenergic neurons is the locus coeruleus, the primary site of norepinephrine (NE) synthesis. Norepinephrine is the main player in neuromodulation and neuroinflammation in the brain (Madden *et al.*, 1995). Indeed, NE binds adrenergic receptors present on all brain cell types. During infection, CNS NE suppresses pro-inflammatory cytokines in microglia and astrocytes to prevent cell damage and hence, control the infection. Also, NE modulates GABAergic neurons thus, balancing neuron signalling and transmission in the brain (Kawaguchi and Shindou, 1998; O'Donnell *et al.*, 2012).

The DBH was down-regulated following *T. gondii* infection that possibly elicited by the host antisense lncRNA dysregulation. The decreased DBH will consequentially decrease the NE synthesis. Lower NE will allow the proinflammatory response in the brain. Neuroinflammation could maintain chronic infection in the brain and suppress tachyzoite activation, so that the host is more likely be predated, and the parasite can be transmitted.

## 6.5 Future investigations

### 6.5.1 Implement other cell lines and *in vivo* tissue

Assessing the catecholamine released by HPLC-ECD for each PC12 cell batch used prior to an assay is important for quality control. This study was performed in a single host cell type from a rat neural cell line. Future experiments could use a human neuron cell line such as BE(2) M17. Also, the experiment can directly use infected brain tissues which would provide abundant information to analyse protein-DNA interactions *in vivo* for further analysis.

### 6.5.2 Broadening the studied promoter-region

The DNA methylation and chromatin modification assays used in this study are limited in terms of the required length of the DNA fragment (an average of 300-500 bp), thus allowing analysis for a limited region size. Broadening or extending the studied loci in the promoter region is recommended for future study by implementing the optimised-MeDIP and ChIP assays developed. It is possible that this study was missing functional loci contributing to DBH transcription activity. The genome-wide bisulphite-sequencing analysis is likely to be exceptionally useful in future studies, particularly because it may give a detailed overview of all CpG site status on the DBH gene and its promoter.

### 6.5.3 Analysis of other related host epigenetic effector proteins

As aforementioned in the proposed mechanism of TGS, there are many associated regulatory factors of the chromatin modification machinery which act as effector proteins that may contribute to DBH gene silencing, such as AGO1, HDAC-1, EZH2, G9A, H3K27me3 and MBDs proteins. The optimised-ChIP method can be used to measure these proteins. It is important to identify each individual epigenetic modification protein and determine their binding-pattern changes at the DBH promoter site upon *T. gondii* infection, hence providing reliable information regarding locus site and time of action and their biological functions in silencing the DBH gene.

### 6.5.4 Characterise the detected-long non-coding RNA transcript at 5'TSS

The detected antisense lncRNA complementary to the protein-coding DBH strand described in this thesis needs continued research. Characterisation of the antisense lncRNA transcript is essential to determine its potential role in DBH transcription regulation. Meanwhile, the functional analysis of the lncRNA can be done by cloning the isolated fragment into an expression vector (e.g. pCR-XL-2-TOPO vector that is specialised for long fragment cloning) and transfecting it into cell cultures, then observing the effect on DBH gene expression. RNA structure can be predicted by *in silico* folding programs (computational models) and determined experimentally by chemical agents or enzymes that can selectively cut or modify RNA bases. Additional detailed methodologies can be referred to in a review presented by Kashi *et al.* (2016).

### **6.5.5 Assess chromatin accessibility changes throughout the neural cell genome with *T. gondii* infection**

Change in heterochromatin state may occur at multiple locations throughout the genome with infection, including the DBH region. Future experiments assaying chromatin structure may include assay for transposase-accessible chromatin with high-throughput sequencing (ATAC-Seq). The ATAC-seq is a method for mapping chromatin accessibility across the genome (Buenrostro *et al.*, 2015). It utilises a hyperactive Tn5 transposase to capture open chromatin sites by cutting exposed DNA sequences into fragments and ligating with sequencing adapters. Adapter-ligated DNA fragments are then isolated, amplified by PCR and used for next-generation sequencing. The number of sequencing reads for a region correlates with how open that chromatin is at a single nucleotide resolution.

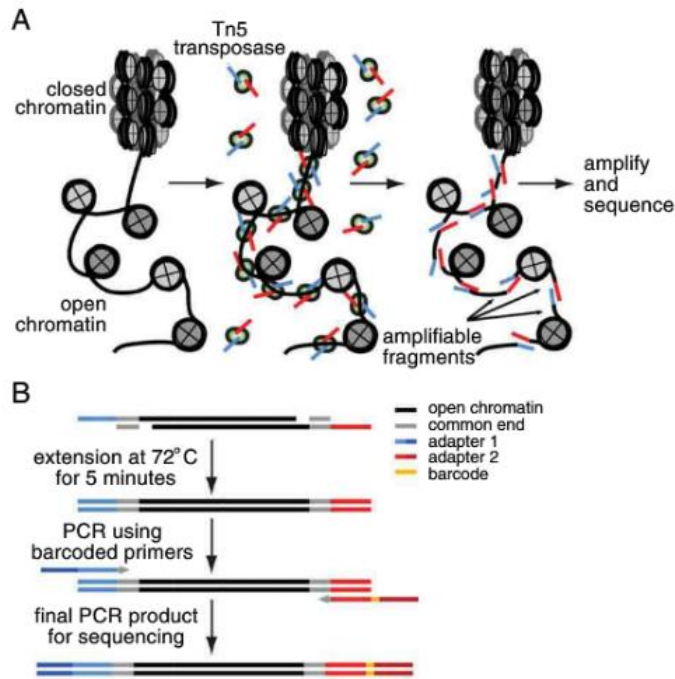


**Figure 6.2 Schematic workflow of the ATAC-seq process.** The assay was established by Buenrostro *et al.* (2015). (A) Transposition by hyperactive Tn5 transposase cut any open chromatin region resulting in fragmented DNAs. (B) Adapters (adapter 1 and adapter 2) were added prior to the PCR amplification by an extension steps at 72 °C. In the subsequent PCR, additional sequence was added to the adapters which include sequencing barcoded primers, and the final PCR product ended with DNA sequencing.

## 6.6 Conclusion

Even though the mechanistic details as to how the RNA and chromatin worlds connect remain unknown, this study attempted to demonstrate the involvement of antisense lncRNAs in silencing a gene through chromatin remodelling pathways, and possibly with the association of DNA methylation. This is the first description of neurotransmitter regulation by lncRNAs. Further details on how *T. gondii* induces lncRNA changes in the host cell's nucleus need further investigation, e.g. which exactly is the critical initiating event for DBH TGS. Elucidating the epigenetic mechanism can provide insight into how *T. gondii* can alter the expression of other genes, and possibly increase our understanding of mechanisms of gene regulation in the mammalian brain.

## List of References

- Afar, R., Silverman, R., Aguanno, A. and Albert, V.R. 1996. Positive and Negative Elements Contribute to the Cell-Specific Expression of the Rat Dopamine Beta-Hydroxylase Gene. *Molecular Brain Research*. **36**(1), pp.79-92.
- Al-Saady, I. 2016. *Immune Response Effect on Dopamine Production During Toxoplasma gondii Infection*. Doctor of Philosophy thesis, University of Leeds.
- Allis, C.D. and Jenuwein, T. 2016. The Molecular Hallmarks of Epigenetic Control. *Nature Reviews Genetics*. **17**, p487.
- Alsaady, I., Tedford, E., Alsaad, M., Bristow, G., Kohli, S., Murray, M., Reeves, M., Vijayabaskar, M., Clapcote, S.J. and Wastling, J. 2019. Downregulation of the Central Noradrenergic System by *Toxoplasma gondii* Infection. *Infection And Immunity*. **87**(2), pp.e00789-00718.
- Amir, R.E., Van den Veyver, I.B., Wan, M., Tran, C.Q., Francke, U. and Zoghbi, H.Y. 1999. Rett Syndrome Is Caused by Mutations in X-Linked MECP2, Encoding Methyl-CpG-Binding Protein 2. *Nature Genetics*. **23**(2), pp.185-188.
- Ando, M., Saito, Y., Xu, G., Bui, N.Q., Medetgul-Ernar, K., Pu, M., Fisch, K., Ren, S., Sakai, A. and Fukusumi, T. 2019. Chromatin Dysregulation and DNA Methylation at Transcription Start Sites Associated with Transcriptional Repression in Cancers. *Nature Communications*. **10**(1), p2188.
- Bak, J., Shim, S.-H., Kwon, Y.-J., Lee, H.-Y., Kim, J.S., Yoon, H. and Lee, Y.J. 2018. The Association between Suicide Attempts and *Toxoplasma gondii* Infection. *Clinical Psychopharmacology And Neuroscience : The Official Scientific Journal Of The Korean College of Neuropsychopharmacology*. **16**(1), pp.95-102.
- Barker-Haliski, M. and White, H.S. 2015. Glutamatergic Mechanisms Associated with Seizures and Epilepsy. *Cold Spring Harbor Perspectives In Medicine*. **5**(8), pa022863.
- Batz, M.B., Hoffmann, S. and Morris, J.G. 2012. Ranking the Disease Burden of 14 Pathogens in Food Sources in the United States Using Attribution Data from Outbreak Investigations and Expert Elicitation. *Journal of Food Protection*. **75**(7), pp.1278-1291.
- Bayer-Santos, E., Marini, M.M. and da Silveira, J.F. 2017. Non-Coding RNAs in Host-Pathogen Interactions: Subversion of Mammalian Cell Functions by Protozoan Parasites. *Frontiers in Microbiology*. **8**, p474.
- Becker, J.S., Nicetto, D. and Zaret, K.S. 2016. H3K9me3-Dependent Heterochromatin: Barrier to Cell Fate Changes. *Trends in Genetics*. **32**(1), pp.29-41.

- Berdoy, M., Webster, J.P. and Macdonald, D.W. 2000. Fatal Attraction in Rats Infected with *Toxoplasma gondii*. *Proceedings of the Royal Society of London. Series B: Biological Sciences*. **267**(1452), pp.1591-1594.
- Bessler, J.B., Andersen, E.C. and Villeneuve, A.M. 2010. Differential Localization and Independent Acquisition of the H3K9me2 and H3K9me3 Chromatin Modifications in the *Caenorhabditis elegans* Adult Germ Line. *PLOS Genetics*. **6**(1), pe1000830.
- Bird, A. 1992. The Essentials of DNA Methylation. *Cell Science*. **70**(1), pp.5-8.
- Bird, A. 2002. DNA Methylation Patterns and Epigenetic Memory. *Genes Development*. **16**(1), pp.6-21.
- Bird, A.P. 1980. DNA Methylation and the Frequency of CpG in Animal DNA. *Nucleic Acids Research*. **8**(7), pp.1499-1504.
- Bird, A.P. and Wolffe, A.P. 1999. Methylation-Induced Repression-Belts, Braces, and Chromatin. *Cell*. **99**(5), pp.451-454.
- Blader, I.J. and Koshy, A.A. 2014. *Toxoplasma gondii* Development of Its Replicative Niche: In Its Host Cell and Beyond. *Eukaryotic Cell*. **13**(8), pp.965-976.
- Blanchard, N., Dunay, I.R. and Schlüter, D. 2015. Persistence of *Toxoplasma gondii* in the Central Nervous System: A Fine-Tuned Balance between the Parasite, the Brain and the Immune System. *Parasite Immunology*. **37**(3), pp.150-158.
- Blumberg, B.M., Gelbard, H.A. and Epstein, L.G. 1994. HIV-1 Infection of the Developing Nervous System: Central Role of Astrocytes in Pathogenesis. *Virus Research*. **32**(2), pp.253-267.
- Bonasio, R. and Shiekhhattar, R. 2014. Regulation of Transcription by Long Noncoding RNAs. *Annual Review of Genetics*. **48**(1), pp.433-455.
- Bouchut, A., Chawla, A.R., Jeffers, V., Hudmon, A. and Sullivan, W.J., Jr. 2015. Proteome-Wide Lysine Acetylation in Cortical Astrocytes and Alterations That Occur During Infection with Brain Parasite *Toxoplasma gondii*. *PLOS ONE*. **10**(3), pe0117966.
- Bougdour, A., Durandau, E., Brenier-Pinchart, M.-P., Ortet, P., Barakat, M., Kieffer, S., Curt-Varesano, A., Curt-Bertini, R.-L., Bastien, O. and Coute, Y. 2013. Host Cell Subversion by *Toxoplasma* GRA16, an Exported Dense Granule Protein That Targets the Host Cell Nucleus and Alters Gene Expression. *Cell Host & Microbe*. **13**(4), pp.489-500.
- Bougdour, A., Tardieux, I. and Hakimi, M.-A. 2014. *Toxoplasma* Exports Dense Granule Proteins Beyond the Vacuole to the Host Cell Nucleus and Rewires the Host Genome Expression. *Cellular Microbiology*. **16**(3), pp.334-343.

- Brenet, F., Moh, M., Funk, P., Feierstein, E., Viale, A.J., Socci, N.D. and Scandura, J.M. 2011. DNA Methylation of the First Exon Is Tightly Linked to Transcriptional Silencing. *PLOS ONE*. **6**(1), pe14524.
- Brooks, J.M., Carrillo, G.L., Su, J., Lindsay, D.S., Fox, M.A. and Blader, I.J. 2015. *Toxoplasma gondii* Infections Alter GABAergic Synapses and Signaling in the Central Nervous System. *MBio*. **6**(6), pp.e01428-01415.
- Brown, C.J., Ballabio, A., Rupert, J.L., Lafreniere, R.G., Grompe, M., Tonlorenzi, R. and Willard, H.F.J.N. 1991. A Gene from the Region of the Human X Inactivation Centre Is Expressed. **349**, p3.
- Brunet, J., Pfaff, A.W., Abidi, A., Unoki, M., Nakamura, Y., Guinard, M., Klein, J.-P., Candolfi, E. and Mousli, M. 2008. *Toxoplasma gondii* Exploits UHRF1 and Induces Host Cell Cycle Arrest at G2 to Enable Its Proliferation. *Cellular Microbiology*. **10**(4), pp.908-920.
- Buenrostro, J.D., Wu, B., Chang, H.Y. and Greenleaf, W.J. 2015. ATAC-Seq: A Method for Assaying Chromatin Accessibility Genome-Wide. *Current Protocols In Molecular Biology*. **109**, pp.21.29.21-21.29.29.
- Bulut-Karslioglu, A., De La Rosa-Velázquez, Inti A., Ramirez, F., Barenboim, M., Onishi-Seebacher, M., Arand, J., Galán, C., Winter, Georg E., Engist, B., Gerle, B., O'Sullivan, Roderick J., Martens, Joost H.A., Walter, J., Manke, T., Lachner, M. and Jenuwein, T. 2014. Suv39h-Dependent H3K9me3 Marks Intact Retrotransposons and Silences Line Elements in Mouse Embryonic Stem Cells. *Molecular Cell*. **55**(2), pp.277-290.
- Burgdorf, K.S., Trabjerg, B.B., Pedersen, M.G., Nissen, J., Banasik, K., Pedersen, O.B., Sørensen, E., Nielsen, K.R., Larsen, M.H., Erikstrup, C., Bruun-Rasmussen, P., Westergaard, D., Thørner, L.W., Hjalgrim, H., Paarup, H.M., Brunak, S., Pedersen, C.B., Torrey, E.F., Werge, T., Mortensen, P.B., Yolken, R.H. and Ullum, H. 2019. Large-Scale Study of *Toxoplasma* and Cytomegalovirus Shows an Association between Infection and Serious Psychiatric Disorders. *Brain, Behavior, and Immunity*. **79**, pp.152-158.
- Butcher, B.A., Fox, B.A., Rommereim, L.M., Kim, S.G., Maurer, K.J., Yarovinsky, F., DeBroski, R.H., Bzik, D.J. and Denkers, E.Y. 2011. *Toxoplasma gondii* Rhopty Kinase ROP16 Activates STAT3 and STAT6 Resulting in Cytokine Inhibition and Arginase-1-Dependent Growth Control. *PLoS Pathogens*. **7**(9), pe1002236.
- Cabral, C.M., Tuladhar, S., Dietrich, H.K., Nguyen, E., MacDonald, W.R., Trivedi, T., Devineni, A. and Koshy, A.A. 2016. Neurons Are the Primary Target Cell for the Brain-Tropic Intracellular Parasite *Toxoplasma gondii*. *PLOS Pathogens*. **12**(2), pe1005447.
- Cai, Y., Chen, H., Mo, X., Tang, Y., Xu, X., Zhang, A., Lun, Z., Lu, F., Wang, Y. and Shen, J. 2014. *Toxoplasma gondii* Inhibits Apoptosis Via a Novel STAT3-Mir-17-92-Bim Pathway in Macrophages. *Cellular Signalling*. **26**(6), pp.1204-1212.
- Çakın Memik, N., Sönmez Tamer, G., Ünver, H. and Yıldız Gündoğdu, Ö. 2015. The Relationship between Pediatric Obsessive Compulsive Disorder and

*Toxoplasma gondii*. *Journal of Obsessive-Compulsive and Related Disorders*. **7**, pp.24-28.

- Cao, J. 2014. The Functional Role of Long Non-Coding RNAs and Epigenetics. *Biological Procedures Online*. **16**(1), p42.
- Chattopadhyaya, B., Di Cristo, G., Wu, C.Z., Knott, G., Kuhlman, S., Fu, Y., Palmiter, R.D. and Huang, Z.J. 2007. GAD67-Mediated GABA Synthesis and Signaling Regulate Inhibitory Synaptic Innervation in the Visual Cortex. *Neuron*. **54**(6), pp.889-903.
- Chen, Y., Wen, G., Rao, F., Zhang, K., Wang, L., Rodriguez-Flores, J.L., Sanchez, A.P., Mahata, M., Taupenot, L. and Sun, P. 2010. Human Dopamine Beta-Hydroxylase (DBH) Regulatory Polymorphism That Influences Enzymatic Activity, Autonomic Function, and Blood Pressure. *Journal of Hypertension*. **28**(1), p76.
- Clough, B. and Frickel, E.-M. 2017. The *Toxoplasma* Parasitophorous Vacuole: An Evolving Host–Parasite Frontier. *Trends in Parasitology*. **33**(6), pp.473-488.
- Coffey, M.J., Jennison, C., Tonkin, C.J. and Boddey, J.A. 2016. Role of the Er and Golgi in Protein Export by Apicomplexa. *Current Opinion in Cell Biology*. **41**, pp.18-24.
- Collas, P. 2010. The Current State of Chromatin Immunoprecipitation. *Molecular Biotechnology*. **45**(1), pp.87-100.
- Combarros, O., Warden, D.R., Hammond, N., Cortina-Borja, M., Belbin, O., Lehmann, M.G., Wilcock, G.K., Brown, K., Kehoe, P.G. and Barber, R. 2010. The Dopamine B-Hydroxylase-1021c/T Polymorphism Is Associated with the Risk of Alzheimer's Disease in the Epistasis Project. *BMC Medical Genetics*. **11**(1), p162.
- Consortium, I.H.G.S. 2001. Initial Sequencing and Analysis of the Human Genome. *Nature Reviews Genetics*. **409**(6822), p860.
- Coppens, I., Sinai, A.P. and Joiner, K.A. 2000. *Toxoplasma gondii* Exploits Host Low-Density Lipoprotein Receptor-Mediated Endocytosis for Cholesterol Acquisition. *The Journal Of Cell Biology*. **149**(1), pp.167-180.
- Courret, N., Darche, S., Sonigo, P., Milon, G., Buzoni-Gâtel, D. and Tardieux, I. 2006. Cd11c- and Cd11b-Expressing Mouse Leukocytes Transport Single *Toxoplasma gondii* Tachyzoites to the Brain. *Blood*. **107**(1), p309.
- Cubells, J.F., Price, L.H., Meyers, B.S., Anderson, G.M., Zabetian, C.P., Alexopoulos, G.S., Nelson, J.C., Sanacora, G., Kirwin, P. and Carpenter, L. 2002. Genotype-Controlled Analysis of Plasma Dopamine B-Hydroxylase Activity in Psychotic Unipolar Major Depression. *Biological Psychiatry*. **51**(5), pp.358-364.
- Dahl, J.A. and Collas, P. 2008. A Rapid Micro Chromatin Immunoprecipitation Assay (ChIP). *Nature Protocols*. **3**(6), p1032.
- Daubner, S.C., Le, T. and Wang, S. 2011. Tyrosine Hydroxylase and Regulation of Dopamine Synthesis. *Archives of Biochemistry and Biophysics*. **508**(1), pp.1-12.

- David, C.N., Frias, E.S., Szu, J.I., Vieira, P.A., Hubbard, J.A., Lovelace, J., Michael, M., Worth, D., McGovern, K.E. and Ethell, I.M. 2016. Glt-1-Dependent Disruption of CNS Glutamate Homeostasis and Neuronal Function by the Protozoan Parasite *Toxoplasma gondii*. *PLoS Pathogens*. **12**(6), pe1005643.
- de Barros, J.L.V.M., Barbosa, I.G., Salem, H., Rocha, N.P., Kummer, A., Okusaga, O.O., Soares, J.C. and Teixeira, A.L. 2017. Is There Any Association between *Toxoplasma gondii* Infection and Bipolar Disorder? A Systematic Review and Meta-Analysis. *Journal of Affective Disorders*. **209**, pp.59-65.
- Dellacasa-Lindberg, I., Hitziger, N. and Barragan, A. 2007. Localized Recrudescence of *Toxoplasma* Infections in the Central Nervous System of Immunocompromised Mice Assessed by in Vivo Bioluminescence Imaging. *Microbes and Infection*. **9**(11), pp.1291-1298.
- Delorme-Walker, V., Abrivard, M., Lagal, V., Anderson, K., Perazzi, A., Gonzalez, V., Page, C., Chauvet, J., Ochoa, W. and Volkmann, N. 2012. Toxofilin Upregulates the Host Cortical Actin Cytoskeleton Dynamics, Facilitating *Toxoplasma* Invasion. *Cell Sci*. **125**(18), pp.4333-4342.
- Derrien, T., Johnson, R., Bussotti, G., Tanzer, A., Djebali, S., Tilgner, H., Guernec, G., Martin, D., Merkel, A. and Knowles, D.G. 2012. The Gencode V7 Catalog of Human Long Noncoding RNAs: Analysis of Their Gene Structure, Evolution, and Expression. *Genome Research*. **22**(9), pp.1775-1789.
- Dimier, I. and Bout, D. 1998. Interferon-Gamma-Activated Primary Enterocytes Inhibit *Toxoplasma gondii* Replication: A Role for Intracellular Iron. *Immunology*. **94**(4), p488.
- Divanovic, S., Sawtell, N.M., Trompette, A., Warning, J.I., Dias, A., Cooper, A.M., Yap, G.S., Arditi, M., Shimada, K. and DuHadaway, J.B. 2011. Opposing Biological Functions of Tryptophan Catabolizing Enzymes During Intracellular Infection. *Journal of Infectious Diseases*. **205**(1), pp.152-161.
- Djebali, S., Davis, C.A., Merkel, A., Dobin, A., Lassmann, T., Mortazavi, A., Tanzer, A., Lagarde, J., Lin, W. and Schlesinger, F. 2012. Landscape of Transcription in Human Cells. *Nature*. **489**(7414), p101.
- Dubey, J., Miller, N.L. and Frenkel, J. 1970. The *Toxoplasma gondii* Oocyst from Cat Feces. *Journal of Experimental Medicine*. **132**(4), pp.636-662.
- Dubey, J.P. 2008. The History of *Toxoplasma gondii*-the First 100 Years. *Journal of Eukaryotic Microbiology*. **55**(6), pp.467-475.
- Dubey, J.P., Ferreira, L.R., Alsaad, M., Verma, S.K., Alves, D.A., Holland, G.N. and McConkey, G.A. 2016. Experimental Toxoplasmosis in Rats Induced Orally with Eleven Strains of *Toxoplasma gondii* of Seven Genotypes: Tissue Tropism, Tissue Cyst Size, Neural Lesions, Tissue Cyst Rupture without Reactivation, and Ocular Lesions. *PLOS ONE*. **11**(5), pe0156255.

- Eckhardt, F., Lewin, J., Cortese, R., Rakyan, V.K., Attwood, J., Burger, M., Burton, J., Cox, T.V., Davies, R. and Down, T.A. 2006. DNA Methylation Profiling of Human Chromosomes 6, 20 and 22. *Nature Genetics*. **38**(12), p1378.
- Estado, V., Stipursky, J., Gomes, F., Mergener, T.C., Frazão-Teixeira, E., Allodi, S., Tibiriçá, E., Barbosa, H.S. and Adesse, D. 2018. The Neurotropic Parasite *Toxoplasma gondii* Induces Sustained Neuroinflammation with Microvascular Dysfunction in Infected Mice. *The American Journal Of Pathology*. **188**(11), pp.2674-2687.
- Esteller, M. 2011. Non-Coding RNAs in Human Disease. *Nature Reviews Genetics*. **12**, p861.
- Fabiani, S., Pinto, B., Bonuccelli, U. and Bruschi, F. 2015. Neurobiological Studies on the Relationship between Toxoplasmosis and Neuropsychiatric Diseases. *Journal of The Neurological Sciences*. **351**(1-2), pp.3-8.
- Faghihi, M.A., Modarresi, F., Khalil, A.M., Wood, D.E., Sahagan, B.G., Morgan, T.E., Finch, C.E., St. Laurent Iii, G., Kenny, P.J. and Wahlestedt, C. 2008. Expression of a Noncoding RNA Is Elevated in Alzheimer's Disease and Drives Rapid Feed-Forward Regulation of B-Secretase. *Nature Medicine*. **14**(7), pp.723-730.
- Feng, J., Chang, H., Li, E. and Fan, G. 2005. Dynamic Expression of De Novo DNA Methyltransferases DNMT3a and DNMT3b in the Central Nervous System. *Journal of Neuroscience Research*. **79**(6), pp.734-746.
- Feng, J., Zhou, Y., Campbell, S.L., Le, T., Li, E., Sweatt, J.D., Silva, A.J. and Fan, G. 2010. DNMT1 and DNMT3a Maintain DNA Methylation and Regulate Synaptic Function in Adult Forebrain Neurons. *Nature Neuroscience*. **13**, p423.
- Fentress, S.J. and Sibley, L.D. 2011. The Secreted Kinase ROP18 Defends *Toxoplasma's* Border. *Bioessays*. **33**(9), pp.693-700.
- Ferguson, D.J.P. and Hutchison, W.M. 1987a. The Host-Parasite Relationship of *Toxoplasma gondii* in the Brains of Chronically Infected Mice. *Virchows Archiv A*. **411**(1), pp.39-43.
- Ferguson, D.J.P. and Hutchison, W.M. 1987b. An Ultrastructural Study of the Early Development and Tissue Cyst Formation of *Toxoplasma gondii* in the Brains of Mice. *Parasitology Research*. **73**(6), pp.483-491.
- Fernandes, C.R.J., Acuña, M.S., Aoki, I.J., Floeter-Winter, M.L. and Muxel, M.S. 2019. Long Non-Coding RNAs in the Regulation of Gene Expression: Physiology and Disease. *Non-Coding RNA*. **5**(1).
- Flegr, J. 2010. Influence of Latent Toxoplasmosis on the Phenotype of Intermediate Hosts. *Folia Parasitol* **57**(2), pp.81-87.
- Flegr, J. 2015. Neurological and Neuropsychiatric Consequences of Chronic *Toxoplasma* Infection. *Current Clinical Microbiology Reports*. **2**(4), pp.163-172.

- Flegr, J., Lenochová, P., Hodný, Z. and Vondrová, M. 2011. Fatal Attraction Phenomenon in Humans-Cat Odour Attractiveness Increased for *Toxoplasma*-Infected Men While Decreased for Infected Women. *PLOS Neglected Tropical Diseases*. **5**(11), pe1389.
- Flegr, J., Lindová, J. and Kodym, P. 2008. Sex-Dependent Toxoplasmosis-Associated Differences in Testosterone Concentration in Humans. *Parasitology*. **135**(4), pp.427-431.
- Flegr, J., Preiss, M., Klose, J., Havlíček, J., Vitáková, M. and Kodym, P. 2003. Decreased Level of Psychobiological Factor Novelty Seeking and Lower Intelligence in Men Latently Infected with the Protozoan Parasite *Toxoplasma gondii*: Dopamine, a Missing Link between Schizophrenia and Toxoplasmosis? *Biological Psychology*. **63**(3), pp.253-268.
- Franco, M., Panas, M.W., Marino, N.D., Lee, M.-C.W., Buchholz, K.R., Kelly, F.D., Bednarski, J.J., Sleckman, B.P., Pourmand, N. and Boothroyd, J.C. 2016. A Novel Secreted Protein, Myr1, Is Central to *Toxoplasma*'s Manipulation of Host Cells. *MBio*. **7**(1), pp.e02231-02215.
- Frommer, M., McDonald, L.E., Millar, D.S., Collis, C.M., Watt, F., Grigg, G.W., Molloy, P.L. and Paul, C.L. 1992. A Genomic Sequencing Protocol That Yields a Positive Display of 5-Methylcytosine Residues in Individual DNA Strands. *Proceedings of the National Academy of Sciences*. **89**(5), pp.1827-1831.
- Fuks, F., Burgers, W.A., Godin, N., Kasai, M. and Kouzarides, T. 2001. DNMT3a Binds Deacetylases and Is Recruited by a Sequence-Specific Repressor to Silence Transcription. *The EMBO journal*. **20**(10), pp.2536-2544.
- Fuks, F., Hurd, P.J., Deplus, R. and Kouzarides, T. 2003. The DNA Methyltransferases Associate with HP1 and the Suv39h1 Histone Methyltransferase. *Nucleic Acids Research*. **31**(9), pp.2305-2312.
- Fuks, J.M., Arrighi, R.B., Weidner, J.M., Mendu, S.K., Jin, Z., Wallin, R.P., Rethi, B., Birnir, B. and Barragan, A. 2012. Gabaergic Signaling Is Linked to a Hypermigratory Phenotype in Dendritic Cells Infected by *Toxoplasma gondii*. *PLoS Pathogens*. **8**(12), pe1003051.
- Furtado, J.M., Winthrop, K.L., Butler, N.J. and Smith, J.R. 2013. Ocular Toxoplasmosis I: Parasitology, Epidemiology and Public Health. *Clinical & Experimental Ophthalmology*. **41**(1), pp.82-94.
- Gade, P. and Kalvakolanu, D.V. 2012. Chromatin Immunoprecipitation Assay as a Tool for Analyzing Transcription Factor Activity. In: Vancura, A. ed. *Transcriptional Regulation: Methods and Protocols*. New York, NY: Springer New York, pp.85-104.
- Gajewski, P.D., Falkenstein, M., Hengstler, J.G. and Golka, K. 2014. *Toxoplasma gondii* Impairs Memory in Infected Seniors. *Brain, Behavior, and Immunity*. **36**, pp.193-199.

- Gale, S.D., Brown, B.L., Berrett, A., Erickson, L.D. and Hedges, D.W. 2014. Association between Latent Toxoplasmosis and Major Depression, Generalised Anxiety Disorder and Panic Disorder in Human Adults. *Folia Parasitologica*. **61**(4), p285.
- Gaskell, E.A., Smith, J.E., Pinney, J.W., Westhead, D.R. and McConkey, G.A. 2009. A Unique Dual Activity Amino Acid Hydroxylase in *Toxoplasma gondii*. *PLOS ONE*. **4**(3), pe4801.
- Gatkowska, J., Wieczorek, M., Dziadek, B., Dzitko, K. and Dlugonska, H. 2013. Sex-Dependent Neurotransmitter Level Changes in Brains of *Toxoplasma gondii* Infected Mice. *Experimental Parasitology*. **133**(1), pp.1-7.
- Gavin, D.P. and Sharma, R.P. 2010. Histone Modifications, DNA Methylation, and Schizophrenia. *Neuroscience Biobehavioral Review*. **34**(6), pp.882-888.
- Geisler, S. and Collier, J. 2013. RNA in Unexpected Places: Long Non-Coding RNA Functions in Diverse Cellular Contexts. *Nature Reviews Molecular Cell Biology*. **14**, p699.
- Goebel, S., Gross, U. and Lüder, C.G. 2001. Inhibition of Host Cell Apoptosis by *Toxoplasma gondii* Is Accompanied by Reduced Activation of the Caspase Cascade and Alterations of Poly (Adp-Ribose) Polymerase Expression. *Journal of Cell Science*. **114**(19), pp.3495-3505.
- Goto, K., Numata, M., Komura, J.-I., Ono, T., Bestor, T.H. and Kondo, H. 1994. Expression of DNA Methyltransferase Gene in Mature and Immature Neurons as Well as Proliferating Cells in Mice. *Differentiation*. **56**(1-2), pp.39-44.
- Grayson, D.R., Jia, X., Chen, Y., Sharma, R.P., Mitchell, C.P., Guidotti, A. and Costa, E. 2005. Reelin Promoter Hypermethylation in Schizophrenia. *Proceedings of the National Academy of Sciences*. **102**(26), pp.9341-9346.
- Greco, D., Zellmer, E., Zhang, Z. and Lewis, E. 1995. Transcription Factor Ap-2 Regulates Expression of the Dopamine Beta-Hydroxylase Gene. *Journal of Neurochemistry*. **65**(2), pp.510-516.
- Greene, L.A. and Tischler, A.S. 1976. Establishment of a Noradrenergic Clonal Line of Rat Adrenal Pheochromocytoma Cells Which Respond to Nerve Growth Factor. *Proceedings of the National Academy of Sciences of the United States of America*. **73**(7), pp.2424-2428.
- Grewal, S.I. and Moazed, D. 2003. Heterochromatin and Epigenetic Control of Gene Expression. *Science*. **301**(5634), pp.798-802.
- Guillemin, G.J., Smythe, G., Takikawa, O. and Brew, B.J. 2005. Expression of Indoleamine 2, 3-Dioxygenase and Production of Quinolinic Acid by Human Microglia, Astrocytes, and Neurons. *Glia*. **49**(1), pp.15-23.
- Guo, J.U., Ma, D.K., Mo, H., Ball, M.P., Jang, M.-H., Bonaguidi, M.A., Balazer, J.A., Eaves, H.L., Xie, B., Ford, E., Zhang, K., Ming, G.-I., Gao, Y. and Song, H. 2011.

Neuronal Activity Modifies the DNA Methylation Landscape in the Adult Brain. *Nature Neuroscience*. **14**(10), pp.1345-1351.

- Gupta, R.A., Shah, N., Wang, K.C., Kim, J., Horlings, H.M., Wong, D.J., Tsai, M.-C., Hung, T., Argani, P. and Rinn, J.L. 2010. Long Non-Coding RNA Hotair Reprograms Chromatin State to Promote Cancer Metastasis. *Nature*. **464**(7291), p1071.
- Haddad, F., Qin, A.X., Giger, J.M., Guo, H. and Baldwin, K.M. 2007. Potential Pitfalls in the Accuracy of Analysis of Natural Sense-Antisense RNA Pairs by Reverse Transcription-PCR. *BMC Biotechnology*. **7**(1), p21.
- Hakimi, M.-A. and Bougdour, A. 2015. *Toxoplasma's* Ways of Manipulating the Host Transcriptome Via Secreted Effectors. *Current Opinion in Microbiology*. **26**, pp.24-31.
- Hakimi, M.-A., Olias, P. and Sibley, L.D. 2017. *Toxoplasma* Effectors Targeting Host Signaling and Transcription. *Clinical Microbiology Reviews*. **30**(3), pp.615-645.
- Halonen, S.K. 2015. Modulation of Host Programmed Cell Death Pathways by the Intracellular Protozoan Parasite, *Toxoplasma gondii*—Implications for Maintenance of Chronic Infection and Potential Therapeutic Applications. *Cell Death-Autophagy, Apoptosis and Necrosis*. IntechOpen.
- Hangauer, M.J., Vaughn, I.W. and McManus, M.T. 2013. Pervasive Transcription of the Human Genome Produces Thousands of Previously Unidentified Long Intergenic Noncoding RNAs. *PLOS Genetics*. **9**(6), pe1003569.
- Hari Dass, S.A. and Vyas, A. 2014. *Toxoplasma gondii* Infection Reduces Predator Aversion in Rats through Epigenetic Modulation in the Host Medial Amygdala. *Molecular Ecology*. **23**(24), pp.6114-6122.
- Harker, K.S., Ueno, N. and Lodoen, M.B. 2015. *Toxoplasma gondii* Dissemination: A Parasite's Journey through the Infected Host. *Parasite Immunology*. **37**(3), pp.141-149.
- Haroon, F., Händel, U., Angenstein, F., Goldschmidt, J., Kreutzmann, P., Lison, H., Fischer, K.-D., Scheich, H., Wetzel, W., Schlüter, D. and Budinger, E. 2012. *Toxoplasma gondii* Actively Inhibits Neuronal Function in Chronically Infected Mice. *PLOS ONE*. **7**(4), pe35516.
- Havlíček, J., Gašová, Z., Smith, A.P., Zvára, K. and Flegr, J. 2001. Decrease of Psychomotor Performance in Subjects with Latent 'Asymptomatic' toxoplasmosis. *Parasitology*. **122**(5), pp.515-520.
- Hawkins, P.G. and Morris, K.V. 2008. RNA and Transcriptional Modulation of Gene Expression. *Cell Cycle*. **7**(5), pp.602-607.
- Hawkins, P.G., Santoso, S., Adams, C., Anest, V. and Morris, K.V. 2009. Promoter Targeted Small RNAs Induce Long-Term Transcriptional Gene Silencing in Human Cells. *Nucleic Acids Research*. **37**(9), pp.2984-2995.

- Healy, D.G., Abou-Sleiman, P.M., Ozawa, T., Lees, A.J., Bhatia, K., Ahmadi, K.R., Wullner, U., Berciano, J., Moller, J.C. and Kamm, C. 2004. A Functional Polymorphism Regulating Dopamine B-Hydroxylase Influences against Parkinson's Disease. *Annals of Neurology: Official Journal of the American Neurological Association the Child Neurology Society*. **55**(3), pp.443-446.
- Henriquez, S., Brett, R., Alexander, J., Pratt, J. and Roberts, C. 2009. Neuropsychiatric Disease and *Toxoplasma gondii* Infection. *Neuroimmunomodulation*. **16**(2), pp.122-133.
- Hervouet, E., Vallette, F.M. and Cartron, P.-F. 2009. DNMT3/Transcription Factor Interactions as Crucial Players in Targeted DNA Methylation. *Epigenetics*. **4**(7), pp.487-499.
- Hill, D. and Dubey, J.P. 2002. *Toxoplasma gondii*: Transmission, Diagnosis and Prevention. *Clinical Microbiology And Infection*. **8**(10), pp.634-640.
- Holland, G.N. 2004. Ocular Toxoplasmosis: A Global Reassessment: Part Ii: Disease Manifestations and Management. *American Journal of Ophthalmology*. **137**(1), pp.1-17.
- Holub, D., Flegr, J., Dragomirecka, E., Rodriguez, M., Preiss, M., Novak, T., Čermák, J., Horáček, J., Kodym, P. and Libiger, J. 2013. Differences in Onset of Disease and Severity of Psychopathology between Toxoplasmosis-Related and Toxoplasmosis-Unrelated Schizophrenia. *Acta Psychiatrica Scandinavica*. **127**(3), pp.227-238.
- Holz-Schietinger, C. and Reich, N.O. 2012. RNA Modulation of the Human DNA Methyltransferase 3a. *Nucleic Acids Research*. **40**(17), pp.8550-8557.
- Horacek, J., Flegr, J., Tintera, J., Verebova, K., Spaniel, F., Novak, T., Brunovsky, M., Bubenikova-Valesova, V., Holub, D., Palenicek, T. and Höschl, C. 2012. Latent Toxoplasmosis Reduces Gray Matter Density in Schizophrenia but Not in Controls: Voxel-Based-Morphometry (Vbm) Study. *The World Journal of Biological Psychiatry*. **13**(7), pp.501-509.
- Howe, D.K. and Sibley, L.D. 1995. *Toxoplasma gondii* Comprises Three Clonal Lineages: Correlation of Parasite Genotype with Human Disease. *The Journal of Infectious Diseases*. **172**(6), pp.1561-1566.
- Hoyle, G., Mercer, E., Palmiter, R. and Brinster, R. 1994. Cell-Specific Expression from the Human Dopamine Beta-Hydroxylase Promoter in Transgenic Mice Is Controlled Via a Combination of Positive and Negative Regulatory Elements. *Journal of Neuroscience*. **14**(5), pp.2455-2463.
- Hu, R.-S., He, J.-J., Elsheikha, H.M., Zhang, F.-K., Zou, Y., Zhao, G.-H., Cong, W. and Zhu, X.-Q. 2018. Differential Brain MicroRNA Expression Profiles after Acute and Chronic Infection of Mice with *Toxoplasma gondii* Oocysts. *Frontiers in Microbiology*. **9**, p2316.

- Huang, Y., Pastor, W.A., Shen, Y., Tahiliani, M., Liu, D.R. and Rao, A. 2010. The Behaviour of 5-Hydroxymethylcytosine in Bisulfite Sequencing. *PLOS ONE*. **5**(1), pe8888.
- Hutchison, W.M., Bradley, M., Cheyne, W.M., Wells, B.W.P. and Hay, J. 1980. Behavioural Abnormalities in *Toxoplasma*-Infected Mice. *Annals of Tropical Medicine & Parasitology*. **74**(3), pp.337-345.
- Ihara, F., Nishimura, M., Muroi, Y., Mahmoud, M.E., Yokoyama, N., Nagamune, K. and Nishikawa, Y. 2016. *Toxoplasma gondii* Infection in Mice Impairs Long-Term Fear Memory Consolidation through Dysfunction of the Cortex and Amygdala. *Infection Immunity*. **84**(10), pp.2861-2870.
- Ingram, W.M., Goodrich, L.M., Robey, E.A. and Eisen, M.B. 2013. Mice Infected with Low-Virulence Strains of *Toxoplasma gondii* Lose Their Innate Aversion to Cat Urine, Even after Extensive Parasite Clearance. *PLOS ONE*. **8**(9), pe75246.
- Iyer, M.K., Niknafs, Y.S., Malik, R., Singhal, U., Sahu, A., Hosono, Y., Barrette, T.R., Prensner, J.R., Evans, J.R. and Zhao, S. 2015. The Landscape of Long Noncoding RNAs in the Human Transcriptome. *Nature Genetics*. **47**(3), p199.
- Jayanthi, S., McCoy, M.T., Chen, B., Britt, J.P., Kourrich, S., Yau, H.-J., Ladenheim, B., Krasnova, I.N., Bonci, A. and Cadet, J.L. 2014. Methamphetamine Downregulates Striatal Glutamate Receptors Via Diverse Epigenetic Mechanisms. *Biological Psychiatry*. **76**(1), pp.47-56.
- Jia, B., Chang, Z., Wei, X., Lu, H., Yin, J., Jiang, N. and Chen, Q. 2014. Plasma Micrnas Are Promising Novel Biomarkers for the Early Detection of *Toxoplasma gondii* Infection. *Parasites Vectors*. **7**(1), p433.
- Jones-Brando, L., Torrey, E.F. and Yolken, R. 2003. Drugs Used in the Treatment of Schizophrenia and Bipolar Disorder Inhibit the Replication of *Toxoplasma gondii*. *Schizophrenia Research*. **62**(3), pp.237-244.
- Jones, J.L. and Dubey, J.P. 2012. Foodborne Toxoplasmosis. *Clinical Infectious Diseases*. **55**(6), pp.845-851.
- Jones, P.A. 2012. Functions of DNA Methylation: Islands, Start Sites, Gene Bodies and Beyond. *Nature Reviews Genetics*. **13**(7), p484.
- Jones, P.L., Jan Veenstra, G.C., Wade, P.A., Vermaak, D., Kass, S.U., Landsberger, N., Strouboulis, J. and Wolffe, A.P. 1998. Methylated DNA and MeCP2 Recruit Histone Deacetylase to Repress Transcription. *Nature Genetics*. **19**, p187.
- Kashi, K., Henderson, L., Bonetti, A. and Carninci, P. 2016. Discovery and Functional Analysis of LncRNAs: Methodologies to Investigate an Uncharacterized Transcriptome. *Biochimica et Biophysica Acta (BBA) - Gene Regulatory Mechanisms*. **1859**(1), pp.3-15.
- Katayama, S., Tomaru, Y., Kasukawa, T., Waki, K., Nakanishi, M., Nakamura, M., Nishida, H., Yap, C., Suzuki, M. and Kawai, J. 2005. Antisense Transcription in the Mammalian Transcriptome. *Science*. **309**(5740), pp.1564-1566.

- Kaushik, M., Lamberton, P.H. and Webster, J.P. 2012. The Role of Parasites and Pathogens in Influencing Generalised Anxiety and Predation-Related Fear in the Mammalian Central Nervous System. *Hormones Behavioral Neuroscience*. **62**(3), pp.191-201.
- Kawaguchi, Y. and Shindou, T. 1998. Noradrenergic Excitation and Inhibition of GABAergic Cell Types in Rat Frontal Cortex. *The Journal of Neuroscience*. **18**(17), p6963.
- Keller, P., Schaumburg, F., Fischer, S.F., Häcker, G., Groß, U. and Lüder, C.G.K. 2006. Direct Inhibition of Cytochrome C-Induced Caspase Activation in Vitro by *Toxoplasma gondii* Reveals Novel Mechanisms of Interference with Host Cell Apoptosis. *FEMS Microbiology Letters*. **258**(2), pp.312-319.
- Khalil, A.M., Guttman, M., Huarte, M., Garber, M., Raj, A., Morales, D.R., Thomas, K., Presser, A., Bernstein, B.E. and van Oudenaarden, A. 2009. Many Human Large Intergenic Noncoding RNAs Associate with Chromatin-Modifying Complexes and Affect Gene Expression. *Proceedings of the National Academy of Sciences*. **106**(28), pp.11667-11672.
- Khan, A., Dubey, J., Su, C., Ajioka, J.W., Rosenthal, B.M. and Sibley, L.D. 2011. Genetic Analyses of Atypical *Toxoplasma gondii* Strains Reveal a Fourth Clonal Lineage in North America. *International Journal For Parasitology*. **41**(6), pp.645-655.
- Kim, D.H., Villeneuve, L.M., Morris, K.V. and Rossi, J.J. 2006. Argonaute-1 Directs SiRNA-Mediated Transcriptional Gene Silencing in Human Cells. *Nature Structural & Molecular Biology*. **13**(9), pp.793-797.
- Kim, M.J., Jung, B.-K., Cho, J., Song, H., Pyo, K.-H., Lee, J.M., Kim, M.-K. and Chai, J.-Y. 2016. Exosomes Secreted by *Toxoplasma gondii*-Infected L6 Cells: Their Effects on Host Cell Proliferation and Cell Cycle Changes. *The Korean Journal of Parasitology*. **54**(2), pp.147-154.
- Konradt, C., Ueno, N., Christian, D.A., DeLong, J.H., Pritchard, G.H., Herz, J., Bzik, D.J., Koshy, A.A., McGavern, D.B., Lodoen, M.B. and Hunter, C.A. 2016. Endothelial Cells Are a Replicative Niche for Entry of *Toxoplasma gondii* to the Central Nervous System. *Nature Microbiology*. **1**, p16001.
- Kornienko, A.E., Guenzl, P.M., Barlow, D.P. and Pauler, F.M. 2013. Gene Regulation by the Act of Long Non-Coding RNA Transcription. *BMC Biology*. **11**(1), p59.
- Koshy, A.A., Dietrich, H.K., Christian, D.A., Melehani, J.H., Shastri, A.J., Hunter, C.A. and Boothroyd, J.C. 2012. *Toxoplasma* Co-opts Host Cells It Does Not Invade. *PLOS Pathogens*. **8**(7), pe1002825.
- Kouzarides, T. 2007. Chromatin Modifications and Their Function. *Cell Sci*. **128**(4), pp.693-705.
- Kriaucionis, S. and Heintz, N. 2009. The Nuclear DNA Base 5-Hydroxymethylcytosine Is Present in Purkinje Neurons and the Brain. *Science*. **324**(5929), pp.929-930.

- Kuo, M.-H. and Allis, C.D. 1999. In Vivo Cross-Linking and Immunoprecipitation for Studying Dynamic Protein:DNA Associations in a Chromatin Environment. *Methods*. **19**(3), pp.425-433.
- Labonté, B., Suderman, M., Maussion, G., Lopez, J.P., Navarro-Sánchez, L., Yerko, V., Mechawar, N., Szyf, M., Meaney, M.J. and Turecki, G. 2013. Genome-Wide Methylation Changes in the Brains of Suicide Completers. *American Journal of Psychiatry*. **170**(5), pp.511-520.
- Lachner, M., O'Carroll, D., Rea, S., Mechtler, K. and Jenuwein, T. 2001. Methylation of Histone H3 Lysine 9 Creates a Binding Site for HP1 Proteins. *Nature*. **410**(6824), pp.116-120.
- Lang, C., Hildebrandt, A., Brand, F., Opitz, L., Dihazi, H. and Lüder, C.G.K. 2012. Impaired Chromatin Remodelling at STAT1-Regulated Promoters Leads to Global Unresponsiveness of *Toxoplasma gondii*-Infected Macrophages to IFN-gamma. *PLOS Pathogens*. **8**(1), pe1002483.
- Lee, T.I., Johnstone, S.E. and Young, R.A. 2006. Chromatin Immunoprecipitation and Microarray-Based Analysis of Protein Location. *Nature Protocols*. **1**(2), pp.729-748.
- Li, B., Carey, M. and Workman, J.L. 2007. The Role of Chromatin During Transcription. *Cell*. **128**(4), pp.707-719.
- Li, L.-C. and Dahiya, R. 2002. Methprimer: Designing Primers for Methylation Pcrs. *Bioinformatics*. **18**(11), pp.1427-1431.
- Li, Y. and Tollefsbol, T.O. 2011. DNA Methylation Detection: Bisulfite Genomic Sequencing Analysis. In: Tollefsbol, T.O. ed. *Epigenetics Protocols*. Totowa, NJ: Humana Press, pp.11-21.
- Lim, A., Kumar, V., Hari Dass, S.A. and Vyas, A. 2013. *Toxoplasma gondii* Infection Enhances Testicular Steroidogenesis in Rats. *Molecular Ecology*. **22**(1), pp.102-110.
- Liu, W., Huang, L., Wei, Q., Zhang, Y., Zhang, S., Zhang, W., Cai, L. and Liang, S. 2018. Microarray Analysis of Long Non-Coding RNA Expression Profiles Uncovers a *Toxoplasma*-Induced Negative Regulation of Host Immune Signaling. *Parasites Vectors*. **11**(1), p174.
- Lüder, C.G.K., Giraldo-Velásquez, M., Sendtner, M. and Gross, U. 1999. *Toxoplasma gondii* in Primary Rat CNS Cells: Differential Contribution of Neurons, Astrocytes, and Microglial Cells for the Intracerebral Development and Stage Differentiation. *Experimental Parasitology*. **93**(1), pp.23-32.
- Luft, B.J. and Remington, J.S. 1992. Toxoplasmic Encephalitis in Aids. *Clinical Infectious Diseases*. **15**(2), pp.211-222.
- Lykins, J., Wang, K., Wheeler, K., Clouser, F., Dixon, A., El Bissati, K., Zhou, Y., Lyttle, C., Rzhetsky, A. and McLeod, R. 2016. Understanding Toxoplasmosis in the

United States through “Large Data” Analyses. *Reviews of Infectious Diseases*. **63**(4), pp.468-475.

MacRae, J.I., Sheiner, L., Nahid, A., Tonkin, C., Striepen, B. and McConville, M.J. 2012. Mitochondrial Metabolism of Glucose and Glutamine Is Required for Intracellular Growth of *Toxoplasma gondii*. *Cell Host & Microbe*. **12**(5), pp.682-692.

Madden, K.S., Sanders, V.M. and Felten, D.L. 1995. Catecholamine Influences and Sympathetic Neural Modulation of Immune Responsiveness. *Annual Review of Pharmacology and Toxicology*. **35**(1), pp.417-448.

Maenz, M., Schlüter, D., Liesenfeld, O., Schares, G., Gross, U. and Pleyer, U. 2014. Ocular Toxoplasmosis Past, Present and New Aspects of an Old Disease. *Progress in Retinal and Eye Research*. **39**, pp.77-106.

Magistri, M., Faghihi, M.A., St Laurent, G. and Wahlestedt, C. 2012. Regulation of Chromatin Structure by Long Noncoding RNAs: Focus on Natural Antisense Transcripts. *Trends in Genetics*. **28**(8), pp.389-396.

Mahmoud, M.E., Fereig, R. and Nishikawa, Y. 2017. Involvement of Host Defense Mechanisms against *Toxoplasma gondii* Infection in Anhedonic and Despair-Like Behaviors in Mice. *Infection Immunity*. **85**(4), pp.e00007-00017.

Markovitz, A.A., Simanek, A.M., Yolken, R.H., Galea, S., Koenen, K.C., Chen, S. and Aiello, A.E. 2015. *Toxoplasma gondii* and Anxiety Disorders in a Community-Based Sample. *Brain, Behavior, and Immunity*. **43**, pp.192-197.

Martianov, I., Ramadass, A., Barros, A.S., Chow, N. and Akoulitchev, A. 2007. Repression of the Human Dihydrofolate Reductase Gene by a Non-Coding Interfering Transcript. *Nature*. **445**(7128), p666.

Martin, H.L., Alsaady, I., Howell, G., Prandovszky, E., Peers, C., Robinson, P. and McConkey, G.A. 2015. Effect of Parasitic Infection on Dopamine Biosynthesis in Dopaminergic Cells. *Neuroscience*. **306**, pp.50-62.

Martinowich, K., Hattori, D., Wu, H., Fouse, S., He, F., Hu, Y., Fan, G. and Sun, Y.E. 2003. DNA Methylation-Related Chromatin Remodeling in Activity-Dependent Bdnf Gene Regulation. *Science*. **302**(5646), pp.890-893.

Martynowicz, J., Augusto, L., Wek, R.C., Boehm, S.L. and Sullivan, W.J. 2019. Guanabenz Reverses a Key Behavioral Change Caused by Latent Toxoplasmosis in Mice by Reducing Neuroinflammation. *MBio*. **10**(2), pp.e00381-00319.

McManus, M.T. and Sharp, P.A. 2002. Gene Silencing in Mammals by Small Interfering RNAs. *Nature Reviews Genetics*. **3**(10), pp.737-747.

McMaster, W.R., Morrison, C.J. and Kobor, M.S. 2016. Epigenetics: A New Model for Intracellular Parasite–Host Cell Regulation. *Trends in Parasitology*. **32**(7), pp.515-521.

- Melzer, T., Cranston, H., Weiss, L. and Halonen, S. 2010. Host Cell Preference of *Toxoplasma gondii* Cysts in Murine Brain: A Confocal Study. *Journal of Neuroparasitology*. **1**.
- Menard, K.L., Haskins, B.E., Colombo, A.P. and Denkers, E.Y. 2018. *Toxoplasma gondii* Manipulates Expression of Host Long Noncoding RNA During Intracellular Infection. *Scientific Reports*. **8**.
- Mercer, T.R., Dinger, M.E. and Mattick, J.S. 2009. Long Non-Coding RNAs: Insights into Functions. *Nature reviews genetics*. **10**(3), p155.
- Mercer, T.R. and Mattick, J.S. 2013. Structure and Function of Long Noncoding RNAs in Epigenetic Regulation. *Nature Structural & Molecular Biology*. **20**, p300.
- Miller, B.H., Zeier, Z., Xi, L., Lanz, T.A., Deng, S., Strathmann, J., Willoughby, D., Kenny, P.J., Elsworth, J.D., Lawrence, M.S., Roth, R.H., Edbauer, D., Kleiman, R.J. and Wahlestedt, C. 2012. MicroRNA-132 Dysregulation in Schizophrenia Has Implications for Both Neurodevelopment and Adult Brain Function. *Proceedings of the National Academy of Sciences*. **109**(8), p3125.
- Miman, O., Kusbeci, O.Y., Aktepe, O.C. and Cetinkaya, Z. 2010a. The Probable Relation between *Toxoplasma gondii* and Parkinson's Disease. *Neuroscience Letters*. **475**(3), pp.129-131.
- Miman, O., Mutlu, E.A., Ozcan, O., Atambay, M., Karlidag, R. and Unal, S. 2010b. Is There Any Role of *Toxoplasma gondii* in the Etiology of Obsessive–Compulsive Disorder? *Psychiatry Research*. **177**(1), pp.263-265.
- Mitra, R., Sapolsky, R.M. and Vyas, A. 2013. *Toxoplasma gondii* Infection Induces Dendritic Retraction in Basolateral Amygdala Accompanied by Reduced Corticosterone Secretion. *Disease Models & Mechanisms*. **6**(2), p516.
- Möhle, L., Parlog, A., Pahnke, J. and Dunay, I.R. 2014. Spinal Cord Pathology in Chronic Experimental *Toxoplasma gondii* Infection. *European Journal of Microbiology Immunology*. **4**(1), pp.65-75.
- Mondal, T., Rasmussen, M., Pandey, G.K., Isaksson, A. and Kanduri, C. 2010. Characterization of the RNA Content of Chromatin. *Genome Research*. **20**(7), pp.899-907.
- Montoya, J.G. and Remington, J.S. 1996. Toxoplasmic Chorioretinitis in the Setting of Acute Acquired Toxoplasmosis. *Clinical Infectious Diseases*. **23**(2), pp.277-282.
- Moore, L.D., Le, T. and Fan, G. 2012. DNA Methylation and Its Basic Function. *Neuropsychopharmacology*. **38**, p23.
- Morgado, P., Sudarshana, D.M., Gov, L., Harker, K.S., Lam, T., Casali, P., Boyle, J.P. and Lodoen, M.B. 2014. Type II *Toxoplasma gondii* Induction of CD40 on Infected Macrophages Enhances Interleukin-12 Responses. *Infection And immunity*. **82**(10), pp.4047-4055.

- Morris, K.V. 2005. Sirna-Mediated Transcriptional Gene Silencing: The Potential Mechanism and a Possible Role in the Histone Code. *Cellular Molecular Life Sciences CMLS*. **62**(24), pp.3057-3066.
- Morris, K.V. 2009. Long Antisense Non-Coding RNAs Function to Direct Epigenetic Complexes That Regulate Transcription in Human Cells. *Epigenetics*. **4**(5), pp.296-301.
- Morris, K.V., Chan, S.W.-L., Jacobsen, S.E. and Looney, D.J. 2004. Small Interfering RNA-Induced Transcriptional Gene Silencing in Human Cells. *Science*. **305**(5688), pp.1289-1292.
- Mozzetta, C., Pontis, J., Fritsch, L., Robin, P., Portoso, M., Proux, C., Margueron, R. and Ait-Si-Ali, S. 2014. The Histone H3 Lysine 9 Methyltransferases G9a and Glp Regulate Polycomb Repressive Complex 2-Mediated Gene Silencing. *Molecular Cell*. **53**(2), pp.277-289.
- Mustapic, M., Presecki, P., Pivac, N., Mimica, N., Hof, P.R., Simic, G., Folnegovic-Smalc, V. and Muck-Seler, D. 2013. Genotype-Independent Decrease in Plasma Dopamine Beta-Hydroxylase Activity in Alzheimer's Disease. *Progress in Neuro-Psychopharmacology Biological Psychiatry*. **44**, pp.94-99.
- Mutskov, V. and Felsenfeld, G. 2004. Silencing of Transgene Transcription Precedes Methylation of Promoter DNA and Histone H3 Lysine 9. *The EMBO journal*. **23**(1), pp.138-149.
- Nan, X., Ng, H.-H., Johnson, C.A., Laherty, C.D., Turner, B.M., Eisenman, R.N. and Bird, A. 1998. Transcriptional Repression by the Methyl-CpG-Binding Protein MeCP2 Involves a Histone Deacetylase Complex. *Nature*. **393**(6683), pp.386-389.
- Nash, P.B., Purner, M.B., Leon, R.P., Clarke, P., Duke, R.C. and Curiel, T.J. 1998. *Toxoplasma gondii*-Infected Cells Are Resistant to Multiple Inducers of Apoptosis. *The Journal of Immunology*. **160**(4), p1824.
- Nelson, J.D., Denisenko, O. and Bomsztyk, K. 2006. Protocol for the Fast Chromatin Immunoprecipitation (ChIP) Method. *Nature Protocols*. **1**(1), p179.
- Newell-Price, J., Clark, A.J.L. and King, P. 2000. DNA Methylation and Silencing of Gene Expression. *Trends in Endocrinology & Metabolism*. **11**(4), pp.142-148.
- Ng, S.-Y., Lin, L., Soh, B.S. and Stanton, L.W. 2013. Long Noncoding RNAs in Development and Disease of the Central Nervous System. *Trends in Genetics*. **29**(8), pp.461-468.
- Notarangelo, F., Wilson, E., Horning, K., Thomas, M., Harris, T., Fang, Q., Hunter, C. and Schwarcz, R. 2014. Evaluation of Kynurenine Pathway Metabolism in *Toxoplasma gondii*-Infected Mice: Implications for Schizophrenia. *Schizophrenia Research*. **152**(1), pp.261-267.
- O'Donnell, J., Zeppenfeld, D., McConnell, E., Pena, S. and Nedergaard, M. 2012. Norepinephrine: A Neuromodulator That Boosts the Function of Multiple Cell

- Types to Optimize CNS Performance. *Neurochemical research*. **37**(11), pp.2496-2512.
- Oka, M., Rodić, N., Graddy, J., Chang, L.-J. and Terada, N. 2006. CpG Sites Preferentially Methylated by DNMT3a in Vivo. *Journal of Biological Chemistry*. **281**(15), pp.9901-9908.
- Okusaga, O., Langenberg, P., Sleemi, A., Vaswani, D., Giegling, I., Hartmann, A.M., Konte, B., Friedl, M., Groer, M.W. and Yolken, R.H. 2011. *Toxoplasma gondii* Antibody Titers and History of Suicide Attempts in Patients with Schizophrenia. *Schizophrenia Research*. **133**(1-3), pp.150-155.
- Ondounda, M., Ilozue, C. and Magne, C. 2016. Cerebro-Meningeal Infections in HIV-Infected Patients: A Study of 116 Cases in Libreville, Gabon. *African Health Sciences*. **16**(2), pp.603-610.
- Orlando, V., Strutt, H. and Paro, R. 1997. Analysis of Chromatin Structure by in Vivo Formaldehyde Cross-Linking. *Methods*. **11**(2), pp.205-214.
- Pang, K.C., Frith, M.C. and Mattick, J.S. 2006. Rapid Evolution of Noncoding RNAs: Lack of Conservation Does Not Mean Lack of Function. *Trends in Genetics*. **22**(1), pp.1-5.
- Parlog, A., Harsan, L.-A., Zagrebelsky, M., Weller, M., von Elverfeldt, D., Mawrin, C., Korte, M. and Dunay, I.R. 2014. Chronic Murine Toxoplasmosis Is Defined by Subtle Changes in Neuronal Connectivity. *Disease Models & Mechanisms*. **7**(4), p459.
- Parlog, A., Schluter, D. and Dunay, I.R. 2015. *Toxoplasma gondii*-Induced Neuronal Alterations. *Parasite Immunology*. **37**(3), pp.159-170.
- Payne, T.M., Molestina, R.E. and Sinai, A.P. 2003. Inhibition of Caspase Activation and a Requirement for Nf-Kb Function in the *Toxoplasma gondii*-Mediated Blockade of Host Apoptosis. *Journal of Cell Science*. **116**(21), pp.4345-4358.
- Pelechano, V. and Steinmetz, L.M. 2013. Gene Regulation by Antisense Transcription. *Nature Reviews Genetics*. **14**(12), p880.
- Penny, G.D., Kay, G.F., Sheardown, S.A., Rastan, S. and Brockdorff, N. 1996. Requirement for Xist in X Chromosome Inactivation. *Nature*. **379**(6561), p131.
- Pittman, K.J. and Knoll, L.J. 2015. Long-Term Relationships: The Complicated Interplay between the Host and the Developmental Stages of *Toxoplasma gondii* During Acute and Chronic Infections. *Microbiol. Mol. Biol. Rev.* **79**(4), pp.387-401.
- Pope, S.M. and Lässer, C. 2013. *Toxoplasma Gondii* Infection of Fibroblasts Causes the Production of Exosome-Like Vesicles Containing a Unique Array of mRNA and miRNA Transcripts Compared to Serum Starvation. *Journal of Extracellular Vesicles*. **2**(1), p22484.

- Prandovszky, E., Gaskell, E., Martin, H., Dubey, J., Webster, J.P. and McConkey, G.A. 2011. The Neurotropic Parasite *Toxoplasma gondii* Increases Dopamine Metabolism. *PLOS ONE*. **6**(9), pe23866.
- Quinn, J.J. and Chang, H.Y. 2015. Unique Features of Long Non-Coding RNA Biogenesis and Function. *Nature Reviews Genetics*. **17**, p47.
- Razin, A. 1998. CpG Methylation, Chromatin Structure and Gene Silencing—a Three-Way Connection. *The EMBO journal*. **17**(17), pp.4905-4908.
- Razin, A. and Cedar, H. 1991. DNA Methylation and Gene Expression. *Microbiology Molecular Biology Reviews*. **55**(3), pp.451-458.
- Rea, S., Eisenhaber, F., O'Carroll, D., Strahl, B.D., Sun, Z.-W., Schmid, M., Opravil, S., Mechtler, K., Ponting, C.P. and Allis, C.D. 2000. Regulation of Chromatin Structure by Site-Specific Histone H3 Methyltransferases. *Nature*. **406**(6796), p593.
- Rice, J.C., Briggs, S.D., Ueberheide, B., Barber, C.M., Shabanowitz, J., Hunt, D.F., Shinkai, Y. and Allis, C.D. 2003. Histone Methyltransferases Direct Different Degrees of Methylation to Define Distinct Chromatin Domains. *Molecular Cell*. **12**(6), pp.1591-1598.
- Rinn, J.L., Kertesz, M., Wang, J.K., Squazzo, S.L., Xu, X., Brugmann, S.A., Goodnough, L.H., Helms, J.A., Farnham, P.J. and Segal, E. 2007. Functional Demarcation of Active and Silent Chromatin Domains in Human HOX Loci by Noncoding RNAs. *Cell Cycle*. **129**(7), pp.1311-1323.
- Riyahi, A.A., Al-Anouti, F., Al-Rayes, M. and Ananvoranich, S. 2006. Single Argonaute Protein from *Toxoplasma gondii* Is Involved in the Double-Stranded RNA Induced Gene Silencing. *International Journal For Parasitology*. **36**(9), pp.1003-1014.
- Roberts, T.C., Morris, K.V. and Weinberg, M.S. 2014a. Perspectives on the Mechanism of Transcriptional Regulation by Long Non-Coding RNAs. *Epigenetics*. **9**(1), pp.13-20.
- Roberts, T.C., Morris, K.V. and Wood, M.J. 2014b. The Role of Long Non-Coding RNAs in Neurodevelopment, Brain Function and Neurological Disease. *Philosophical Transactions of the Royal Society B: Biological Sciences*. **369**(1652), p20130507.
- Robinson, M.D., Storzaker, C., Statham, A.L., Coolen, M.W., Song, J.Z., Nair, S.S., Strbenac, D., Speed, T.P. and Clark, S.J. 2010. Evaluation of Affinity-Based Genome-Wide DNA Methylation Data: Effects of CpG Density, Amplification Bias, and Copy Number Variation. *Genome Research*. **20**(12), pp.1719-1729.
- Rowley, N.M., Madsen, K.K., Schousboe, A. and Steve White, H. 2012. Glutamate and GABA Synthesis, Release, Transport and Metabolism as Targets for Seizure Control. *Neurochemistry International*. **61**(4), pp.546-558.
- Rozenfeld, C., Martinez, R., Figueiredo, R.T., Bozza, M.T., Lima, F.R., Pires, A.L., Silva, P.M., Bonomo, A., Lannes-Vieira, J. and De Souza, W. 2003. Soluble Factors

Released by *Toxoplasma gondii*-Infected Astrocytes Down-Modulate Nitric Oxide Production by Gamma Interferon-Activated Microglia and Prevent Neuronal Degeneration. *Infection Immunity*. **71**(4), pp.2047-2057.

- Rozenfeld, C., Martinez, R., Seabra, S., Sant'Anna, C., Gonçalves, J.G.R., Bozza, M., Moura-Neto, V. and De Souza, W. 2005. *Toxoplasma gondii* Prevents Neuron Degeneration by Interferon-gamma-Activated Microglia in a Mechanism Involving Inhibition of Inducible Nitric Oxide Synthase and Transforming Growth Factor-B1 Production by Infected Microglia. *The American Journal Of Pathology*. **167**(4), pp.1021-1031.
- Saayman, S., Ackley, A., Turner, A.-M.W., Famiglietti, M., Bosque, A., Clemson, M., Planelles, V. and Morris, K.V. 2014. An HIV-Encoded Antisense Long Noncoding RNA Epigenetically Regulates Viral Transcription. *Molecular Therapy*. **22**(6), pp.1164-1175.
- Sabou, M., Doderer-Lang, C., Leyer, C., Konjic, A., Kubina, S., Lennon, S., Rohr, O., Viville, S., Cianféroni, S., Candolfi, E., Pfaff, A.W. and Brunet, J. 2019. *Toxoplasma gondii* ROP16 Kinase Silences the Cyclin B1 Gene Promoter by Hijacking Host Cell UHRF1-Dependent Epigenetic Pathways. *Cellular and Molecular Life Sciences*.
- Saeij, J.P., Boyle, J.P. and Boothroyd, J.C. 2005. Differences among the Three Major Strains of *Toxoplasma gondii* and Their Specific Interactions with the Infected Host. *Trends in Parasitology*. **21**(10), pp.476-481.
- Salvioni, A., Belloy, M., Lebourg, A., Bassot, E., Cantaloube-Ferrieu, V., Vasseur, V., Blanié, S., Liblau, R.S., Suberbielle, E., Robey, E.A. and Blanchard, N. 2019. Robust Control of a Brain-Persisting Parasite through MHC I Presentation by Infected Neurons. *Cell Reports*. **27**(11), pp.3254-3268.e3258.
- Samojłowicz, D., Twarowska-Malczyńska, J., Borowska-Solonyńko, A., Poniowski, Ł.A., Sharma, N. and Olczak, M. 2019. Presence of *Toxoplasma gondii* Infection in Brain as a Potential Cause of Risky Behavior: A Report of 102 Autopsy Cases. *European Journal of Clinical Microbiology Infectious Diseases*. **38**(2), pp.305-317.
- Sarciron, M. and Gherardi, A. 2000. Cytokines Involved in Toxoplasmic Encephalitis. *Scandinavian Journal of Immunology*. **52**(6), pp.534-543.
- Scallan, E., Hoekstra, R.M., Angulo, F.J., Tauxe, R.V., Widdowson, M.-A., Roy, S.L., Jones, J.L. and Griffin, P.M. 2011. Foodborne Illness Acquired in the United States--Major Pathogens. *Emerging Infectious Diseases*. **17**(1), pp.7-15.
- Schaeffer, M., Han, S.-J., Chtanova, T., van Dooren, G.G., Herzmark, P., Chen, Y., Roysam, B., Striepen, B. and Robey, E.A. 2009. Dynamic Imaging of T Cell-Parasite Interactions in the Brains of Mice Chronically Infected with *Toxoplasma gondii*. *The Journal of Immunology*. **182**(10), pp.6379-6393.
- Schlüter, D., Deckert, M., Hof, H. and Frei, K. 2001. *Toxoplasma gondii* Infection of Neurons Induces Neuronal Cytokine and Chemokine Production, but Gamma

Interferon- and Tumor Necrosis Factor-Stimulated Neurons Fail to Inhibit the Invasion and Growth of *T. gondii*. *Infection And Immunity*. **69**(12), pp.7889-7893.

Schübeler, D. 2015. Function and Information Content of DNA Methylation. *Nature*. **517**(7534), p321.

Schübeler, D., Lorincz, M.C., Cimborá, D.M., Telling, A., Feng, Y.-Q., Bouhassira, E.E. and Groudine, M. 2000. Genomic Targeting of Methylated DNA: Influence of Methylation on Transcription, Replication, Chromatin Structure, and Histone Acetylation. *Molecular and Cellular Biology*. **20**(24), p9103.

Schwarcz, R. and Hunter, C.A. 2007. *Toxoplasma gondii* and Schizophrenia: Linkage through Astrocyte-Derived Kynurenic Acid? *Schizophrenia Bulletin*. **33**(3), pp.652-653.

Schwarcz, R. and Pellicciari, R. 2002. Manipulation of Brain Kynurenines: Glial Targets, Neuronal Effects, and Clinical Opportunities. *Journal of Pharmacology Experimental Therapeutics*. **303**(1), pp.1-10.

Seizova, S., Garnham, A.L., Coffey, M.J., Whitehead, L.W., Rogers, K.L. and Tonkin, C. 2019. *Toxoplasma gondii* Bradyzoites Elicit Transcriptional Changes in Host Cells to Prevent Ifny-Mediated Cell Death. *Cell Press*.

Shen, L., Guo, Y., Chen, X., Ahmed, S. and Issa, J.-P.J. 2007. Optimizing Annealing Temperature Overcomes Bias in Bisulfite PCR Methylation Analysis. *Biotechniques*. **42**(1), pp.48-58.

Shogren-Knaak, M., Ishii, H., Sun, J.-M., Pazin, M.J., Davie, J.R. and Peterson, C.L. 2006. Histone H4-K16 Acetylation Controls Chromatin Structure and Protein Interactions. *Science*. **311**(5762), pp.844-847.

Sibley, L.D., Khan, A., Ajioka, J.W. and Rosenthal, B.M. 2009. Genetic Diversity of *Toxoplasma gondii* in Animals and Humans. *Philosophical Transactions Of The Royal Society Of London. Series B, Biological Sciences*. **364**(1530), pp.2749-2761.

Sibley, L.D., Messina, M. and Niesman, I.R. 1994. Stable DNA Transformation in the Obligate Intracellular Parasite *Toxoplasma gondii* by Complementation of Tryptophan Auxotrophy. *Proceedings of the National Academy of Sciences*. **91**(12), pp.5508-5512.

Sigova, A.A., Mullen, A.C., Molinie, B., Gupta, S., Orlando, D.A., Guenther, M.G., Almada, A.E., Lin, C., Sharp, P.A., Giallourakis, C.C. and Young, R.A. 2013. Divergent Transcription of Long Noncoding RNA/mRNA Gene Pairs in Embryonic Stem Cells. *Proceedings of the National Academy of Sciences*. **110**(8), p2876.

Sikes, M.L., Bradshaw, J.M., Ivory, W.T., Lunsford, J.L., McMillan, R.E. and Morrison, C.R. 2009. A Streamlined Method for Rapid and Sensitive Chromatin Immunoprecipitation. *Journal of Immunological Methods*. **344**(1), pp.58-63.

Silva, N.M., Manzan, R.M., Carneiro, W.P., Milanezi, C.M., Silva, J.S., Ferro, E.A.V. and Mineo, J.R. 2010. *Toxoplasma Gondii*: The Severity of Toxoplasmic Encephalitis

in C57bl/6 Mice Is Associated with Increased Alcam and Vcam-1 Expression in the Central Nervous System and Higher Blood–Brain Barrier Permeability. *Experimental parasitology*. **126**(2), pp.167-177.

- Silva, N.M., Rodrigues, C.V., Santoro, M.M., Reis, L.F., Alvarez-Leite, J.I. and Gazzinelli, R.T. 2002. Expression of Indoleamine 2, 3-Dioxygenase, Tryptophan Degradation, and Kynurenine Formation During in Vivo Infection with *Toxoplasma gondii*: Induction by Endogenous Gamma Interferon and Requirement of Interferon Regulatory Factor 1. *Infection Immunity*. **70**(2), pp.859-868.
- Sinai, A., Payne, T., Carmen, J., Hardi, L., Watson, S. and Molestina, R. 2004. Mechanisms Underlying the Manipulation of Host Apoptotic Pathways by *Toxoplasma gondii*. *International Journal For Parasitology*. **34**(3), pp.381-391.
- Skallova, A., Kodym, P., Frynta, D. and Flegr, J. 2006. The Role of Dopamine in *Toxoplasma*-Induced Behavioural Alterations in Mice: An Ethological and Ethopharmacological Study. *Parasitology*. **133**(5), pp.525-535.
- Smith, Z.D. and Meissner, A. 2013. DNA Methylation: Roles in Mammalian Development. *Nature Reviews Genetics*. **14**(3), p204.
- Stewart, M.D., Li, J. and Wong, J. 2005. Relationship between Histone H3 Lysine 9 Methylation, Transcription Repression, and Heterochromatin Protein 1 Recruitment. *Molecular and Cellular Biology*. **25**(7), p2525.
- Stibbs, H. 1985. Changes in Brain Concentrations of Catecholamines and Indoleamines in *Toxoplasma gondii* Infected Mice. *Annals of Tropical Medicine Parasitology*. **79**(2), pp.153-157.
- Stirzaker, C., Song, J.Z., Davidson, B. and Clark, S.J. 2004. Transcriptional Gene Silencing Promotes DNA Hypermethylation through a Sequential Change in Chromatin Modifications in Cancer Cells. *Cancer Research*. **64**(11), p3871.
- Strahl, B.D. and Allis, C.D. 2000. The Language of Covalent Histone Modifications. *Nature*. **403**(6765), p41.
- Syn, G., Anderson, D., Blackwell, J.M. and Jamieson, S.E. 2018. Epigenetic Dysregulation of Host Gene Expression in *Toxoplasma* Infection with Specific Reference to Dopamine and Amyloid Pathways. *Infection, Genetics and Evolution*. **65**, pp.159-162.
- Taft, R.J., Pang, K.C., Mercer, T.R., Dinger, M. and Mattick, J.S. 2010. Non-Coding RNAs: Regulators of Disease. *The Journal of Pathology*. **220**(2), pp.126-139.
- Tahiliani, M., Koh, K.P., Shen, Y., Pastor, W.A., Bandukwala, H., Brudno, Y., Agarwal, S., Iyer, L.M., Liu, D.R. and Aravind, L. 2009. Conversion of 5-Methylcytosine to 5-Hydroxymethylcytosine in Mammalian DNA by Mll Partner Tet1. *Science*. **324**(5929), pp.930-935.
- Tamaru, H. and Selker, E.U. 2001. A Histone H3 Methyltransferase Controls DNA Methylation in *Neurospora crassa*. *Nature*. **414**(6861), p277.

- Tamaru, H., Zhang, X., McMillen, D., Singh, P.B., Nakayama, J.-i., Grewal, S.I., Allis, C.D., Cheng, X. and Selker, E.U. 2003. Trimethylated Lysine 9 of Histone H3 Is a Mark for DNA Methylation in *Neurospora crassa*. *Nature Genetics*. **34**(1), p75.
- Tanaka, S., Nishimura, M., Ihara, F., Yamagishi, J., Suzuki, Y. and Nishikawa, Y. 2013. Transcriptome Analysis of Mouse Brain Infected with *Toxoplasma gondii*. *Infection And Immunity*. **81**(10), pp.3609-3619.
- Tate, P.H. and Bird, A.P. 1993. Effects of DNA Methylation on DNA-Binding Proteins and Gene Expression. *Current Opinion in Genetics & Development*. **3**(2), pp.226-231.
- Tedford, E.R. 2018. *Neurophysiological Changes During Chronic Toxoplasma gondii Infection*. PhD thesis, University of Leeds.
- Tenter, A.M., Heckeroth, A.R. and Weiss, L.M. 2000. *Toxoplasma gondii*: From Animals to Humans. *International Journal For Parasitology*. **30**(12-13), pp.1217-1258.
- Thomas, F., Lafferty Kevin, D., Brodeur, J., Elguero, E., Gauthier-Clerc, M. and Missé, D. 2012. Incidence of Adult Brain Cancers Is Higher in Countries Where the Protozoan Parasite *Toxoplasma gondii* Is Common. *Biology Letters*. **8**(1), pp.101-103.
- Ting, A.H., Schuebel, K.E., Herman, J.G. and Baylin, S.B. 2005. Short Double-Stranded RNA Induces Transcriptional Gene Silencing in Human Cancer Cells in the Absence of DNA Methylation. *Nature Genetics*. **37**(8), pp.906-910.
- Torrey, E.F., Bartko, J.J., Lun, Z.-R. and Yolken, R.H. 2006. Antibodies to *Toxoplasma gondii* in Patients with Schizophrenia: A Meta-Analysis. *Schizophrenia Bulletin*. **33**(3), pp.729-736.
- Torrey, E.F. and Yolken, R.H. 2003. *Toxoplasma gondii* and Schizophrenia. *Emerging Infectious Diseases*. **9**(11), p1375.
- Tsai, M.-C., Manor, O., Wan, Y., Mosammamaparast, N., Wang, J.K., Lan, F., Shi, Y., Segal, E. and Chang, H.Y. 2010. Long Noncoding RNA as Modular Scaffold of Histone Modification Complexes. *Science*. **329**(5992), p689.
- Tucker, K.L. 2001. Methylated Cytosine and the Brain: A New Base for Neuroscience. *Neuron*. **30**(3), pp.649-652.
- Turner, B.M. 2007. Defining an Epigenetic Code. *Nature Cell Biology*. **9**(1), p2.
- Tyebji, S., Seizova, S., Hannan, A.J. and Tonkin, C.J. 2019. Toxoplasmosis: A Pathway to Neuropsychiatric Disorders. *Neuroscience & Biobehavioral Reviews*. **96**, pp.72-92.
- Unoki, M., Brunet, J. and Mousli, M. 2009. Drug Discovery Targeting Epigenetic Codes: The Great Potential of UHRF1, Which Links DNA Methylation and Histone Modifications, as a Drug Target in Cancers and Toxoplasmosis. *Biochemical Pharmacology*. **78**(10), pp.1279-1288.

- Vadaie, N. and Morris, K.V. 2013. Long Antisense Non-Coding RNAs and the Epigenetic Regulation of Gene Expression. *Biomolecular Concepts*. **4**(4), pp.411-415.
- Viré, E., Brenner, C., Deplus, R., Blanchon, L., Fraga, M., Didelot, C., Morey, L., Van Eynde, A., Bernard, D. and Vanderwinden, J.-M. 2006. The Polycomb Group Protein EZH2 Directly Controls DNA Methylation. *Nature*. **439**(7078), p871.
- Vyas, A. 2015. Mechanisms of Host Behavioral Change in *Toxoplasma gondii* Rodent Association. *PLOS Pathogens*. **11**(7), pe1004935.
- Vyas, A., Kim, S.-K., Giacomini, N., Boothroyd, J.C. and Sapolsky, R.M. 2007. Behavioral Changes Induced by *Toxoplasma* Infection of Rodents Are Highly Specific to Aversion of Cat Odors. *Proceedings of the National Academy of Sciences*. **104**(15), pp.6442-6447.
- Weber, M., Davies, J.J., Wittig, D., Oakeley, E.J., Haase, M., Lam, W.L. and Schübeler, D. 2005. Chromosome-Wide and Promoter-Specific Analyses Identify Sites of Differential DNA Methylation in Normal and Transformed Human Cells. *Nature Genetics*. **37**, p853.
- Weber, M., Hellmann, I., Stadler, M.B., Ramos, L., Pääbo, S., Rebhan, M. and Schübeler, D. 2007. Distribution, Silencing Potential and Evolutionary Impact of Promoter DNA Methylation in the Human Genome. *Nature Genetics*. **39**, p457.
- Weber, M. and Schübeler, D. 2007. Genomic Patterns of DNA Methylation: Targets and Function of an Epigenetic Mark. *Current Opinion In Cell Biology*. **19**(3), pp.273-280.
- Webster, J., Lamberton, P., Donnelly, C. and Torrey, E. 2006. Parasites as Causative Agents of Human Affective Disorders? The Impact of Anti-Psychotic, Mood-Stabilizer and Anti-Parasite Medication on *Toxoplasma gondii*'s Ability to Alter Host Behaviour. *Proceedings of the Royal Society B: Biological Sciences*. **273**(1589), pp.1023-1030.
- Webster, J.P. 1994. The Effect of *Toxoplasma gondii* and Other Parasites on Activity Levels in Wild and Hybrid Rattus Norvegicus. *Parasitology*. **109**(5), pp.583-589.
- Webster, J.P. 2007. The Effect of *Toxoplasma gondii* on Animal Behavior: Playing Cat and Mouse. *Schizophrenia Bulletin*. **33**(3), pp.752-756.
- Webster, J.P. and McConkey, G.A. 2010. *Toxoplasma gondii*-Altered Host Behaviour: Clues as to Mechanism of Action. *Folia parasitologica*. **57**(2), p95.
- Weinberg, M.S. and Morris, K.V. 2013. Long Non-Coding RNA Targeting and Transcriptional De-Repression. *Nucleic Acid Therapeutics*. **23**(1), pp.9-14.
- Weinberg, M.S. and Morris, K.V. 2016. Transcriptional Gene Silencing in Humans. *Nucleic Acids Research*. **44**(14), pp.6505-6517.
- Weinberg, M.S., Villeneuve, L.M., Ehsani, A., Amarzguioui, M., Aagaard, L., Chen, Z.-X., Riggs, A.D., Rossi, J.J. and Morris, K.V. 2006. The Antisense Strand of Small

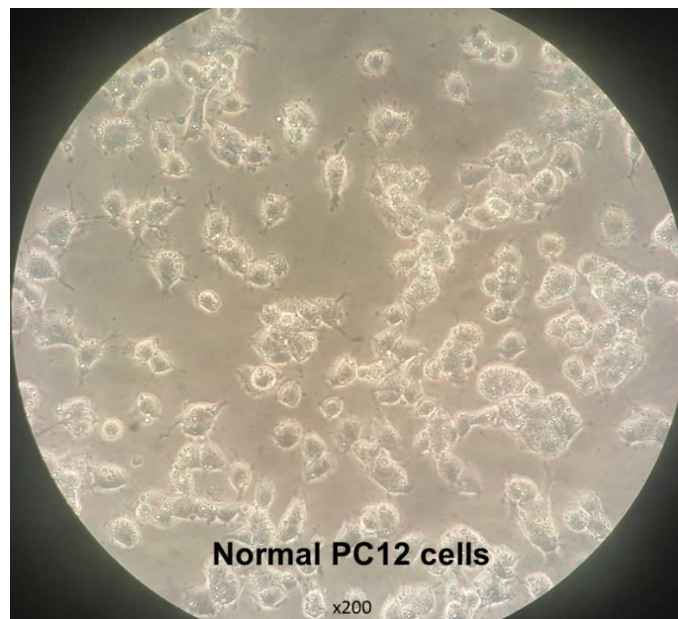
Interfering RNAs Directs Histone Methylation and Transcriptional Gene Silencing in Human Cells. *RNA*. **12**(2), pp.256-262.

- Weiss, L.M. and Dubey, J.P. 2009. Toxoplasmosis: A History of Clinical Observations. *International Journal for Parasitology*. **39**(8), pp.895-901.
- Whitehead, J., Pandey, G.K. and Kanduri, C. 2009. Regulation of the Mammalian Epigenome by Long Noncoding RNAs. *Biochimica et Biophysica Acta (BBA) - General Subjects*. **1790**(9), pp.936-947.
- Wockner, L.F., Noble, E.P., Lawford, B.R., Young, R.M., Morris, C.P., Whitehall, V.L. and Voisey, J. 2014. Genome-Wide DNA Methylation Analysis of Human Brain Tissue from Schizophrenia Patients. *Translational Psychiatry*. **4**(1), pe339.
- Wohlfert, E.A., Blader, I.J. and Wilson, E.H. 2017. Brains and Brawn: *Toxoplasma* Infections of the Central Nervous System and Skeletal Muscle. *Trends in Parasitology*. **33**(7), pp.519-531.
- Wutz, A. 2003. Xist RNA Associates with Chromatin and Causes Gene Silencing. *Noncoding RNAs: Molecular biology molecular medicine. Georgetown : Landes Bioscience*. pp.49-65.
- Xiao, J., Li, Y., Prandovszky, E., Karuppagounder, S.S., Talbot, C.C., Dawson, V.L., Dawson, T.M. and Yolken, R.H. 2014. MicroRNA-132 Dysregulation in *Toxoplasma gondii* Infection Has Implications for Dopamine Signaling Pathway. *Neuroscience*. **268**, pp.128-138.
- Xie, S., Wang, Z., Okano, M., Nogami, M., Li, Y., He, W.-W., Okumura, K. and Li, E. 1999. Cloning, Expression and Chromosome Locations of the Human DNMT3 Gene Family. *Gene*. **236**(1), pp.87-95.
- Yeivin, A. and Razin, A. 1993. Gene Methylation Patterns and Expression. *DNA Methylation*. Springer, pp.523-568.
- Yong, W.-S., Hsu, F.-M. and Chen, P.-Y. 2016. Profiling Genome-Wide DNA Methylation. *Epigenetics & Chromatin*. **9**(1), p26.
- Yu, J.-Y., DeRuiter, S.L. and Turner, D.L. 2002. RNA Interference by Expression of Short-Interfering RNAs and Hairpin RNAs in Mammalian Cells. *Proceedings of the National Academy of Sciences*. **99**(9), p6047.
- Zeiner, G.M., Norman, K.L., Thomson, J.M., Hammond, S.M. and Boothroyd, J.C. 2010. *Toxoplasma gondii* Infection Specifically Increases the Levels of Key Host MicroRNAs. *PLOS ONE*. **5**(1), pe8742.
- Zhao, J., Sun, B.K., Erwin, J.A., Song, J.-J. and Lee, J.T. 2008. Polycomb Proteins Targeted by a Short Repeat RNA to the Mouse X Chromosome. *Science*. **322**(5902), p750.

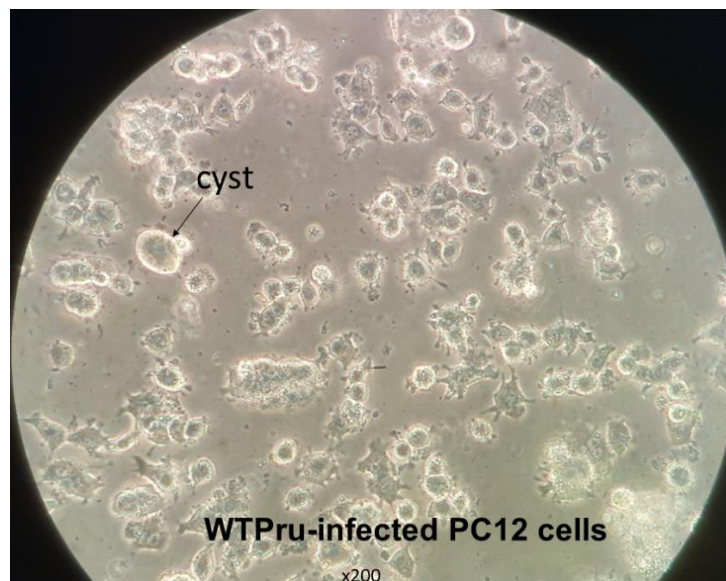
## Appendix A

### A.1 Photos of normal PC12 cells and *T. gondii* parasites in PC12 and HFF cells

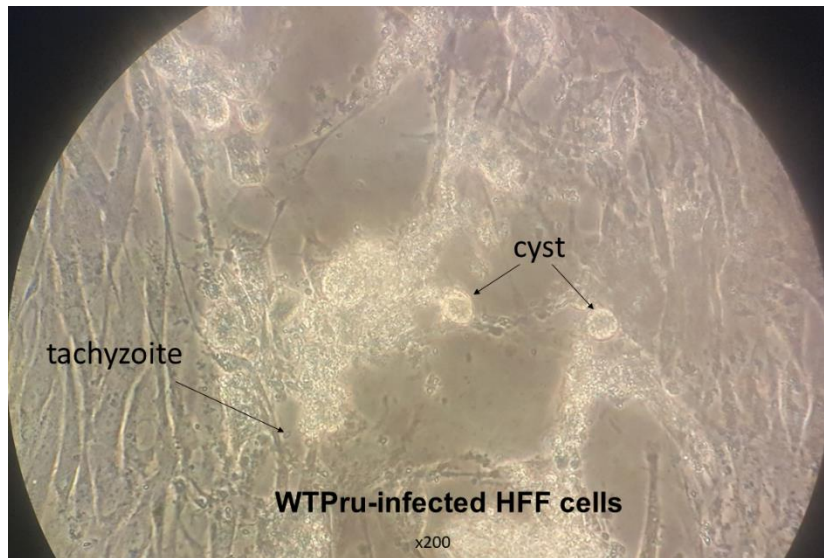
#### A.1.1 Normal rat neural PC12 cells



#### A.1.2 WTPru *T. gondii*-Infected PC12 cells



**A.1.3 WTPru *T.gondii*-infected HFF cells (after pH induction)**



## Appendix B

### B.1 DBH gene expression in MOI infection of *T. gondii*-infected PC12 cells with respect to the housekeeping gene, rat GAPDH, on day five post-infection, analysed by RT-qPCR

The assay was done for three biological repeats (Repeat 1-3). Values of Cqs (triplicates) and data analysis of the RT-qPCR as in the following tables. Data analysis was calculated by implementing  $-\Delta Cq$  method ( $\Delta Cq = Cq \text{ sample} - Cq \text{ GAPDH}$ ). The  $\Delta Cq$  was the difference in Cq values, between Cq sample and Cq of the reference gene (GAPDH) by which the average of Cq GAPDH was subtracted from the average Cq sample. This method was implemented throughout the gene expression assays used in this study.

#### B.1.1 Repeat 1

	Biological Repeat 1							
	Cq DBH				Cq GAPDH			
	Cq 1	Cq 2	Cq 3	Average	Cq 1	Cq 2	Cq 3	Average
<b>Un-infected Day 5</b>	20.06	20.09	20.61	<b>20.25</b>	18.97	18.78	18.92	<b>18.89</b>
<b>Infected 1:1</b>	22.09	22.31	22.30	<b>22.23</b>	19.45	19.40	19.46	<b>19.44</b>
<b>Infected 2:1</b>	21.99	22.25	22.32	<b>22.19</b>	19.89	19.79	19.63	<b>19.77</b>
<b>Infected 3:1</b>	22.11	22.01	22.39	<b>22.17</b>	19.95	19.75	19.83	<b>19.84</b>
<b>Infected 4:1</b>	22.47	22.56	22.80	<b>22.61</b>	20.16	20.32	20.21	<b>20.23</b>
<b>Infected 5:1</b>	22.86	23.25	23.18	<b>23.10</b>	20.34	20.36	20.28	<b>20.33</b>

	Biological Repeat 1			
	Average Cq DBH	Average Cq GAPDH	DBH-GAPDH 1	SEM (triplicate wells)
<b>Un-infected Day 5</b>	20.25	18.89	-1.36	0.18
<b>Infected 1:1</b>	22.23	19.44	-2.80	0.07
<b>Infected 2:1</b>	22.19	19.77	-2.42	0.10
<b>Infected 3:1</b>	22.17	19.84	-2.33	0.11
<b>Infected 4:1</b>	22.61	20.23	-2.38	0.10
<b>Infected 5:1</b>	23.10	20.33	-2.77	0.12

## B.1.2 Repeat 2

	Biological Repeat 2							
	Cq DBH				Cq GAPDH			
	Cq 1	Cq 2	Cq 3	Average	Cq 1	Cq 2	Cq 3	Average
<b>Un-infected Day 5</b>	21.81	21.67	21.83	<b>21.77</b>	19.67	19.64	19.8	<b>19.70</b>
<b>Infected 1:1</b>	24.59	24.72	25.06	<b>24.79</b>	20.24	20.21	20.26	<b>20.24</b>
<b>Infected 2:1</b>	26.62	26.74	26.76	<b>26.71</b>	21.29	21.39	21.36	<b>21.35</b>
<b>Infected 3:1</b>	23.83	24.08	24.21	<b>24.04</b>	21.28	21.43	21.32	<b>21.34</b>
<b>Infected 4:1</b>	23.53	23.56	23.52	<b>23.54</b>	22.16	22.09	22.07	<b>22.11</b>
<b>Infected 5:1</b>	24.66	24.98	24.87	<b>24.84</b>	21.55	21.42	21.43	<b>21.47</b>

	Biological Repeat 2			
	Average Cq DBH	Average Cq GAPDH	DBH-GAPDH 1	SEM (triplicate wells)
<b>Un-infected Day 5</b>	21.77	19.70	-2.07	0.05
<b>Infected 1:1</b>	24.79	20.24	-4.55	0.14
<b>Infected 2:1</b>	26.71	21.35	-5.36	0.04
<b>Infected 3:1</b>	24.04	21.34	-2.70	0.11
<b>Infected 4:1</b>	23.54	22.11	-1.43	0.01
<b>Infected 5:1</b>	24.84	21.47	-3.37	0.09

## B.1.3 Repeat 3

	Biological Repeat 3							
	Cq DBH				Cq GAPDH			
	Cq 1	Cq 2	Cq 3	Average	Cq 1	Cq 2	Cq 3	Average
<b>Un-infected Day 5</b>	23.67	23.28	23.42	<b>23.46</b>	20.33	20.36	20.44	<b>20.38</b>
<b>Infected 1:1</b>	23.73	23.21	23.34	<b>23.43</b>	20.93	20.75	20.68	<b>20.79</b>
<b>Infected 2:1</b>	21.91	21.54	21.43	<b>21.63</b>	20.20	20.12	20.07	<b>20.13</b>
<b>Infected 3:1</b>	24.25	23.82	24.10	<b>24.06</b>	20.79	20.64	20.57	<b>20.67</b>
<b>Infected 4:1</b>	25.31	24.89	25.21	<b>25.14</b>	22.14	21.87	22.03	<b>22.01</b>
<b>Infected 5:1</b>	26.84	26.74	27.17	<b>26.92</b>	23.53	23.52	23.65	<b>23.57</b>

	Biological Repeat 3			
	Average Cq DBH	Average Cq GAPDH	DBH-GAPDH 1	SEM (triplicate wells)
<b>Un-infected Day 5</b>	23.46	20.38	-3.08	0.11
<b>Infected 1:1</b>	23.43	20.79	-2.64	0.16
<b>Infected 2:1</b>	21.63	20.13	-1.50	0.15
<b>Infected 3:1</b>	24.06	20.67	-3.39	0.13
<b>Infected 4:1</b>	25.14	22.01	-3.12	0.13
<b>Infected 5:1</b>	26.92	23.57	-3.35	0.13

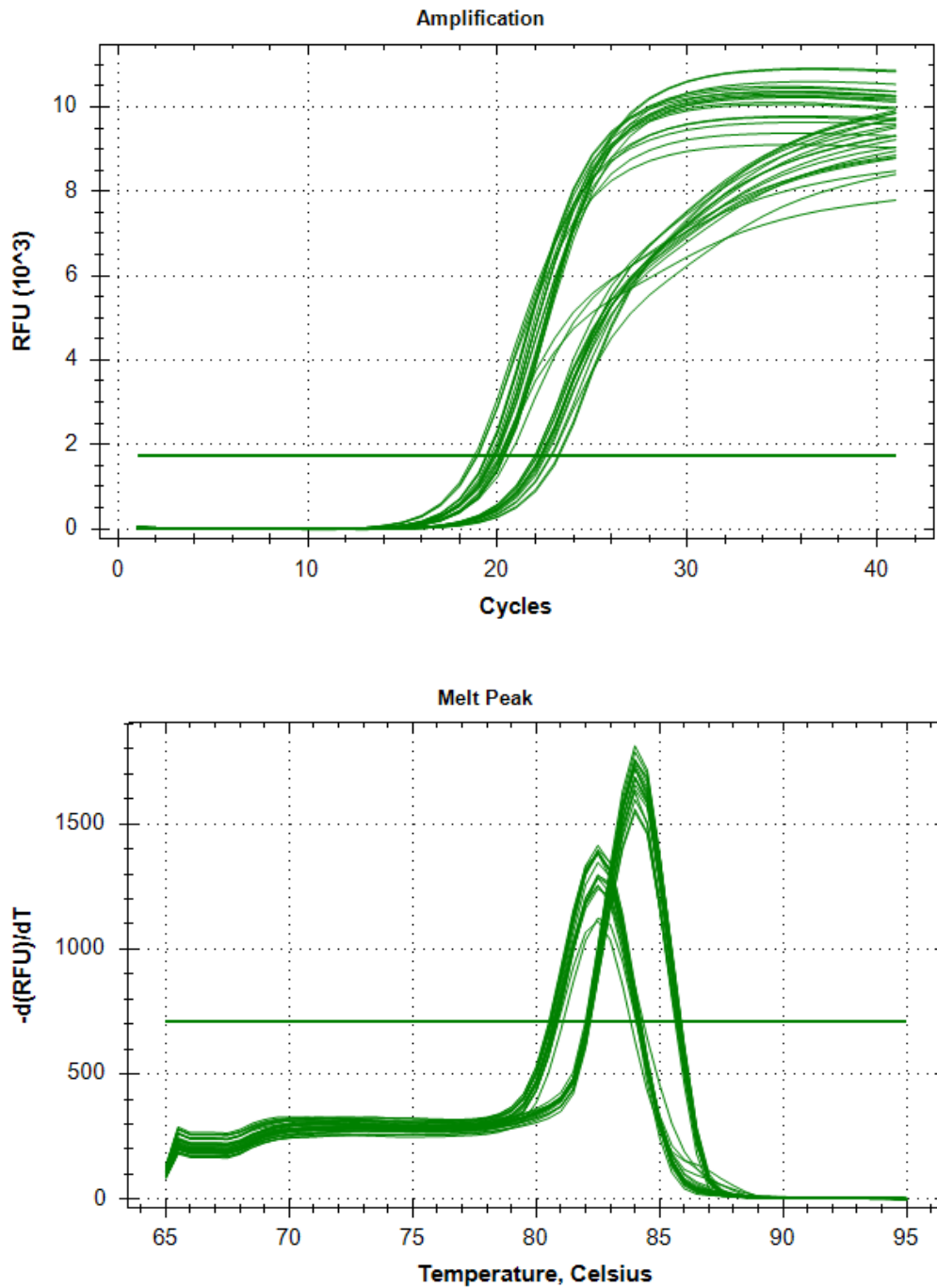
**B.1.4 Average  $\Delta Cq$  values**

All these three sets data (B.1.1 – B.1.3) were averaged and a graph was plotted as in Figure 4.2, plotting the DBH gene expression ( $-\Delta Cq$ ) relative to samples.

	<b>Set 1</b>	<b>Set 2</b>	<b>Set 3</b>	<b>AVERAGE <math>\Delta Cq</math></b>	<b>SEM</b>
Un-infected	-1.36	-2.07	-3.08	<b>-2.17</b>	0.498
Infected 1:1	-2.80	-4.55	-2.64	<b>-3.33</b>	0.613
Infected 2:1	-2.42	-5.36	-1.50	<b>-3.09</b>	1.165
Infected 3:1	-2.33	-2.70	-3.39	<b>-2.80</b>	0.312
Infected 4:1	-2.38	-1.43	-3.12	<b>-2.31</b>	0.490
Infected 5:1	-2.77	-3.37	-3.35	<b>-3.16</b>	0.197

**B.1.5 Amplification curve and melt curve.**

Graph below showed the amplification and melt peak curve of biological repeat Set 1 as an example of peaks shown in Bio-Rad CFX Manager (USA) software. One single peak was observed for each gene indicating a correct amplification product. Analysis was done with relative to the GAPDH reference gene.



## B.2 DBH gene expression of day 1, 3 and 5

Two biological repeat was done for this assay. The assay was done for two biological repeats (Repeat 1-2). Data analysis of RT-qPCR was shown as in the following table.

### B.2.1 Repeat 1

	Biological Repeat 1								
	Cq DBH				Cq GAPDH				Average Cq (DBH - GAPDH)
	Cq 1	Cq 2	Cq 3	Average	Cq 1	Cq 2	Cq 3	Average	
Un-infected Day 1	30.34	30.04	29.98	<b>30.12</b>	24.24	24.84	24.62	<b>24.57</b>	<b>-5.55</b>
Infected Day 1	29.36	29.48	29.94	<b>29.59</b>	23.65	24.06	23.70	<b>23.80</b>	<b>-5.79</b>
Un-infected Day 3	27.93	28.06	27.85	<b>27.95</b>	21.83	21.89	22.03	<b>21.92</b>	<b>-6.03</b>
Infected Day 3	28.99	27.44	27.78	<b>28.07</b>	21.82	22.05	21.78	<b>21.88</b>	<b>-6.19</b>
Un-infected Day 5	26.65	26.39	26.93	<b>26.66</b>	21.25	21.36	21.11	<b>21.24</b>	<b>-5.42</b>
Infected Day 5	28.98	29.39	29.22	<b>29.20</b>	22.57	22.92	22.68	<b>22.72</b>	<b>-6.47</b>

	Average Cq (DBH - GAPDH)		SEM (triplicate wells)	
	Un-infected	Infected	Un-infected	Infected
Day 1	-5.55	-5.79	0.11	0.18
Day 3	-6.03	-6.19	0.06	0.47
Day 5	-5.42	-6.47	0.16	0.12

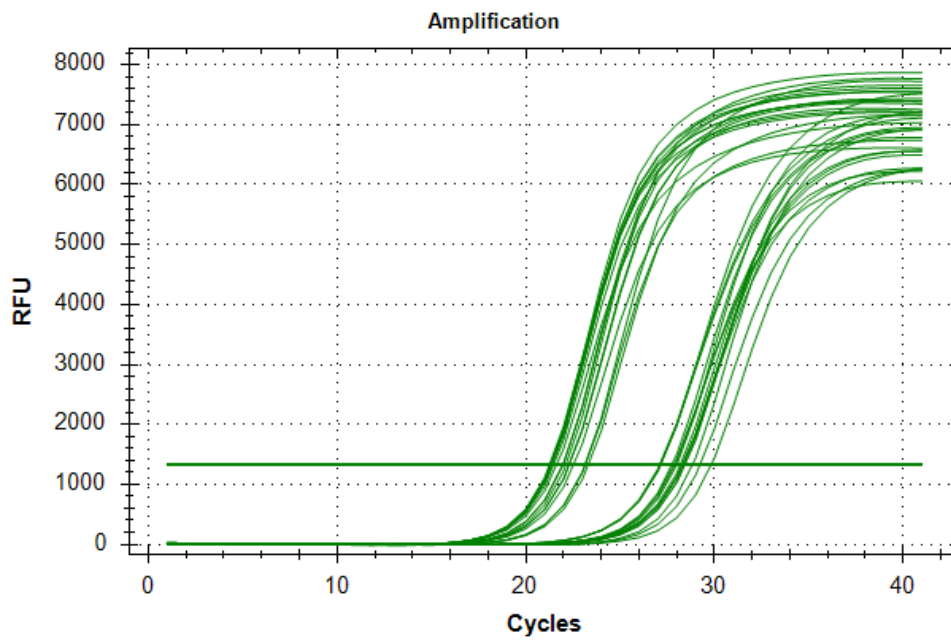
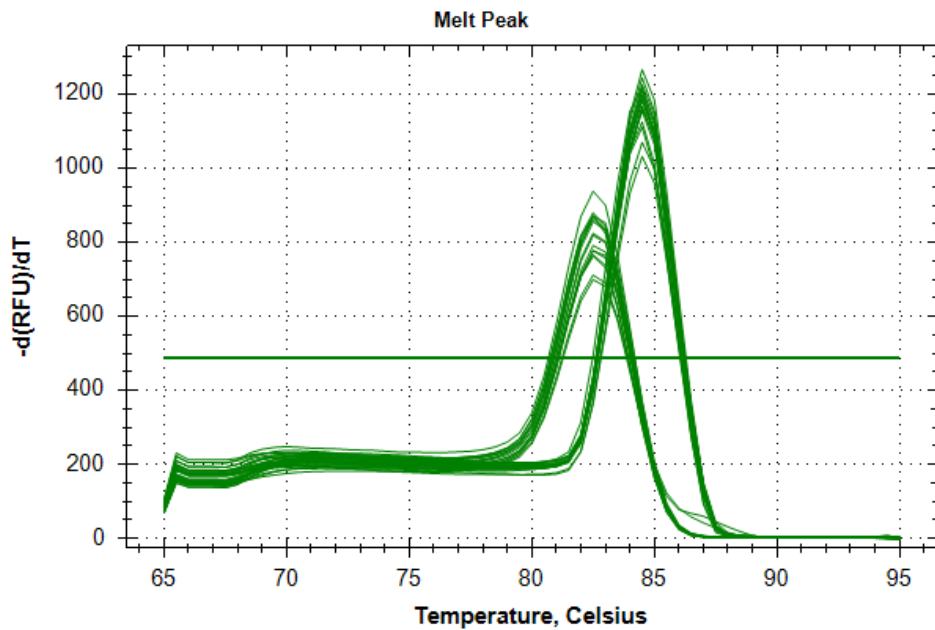
### B.2.2 Repeat 2

	Biological Repeat 2								
	Cq DBH				Cq GAPDH				Average Cq (DBH - GAPDH)
	Cq 1	Cq 2	Cq 3	Average	Cq 1	Cq 2	Cq 3	Average	
Un-infected Day 1	28.42	28.61	28.59	<b>28.54</b>	22.31	22.29	22.53	<b>22.38</b>	<b>-6.16</b>
Infected Day 1	29.83	29.24	28.84	<b>29.30</b>	23.14	23.32	23.17	<b>23.21</b>	<b>-6.09</b>
Un-infected Day 3	27.10	27.14	27.16	<b>27.13</b>	22.13	21.96	22	<b>22.03</b>	<b>-5.10</b>
Infected Day 3	27.85	27.93	27.75	<b>27.84</b>	21.26	21.64	21.3	<b>21.40</b>	<b>-6.44</b>
Un-infected Day 5	28.30	28.20	28.02	<b>28.17</b>	21.38	21.32	21.35	<b>21.35</b>	<b>-6.82</b>
Infected Day 5	28.30	28.32	28.43	<b>28.35</b>	21.48	21.38	21.34	<b>21.40</b>	<b>-6.95</b>

	Average Cq (DBH - GAPDH)		SEM (triplicate wells)	
	Un-infected	Infected	Un-infected	Infected
Day 1	-6.16	-6.09	0.06	0.29
Day 3	-5.10	-6.44	0.02	0.05
Day 5	-6.82	-6.95	0.08	0.04

**B.2.3 Amplification and melt peak curve data of biological repeat Set 2 of DBH gene.**

Graph below showed the amplification and melt peak curve data of biological repeat Set 1. One single peak was observed for each gene. Analysis was done with relative to the GAPDH reference gene.



**B.3 BAG1 gene expression relative to rat GAPDH expression in *T. gondii*-infected PC12 cells at 1, 3, and 5 days post-infection, analysed by RT-qPCR.**

Two biological repeat was done for this assay. The assay was done for two biological repeats with triplicate samples in RT-qPCR (Repeat 1-2). Data analysis of RT-qPCR as in the following table.

**B.3.1 Repeat 1 and Repeat 2**

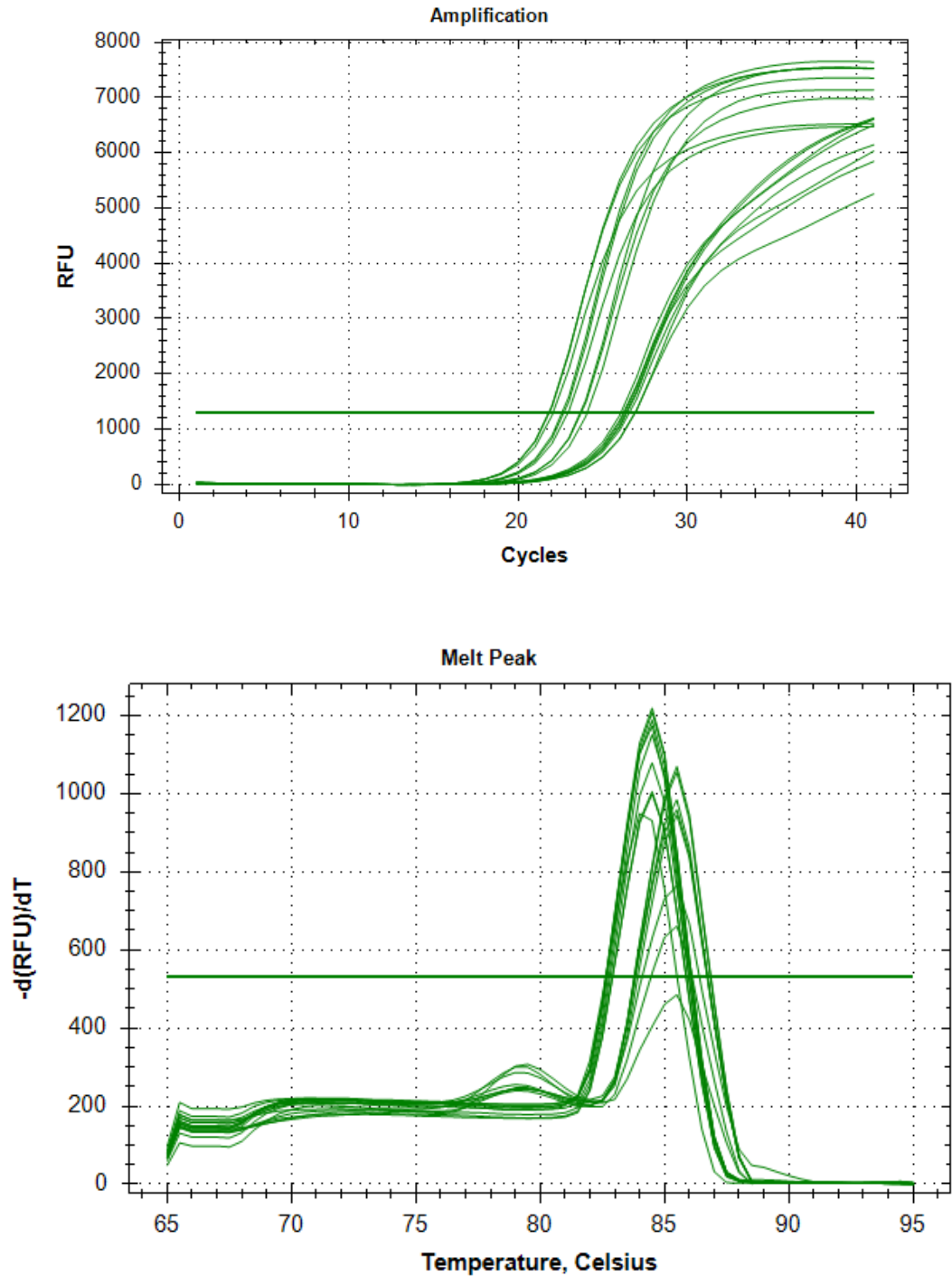
		Repeat 1								
bradyzoite marker	BAG1				Cq GAPDH				Average $\Delta$ Cq (BAG1 - GAPDH)	
	Cq 1	Cq 2	Cq 3	Average	Cq 1	Cq 2	Cq 3	Average		
Infected Day 1	33.7	33.76	33.25	<b>33.57</b>	23.65	24.06	23.7	<b>23.80</b>	<b>-9.77</b>	
Infected Day 3	29.43	29.03	29.23	<b>29.23</b>	21.82	22.05	21.78	<b>21.88</b>	<b>-7.35</b>	
Infected Day 5	30.39	30.35	30.19	<b>30.31</b>	22.57	22.92	22.68	<b>22.72</b>	<b>-7.59</b>	

		Repeat 2								
bradyzoite marker	BAG1				Cq GAPDH				Average $\Delta$ Cq (BAG1 - GAPDH)	
	Cq 1	Cq 2	Cq 3	Average	Cq 1	Cq 2	Cq 3	Average		
Infected Day 1	34.01	33.34	33.93	<b>33.76</b>	23.14	23.32	23.17	<b>23.21</b>	<b>-10.55</b>	
Infected Day 3	30.09	29.96	30.03	<b>30.03</b>	21.26	21.64	21.30	<b>21.40</b>	<b>-8.63</b>	
Infected Day 5	29.45	29.62	29.65	<b>29.57</b>	21.48	21.38	21.34	<b>21.40</b>	<b>-8.17</b>	

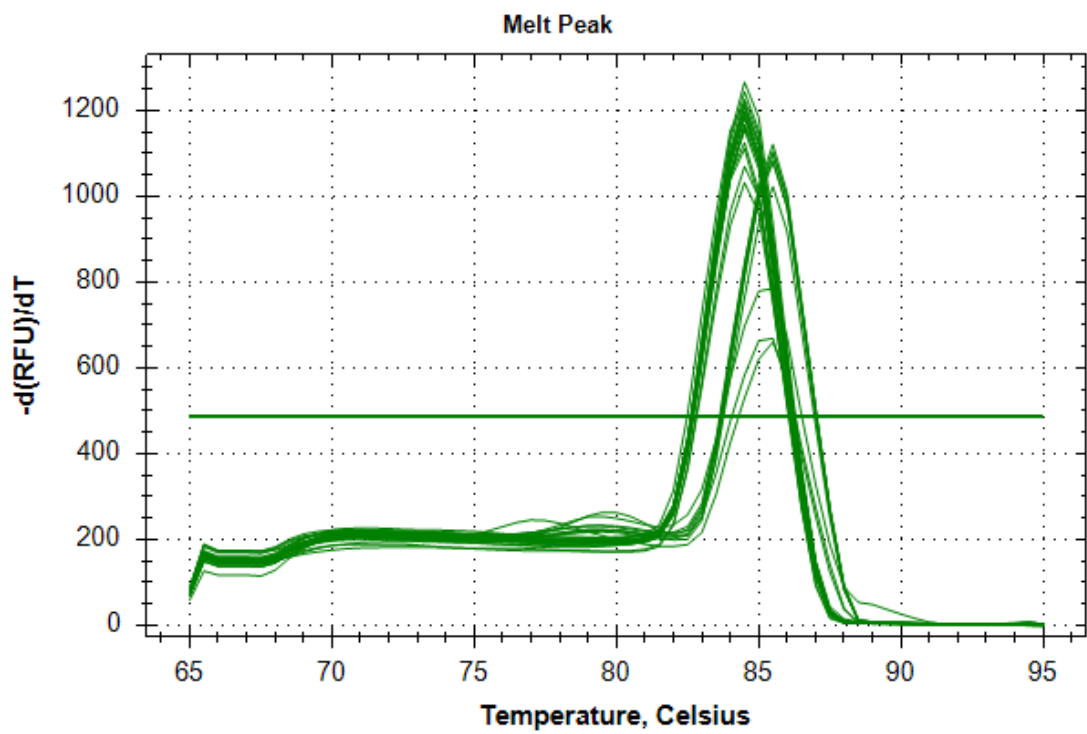
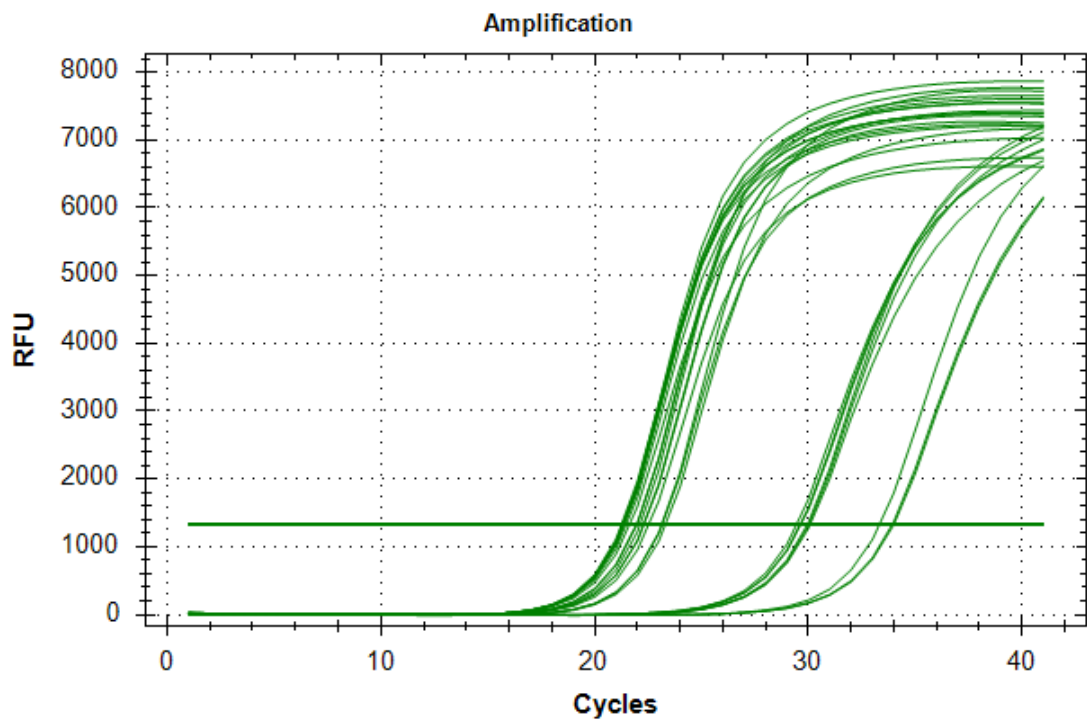
BAG 1	SET 1	SET 2	Average $\Delta$ Cq	SEM
Day 1	-9.77	-10.55	-10.16	0.392
Day 3	-7.35	-8.63	-7.99	0.640
Day 5	-7.59	-8.17	-7.88	0.293

**B.3.2 Amplification and melt curve data BAG 1**

Both amplification and melt curve graphs for each repeat as shown in the following figures:

**B.3.2.1 Repeat 1**

## B.3.2.2 Repeat 2



**B.4 Toxo-actin gene expression relative to rat GAPDH expression in *T. gondii*-infected PC12 cells at 1, 3, and 5 days post-infection, analysed by RT-qPCR.**

Two biological repeat was done for this assay. The assay was done for two biological repeats (Repeat 1-2). Data analysis of RT-qPCR as in the following table.

**B.4.1 Repeat 1 and Repeat 2**

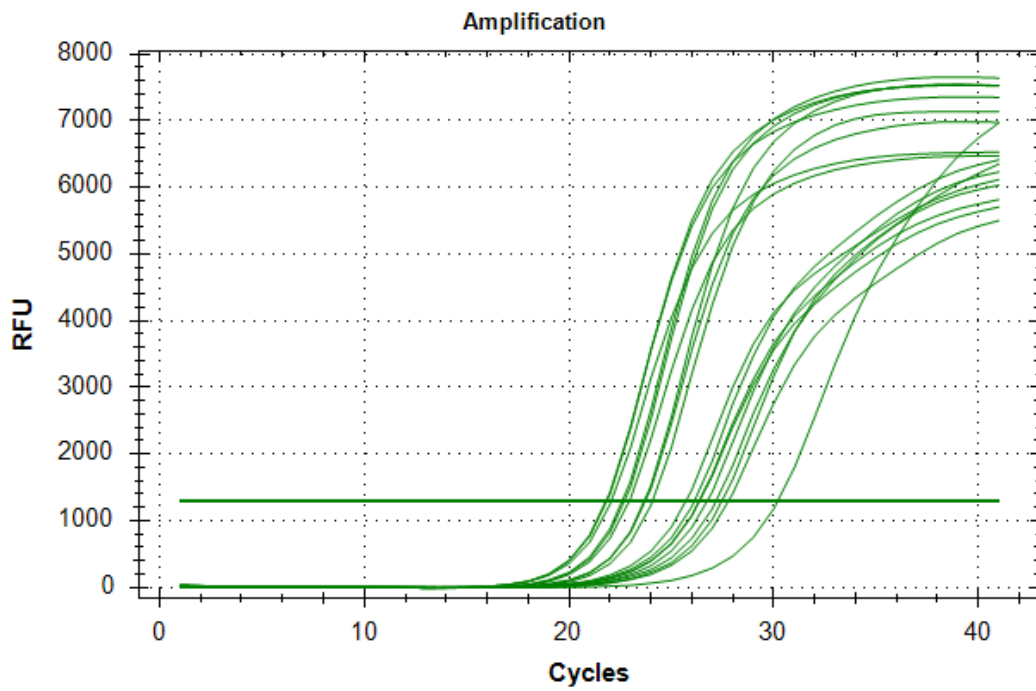
		Repeat 1								
		Toxo-actin				Cq GAPDH				Average $\Delta$ Cq (BAG1 - GAPDH)
		Cq 1	Cq 2	Cq 3	Average	Cq 1	Cq 2	Cq 3	Average	
Infected Day 1		34.18	34.79	33.99	<b>34.32</b>	23.65	24.06	23.7	<b>23.80</b>	<b>-10.52</b>
Infected Day 3		29.24	29.18	28.94	<b>29.12</b>	21.82	22.05	21.78	<b>21.88</b>	<b>-7.24</b>
Infected Day 5		31.34	31.06	30.62	<b>31.01</b>	22.57	22.92	22.68	<b>22.72</b>	<b>-8.28</b>

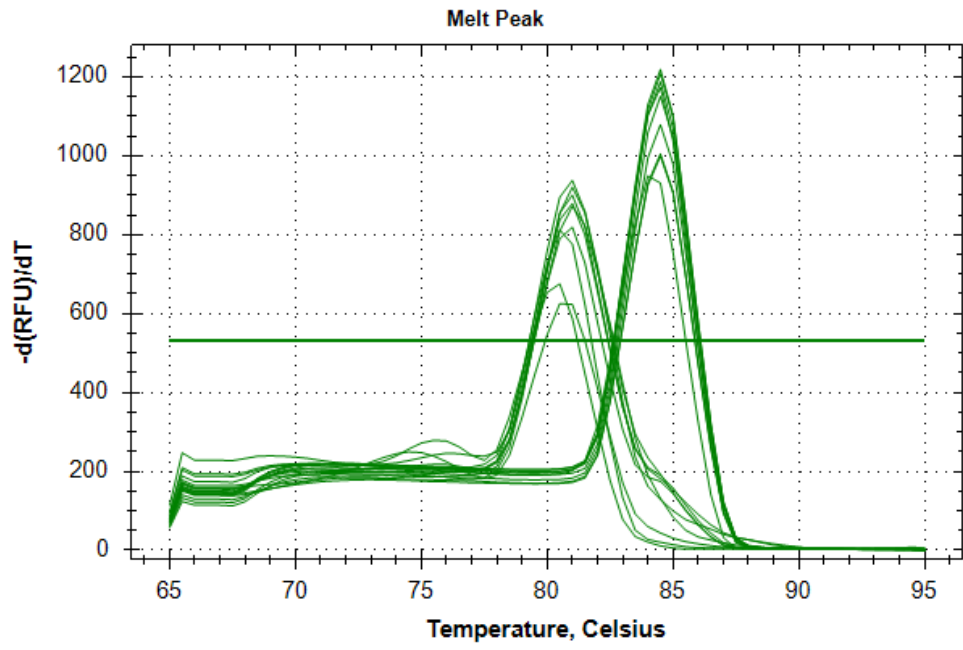
		Repeat 2								
		Toxo-actin				Cq GAPDH				Average $\Delta$ Cq (BAG1 - GAPDH)
		Cq 1	Cq 2	Cq 3	Average	Cq 1	Cq 2	Cq 3	Average	
Infected Day 1		34.76	33.76	33.74	<b>34.09</b>	23.14	23.32	23.17	<b>23.21</b>	<b>-10.88</b>
Infected Day 3		30.86	30.31	30.25	<b>30.47</b>	21.26	21.64	21.30	<b>21.40</b>	<b>-9.07</b>
Infected Day 5		31.17	30.27	30.3	<b>30.58</b>	21.48	21.38	21.34	<b>21.40</b>	<b>-9.18</b>

Actin	SET 1	SET 2	Average $\Delta$ Cq	SEM
Day 1	-10.52	-10.88	-10.70	0.180
Day 3	-7.24	-9.07	-8.16	0.918
Day 5	-8.28	-9.18	-8.73	0.448

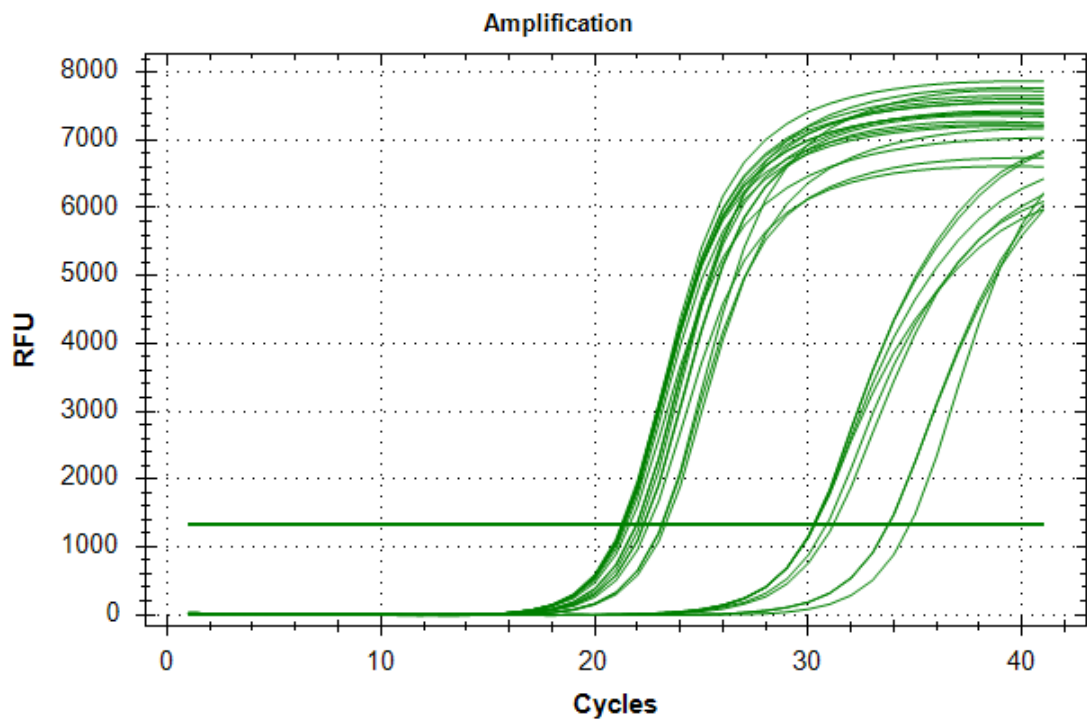
**B.4.2 Amplification and melt curve Toxo-actin.**

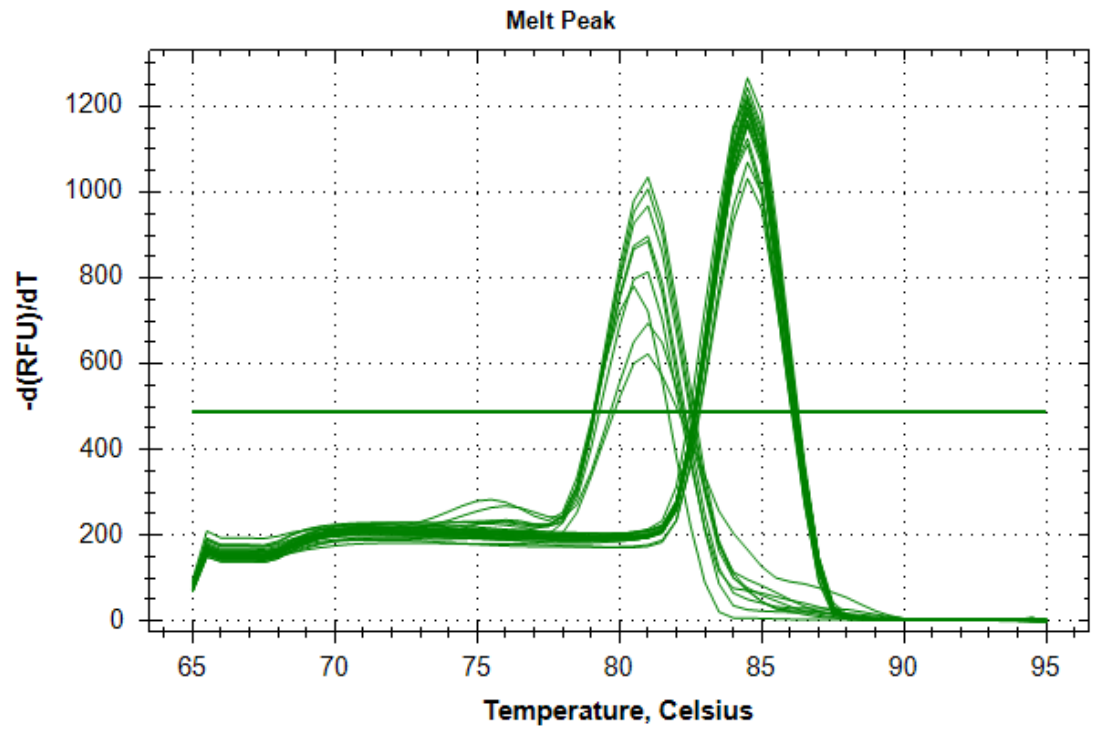
Both amplification and melt curve graphs for each repeat as shown in the following figures:

**B.4.2.1 Repeat 1**



**B.4.2.2 Repeat 2**







**C.1.2 Primer Set 3**

The sequence was matched with *Rattus norvegicus* DBH promoter gene sequence (sequence ID: L12409.1, range 1: 633 to 959).

Score	Expected	Identities	Gaps	Strand
604 bits(327)	5e-169	327/327(100%)	0/327(0%)	Plus/Minus

```

Query 1   GCCAGGCTGTACCTAATCACATTTGTCTGGTGGGGAATTCAATTGTCCTGGTGGCTCTCC 60
          |
          |
          |
Sbjct 959  GCCAGGCTGTACCTAATCACATTTGTCTGGTGGGGAATTCAATTGTCCTGGTGGCTCTCC 900

Query 61  CACCAGCCCATGCCCTGGGGCAAACACTTTGCTCCGATCCTCCCCTAATTGACACTAATG 120
          |
          |
          |
Sbjct 899  CACCAGCCCATGCCCTGGGGCAAACACTTTGCTCCGATCCTCCCCTAATTGACACTAATG 840

Query 121 ACGCATGGACATCATCAAGAGAATCGAAGCAGAATGGCCATGTCCTCCAATGGATCTCTG 180
          |
          |
          |
Sbjct 839  ACGCATGGACATCATCAAGAGAATCGAAGCAGAATGGCCATGTCCTCCAATGGATCTCTG 780

Query 181  ACGCCTGTTGGAAACAGCTACTCTCTGCAGACATAGGTCCCAAGGACACCTCCAGCCAGG 240
          |
          |
          |
Sbjct 779  ACGCCTGTTGGAAACAGCTACTCTCTGCAGACATAGGTCCCAAGGACACCTCCAGCCAGG 720

Query 241  CCCTGCTGAATGCCTCATAGGCAGTCAGGGCCTCTCTACCTGCTCCAAGTCAAG 300
          |
          |
          |
Sbjct 719  CCCTGCTGAATGCCTCATAGGCAGTCAGGGCCTCTCTACCTGCTCCAAGTCAAG 660

Query 301  GGGCTCCTTCCTGAGTGACAGTGAGTG 327
          |
          |
          |
Sbjct 659  GGGCTCCTTCCTGAGTGACAGTGAGTG 633

```

**C.1.3 Primer Set 4**

The sequence was matched with *Rattus norvegicus* DBH promoter gene sequence (sequence ID: L12409.1, range 1: 633 to 830).

Score	Expected	Identities	Gaps	Strand
366 bits(198)	2e-97	198/198(100%)	0/198(0%)	Plus/Minus

```

Query 1   CATCATCAAGAGAATCGAAGCAGAATGGCCATGTCCTCCAATGGATCTCTGACGCCTGTT 60
          ||||||||||||||||||||||||||||||||||||||||||||||||||||||||
Sbjct 830  CATCATCAAGAGAATCGAAGCAGAATGGCCATGTCCTCCAATGGATCTCTGACGCCTGTT 771

Query 61  GGAAACAGCTACTCTCTGCAGACATAGGTCCCAAGGACACCTCCAGCCAGGCCCTGCTGA 120
          ||||||||||||||||||||||||||||||||||||||||||||||||||||||||
Sbjct 770  GGAAACAGCTACTCTCTGCAGACATAGGTCCCAAGGACACCTCCAGCCAGGCCCTGCTGA 711

Query 121 ATGCCTCATAGGCAGTCAGGGCCTCTCTACCTGCTCCAAGTCAAGGGGCTCCTT 180
          ||||||||||||||||||||||||||||||||||||||||||||||||||||||||
Sbjct 710  ATGCCTCATAGGCAGTCAGGGCCTCTCTACCTGCTCCAAGTCAAGGGGCTCCTT 651

Query 181  CCTGAGTGACAGTGAGTG 198
          ||||||||||||||||
Sbjct 650  CCTGAGTGACAGTGAGTG 63

```